# THERMALLY EFFICIENT

# ADVANCED DIESEL EXHAUST AFTERTREATMENT

# FOR CLEANER VEHICLES

By

ISALINE LEFORT

A thesis submitted to

The University of Birmingham

For the degree of

DOCTOR OF PHILOSOPHY

School of Mechanical Engineering

University of Birmingham

July 2015

UNIVERSITY OF BIRMINGHAM

**University of Birmingham Research Archive**

**e-theses repository**

This unpublished thesis/dissertation is copyright of the author and/or third parties. The intellectual property rights of the author or third parties in respect of this work are as defined by The Copyright Designs and Patents Act 1988 or as modified by any successor legislation.

Any use made of information contained in this thesis/dissertation must be in accordance with that legislation and must be properly acknowledged. Further distribution or reproduction in any format is prohibited without the permission of the copyright holder.

# ABSTRACT

Increased diesel vehicle use and growing concerns about the health and environmental effects of exhaust gas pollutants lead to a greater attention upon the reduction of vehicle emissions. The development of driving patterns and vehicle technologies lead to lower average exhaust gas temperatures. This can limit the diesel aftertreatment system's ability to meet increasingly stringent emissions legislation. A thermally efficient aftertreatment system can be produced through advanced and novel catalyst designs. The research work presented in this thesis investigates diesel oxidation catalyst (DOC) and exhaust gas properties that can enhance aftertreatment performance at low temperatures.

Firstly, an advanced two-catalyst configuration is designed that widens the aftertreatment system operating temperature window. Catalyst cell density, wall thickness and material choices were optimised using theoretical equations, modelling tools and an experimental approach.

Secondly, strategies were developed to assist the aftertreatment low-temperature activity through the understanding of exhaust species interactions (inhibition and promotion) within the catalyst. This was achieved by varying the exhaust composition at the catalyst inlet, using alternative fuels and combustion modes.

Finally, a catalyst component combining a filtration/oxidation function (partial-flow filter) was found to promote particulate removal while reducing the need for diesel particulate filter active regeneration.

Graphical Abstract

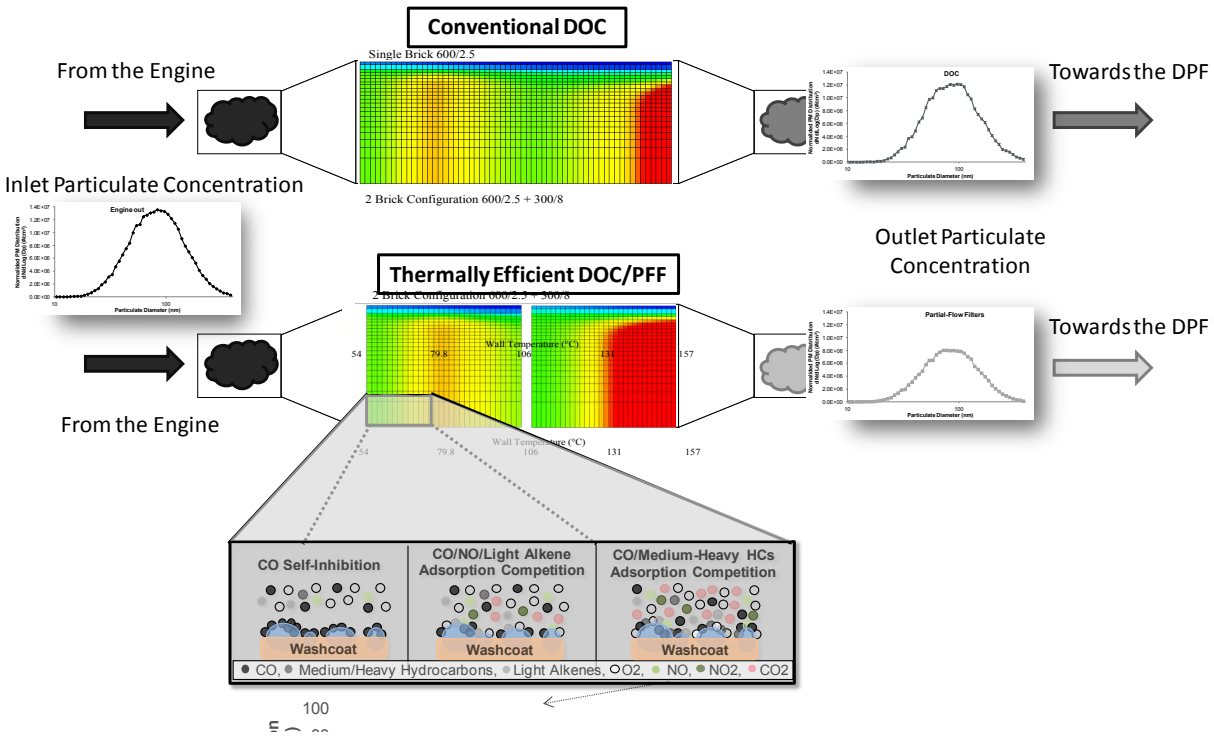

# ACKNOWLEDGEMENT

I would like to express my appreciation and thanks to all the people who helped me throughout this PhD and allowed the completion of this work. First of all, I would like to thank my supervisor, Dr. Athanasios Tsolakis, for his guidance, technical knowledge and support during these years at the University. My co-supervisor, Professor Miroslaw Wyszynski is also acknowledged for his welcome and support. Thank you also to Jaguar Land Rover for the technical and financial support that was greatly appreciated and I would like to especially thank Ken Hansen, Jonathan Hartland, David Sellick, Aden Bott and Karl Wright from Jaguar Land Rover. A special thanks to the staff from the School of Mechanical Engineering of the University of Birmingham and especially Helen Booth for her kindness and precious help with the administrative matters, and the technicians, Carl Hingley, Peter Thornton, Lee Gauntlett and Jack Garrod, for their excellent manufacturing skills that allowed the creation of some of the exhaust parts used in this study. Thank you also to all my colleagues and friends, Jose Martin Herreros, Maria Bogarra Macias, Soheil Zeraati Rezaei, Shahriar Parisouz, Mohammedreza Hamedi, Yasser Al Qahtani and Chongming Wang, who with their presence and kind attention, made this whole PhD experience so fruitful in learning, discoveries and enjoyment. A special thought to Umar Musbahu who, with his constant smile even during the difficult times, was inspiring and always positive. Finally, I would like to thank my parents, Pascal and Pascale Lefort, and my sister Anaïs, for their moral support and encouragements, despite the distance, and for always cheering me up. Last but not least, thank you also to my boyfriend Paul Rounce, for having always believed I would succeed in this enterprise “despite my handicap of being French”...!

ISALINE LEFORT

July 2015

# TABLE OF CONTENTS

**1. INTRODUCTION ..... 1**
1.1. Background: Diesel Engine and Emissions ..... 1
1.1.1. Diesel Engines ..... 1
1.1.2. Exhaust Emissions Formation and Effect on Human Health and the Environment 2
1.1.3. Pollutants Removal in Diesel Exhaust System ..... 5
1.2. Motivation: Low Exhaust Temperature Challenge ..... 9
1.2.1. Development of Engines with Increasing Efficiency ..... 9
1.2.2. Development of the Driving Pattern ..... 11
1.2.3. Effect of the Hybridisation of the Powertrain ..... 13
1.3. Strategies to Improve the Low-Temperature Catalyst Activity ..... 14
1.4. Scope, Aim and Objectives ..... 16
1.5. Thesis Outline ..... 17
**2. LITERATURE REVIEW ..... 21**
2.1. Catalyst Design ..... 21
2.1.1. Catalyst Physical Properties ..... 21
2.1.1.1. Substrate Internal Dimensions ..... 22
2.1.1.2. Substrate Material ..... 25
2.1.2. Catalyst Chemical Properties ..... 26
2.2. Influence of the Exhaust Gas Composition on the Catalyst Activity ..... 29
2.2.1. Exhaust Gas Physical Properties ..... 29
2.2.1.1. Exhaust Gas Temperature ..... 29
2.2.1.2. Exhaust Gas Flow Rate ..... 30
2.2.2. Exhaust Gas Chemical Properties ..... 31
2.2.2.1. Oxygen Exhaust Concentration ..... 31
2.2.2.2. Exhaust Pollutants Concentration and Composition ..... 32
2.2.2.3. Particulate Matter Accumulation ..... 33
2.3. Catalyst Design: Combination of Filtration and Oxidation Functions ..... 35
2.3.1. Thermal Management of the Aftertreatment System ..... 35
2.3.2. Benefits and Requirements of the Pre-Filter Component ..... 36
2.3.3. Potential Substrates ..... 36
2.3.4. Presentation of the Partial-Flow Filters ..... 37
2.3.4.1. Characteristics and Properties of Partial-Flow Filters ..... 37

2.3.4.2. Partial-Flow Filters ..... 39
**3. EXPERIMENTAL FACILITIES ..... 42**
3.1. Engine and Fuels ..... 42
3.1.1. Diesel Engine and Instrumentation ..... 42
3.1.2. Liquid Fuels ..... 43
3.1.3. Gaseous Components Additions ..... 44
3.2. Engine Exhaust System and Aftertreatment ..... 45
3.2.1. Exhaust System and Instrumentation ..... 45
3.2.2. Diesel Oxidation Catalysts and Particulate Filters ..... 47
3.3. Exhaust Gas Emission Analysis ..... 50
3.3.1. Fourier Transform Infrared Spectrometry (FTIR) ..... 50
3.3.2. AVL DiGas ..... 51
3.3.3. Scanning Mobility Particle Sizer (SMPS) ..... 51
3.3.4. Thermogravimetric Analysis (TGA) ..... 52
3.3.5. Transmission Electronic Microscope (TEM) ..... 53
3.4. Experimental Errors and Repeatability ..... 54
3.5. Software Used for the Modelling of the Aftertreatment System ..... 55
**4. A THERMALLY EFFICIENT DOC CONFIGURATION TO IMPROVE LOW-TEMPERATURE ACTIVITY ..... 58**
4.1. Methodology ..... 58
4.1.1. Theoretical Study Assumptions ..... 58
4.1.2. Input Data for the Modelling and Simulation Study ..... 59
4.1.3. Set-Up and Methodology for the Experimental Study ..... 59
4.1.4. Model Setup for the Alternative Driving Cycles Study ..... 64
4.2. Results of the Theoretical Study ..... 64
4.2.1. Presentation of the Equations ..... 65
4.2.2. Effect of Cell Density/Wall Thickness on the Catalyst Activity and Durability ..... 68
4.3. Simulation Study ..... 75
4.3.1. Simulation of the Thermal Behaviour and Conversion Efficiency of the Selected Catalysts ..... 75
4.3.1.1. Cold Start – Warming Phases ..... 75
4.3.1.2. Cooling Phases ..... 77
4.3.2. Two-Catalyst Configurations ..... 80
4.3.2.1. Selection of the Second Catalyst ..... 81

4.3.2.2. $NO_2$ Production from the Two-Brick Configuration ..... 89
4.4. Experimental Study of the Two-Brick Configurations ..... 90
4.4.1. Thermal Behaviour of the Two-Brick Configurations with Genuine Diesel Exhaust Gas ..... 90
4.4.2. Conversion Efficiency ..... 100
4.4.2.1. Carbon Monoxide (CO) ..... 100
4.4.2.2. Long-Chain Hydrocarbons (HC) ..... 102
4.4.2.3. Nitrogen Oxides ($NO_x$) ..... 104
4.5. Simulations of Alternative Driving Cycles ..... 107
4.5.1. Validation of the Axisuite Model ..... 107
4.5.2. Thermal Behaviour during Alternative Driving Cycles ..... 110
4.5.2.1. Paris Cycle ..... 110
4.5.2.2. Urban Parts of the NEDC with Stop/Start Strategy ..... 112
4.6. Summary and Conclusions ..... 114
**5. EFFECT OF THE EXHAUST GAS COMPOSITION ON THE DOC ACTIVITY 115**
5.1. Methodology ..... 115
5.1.1. Exhaust Species Interaction Study ..... 115
5.1.2. Oxygen Study ..... 116
5.1.3. PM Effect on the DOC Activity Study ..... 117
5.2. Results and Discussion on the Study on Interactions Between Exhaust Gas Pollutants ..... 119
5.2.1. Exhaust Gas Composition ..... 120
5.2.2. CO Oxidation ..... 122
5.2.3. HC Oxidation ..... 128
5.2.3.1. Medium-Heavy Hydrocarbons ..... 128
5.2.3.2. Light Hydrocarbons ..... 132
5.2.4. Evolution of the Distribution of Hydrocarbon Species during Light-Off ..... 133
5.2.5. Strategies to Reduce Exhaust Gas Interactions and Promote Low-Temperature Activity ..... 135
5.3. Oxygen Exhaust Gas Concentration ..... 137
5.3.1. Background Study ..... 137
5.3.2. Results and Discussions from the Oxygen Concentration Study ..... 138
5.3.2.1. Exhaust Gas Composition ..... 138
5.3.2.2. Oxygen Effect on CO from Diesel Fuel Combustion ..... 140

5.3.2.3. Oxygen Effect on CO and HCs from Dual-Fuel Combustion ..... 145
5.4. Effect of the Exhaust PM on the Diesel Oxidation Catalyst Activity ..... 147
5.4.1. Effect of EGR Strategy on the DOC Activity ..... 147
5.4.1.1. Gaseous Exhaust Species ..... 147
5.4.1.2. Effect of EGR on the Soot Profile and PM Removal in the DOC ..... 148
5.4.2. Effect of Particulate Matter on the DOC Activity ..... 149
5.4.2.1. Gaseous Exhaust Species Oxidation ..... 149
5.4.2.2. Particulate Matter Removal ..... 151
5.5. Summary and Conclusions ..... 155
**6. COMBINATION OF FILTRATION AND OXIDATION FUNCTIONS TO IMPROVE THE DPF THERMAL MANAGEMENT ..... 156**
6.1. Methodology ..... 156
6.1.1. Filtration and Oxidation Mechanisms and Efficiencies ..... 156
6.1.2. Long-Term Filtration and Oxidation Activity ..... 158
6.1.3. Partial-Flow Filters Passive Regeneration Study ..... 159
6.1.3.1. Passive Regeneration of the PM-Metalit ..... 159
6.1.3.2. Passive Regeneration of the POC ..... 160
6.1.4. Combined PFF+DPF System ..... 160
6.2. Study of the Filtration Mechanisms ..... 160
6.2.1. Partial-Flow Filters ..... 161
6.2.1.1. PM-Metalit ..... 161
6.2.1.2. POC ..... 165
6.2.2. Flow-Through Catalysts ..... 169
6.2.2.1. LS Catalyst ..... 170
6.2.2.2. Conventional Flow-Through DOC ..... 174
6.3. Comparisons Between the PFFs and Flow-Through Catalysts ..... 178
6.3.1. Filtration Efficiency ..... 178
6.3.1.1. Study of the Filtration Efficiency at 25 000/h SV – 200°C ..... 178
6.3.1.2. Study of the Filtration Efficiency at 28 000/h SV – 250°C ..... 178
6.3.1.3. Study of the Filtration Efficiency at 40 000/h SV – 330°C ..... 180
6.3.1.4. Study of the Filtration Efficiency at 44 000/h SV – 420°C ..... 181
6.3.2. Filtration Efficiency at Idle Engine Condition ..... 182
6.3.3. Catalyst Oxidation Efficiency ..... 184
6.3.4. Comparison of the Long-Term Activity ..... 187

6.3.4.1. Long-Term Filtration Efficiency ..... 187
6.3.4.2. Long-Term Oxidation Efficiency of the POC, LS and DOC ..... 190
6.3.5. Passive Regeneration ..... 192
6.3.5.1. Passive Regeneration of the PM-Metalit ..... 192
6.3.5.2. Passive Regeneration of the POC ..... 195
6.3.6. Temperature and Pressure Comparison Between PFF and Flow-Through Catalysts ..... 197
6.4. Investigation of a PFF + DPF System ..... 200
6.4.1. Effect of the PFF on the Particulates Supplied to the DPF ..... 200
6.4.1.1. Particulate Concentration, Size and Composition ..... 200
6.4.1.2. Particulate Morphology and Microstructure ..... 202
6.4.1.3. Particulate Reactivity ..... 204
6.4.2. Efficiency of a Combined PFF and DPF System ..... 205
6.4.2.1. Filtration Efficiency ..... 205
6.4.2.2. Soot Accumulation and Pressure Increase in the DPF ..... 208
6.5. Summary and Conclusions ..... 209
**7. CONCLUSIONS AND FUTURE WORK ..... 210**
7.1. A Thermally Efficient DOC Configuration to Improve Low-Temperature Activity 210
7.2. Effect of the Exhaust Gas Composition on the DOC Activity ..... 211
7.2.1. Interactions Between Exhaust Gas Pollutants ..... 211
7.2.2. Oxygen Exhaust Gas Concentration ..... 212
7.2.3. Effect of Soot Accumulation on the DOC Activity ..... 213
7.3. Combination of Filtration and Oxidation Functions to Improve the DPF Thermal Management ..... 213
7.4. Closing Remarks ..... 214
**AUTHOR PUBLICATIONS ..... 216**
**AWARDS ..... 217**
**APPENDICES ..... 218**
A.1. Legislation Driving Cycles ..... 218
**REFERENCES ..... 223**

# LIST OF FIGURES

Figure 1-1. Average diesel penetration in 15 countries of Europe and by country in percent of share of new cars registered ..... 1
Figure 1-2. Relation between the particulate size and their deposition rate and location in the human body, fitted with a typical particulate size distribution from the engine used in this study ..... 5
Figure 1-3. Yearly published items containing the term “catalytic converter” from 1957 to 2014 ..... 6
Figure 1-4. Exhaust temperature measured at different locations in the exhaust system of a Volvo S60 operating an EU III cycle ..... 10
Figure 1-5. Fraction of CO and THCs emitted at the different stages of the NEDC, based on the emissions of an EU5 diesel engine ..... 12
Figure 1-6. Percentage of time at temperature over the NEDC, based on an EU5 diesel engine ..... 12
Figure 1-7. Example of catalyst improved light-off for CO conversion efficiency ..... 14
Figure 1-8. Example of in-situ catalyst improved temperature ..... 15
Figure 1-9. Schematic summarising the scope of the research work presented in this thesis ..... 17
Figure 2-1. Estimation of the influence of the cell density/wall thickness and cell shape on the catalyst light-off factor, pressure drop and mechanical durability ..... 23
Figure 2-2. Effect of the addition of palladium in a platinum catalyst on CO conversion efficiency at two different CO and HC exhaust gas concentrations ..... 27
Figure 2-3. The cost of platinum and palladium from 1992 to 2014 ..... 28
Figure 2-4. Cell area for various cell densities and wall thicknesses ..... 34
Figure 2-5. Schematic of the filtration mechanisms taking place within the PM-Metalit ..... 39
Figure 2-6. Layers arrangement in the POC and flow path within the filter ..... 40
Figure 2-7. View from a single channel in the LS catalyst and schematic of the flow behaviour within the channel ..... 41
Figure 3-1. Schematic of the experimental set-up ..... 46
Figure 3-2. Pictures of the aftertreatment components studied ..... 48
Figure 3-3. Typical particulate size distribution for the engine used in this study ..... 52
Figure 3-4. Comparison of the DOC outlet temperature as predicted by Axisuite, with the measured one from an engine over an NEDC ..... 56

Figure 4-1. Variations (error bars) in the exhaust gas concentration during the repetition of the engine operating conditions for the different combinations of catalysts ..... 63
Figure 4-2. Effect of the cell density/wall thickness on the improvement or reduction in light-off factor compared to the reference substrate ..... 70
Figure 4-3. Effect of the cell density/wall thickness on the improvement or reduction in conversion efficiency factor compared to the reference substrate ..... 70
Figure 4-4. Effect of the cell density/wall thickness on the improvement or reduction in pressure losses compared to the reference substrate ..... 71
Figure 4-5. Effect of the cell density/wall thickness on the improvement or reduction in mechanical durability compared to the reference substrate ..... 71
Figure 4-6. Effect of the cell density/wall thickness on the increase or decrease of the cell area compared to the 400/4 reference substrate ..... 72
Figure 4-7. Effect of the cell density/wall thickness on the catalysts outlet CO and THC cumulative emissions during the first 200 seconds of the NEDC (light-off phase) ..... 75
Figure 4-8. Effect of the cell density/wall thickness on the catalysts outlet temperature during the first 200 seconds of the NEDC with the engine-out CO and HC emissions ..... 76
Figure 4-9. Effect of the cell density/wall thickness on the catalysts outlet CO and THC cumulative emissions during acceleration/deceleration phases of the NEDC ..... 77
Figure 4-10. Effect of the cell density/wall thickness on the catalysts outlet temperature during acceleration/deceleration phases of the NEDC with the engine-out CO and HC emissions ..... 78
Figure 4-11. Comparison of the gain in total conversion efficiency when replacing the reference 400/4 catalyst by a single catalyst or a two-catalyst combination ..... 82
Figure 4-12. Comparison of the pressure increase when replacing the reference 400/4 catalyst by a single catalyst or a two-catalyst combination ..... 83
Figure 4-13. Effect of the two-brick configurations on the catalysts outlet temperature during acceleration/deceleration phases of the NEDC, with engine-out CO and HC emissions ..... 84
Figure 4-14. Effect of the two-brick configurations on the catalyst outlet CO and THC cumulative emissions compared to the 400/4 and 600/2.5 single catalysts over an NEDC .... 84
Figure 4-15. Temperature distribution in the catalysts (400/4 reference catalyst versus two-brick configuration) at the 290$^{th}$ second of the NEDC (warming phase) ..... 86
Figure 4-16. Temperature distribution in the catalysts (600/2.5 versus two-brick configuration) at the 230$^{th}$ second of the NEDC (cooling phase) ..... 87

Figure 4-17. Effect of the two-brick configuration 600/2.5 + 300/8 on $NO_2$ production, compared to the reference 400/4 catalyst, during an NEDC ..... 89
Figure 4-18. Catalysts inlet and outlet temperatures and temperature losses for the different combinations, during the warming phase of the experiment ..... 90
Figure 4-19. Evolution of the exhaust gas concentration and catalyst temperature during the release of the stored hydrocarbons in the 400/4 catalyst ..... 92
Figure 4-20. Evolution of the $NO_x$ exhaust concentration and catalyst temperature during the release of the stored hydrocarbons in the 400/4 catalyst ..... 93
Figure 4-21. Catalyst inlet and outlet temperatures for the different combinations during the first exothermic event ..... 93
Figure 4-22. Catalyst inlet and outlet temperatures for the different combinations during the second exothermic event ..... 95
Figure 4-23. Catalyst inlet and outlet temperatures and temperature losses for the different combinations during a cooling event ..... 97
Figure 4-24. Temperature losses over the combinations of catalysts during a cooling at rest 98
Figure 4-25. Temperature losses over the various combinations of catalysts during the steady-state phases of the experiment ..... 99
Figure 4-26. CO conversion efficiency for the combinations of catalysts based on their inlet and outlet temperatures ..... 100
Figure 4-27. Heavy-hydrocarbons conversion efficiency for the combinations of catalysts based on their inlet and outlet temperatures ..... 102
Figure 4-28. $NO_x$ conversion efficiency for the combinations of catalysts based on their inlet and outlet temperatures ..... 104
Figure 4-29. $NO_2$ production/consumption in the combinations of catalysts based on their inlet and outlet temperatures ..... 105
Figure 4-30. NO conversion efficiency for the combinations of catalysts based on their inlet and outlet temperatures ..... 106
Figure 4-31. Catalyst inlet and outlet temperature profile measured and modelled during the experiment for the configurations studied ..... 108
Figure 4-32. Vehicle speed during the Paris cycle ..... 110
Figure 4-33. Temperature profiles for the catalysts configurations during the Paris cycle ... 111
Figure 4-34. Vehicle speed during the urban part of the NEDC ..... 112
Figure 4-35. Catalyst temperature profiles during the urban parts of the NEDC with a Stop/Start strategy ..... 113

Figure 5-1. Typical CO light-off curves at 30 000/h with 12% oxygen under diesel and dual-fuel combustion exhaust gases with the use of EGR ..... 116
Figure 5-2. Variations in the catalyst inlet exhaust gas concentration during the 8 hour experiment ..... 118
Figure 5-3. Engine exhaust gas compositions from the combustion of alternative fuels and exhaust hydrocarbon species concentrations from the engine operation on dual-fuelling .... 120
Figure 5-4. CO light-off curves for the different exhaust gas compositions ..... 122
Figure 5-5. Light-off curves for light alkene and alkane hydrocarbons for the dual-fuel combustion modes ..... 123
Figure 5-6. Effect of the different exhaust gas compositions on the required catalyst inlet temperature to reach 10%, 50% and 100% CO conversion efficiency ..... 125
Figure 5-7. Medium-heavy hydrocarbon light-off curves for the different exhaust gas compositions ..... 126
Figure 5-8. Mechanisms affecting CO oxidation (light-off curve and state of the catalyst surface) ..... 127
Figure 5-9. NO and $NO_2$ catalyst outlet concentration during the temperature ramp for the different exhaust gas compositions ..... 130
Figure 5-10. Catalyst inlet temperature required to reach 50% CO oxidation and for medium-heavy hydrocarbon oxidation to start, for the different exhaust gas compositions ..... 131
Figure 5-11. Hydrocarbon speciation and distribution for diesel exhaust gas ..... 134
Figure 5-12. Hydrocarbon speciation and distribution for dual-fuel combustion exhaust gas and comparison with diesel hydrocarbon concentration ..... 134
Figure 5-13. Simulation of the exhaust composition, DOC temperature and conversion efficiency of a diesel engine over an NEDC ..... 137
Figure 5-14. Concentrations at the catalyst inlet for the single diesel fuel combustion and dual-fuel combustion with propane, both using EGR strategy ..... 139
Figure 5-15. Concentrations at the catalyst inlet of individual hydrocarbon species for single diesel fuel combustion and dual-fuel combustion with propane, both using EGR strategy .. 139
Figure 5-16. Effect of oxygen exhaust concentration on CO conversion efficiency at 100°C and 30 000/h space velocity ..... 140
Figure 5-17. Effect of oxygen exhaust concentration on CO conversion efficiency at 120°C and 30 000/h space velocity ..... 141
Figure 5-18. Effect of oxygen exhaust concentration and space velocity on CO conversion efficiency at 135°C ..... 142

Figure 5-19. Effect of oxygen exhaust concentration and space velocity on CO conversion efficiency at 150°C ..... 143
Figure 5-20. Summary of the effect of oxygen exhaust concentration on CO conversion efficiency in the DOC, at 30 000/h space velocity ..... 144
Figure 5-21. Effect of oxygen exhaust concentration on CO, propylene and ethylene conversion efficiency at 40 000/h space velocity ..... 145
Figure 5-22. Effect of EGR on the exhaust gas concentration at the catalyst inlet and outlet ..... 148
Figure 5-23. Effect of EGR on the engine-out particulate profile and concentration..... 149
Figure 5-24. Effect of the duration of the test on the conversion efficiency over the DOC for NO, $NO_2$, CO and HCs ..... 150
Figure 5-25. Effect of the duration of the test on NO and $NO_2$ catalyst outlet concentrations ..... 150
Figure 5-26. Effect of the duration of the test on the particulate removal over the DOC ..... 152
Figure 5-27. Evolution of the particulate geometric mean diameter at the catalyst inlet and outlet, over the duration of the experiment ..... 153
Figure 5-28. Effect of the duration of the test on the DOC filtration efficiency in terms of particulate size ..... 154
Figure 5-29. DOC front face before the experiment and once removed from the exhaust system after the 8 hour test ..... 155
Figure 6-1. Engine-out PM profile and mass and number weighting over the particulate diameter for the idle engine condition ..... 158
Figure 6-2. PM-Metalit filtration efficiency for different PM profiles at 34 000/h space velocity..... 161
Figure 6-3. PM-Metalit filtration efficiency for different PM profiles at 48 000/h space velocity..... 162
Figure 6-4. PM number and mass filtration efficiency over the PM-Metalit for the different space velocities and PM profiles..... 162
Figure 6-5. PM-Metalit filtration efficiency at comparable PM profiles for two different space velocities ..... 163
Figure 6-6. PM-Metalit filtration efficiency at comparable PM profiles for two different space velocities ..... 164
Figure 6-7. Effect of the space velocity on PM number and mass filtration efficiency over the PM-Metalit for comparable PM profiles..... 165

Figure 6-8. POC filtration efficiency for different PM profiles at 28 000/h space velocity..166
Figure 6-9. POC filtration efficiency for different PM profiles at 40 000/h space velocity..166
Figure 6-10. PM number and mass filtration efficiency over the POC for the different space velocities and PM profiles .....167
Figure 6-11. POC filtration efficiency at comparable PM profiles for two different space velocities .....168
Figure 6-12. POC filtration efficiency at comparable PM profiles for two different space velocities .....168
Figure 6-13. Effect of the space velocity on PM number and mass filtration efficiency over the POC for comparable PM profiles.....169
Figure 6-14. LS filtration efficiency for different PM profiles at 25 000/h space velocity...170
Figure 6-15. LS filtration efficiency for different PM profiles at 44 000/h space velocity...171
Figure 6-16. PM number and mass filtration efficiency over the LS catalyst for the various space velocities and PM profiles.....172
Figure 6-17. LS filtration efficiency at comparable PM profiles for three different space velocities .....173
Figure 6-18. Effect of the space velocity on PM number and mass filtration efficiency over the LS catalyst for comparable PM profiles .....173
Figure 6-19. DOC filtration efficiency for different PM profiles at 28 000/h space velocity174
Figure 6-20. DOC filtration efficiency for different PM profiles at 40 000/h space velocity175
Figure 6-21. PM number and mass filtration efficiency over the DOC catalyst for the various space velocities and PM profiles.....175
Figure 6-22. DOC filtration efficiency at comparable PM profiles for three different space velocities .....176
Figure 6-23. Effect of the space velocity on PM number and mass filtration efficiency over the DOC catalyst for comparable PM profiles.....177
Figure 6-24. PM filtration efficiency per particulate size and in terms of mass and number for comparable engine-out particulate profiles at 25 000/h space velocity.....178
Figure 6-25. PM filtration efficiency per particulate size and in terms of mass and number for comparable engine-out particulate profiles at 28 000/h space velocity.....179
Figure 6-26. PM filtration efficiency per particulate size and in terms of mass and number for comparable engine-out particulate profiles at 40 000/h space velocity.....180
Figure 6-27. PM filtration efficiency per particulate size and in terms of mass and number for comparable engine-out particulate profiles at 44 000/h space velocity.....181

Figure 6-28. PM removal over the different components at idle conditions, in terms of filtration per diameter and PM number and mass filtration ..... 183
Figure 6-29. CO conversion efficiency at various engine operating conditions for the three catalysts (POC, LS catalyst and DOC) ..... 184
Figure 6-30. Heavy hydrocarbons conversion efficiency at various engine operating conditions for the three catalysts (POC, LS catalyst and DOC) ..... 185
Figure 6-31. $NO_2$ concentration at the outlet of the three catalysts (POC, LS and DOC) at various engine conditions ..... 186
Figure 6-32. PM number and mass filtration efficiency of the PM-Metalit based on particulate diameters at different soot loadings ..... 188
Figure 6-33. PM number and mass filtration efficiency of the POC based on particulate diameters for different soot loadings ..... 188
Figure 6-34. PM number and mass filtration efficiency and filtration efficiency based on particulate diameters during the loading period for the LS catalyst ..... 189
Figure 6-35. PM number and mass filtration efficiency and filtration efficiency based on particulate diameters during the loading period for the conventional DOC ..... 189
Figure 6-36. Effect of the duration of the experiment on the catalyst outlet exhaust gas concentration (NO, $NO_2$, CO and HC). ..... 191
Figure 6-37. Inlet and outlet exhaust gas emissions for the engines conditions selected to study the passive regeneration of the PM-Metalit ..... 193
Figure 6-38. The influence of $NO_2$ concentration on the other exhaust gas emissions at the PM-Metalit outlet, at 420°C ..... 194
Figure 6-39. Effect of the regeneration on the PM number and mass filtration efficiency and filtration per particulate diameter for the PM-Metalit ..... 195
Figure 6-40. Exhaust gas concentration during the regeneration process, at 360°C ..... 196
Figure 6-41. Effect of the regeneration on the PM number and mass filtration efficiency and filtration per particulate diameter for the POC ..... 196
Figure 6-42. Temperature reduction over the different components for various engine operating conditions ..... 197
Figure 6-43. PM size distribution in the engine-out and at the outlet of the LS catalyst, conventional DOC, POC, PM-Metalit and DPF ..... 199
Figure 6-44. Effect of the removal of the particulate volatile fraction on the POC and PM-Metalit number and mass filtration efficiency, at idle, with thermodenuder (particulate solid fraction only) and without the thermodenuder (solid + volatile) ..... 201

Figure 6-45. Particulate matter characteristics after the POC: (a) morphology, (b) micro-structure and (c) microstructural parameters .....203
Figure 6-46. Weight derivative of the soot collected upstream and downstream of the PM-Metalit and the POC.....204
Figure 6-47. PM number and mass filtration for the DPF, PM-Metalit+DPF and POC+DPF configurations .....206
Figure 6-48. PM filtration efficiency based on the particulate diameter for the DPF, PM-Metalit and POC of the configurations studied.....207
Figure 6-49. PM filtration efficiency based on the particulate diameter for the DPF, PM-Metalit+DPF and POC+DPF configurations .....208
Figure 6-50. Pressure increase across the DPF during the loading period .....209
Figure A-1. Vehicle speed against time during an NEDC.....219
Figure A-2. Vehicle speed against time during the FTP-75 .....220
Figure A-3. Vehicle speed against time for the Japan 10-15 cycle and JC08 cycle.....221
Figure A-4. Vehicle speed against time for the WLTP .....222

# LIST OF TABLES

Table 1-1. Health and environmental effects of the main components of diesel exhaust gas ...4
Table 3-1. Engine characteristics ....42
Table 3-2. Properties of the liquid fuels ....44
Table 3-3. Properties of the gaseous propane ....45
Table 3-4. Oxidation catalysts and filters used in the experiments ....49
Table 3-5. Properties of the PM-Metalit ....50
Table 3-6. Properties of the POC fleece ....50
Table 4-1. Catalysts combinations used in the experimental study ....60
Table 4-2. Mass and thermal capacity of the catalysts configurations studied ....61
Table 4-3. Space velocity in the catalysts combinations for the selected engine operating conditions ....62
Table 4-4. Areas representing the improved properties compared to the 400/4 substrate for different "cell density/wall thickness" configurations ....73
Table 4-5. Chosen substrates with their improved or deteriorated properties compared to the reference 400/4 substrate, based on the theoretical equations results ....74
Table 4-6. Summary of the conversion gain/loss and average backpressure increase over the NEDC for the alternative catalysts substrates compared to the reference 400/4 substrate ....79
Table 4-7. Summary of the conversion gain/loss and average backpressure increase over the NEDC for the two-catalyst configurations with a 5 mm gap compared to the reference 400/4 substrate ....88
Table 4-8. Pressure increase calculated for the Axisuite model ....109

# LIST OF EQUATIONS

Equation 1. Light-off factor ..... 63
Equation 2. Heat transfer factor ..... 63
Equation 3. Conversion efficiency factor ..... 64
Equation 4. Mass transfer factor ..... 64
Equation 5. Pressure losses ..... 64
Equation 6. Pressure loss equation simplified with assumptions ..... 65
Equation 7. 2D Iso-static strength ..... 65
Equation 8. Estimated tensile strength of the wall ..... 65
Equation 9. Average shear stress ..... 65
Equation 10. Open frontal area equation, function of the cell density and wall thickness ..... 66
Equation 11. Geometric surface area, function of the cell density and wall thickness ..... 67
Equation 12. Hydraulic diameter, function of the cell density and wall thickness ..... 67
Equation 13. Light-off factor (simplified equation) ..... 67
Equation 14. Conversion efficiency factor (simplified equation) ..... 67
Equation 15. Pressure losses (simplified equation) ..... 67
Equation 16. 2D-iso static strength (simplified equation) ..... 67
Equation 17. Average shear stress (simplified equation) ..... 67

# NOTATION LIST

| Symbol | Units | |
|---|---|---|
| A | $m^2$ | Cross sectional area |
| CEF | $/m^3$ | Conversion efficiency factor |
| d | nm | Particulate diameter |
| $D_h$ | m | Hydraulic diameter |
| $\Delta P$ | Pa | Pressure losses |
| $\Delta P'$ | Pa | Pressure losses simplified with assumptions |
| f | | Friction factor |
| GSA | $m^2/m^3$ | Geometric surface area |
| H | $m/m^3$ | Heat transfer factor |
| L | m | Cell pitch |
| $\lambda$ | m | Channel length |
| LOF | °C/J | Light-off factor |
| M | $m/m^3$ | Mass transfer factor |
| M* | $J/°C/m^3$ | Substrate thermal mass |
| $\mu_g$ | Pa.s | Dynamic viscosity |
| Nu | | Nusselt number |
| OFA | | Open frontal area |
| P | | Fractional substrate wall porosity |
| Q | $m^3/s$ | Volumetric flow rate |
| Re | | Reynolds number |
| Sh | | Sherwood number |
| $\sigma_o$ | MPa | Tensile strength of non-porous cordierite |
| $\sigma_{2D\text{-}iso}$ | MPa | 2D Iso-static strength |
| $\sigma_w$ | MPa | Estimated tensile strength of the wall |
| t | m | Wall thickness |
| $\tau_{AV}$ | MPa | Average shear stress |

# LIST OF ABBREVIATIONS

| | |
|---|---|
| Ag | Silver |
| $Al_2O_3$ | Alumina |
| $CH_4$ | Methane |
| $C_2H_2$ | Acetylene |
| $C_2H_4$ | Ethylene |
| $C_2H_6$ | Ethane |
| $C_3H_6$ | Propylene |
| $C_3H_8$ | Propane |
| CCC | Close-couple catalyst |
| $CeO_2$ | Cerium dioxide |
| $CH_2O$ | Formaldehyde |
| Co | Cobalt |
| CO | Carbon monoxide |
| $CO_2$ | Carbon dioxide |
| CPC | Condensation particle counter |
| Cpsi | Cell per $in^2$ |
| Cu | Copper |
| DMA | Differential mobility analyser |
| DOC | Diesel oxidation catalyst |
| DPF | Diesel particulate filter |
| EAMA | European automobile manufacturers association |
| EGR | Exhaust gas recirculation |
| EPA | Environmental Protection Agency |
| EUDC | Extra-urban driving cycle |
| Fe | Iron |
| FTIR | Fourier transform infrared |
| FTP | Federal test procedure |
| GHSV | Gas hourly space velocity |
| GTL | Gas-to-liquid |
| $H_2O$ | Water |
| HC | Hydrocarbon |
| HGV | Heavy-goods vehicle |
| $HO_2$ | Hydroperoxyl |
| HWFET | Highway fuel economy test |
| IARC | International Agency for Research on Cancer |
| IC | Internal combustion |
| Ir | Iridium |
| Mil | Milli-inch |
| $N_2O$ | Nitrous oxide |
| NEDC | New European driving cycle |
| $NH_3$ | Ammonia |
| Ni | Nickel |
| NO | Nitrogen oxide |
| $NO_2$ | Nitrogen dioxide |
| $NO_x$ | Nitrogen oxides |
| Nu | Nusselt number |
| Pd | Palladium |
| PEMS | Portable emission measurement systems |
| PFF | Partial-flow filter |
| PGM | Precious metal group |
| PM | Particulate matter |
| POC | Particle oxidation catalyst |
| Pt | Platinum |
| Rh | Rhodium |
| RME | Rapeseed methyl ester |
| Ru | Ruthenium |

| | |
|---|---|
| SCR | Selective catalytic reduction |
| $SiO_2$ | Silicon dioxide |
| SOF | Soluble organic fraction |
| SV | Space velocity |
| THC | Total hydrocarbons |
| $TiO_2$ | Titanium dioxide |
| UFC | Under-floor catalyst |
| ULSD | Ultra-low sulphur diesel |
| WLTP | Worldwide harmonized light-duty vehicle test procedure |

# 1. INTRODUCTION

## 1.1. BACKGROUND: DIESEL ENGINE AND EMISSIONS

### 1.1.1. Diesel Engines

Diesel engines now represent on average over 50% of the new car registrations (passenger and commercial vehicles) for 15 countries of the European Union (Figure 1-1), based on the data from the European Automobile Manufacturer's Association (EAMA, 2013), and its share of the world market is still increasing, according to a press release from Bosch Mobility Solutions (2013). This is mainly due to the lower fuel consumption and higher robustness of the diesel engines, as well as the introduction of new advanced technologies that improve the engine performance and emissions.

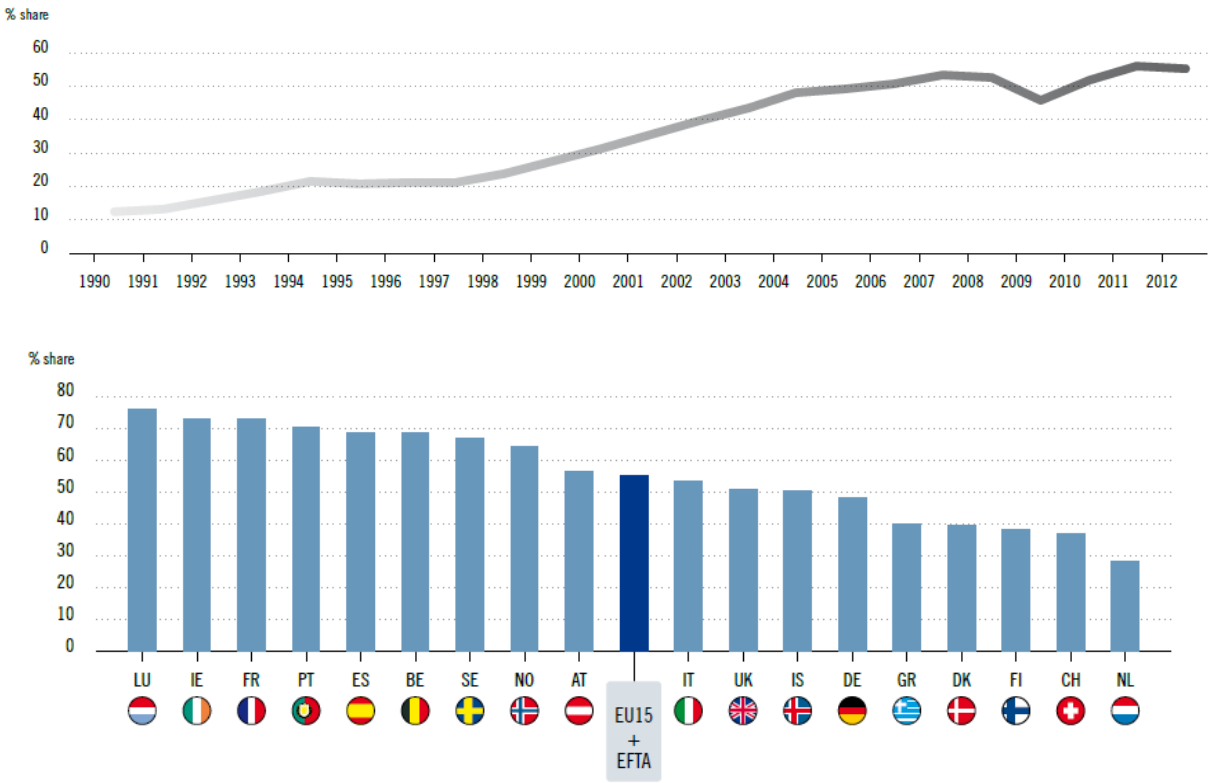


**Figure 1-1.** Average diesel penetration in 15 countries of Europe (top graph) and by country (bottom graph) in percent of share of new cars registered

With this increase in the number of diesel vehicles on the roads comes the question of the effect of their exhaust emissions on human health and the environment and how to efficiently reduce these emissions.

### 1.1.2. Exhaust Emissions Formation and Effect on Human Health and the Environment

In 2012, the International Agency for Research on Cancer (IARC) changed the classification of diesel engine exhaust gas from *possibly carcinogenic to human* (Group 2A) in 1988 to *carcinogenic to human* (Group 1). The products of the incomplete combustion in a diesel engine are released as exhaust gases, composed of gaseous and solid components, that can affect to a significant extent the environment and is toxic to the human beings exposed to them.

Carbon monoxide (CO) and total hydrocarbons (THCs) are the products of incomplete combustion due to a local lack of oxygen (under mixing) or excessive oxygen (over mixing) in the combustion chamber. THCs can also be the product of the fuel spray impacting and condensing on cold cylinder walls or the flame quenching, resulting in unburned fuel. These events can especially happen during cold starts and at low loads when the engine temperature remains limited. Moreover, at cold start, more fuel can be injected to compensate for these losses in spraying and wall wetting. These higher fuel-air ratios and localised rich conditions can also increase engine-out CO and THC emissions.

Other gaseous pollutants present in the diesel exhaust gas are the nitrogen oxides ($NO_x$), composed in majority of nitrogen oxide (NO) but also nitrogen dioxide ($NO_2$) and nitrous oxide ($N_2O$). NO is formed mostly from the reaction of the oxygen and nitrogen composing the intake charge air through various reactions such as the one defined by Zeldovich (1946). It can also be formed from nitrogen-containing compounds in the fuel but this reaction

accounts for a smaller portion of NO. The formation of NO is governed by some combustion properties such as high flame temperature, local oxygen concentration and residence time (flame speed). Sudden accelerations in the driving pattern could, for example, increase the quantity of NO produced. $NO_2$ is formed from the reaction of NO with oxygen. This reaction is especially promoted by hydroperoxyl ($HO_2$) from unburned fuel reacting with oxygen at low temperature (Hori *et al.*, 1992). $NO_2$ formation requires specific conditions to take place (low equivalence ratio, lower combustion temperature) that limit $NO_2$ reduction back to NO (Pipho *et al.*, 1991). $N_2O$, formed through the reaction of oxygen atoms with $N_2$ at sufficiently high pressure, accounts for only a small fraction of the total $NO_x$ concentration produced by a diesel engine.

Finally, diesel engines have been especially recognised for their production of significant quantities of particulate matter (PM). PM is composed of two phases: gaseous compounds (which include volatile hydrocarbons) and solid compounds (soot) formed of an agglomeration of primary particles. These primary particles are produced in the combustion chamber, in the fuel-rich zone of the spray core. Their production is especially promoted by incomplete combustion from low chamber temperature. Depending on the diameter (d) of the particulates, they are classified between nanoparticles ($d < 50$ nm), ultrafine particles ($d < 100$ nm), fine particles ($d < 2.5$ μm) and PM10 ($d < 10$μm).

It can be noticed that cold engine operating conditions and low loads are important factors that can increase the quantity of pollutants produced during the combustion event and released to the atmosphere through the vehicle exhaust system. Moreover, these operating conditions are the ones usually encountered in urban environment when low vehicle speed, stop/start, acceleration and idle phases are frequent (Windeatt *et al.*, 2012). It is also in these urban environments that humans are more exposed to vehicle exhaust gases and their detrimental effect on health (Table 1-1 and Figure 1-2).

**Table 1-1.** Health and environmental effects of the main components of diesel exhaust gas, adapted from Carel (1998), Hawley *et al.* (1998) and Sher (1998)

| Pollutant | Health Effect | Environmental Effect |
|---|---|---|
| **CO** | Affects oxygen supply to tissues and cells by reducing haemoglobin oxygen-carrying capacity when binding with it (higher affinity than oxygen). | |
| **THCs** | Promotes the formation of photochemical smog that can affect the respiratory system. | Reaction with ultraviolet radiation produces photochemical smog.<br>Greenhouse gas (methane). |
| **$NO_x$** | Promotes the formation of photochemical smog that can affect the respiratory system.<br>Irritation within the respiratory system. | Initiates photochemical smog.<br>Acid rain from the reaction with sulphur dioxide ($SO_2$) producing strong acid soluble in water.<br>Destroys ozone in stratosphere. |
| **PM** | Deposition in the respiratory system<br>Smaller particulates are especially considered dangerous (penetrate deeper, more easily embedded, higher surface area to carry potentially carcinogenic chemicals) (Figure 1-2). | Soot deposition on buildings.<br>Reduces atmospheric visibility.<br>Black carbon particles can contribute to global warming. |

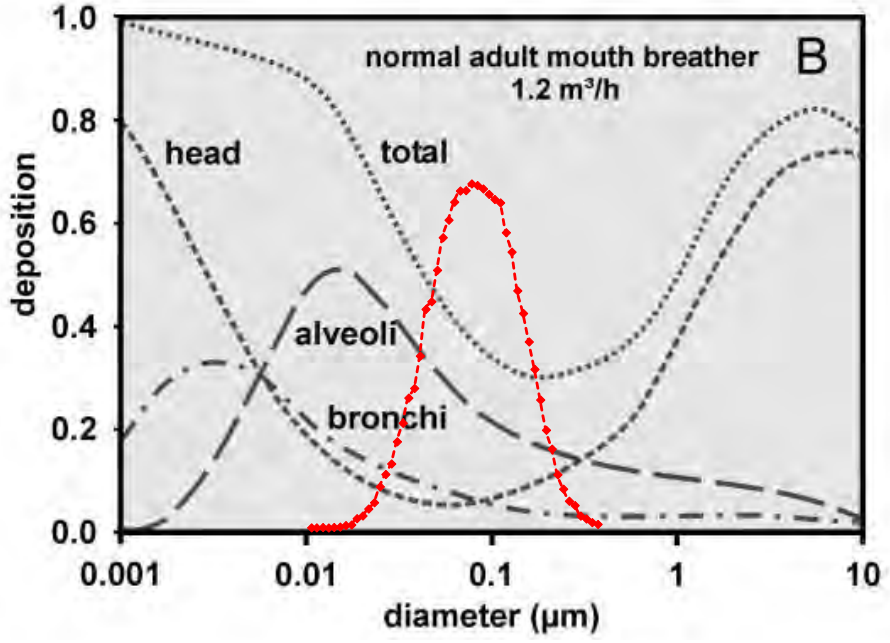


**Figure 1-2.** Relation between the particulate size and their deposition rate and location in the human body, fitted with a typical particulate size distribution from the engine used in this study (red), adapted from Geiser & Kreyling (2010)

To reduce these emissions and their effects on human health and the environment, the legal limits in the concentration of pollutants allowed to be emitted by a vehicle are continuously reducing worldwide (Delphi Emission Handbook, 2014). These limits impose the implementation of aftertreatment components in the exhaust system to promote the removal of pollutants before release to the atmosphere.

### 1.1.3. Pollutants Removal in Diesel Exhaust System

Since the submission of the first patent for a catalytic converter in 1956 by Houdry, exhaust aftertreatment components have been undergoing a dazzling evolution, promoted by ever tightening emission legislation. Figure 1-3 shows that before 1970, the interest in catalytic converters for automotive applications remained limited, based on the number of publications in the literature. It only started to increase from 1973, the date of the first

production catalytic converter, and was promoted by the new emission legislation in California in 1975 with the introduction of the FTP-75 (Federal Test Procedure) cycle. In the 1980s, efforts were taken to reduce the concentration of lead (used as an octane booster in gasoline) which poisoned the catalysts, enabling further aftertreatment development. The arrival of the first phase of emission legislation in Europe (Euro 1) and in the United States (Tier 1) in 1992 and 1994, respectively, greatly promoted the development of catalytic converters and from then, the number of publications on this subject has significantly increased.

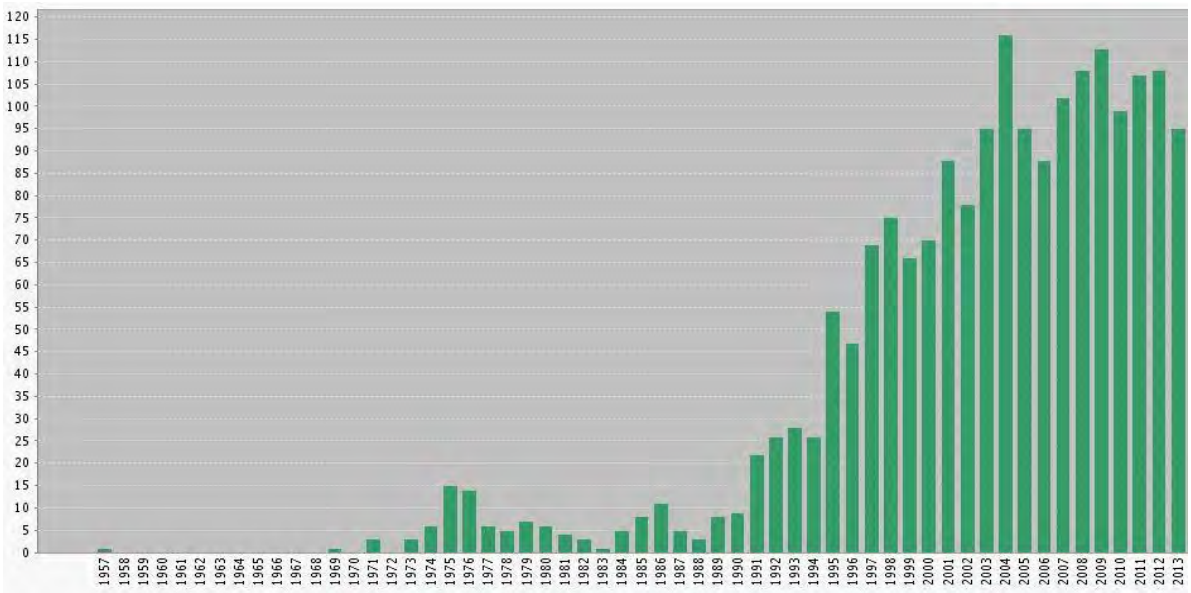


**Figure 1-3.** Yearly published items containing the term "catalytic converter" from 1957 to 2014, produced from Web of Science (2014)

The catalytic converter is composed of three main constituents: the substrate, the washcoat and the catalytic component (Heck *et al.*, 2009).

The substrate supports and provides a surface area for the coated material. The most commonly used substrate shape is the cylindrical honeycomb monolith, composed of channels running along the length of the component onto which the catalytic material can be coated. In the case of filter components used for the removal of particulates, the substrate can

be made of a more porous material, onto which the particulates can accumulate. In that case, the substrate is composed of alternatively plugged channels at the entrance and at the exit of the substrate that will force the exhaust gas to flow-through the walls in order to exit the component.

The washcoat is used to increase the surface area onto which the catalytic component is coated, while assuring the durability and thermal stability of the catalyst by limiting potential sintering. It can also promote the activity and selectivity of the catalyst by interacting with the coated catalytic material and assuring specific functions (oxygen carrier, hydrocarbon trap). The washcoat can be composed of one or more chemical components, such as aluminium oxide ($Al_2O_3$), titanium dioxide ($TiO_2$), silicon dioxide ($SiO_2$), cerium dioxide ($CeO_2$), zeolites, coated onto the walls of the substrate channels.

The catalytic component is responsible for reducing the temperature required for a reaction to take place. Different groups of materials can be found in automotive catalysts: precious metals (such as platinum (Pt), palladium (Pd), rhodium (Rh), iridium (Ir) and ruthenium (Ru)) or base metals (iron (Fe), cobalt (Co), nickel (Ni), silver (Ag) and copper (Cu)). The choice of catalytic components depends on the nature of the reaction that needs promoting (oxidation or reduction), as different catalytic converters are used for the removal of specific exhaust pollutants.

*Diesel Oxidation Catalyst (DOC)*

The DOC is used to oxidise hydrocarbons (HC) and CO. It can also promote the oxidation of NO to $NO_2$ to enhance soot oxidation at lower temperature in the downstream particulate filter (Schejbal *et al.*, 2010) or assist the selective catalytic reduction (SCR) of $NO_x$ in the SCR catalyst (Koebel *et al.*, 2002).

*$NO_x$ Selective Catalytic Reduction (SCR) Catalyst*

The reduction of $NO_x$ emissions can be particularly challenging in diesel exhaust gas, due to the high oxygen exhaust concentration. In current production vehicles, the reductant used for this reaction is injected urea, decomposing into ammonia ($NH_3$) upstream of the catalyst. Another source of reactant that has been studied, but yet not been considered as effective as ammonia, is hydrocarbons (Klingstedt *et al.*, 2004; Lindfors *et al.*, 2004; Zhang *et al.*, 2010; Traa *et al.*, 1999). As previously said, $NO_2$ can also assist in reducing $NO_x$ emissions through the fast-SCR reaction, a higher rate $NO_x$ reduction reaction requiring an equimolar quantity of $NO_2$ and NO to be supplied to the SCR catalyst.

*Diesel Particulate Filter (DPF)*

The DPF's purpose is to remove the particulate matter contained in diesel exhaust gas. During the trapping process, the accumulation of these particulates within the filter walls leads to an increase in exhaust backpressure which can affect the engine power output and fuel consumption. Therefore, a frequent regeneration of the filter is necessary, at temperatures over 600°C, to burn the accumulated particulates using the oxygen present in the exhaust gas and clean the filter. Typical diesel engine driving conditions do not allow the exhaust to reach this range of temperature and therefore the use of "active regeneration" events with specific injection strategies (post or late injections) are necessary to temporarily reach the required exhaust temperature. It is also possible to oxidise particulates at lower temperatures (from 250°C) in the presence of $NO_2$ (Schejbal *et al.*, 2010; Görsmann, 2005) but this "passive regeneration" is usually restricted by the limited concentration of $NO_2$ produced at the DOC outlet.

The use of catalytic converters as previously presented has now become mandatory to meet modern vehicle emission limits. Despite the presence of catalytic materials to reduce the temperature required for the removal of pollutants, the evolution of automotive technologies leads to continuously decreasing exhaust gas temperature which challenges the catalyst activity.

## 1.2. MOTIVATION: LOW EXHAUST TEMPERATURE CHALLENGE

### 1.2.1. Development of Engines with Increasing Efficiency

The growing concerns regarding greenhouse gas emissions such as carbon dioxide ($CO_2$), as well as customer attention to fuel consumption due to fluctuating fuel prices, promote the development of ever more efficient engines. The use of advanced fuel injection strategies together with optimised engine component design enable greater combustion efficiency which comes with a decrease in the exhaust gas temperature.

Moreover, since their first introduction on a production car in the late 1970s, turbochargers have been widely developed and implemented on diesel vehicles, to increase the engine power output by allowing more air into the combustion chamber (increasing the overall volumetric efficiency). The turbine in the exhaust system acts as a heat sink which can greatly reduce the exhaust gas temperature during warm-up, limiting the aftertreatment system efficiency. The effect of the turbocharger on the exhaust temperature is clearly evident in Figure 1-4. The location of the catalyst, either close-coupled (CCC, close to the exhaust manifold) or under-floor (UFC, further away in the exhaust line) also influences the temperature received by the component and the heat loss to the ambient.

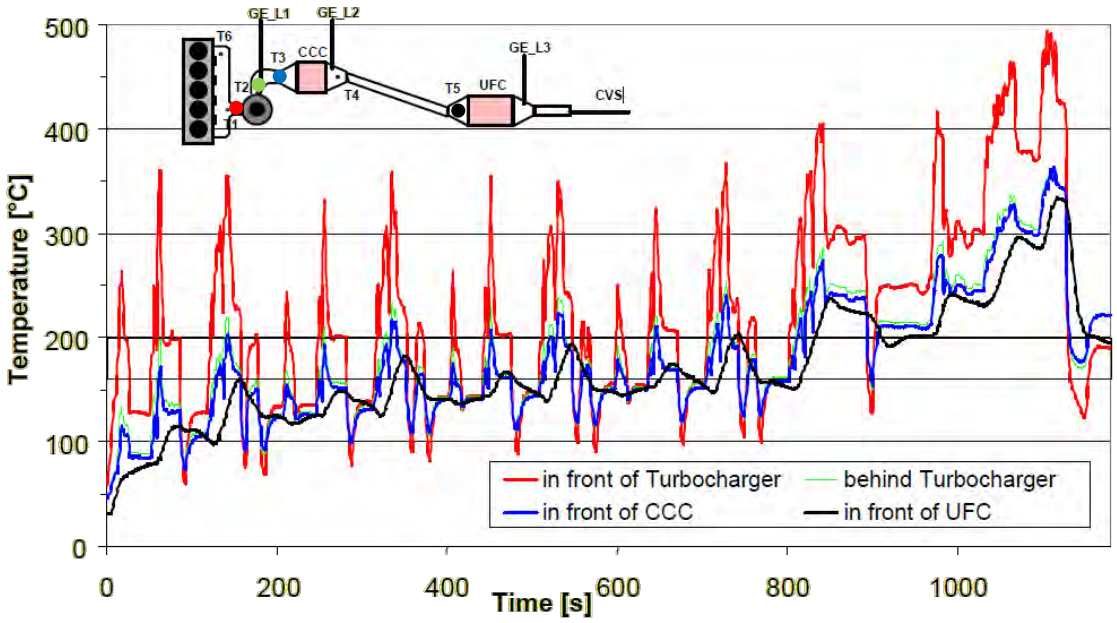


**Figure 1-4.** Exhaust temperature measured at different locations in the exhaust system of a Volvo S60 operating an EU III cycle (Diefke *et al.*, 2003)

Nowadays, turbochargers are widely used on diesel vehicles, especially with the new downsizing trend that allows a reduction of the engine size without sacrificing the output power. The use of additional technologies such as the exhaust gas recirculation (EGR) to reduce $NO_x$ engine-out emissions can affect the combustion process and lead to further reduction in exhaust gas temperature. The extent to which the temperature is reduced depends on the percentage of EGR used, the temperature of the re-circulated exhaust gas, the fuel injection strategies and the engine operating conditions (Agarwal *et al.*, 2004; Agarwal *et al.*, 2011; Saichaitanya *et al.*, 2013). The search for the reduction of the $NO_x$-PM trade-off also promotes the development of advanced low-temperature combustion modes that lead to an increase in CO and HC emissions (Imtenan *et al.*, 2014) while reducing the exhaust gas temperature.

### 1.2.2. Development of the Driving Pattern

The development of urban centres and the increase in the number of vehicles on the road tend to create ever more congested areas, shifting the driving pattern towards the increasing use of idle, stop/start and low load phases where the exhaust gas temperature remains limited (Windeatt *et al.*, 2012). Additionally, the current trend in legal drive cycles, designed to reproduce the local driving pattern (speed limit and driving conditions) to evaluate a vehicle emissions, is to emphasise on real-world driving conditions (Appendix 1). This especially includes cold starts, transient phases and urban driving conditions with idle and low load phases, which are more representative of the regular use of a vehicle (Färnlund & Engström, 2001).

It is particularly during these urban driving phases that the exhaust gas temperature is the lowest and therefore more likely to limit the catalyst efficiency in removing exhaust gas pollutants. Additionally, humans are directly in contact with exhaust gaseous and solid emissions in urban environments which explains a stronger focus on monitoring exhaust emissions during urban type driving conditions.

Figure 1-5 highlights that a greater concentration of CO (32% of the total emissions over the cycle) is produced during the first ECE-15 (urban driving cycle) of the NEDC, when the catalyst temperature is below the light-off temperature and the oxidation activity remains limited (Campbell & Martin, 1995; Ye *et al.*, 2011). THCs present a different spectrum as most of their emissions are produced in the second half of the cycle during accelerations and decelerations when the exhaust temperature undergoes sudden changes.

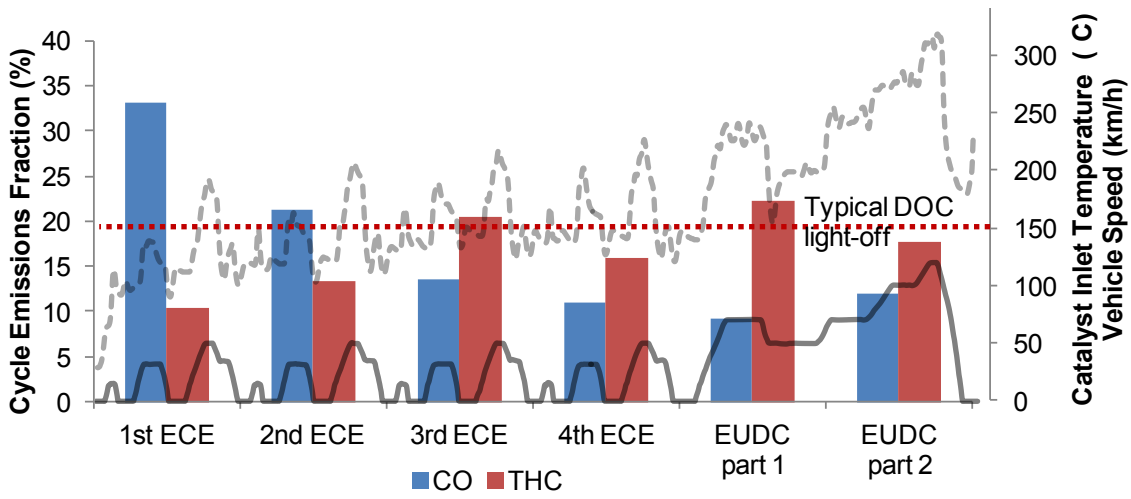


**Figure 1-5.** Fraction of CO and THCs emitted at the different stages of the NEDC, based on the emissions of an EU5 diesel engine

Figure 1-6 shows that during close to 50% of the NEDC, the exhaust gas temperature remains below 150°C, which typically represents the minimum temperature needed to achieve a certain degree of catalytic performance, depending on the catalyst physical and chemical properties.

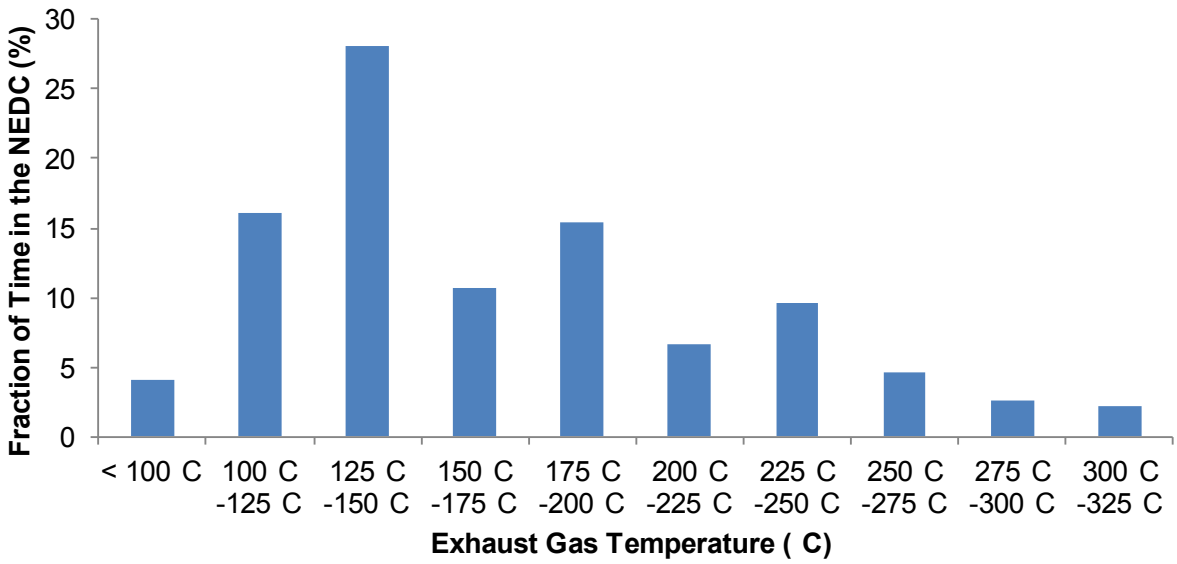


**Figure 1-6.** Percentage of time at temperature over the NEDC, based on an EU5 diesel engine

### 1.2.3. Effect of the Hybridisation of the Powertrain

Finally, the potential use of hybrid electric vehicles utilising multiple sources of power (electric motor/generator and internal combustion (IC) engine) can lead the thermal engine to operate on shorter but more transient periods. Depending on the degree of hybridisation and the energy management system, these relatively frequent intermittent operating phases could significantly affect the exhaust gas temperatures and catalyst activity. On the one hand, the possibility for hybrid vehicles to run the IC engine at its most efficient operating points as frequently as possible can attenuate these decreases in temperature and the production of pollutants. On the other hand, these intermittent operating conditions could lead the engine to cool down more often and when solicited again, produce the usual high emissions from cold operating conditions, leading to possibly multiple cold-starts during a journey (Koltsakis *et al.*, 2011). These developments require quick aftertreatment thermal response to promote catalyst warm-up and effectively deal with the vehicle emissions on the shortest time scale.

It becomes evident that efficient thermal management is necessary for the diesel aftertreatment system to widen its operating temperature window, especially by promoting the activity at lower temperatures, to cope with the decreasing average exhaust gas temperatures and ever tightening emission limits.

## 1.3. STRATEGIES TO IMPROVE THE LOW-TEMPERATURE CATALYST ACTIVITY

Two different strategies can be employed to develop thermally efficient aftertreatment components and promote an earlier start of the catalytic activity, without modifying the temperature of the exhaust gas exiting the combustion chamber (no changes in the engine calibration).

The first strategy is to enhance the catalyst conversion efficiency at a given temperature and especially allow its activity to start or reach greater conversion at lower temperatures (Figure 1-7). This can be achieved through optimisation of the catalyst chemical properties i.e. choice of washcoat and PGM formulation, loading and coating technology. It can also be promoted through the understanding of the interactions (inhibition or promotion) between exhaust species that can limit their catalytic oxidation.

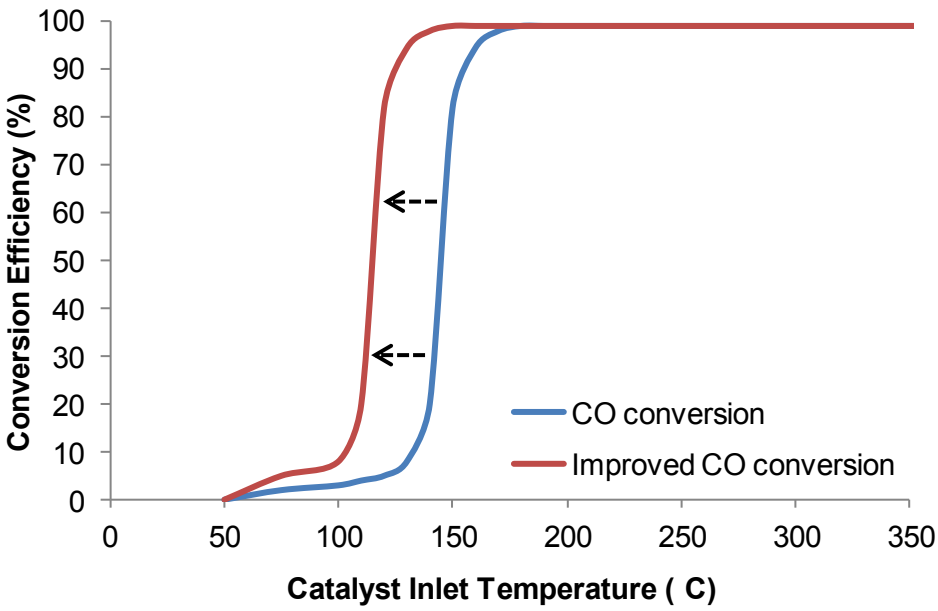


**Figure 1-7.** Example of catalyst improved light-off for CO conversion efficiency

The second strategy relies on promoting the activity through optimisation of the temperature reaching the catalyst (Figure 1-8). For a given temperature profile exiting the combustion chamber, greater temperatures can reach the catalytic sites by optimising the component location along the exhaust line or by reducing the thermal mass through catalyst design i.e. optimisation of its external (aspect ratio) and internal dimensions (cell density and wall thickness) as well as material choices.

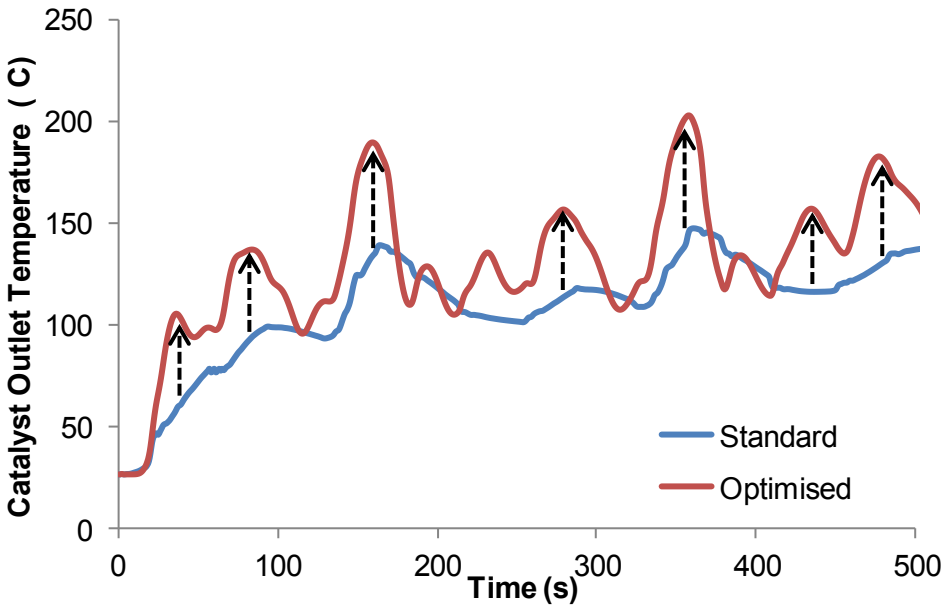


**Figure 1-8.** Example of in-situ catalyst improved temperature

The complexity of the problem is to find the balance between the promotion of low-temperature pollutants removal and the possible subsequent degradation in the engine fuel consumption and increased $CO_2$. The development of new strategies and designs needs also to consider the cost, quality, durability and package-related attributes, to provide practical implementation of the solutions proposed.

## 1.4. SCOPE, AIM AND OBJECTIVES

The aim of this thesis is to investigate and present some strategies that enhance the diesel aftertreatment catalytic activity at low temperature, to promote the removal of exhaust pollutants over a larger range of engine operating conditions.

While it is possible to widen the catalyst operating temperature window through the optimisation of a single specific parameter, the work presented in this thesis focuses on a more extensive approach, proposing various strategies related to the properties of the exhaust gas entering the catalyst and characteristics of the aftertreatment component itself which are the main factors affecting the catalyst activity. The focus is especially given on enhancing the catalytic activity for a given engine-out temperature, i.e. no engine calibration or advanced exhaust design were investigated to modify the temperature profile entering the catalyst.

In addition, the investigation concentrates on enhancing the thermal behaviour of the oxidation catalyst as it is usually the first component in the exhaust system line and therefore, its thermal management would affect the activity of the downstream components. It is considered that the design solutions and strategies presented here can be combined and reach wider applications as they can also be used for other aftertreatment components (e.g. SCR, lean $NO_x$ trap or DPF) and their combination of functions, as a means to enhance their low-temperature activity.

## 1.5. THESIS OUTLINE

The development of thermally efficient diesel exhaust aftertreatment, as presented in this thesis (Figure 1-9) required to consider some parameters external to the catalyst such as the exhaust gas properties, as well as parameters closely related to the catalyst (physical properties and combination of functions).

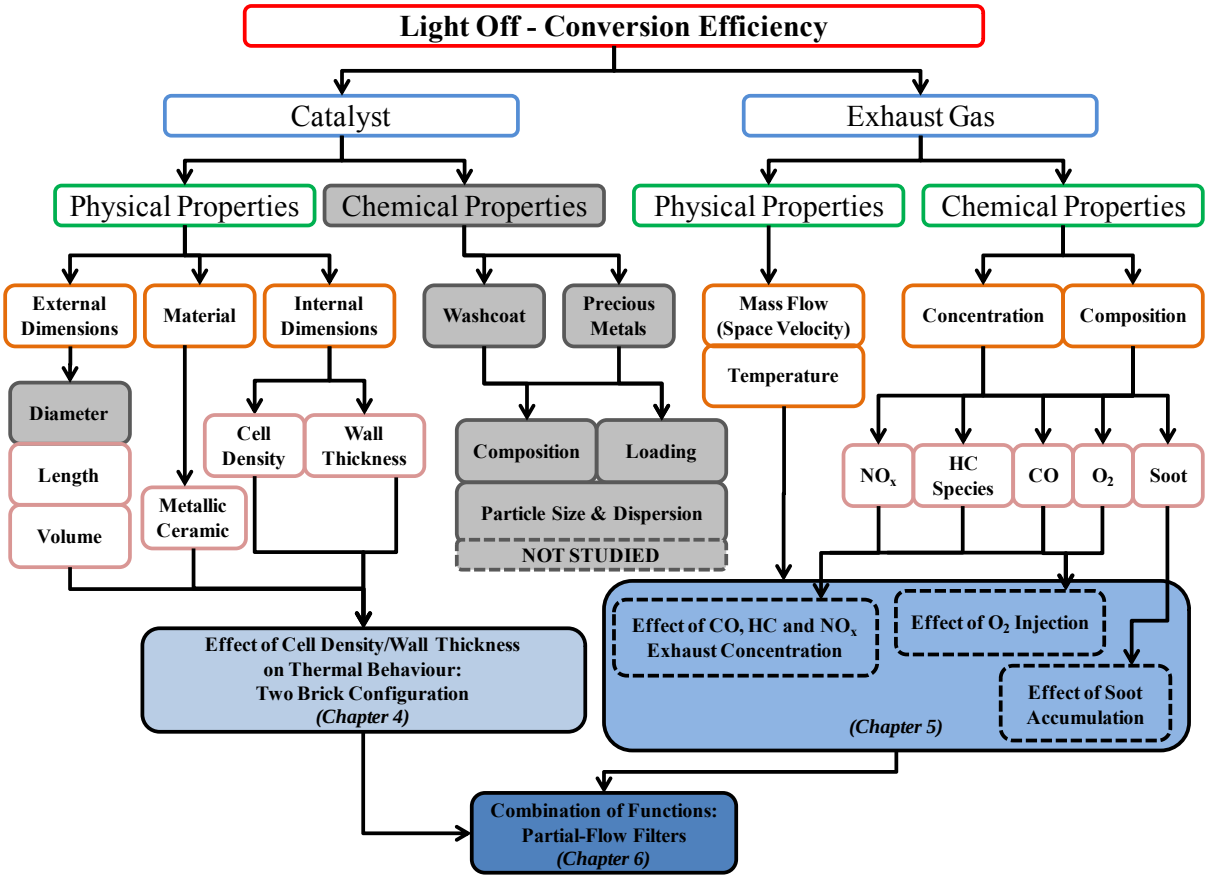


**Figure 1-9.** Schematic summarising the scope of the research work presented in this thesis (grey-shaded areas not developed in this work)

Chapter one introduces the background related to the diesel exhaust aftertreatment system and its thermal requirements, as well as the solutions proposed and directions of study presented in this work.

Chapter two provides the state of the art of the literature related to diesel exhaust aftertreatment thermal management and presents the past and current strategies studied and developed in the automotive industry to efficiently remove vehicle pollutants.

Chapter three presents the experimental set-up in terms of engine instrumentation, gaseous emission and particulate equipment analysers and aftertreatment components used in this study to produce the findings presented in the following chapters.

Chapter four focuses on improving the oxidation efficiency and thermal behaviour of a reference catalyst through the optimisation of the substrate internal dimensions (cell density and wall thickness) without modifying its external dimensions (diameter and length).

The first part of this study investigates the relationships between cell density/wall thickness and some parameters critical to the catalyst activity (light-off capacity, conversion efficiency, pressure losses and durability) using theoretical formulae developed in the literature. The outcomes of this study provide a selection of catalysts whose thermal behaviours are then simulated using the modelling software Axisuite, to allow further selection before engine experiments. The chosen combinations are then experimentally tested on an engine test bench to quantify the gains in terms of thermal behaviour and conversion efficiency with genuine diesel exhaust gas. While the cycle used in the experimental part contains engine conditions representing acceleration and decelerations phases, it does not reproduce everyday driving conditions due to its lack of transient phases and low load. Therefore, to complement the study, a model of the catalyst configurations was developed based on the results from the experimental tests, to evaluate their thermal behaviour for two

different simulated drive cycles under conditions that challenge the catalyst activity (Paris cycle and the urban part of the NEDC with stop/start strategy).

Chapter five examines the effects of the working environment on the catalyst activity, i.e. the exhaust gas composition (gaseous and solid). By understanding the interactions between exhaust gas species (promotion and inhibition), it is possible to optimise the mechanisms that enhance the low-temperature activity and limit the ones that inhibit it.

In the first part, the engine is operated with alternative fuels and combustion modes, to produce a variety of exhaust gases (CO, HC and $NO_x$) for which the catalyst oxidation activity is investigated. The correlations between the light-off curves and the exhaust compositions provide some understanding of exhaust species interactions in genuine exhaust gas and how they affect the catalyst activity. The findings help identifying specific exhaust gas compositions as well as catalyst design strategies which, combined together, can limit the inhibitions and promote the activity at low temperatures.

In the second part, oxygen exhaust content was varied to understand the effect of oxygen on triggering and promoting the oxidation activity, especially at low temperatures. The outcomes of this study provide guidelines into the conditions required, in terms of exhaust gas temperature and space velocity, to efficiently promote the catalytic activity through oxygen addition.

Finally, the third part of this chapter focuses on the effect of the solid portion of the exhaust gas on the catalyst activity, by investigating the possibility of soot accumulation on the face and channels of a high cell density catalyst and assessing the potential risk of soot plugging degrading the oxidation efficiency. This last section provides an insight into the limited particulate removal taking place within the oxidation catalyst, which could be improved using an alternative substrate design, as developed in the following chapter.

Chapter six presents the potential of using an oxidation catalyst that would also combine a filtration function to assist the DPF in removing particulates and allow a reduction in the duration/frequency of the active regeneration events. This would also take advantage of the close-coupled location of the oxidation catalyst, supplying warmer exhaust gas to promote a more frequent oxidation of the soot accumulated. Three different components are selected for this study: two partial-flow filters (PFF) and a flow-through catalyst with advanced channel design. Their filtration mechanisms and oxidation efficiencies, long-term activity and regenerative behaviour are investigated and compared with those of a conventional flow-through catalyst at different engine operating conditions, varying the exhaust gas temperatures, flow rates and particulate matter profiles.

The characteristics (size distribution, composition, microstructure and reactivity) of the particulates the PFF would supply to the downstream filter are also investigated. This is followed by an analysis of the synergy of a combined PFF+DPF system and its results in terms of filtration efficiency, DPF backpressure and soot loading, to estimate the benefit of such a system and the potential effects on DPF active regenerations.

Finally, chapter seven presents a summary of the findings and provides guidelines for future work to continue the development of thermally efficient diesel exhaust aftertreatment.

After having presented the challenges and requirements in terms of thermal management of the diesel exhaust aftertreatment, an overview of the state of the art in the research and development related to the subject is necessary to understand the trends and directions taken in this thesis.

# 2. LITERATURE REVIEW

The implementation of emissions regulations requires ever increasing catalyst efficiency over a wide operating temperature window (Snyder *et al.*, 1972; Barnes & Klimisch, 1973). This has been promoting the research and development of strategies to allow the catalyst to be active soon after engine start and maintain its activity over varied operating conditions. Nowadays, the tightening of the authorised emission levels and the evolution of the driving patterns and powertrain development lead to ever lower diesel exhaust gas temperatures, challenging the aftertreatment efficiency and therefore the removal of exhaust pollutants at specific conditions (cold start, idle and low loads). This stimulates development and research studies to find ways to promote the catalytic activity at lower temperature.

## 2.1. CATALYST DESIGN

Choices in the catalyst properties and its design can allow improvement in the low-temperature activity, by enhancing the catalyst warming capacity and reducing its light-off temperature. These can be promoted through two paths: modifications of the catalyst physical properties (substrate dimensions, structure and material choices) and/or its chemical properties (choices of washcoat, precious metal formulations, loading and coating techniques).

### 2.1.1. Catalyst Physical Properties

The dimensions (internal/external) and material of the substrate can greatly affect some of the catalyst properties, such as the conversion efficiency, its thermal behaviour and mechanical/thermal durability, as well as the creation of undesirable backpressure (flow restriction) that can lead to power loss and fuel penalty (Pannone & Mueller, 2001). Another

area for catalyst design optimisation can be through the modification of the cell density and wall thickness of the substrate.

#### *2.1.1.1. Substrate Internal Dimensions*

Different channel shapes exist for ceramic honeycomb substrate, such as square, hexagonal and triangular (Gulati, 2001; Gulati, 2005). Based on equations developed by Gulati (2001) and presented in section 4.2.1, it is possible to estimate and compare the effect of changing the cell shape on the catalysts warming capacity (light-off), the creation of backpressure and the mechanical durability of the component (Figure 2-1).

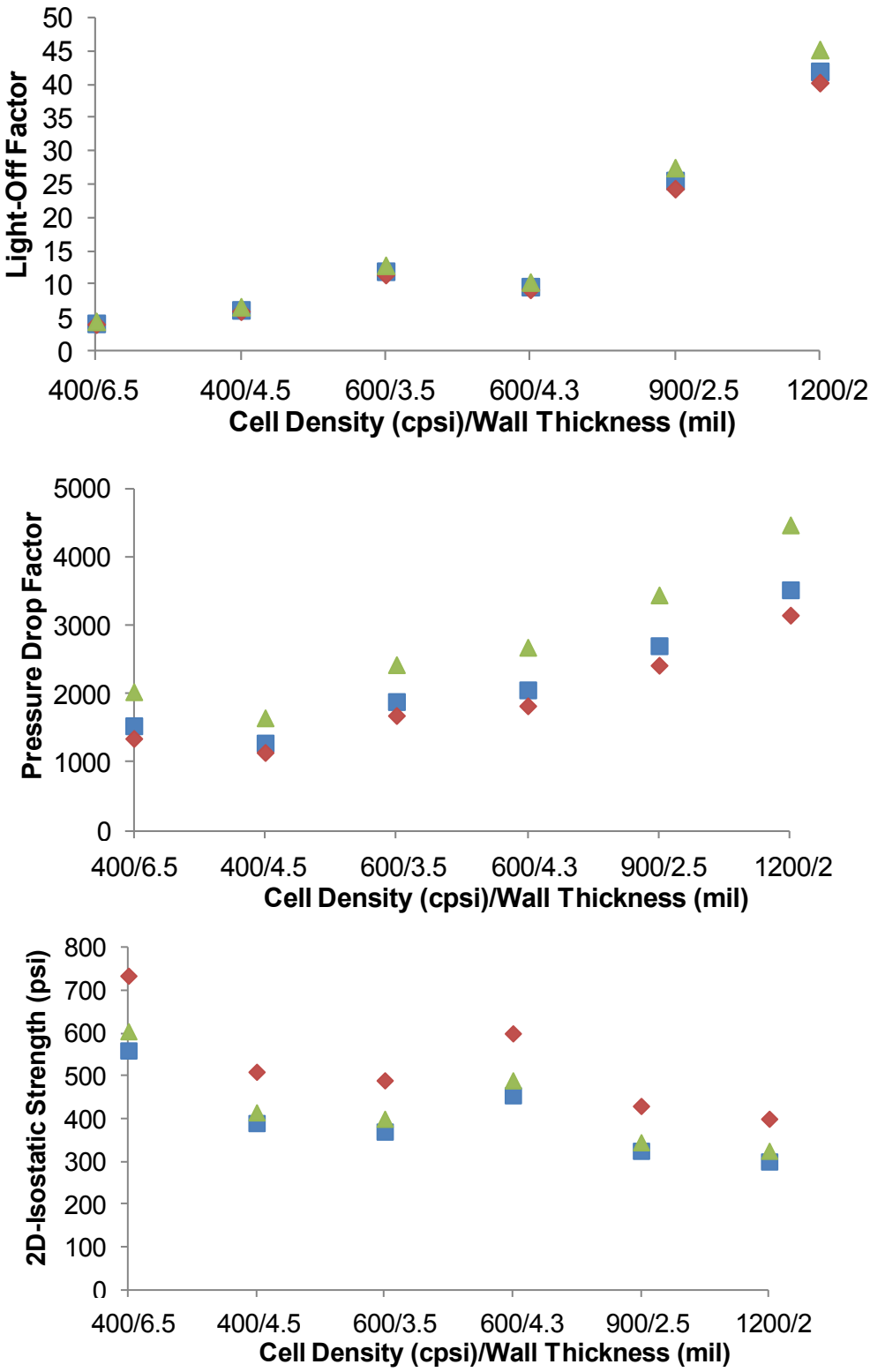


**Figure 2-1.** Estimation of the influence of the cell density/wall thickness and cell shape on the catalyst light-off factor (top graph), pressure drop (middle graph) and mechanical durability (bottom graph), the symbols representing the shape of the cell (square, triangular and hexagonal (diamond symbols))

The shape that shows the best compromise is the square channel (the hexagonal shape leading to a cost increase), which is the prevalent shape in exhaust aftertreatment systems, providing a great choice among the substrates available in production.

Another physical dimension that can influence the catalyst behaviour is its internal dimension, i.e. the cell density and the thickness of the walls between the channels (Umehara *et al.*, 2000; Hughes *et al.*, 2006). It is possible to increase the exhaust gas/catalyst contact area by increasing the cell density (Hughes & Flörchinger, 2002) and enhance the heat and mass transfer in the channels by reducing the cell hydraulic diameter (Marsh *et al.*, 2001). Moreover, thinner walls reduce the substrate thermal mass (Hughes & Flörchinger, 2002). High cell densities tend to increase the pressure created by friction losses along the channels, due to an increased surface of contact (Ichikawa *et al.*, 1999; Schmidt *et al.*, 1999), while thin walls allow a greater open frontal area, reducing the pressure losses from the contraction at the entrance of the catalyst. Finally, thin walls and high cell densities can also affect the durability required to withstand mechanical stresses during the canning process and throughout the lifetime of the catalyst (Chen *et al.*, 2003) as well as the thermal strains imposed by the environment (Li *et al.*, 2012). Some trade-offs exist between conversion efficiency, pressure increase, light-off and mechanical durability from modifying the cell density and wall thickness of the substrate. Therefore, the idea of combining two substrates with different cell density and wall thickness that can counteract each other drawbacks have been previously developed. One example of this technology is the “hybrid catalyst”, a combination of a thin foil metallic substrate that promotes a quick light-off followed by a thicker foil metallic substrate acting as a thermal mass, developed by Emitec (Reizig *et al.*, 2001; Hosogai *et al.*, 2003). The configuration presented put the emphasis on varying only the metallic foil thickness and the study essentially concentrates on the total oxidation efficiency during a driving cycle. The outcomes are relative to this specific application and

do not develop general understanding of the effect of varying the foil thickness or increasing the cell density on the thermal behaviour or oxidation activity during specific phases (warming or cooling). Additionally, the shares in terms of catalytic activity between the first and the second catalyst of the configuration are not presented in this work. The work developed in chapter four provides complementary information about the influence of different cell density/wall thickness combinations, as well as material choices, to design thermally optimised catalyst configurations.

#### *2.1.1.2. Substrate Material*

For a common cordierite catalyst, the mass of the substrate represents around 64% of the total mass of the component, the washcoat 35% and the catalytic material 1%. While these values vary from one catalyst to another, depending on the coating loading and substrate material, the bulk of the catalyst mass still lays in the substrate. Different materials and designs have been developed and tested in the search for improving the substrate properties (Jatkar, 1997; Koltsakis *et al.*, 2007; Sun *et al.*, 2008; Kalam *et al.*, 2009; Bach & Eggenschwiler, 2011; Hirose *et al.*, 2012), but two main materials have been proven to be reliable, i.e. ceramic cordierite and iron-chromium-aluminium (Fe-Cr-Al) metallic alloys, for their thermal properties and mechanical durability. Metallic substrates promote a higher and more homogeneous temperature distribution profile within the catalyst due to their enhanced thermal conductivity (Jasper *et al.*, 1991). They also allow the use of higher cell densities and thinner walls while maintaining a minimum mechanical strength and thermal durability (Brück *et al.*, 2001a; Mueller-Haas *et al.*, 2003). Some concerns have been raised about washcoat adhesion on the metallic substrate walls, due to the limited roughness of the non-porous surface and the differences in terms of thermal expansion between substrate and washcoat. Moreover, from a cost point of view, these substrates are on average more

expensive than their ceramic counterparts. Nevertheless, the interest in metallic substrates is still growing in passenger cars, especially for specific applications where the need for a low backpressure and improved conversion efficiency justifies the cost increase.

While the substrate physical properties can influence the catalyst behaviour, the choice of a suitable catalytic material is essential to promote the activity, especially at low temperature.

### 2.1.2. Catalyst Chemical Properties

The washcoat and catalytic materials are the cores of the activity of the aftertreatment component. The choices in materials, loading and physical/chemical states on the substrate walls are essential features affecting the catalyst activity. While the washcoat function is to increase the wall surface area and assure the thermal stability of the coated components, the catalytic material, usually of the platinum group metal (PGM) type, is the main parameter responsible for the catalytic activity (Yao, 1984; Meng *et al.*, 1997; Patterson *et al.*, 2000). The choice of catalytic material is governed not only by the cost and the requirements in terms of activity but also by its durability. The catalyst needs to maintain its activity despite the harsh operating environment, causing possible deactivation from thermal aging (sintering mechanisms) and species poisoning, limiting physical access to the catalytic material or reducing its activity (Andersson *et al.*, 2007; Winkler *et al.*, 2009; Li *et al.*, 2012; Wiebenga *et al.*, 2012).

While platinum has been the favoured catalyst choice in terms of low-temperature oxidation efficiency, its activity can be greatly reduced after thermal aging (Watanabe *et al.*, 2007; Kallinen *et al.*, 2009; Kim *et al.*, 2011). This promoted the development of catalytic coatings combining several PGMs, such as platinum with palladium. This combination was found to enhance the activity compared to the use of platinum only at conditions such as high CO and HC exhaust concentrations (Figure 2-2). This is thought be due to Pt/Pd interactions,

promoting the coexistence of active catalytic states on the washcoat (Skoglundh *et al.*, 1991; Morlang *et al.*, 2005; Pfeifer *et al.*, 2007). Moreover, the addition of palladium with platinum promotes a better resistance to thermal sintering, maintaining a greater oxidation activity over the catalyst lifetime (Pfeifer *et al.*, 2007; Kallinen *et al.*, 2009; Glover *et al.*, 2011; Kim *et al.*, 2011).

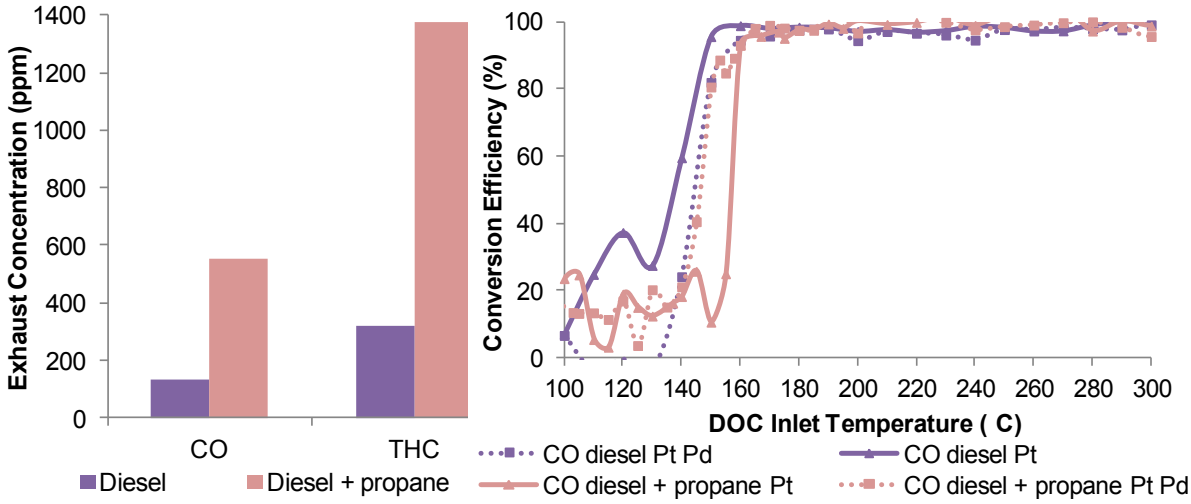


**Figure 2-2.** Effect of the addition of palladium in a platinum catalyst on CO conversion efficiency (right) at two different CO and HC exhaust gas concentrations (left)

Finally, the replacement of a portion of platinum by palladium also allows a cost reduction of the catalyst due to their differences in material prices (Figure 2-3).

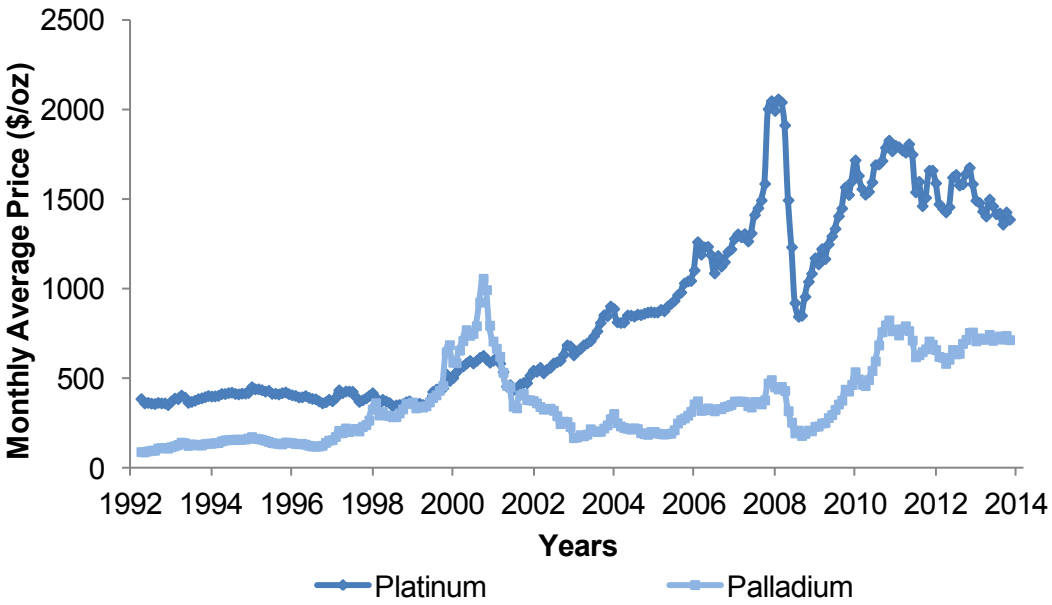


**Figure 2-3.** The cost of platinum and palladium from 1992 to 2014, adapted from Johnson Matthey (2014)

Another trend in catalytic coating research is the development of PGM-free or reduced PGM coating as a means of cost reduction and to limit the dependence towards the producing countries (Holroyd, 2006; Shigapov *et al.*, 2008; Southward *et al.*, 2010; Ishizaki *et al.*, 2012). However, these new catalytic formulations still require substantial development, and their activity and durability need further investigation before becoming as reliable as platinum group metals which are still the most used catalytic coating for the oxidation catalysts.

While extensive studies are still investigating the best catalytic choices for specific operating conditions, combining low-temperature activity, long-term durability and minimal cost, the research work presented in this thesis intentionally discarded this aspect as it would be a whole research study on its own. From the outcomes summarised in the previous paragraph, a platinum/palladium coating was chosen during this study as a good compromise in terms of activity, durability and cost. Some of the strategies and designs presented in this

work for improved low-temperature catalyst activity could be used to enable PGM loading reduction (cost saving).

As previously mentioned, the severe environment in which the catalyst has to operate can affect its performance. It is therefore necessary to investigate how the physical and chemical properties of the exhaust gas flowing through the catalyst can influence its activity.

## 2.2. INFLUENCE OF THE EXHAUST GAS COMPOSITION ON THE CATALYST ACTIVITY

### 2.2.1. Exhaust Gas Physical Properties

#### *2.2.1.1. Exhaust Gas Temperature*

First and foremost, out of the exhaust gas properties, the temperature is the primary parameter that affects the catalyst activity, as the active sites require heat to assure their catalytic functions. The temperature profile supplied to the catalyst can be influenced by engine calibration strategies through modification of the fuel injection and valve timing to increase the temperature of the exhaust gas exiting the combustion chamber (Lancefield *et al.*, 2000; Parks *et al.*, 2007; Honardar *et al.*, 2011). Electrically heated catalysts have also been developed to promote the catalyst warming-up process when the exhaust gas temperature remains limited (Pace & Presti, 2011). Another strategy is to reduce the heat losses between the exhaust manifold and the catalyst, through exhaust pipe design, choice of materials and insulation (Adamczyk *et al.*, 1999; Kandylas & Stamatelos, 1999; Korin *et al.* 1999; Kyu-Hyun *et al.*, 2000; Laurell *et al.*, 2013), or optimise the heat received by the catalyst itself through insulation and heat storage of the can housing the aftertreatment system (Burch & Biel, 1999; Korin *et al.*, 1999). The presence of other components under the car, as well as the space available can limit the possibilities for improvement in the design of the exhaust pipe. As for the piping and insulation materials, their choices are governed by

thermal and mechanical durability, as well as cost, which often greatly reduce the range of materials that can be considered. Finally, the aftertreatment location in the exhaust system, either close-coupled or under-floor can also affect the temperature of the exhaust gas entering the system (Saroglia *et al.*, 2002; Diefke *et al.*, 2003; Alkidas *et al.*, 2004; Carberry *et al.*, 2005; Konieczny *et al.*, 2008). The location of the aftertreatment system can be limited by many factors including bodywork, other powertrain and aftertreatment components, internal floor line and ground clearance. One approach to take advantage of a closely located component is to combine multiple functions within it, to allow maximum exploitation of the heat received without altering the space required for the system, as presented in 2.3.2.

In addition to the temperature, the exhaust gas flow rate can also affect the removal of exhaust pollutants by the aftertreatment system.

#### *2.2.1.2. Exhaust Gas Flow Rate*

The exhaust gas flow rate directly affects the residence time of the exhaust species within the catalyst, and therefore can limit their capacity to reach and interact with the coated walls (Voltz *et al.*, 1973; Mallamo *et al.*, 2013) limiting the catalyst conversion efficiency. The exhaust gas flow rate is related to the gas hourly space velocity (GHSV) or space velocity (SV), calculated as the ratio of the volumetric flow rate on the catalyst volume. This term defines the quantity of exhaust gas in terms of substrate (reactor) volume that can be treated in a unit of time, usually per hour. The higher the volume of exhaust gas treated, the lower the contact time between the active sites and exhaust species. The space velocity can be influenced by a change of flow rate (from the engine operating conditions) and/or by the catalyst volume. In this study, the space velocity was varied for certain tests in order to study the effectiveness of some strategies at different exhaust flow rates or for a reduced catalyst volume, as a means for space saving under the car.

Added to the physical properties, the exhaust gas chemical composition and concentration could also affect the catalyst activity.

### 2.2.2. Exhaust Gas Chemical Properties

#### *2.2.2.1. Oxygen Exhaust Concentration*

Among the various diesel exhaust gas species, oxygen is the main promoting parameter for CO and HC oxidation as an increase in its concentration enhances the reaction rate of the oxidation (Cant *et al.*, 1978; Yao, 1984; Berlowitz *et al.*, 1988; Royer & Duprez, 2011). Secondary air injections in the exhaust, upstream of the catalyst, coupled with other emission reduction strategies (lean A/F ratio, injection strategies) have already been investigated in gasoline engines, to reduce engine-out emissions and enhance the catalyst light-off performance (Lafyatis *et al.*, 1998; Son *et al.*, 1999; Sim *et al.*, 2001; Borland & Zhao, 2002). These strategies are justified by the lower oxygen content of gasoline exhaust gases compared to diesel ones, which could limit the oxidation reactions at low temperatures. However, the use of EGR strategy in diesel engines, for the reduction of $NO_x$ formation during the combustion process, decreases the quantity of oxygen available in the exhaust by replacing part of the intake charge air by inert exhaust gases (Ladommatos *et al.*, 1996). Additionally, some cold-start strategies require greater equivalence ratio to counteract the condensation of fuel at low temperatures, reducing the oxygen content in diesel exhaust gas during the warming-up phase of the engine (Hadavi *et al.*, 2013). Some studies have previously highlighted the interest of using an oxygen enriched intake air to improve diesel combustion and reduce some of the emissions produced in the combustion chamber (Lahiri *et al.*, 1997; Rakopoulos *et al.*, 2004; Nguyen *et al.*, 2011; Rajkumar & Govindarajan, 2011). Other studies investigated the injection of oxygen at the end of the combustion cycle to oxidise some of the soot formed in the chamber (Chanda *et al.*, 2000; Mather *et al.*, 2002;

Poola *et al.*, 2004). These studies concentrate on reducing the formation of exhaust pollutants at the source (combustion chamber) through the addition of oxygen but do not give an insight on the effect of oxygen addition on pollutants removal in the aftertreatment system. As part of investigating the effect of the exhaust gas composition on the catalyst activity, the role of oxygen addition upstream of the DOC to promote low-temperature oxidation was studied in section 5.3.

As well as oxygen, the presence and concentration of certain exhaust species can affect the oxidation activity, especially those that are targeted by the emission legislation, i.e. CO, HC and $NO_x$.

#### *2.2.2.2. Exhaust Pollutants Concentration and Composition*

The purpose of the DOC is to promote the oxidation of some exhaust species by contact with the catalytic sites coated on the channel walls. The fact that several species can react on the same active sites leads to possible interactions within the catalyst, eventually affecting the activity (promotion or inhibition), especially at low temperatures.

These interactions between exhaust species have been researched and modelled using synthetic mixtures of gases to represent engine exhaust gas in order to understand the kinetics and oxidation mechanisms within the catalyst (Voltz *et al.*, 1973; Yao, 1980; Yao, 1984; Mabilon *et al.*, 1995; Patterson *et al.*, 2000; Diehl *et al.*, 2010; Al-Harbi *et al.*, 2012). The majority of these studies focus on tracing the behaviour of an individual or a limited number of exhaust species in a synthetic gas mixture with a known and controlled composition. However, a specific exhaust species can have different oxidation behaviour depending on whether it is studied on its own or as part of a mixture (Patterson *et al.*, 2000). The number of studies using actual engine exhaust gas to examine the interactions between different species remains limited and focused upon exhaust gases from conventional fuel combustion (Katare

*et al.*, 2007; Knafl *et al.*, 2007; Lafossas *et al.*, 2011; Watling *et al.*, 2012). The use of genuine exhaust gas allows a valuable comparison with vehicle emissions met on the road and targeted by the emission legislation for air pollution. At an engine operating condition where the exhaust temperature is limited, pollutant removal could still take place, by encouraging promoting effects and limiting any inhibition of the DOC activity. This could be achieved with a better understanding of these species interactions on CO and HC oxidation to eventually support the design of the aftertreatment system (section 5.2.).

In addition to the gaseous exhaust compounds, the solid portion of the exhaust gas (soot) can also have an effect on the catalyst activity.

#### *2.2.2.3. Particulate Matter Accumulation*

The PM profile produced by diesel engines can show high concentrations and emissions of large particulates (Ntziachristos *et al.*, 2004; Schreiber *et al.*, 2007). Due to its location upstream of the particulate filter, the oxidation catalyst can directly suffer from the engine-out soot emissions that could accumulate on the front face and in the catalyst channels, and obstruct the access to the coated catalytic material, decreasing the catalyst efficiency and possibly increasing the backpressure. While this effect can be limited for low and medium cell density substrates, it can become problematic when high cell density substrates are used, due to a significant reduction in the cell hydraulic diameter. Figure 2-4 shows that the cell area of a substrate can be greatly reduced when increasing the cell density, while wall thickness reduction cannot effectively counteract this effect. Previous studies have highlighted cell plugging within three-way catalysts in gasoline exhaust system, due to manganese based additives in the fuel (Shimizu & Ohtaka, 2007) but fewer studies concentrate on the risk of face plugging and soot deposition on the walls of diesel oxidation catalysts. While the standard 400 cpsi catalyst used in diesel exhaust system offers a cell area

large enough to prevent soot accumulation, the tendency to use higher cell density substrates, such as 600 cpsi, to increase the conversion efficiency and warming capacity, could present a potential risk for cell plugging which needs to be assessed (section 5.4).

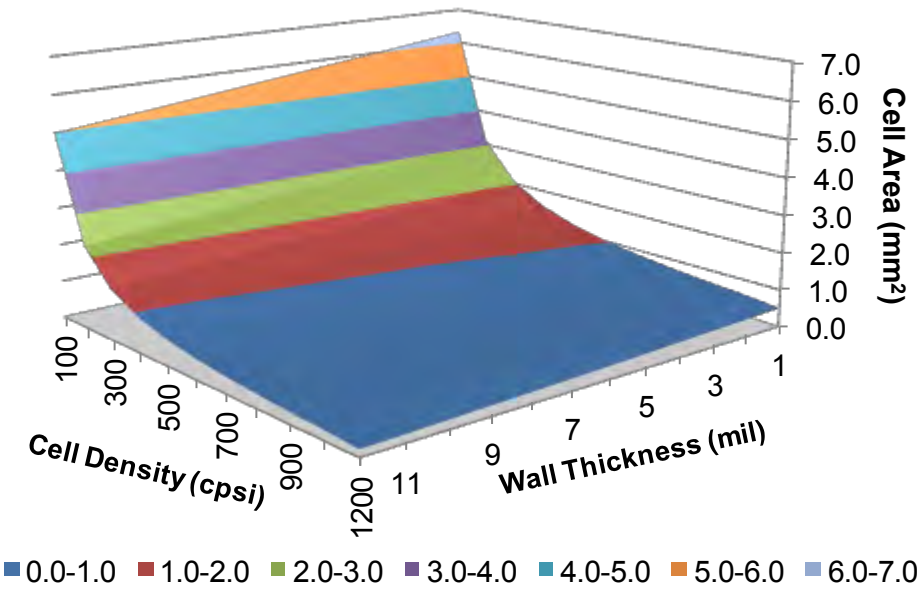


**Figure 2-4.** Cell area for various cell densities and wall thicknesses, based on the equations defined in Gulati (2001)

The study of the interactions between the catalyst and the exhaust gas particulates also points out the limited filtration behaviour of the DOC (Pataky *et al.*, 1994; Johnson & Kittelson, 1996). Therefore, as a matter of thermal management of the aftertreatment system, the focus is shifted towards improving the filtration function of the catalyst to assist the main DPF filtration and reduce the need for active regeneration events.

## 2.3. CATALYST DESIGN: COMBINATION OF FILTRATION AND OXIDATION FUNCTIONS

### 2.3.1. Thermal Management of the Aftertreatment System

Combining functions within one aftertreatment component permits a reduction in the number or dimensions of the components required in the exhaust line. This allows an optimisation of the use of the exhaust heat provided to the aftertreatment system, promotes space saving under the car, as well as a possible cost and backpressure reduction. Different combinations of functions have been studied and the currently most used one is the coated DPF, which oxidises CO, HC and NO while trapping particulates (Johansen *et al.*, 2007; Merlone Borla *et al.*, 2011). Other combinations of functions such as an SCR formulation coated on a filter (Ballinger *et al.*, 2009; Cavataio *et al.*, 2009) or $NO_x$ storage on DOC (Millo & Vezza, 2012) are also being developed. Some catalysts defined as four-way converters, combining oxidation, reduction and filtration functions have been developed in the past for diesel aftertreatment system (Page *et al.*, 1999; Millet *et al.*, 2009) but their efficiency seems to be limited by the necessity to operate at richer conditions to allow $NO_x$ reduction and by the effect of soot deposition on the coating efficiency. Moreover, the lower temperatures reached in diesel exhaust gas compared to gasoline reduce the reaction rates in the four-way catalyst which can promote interactions between active sites and exhaust/intermediate species produced, affecting the conversion efficiency. Another possibility to combine functions, especially for $NO_x$ reduction purposes, is through catalyst zoning (Sultana *et al.*, 2009; Theis *et al.*, 2011) and layer design (Onodera *et al.*, 2008; Liu *et al.*, 2013) where the different catalytic coatings are not mixed together but physically separated within the same component. While most of the combinations of functions concentrate on coating a wall-flow filter or improving the selective reduction of $NO_x$, fewer

studies have been investigating the combination of oxidation and filtration functions on a non wall-flow filter.

### 2.3.2. Benefits and Requirements of the Pre-Filter Component

The aim of combining oxidation and filtration functions within the oxidation catalyst is not to replace the main DPF but to assist it in its particulate removal function and reduce the need for regenerative events by decreasing either their frequency or duration, and therefore their impact on fuel consumption. This also takes advantage of the close-coupled position of the catalyst, supplying higher exhaust gas temperatures to allow a more frequent oxidation of the trapped particulates. Moreover, the oxidation function could also promote $NO_2$ production where the particulates are deposited, further enhancing the soot removal through passive regeneration. However, the additional filtration function needs to have a limited effect on the system overall backpressure increase, to limit any degradation of the engine power output. The component should also not require any active regeneration as this would create complex interactions with the main DPF regenerations as well as reduce the potential gain in fuel economy. Furthermore, this pre-filter DOC should have a limited effect on the temperature profile supplied to the downstream DPF as it could degrade the efficiency of the regeneration event. Finally, the pre-filter component would also need to show a similar or improved CO and HC oxidation capability, compared to the DOC, while allowing the required filtration efficiency.

### 2.3.3. Potential Substrates

Due to the requirements in low backpressure and passive regeneration, the use of a wall-flow filter as a substrate medium for the pre-filter was dismissed (Gaiser & Mucha, 2004). The use of an open-flow filter, such as foam or fibre filters (Koltsakis *et al.*, 2006; Koltsakis

*et al.*, 2008; Merlone Borla *et al.*, 2011) would lead to similar issues to those seen in wall-flow filters, as it would require some active regeneration to remove the accumulated soot. Moreover, the increase in pressure as it becomes loaded could still greatly affect the exhaust line total backpressure, despite being lower than for the wall-flow filters (Miller *et al.*, 2002; Brillant & Zikoridse, 2005; Koltsakis *et al.*, 2006). Another type of filter that has been recently developed and shows interesting features for the pre-filter application is the partial-flow filter.

### 2.3.4. Presentation of the Partial-Flow Filters

#### *2.3.4.1. Characteristics and Properties of Partial-Flow Filters*

PFFs have previously been studied as series production and retrofit solutions for PM removal in heavy-duty vehicles and off-road applications (Vakkilainen & Lylykangas, 2004; Jacobs *et al.*, 2006; Liu *et al.*, 2008; Kramer *et al.*, 2009). They have also been studied as potential hydrolysis catalysts, located upstream of the SCR component, to promote urea decomposition to ammonia while assuming a particulate trapping function (Maus & Brück, 2007; Rice *et al.*, 2008; Brück *et al.*, 2009). Moreover, it is currently investigated as a possible solution for future legislation imposing a tighter limit in the particulate mass and number emissions from gasoline direct injection engine (Karjalainen *et al.*, 2012; Kinnunen *et al.*, 2012; Happonen *et al.*, 2013). While these studies extensively investigate the PFF filtration and oxidation efficiency, they either concentrate on specific applications (drive cycles) or present the total particulate removal efficiency, without analysing the filtration patterns for different particulate sizes.

The filtration in these components is achieved through a specific channel design disturbing the flow trajectory and directing it towards the porous substrate walls, where the particulates are trapped (Andreassi *et al.*, 2002; Lehtoranta *et al.*, 2009). Once loaded, the exhaust flow

can still bypass the filtering membrane, leaving the PFF to behave as a flow-through substrate. This design leads to a much lower backpressure increase over the loading phase compared to wall-flow filters, limiting the impact on engine output power (Vakkilainen & Lylykangas, 2004; Lehtoranta *et al.*, 2007; Liu *et al.*, 2008; Lehtoranta *et al.*, 2009). Moreover, it is maintenance free and does not require any active regeneration as the accumulated soot is burned following the continuous regeneration mechanism, using $NO_2$ and an exhaust gas temperature over 250°C (Brück *et al.*, 2001b; Okawara *et al.*, 2005; Lehtoranta *et al.*, 2009). Finally, partial-flow filters have a lower tendency to accumulate significant amount of lubrication oil ashes, which reduces the need for periodic ash removal (Torbati *et al.*, 2013). These advantages make the partial-flow filter a good candidate for the pre-filter application as its use leads to less constraints and complexity in terms of maintenance and usage compared to other filters. Focusing on the filtration efficiency, the PFF shows a good filtration for ultra-fine particulates (Heikkilä *et al.*, 2009) which are particularly dangerous for health (Geiser & Kreyling, 2010). While the PFF overall filtration efficiency remains limited (20-50%) compared to the 95-99% filtration found in wall-flow filters (Vaaraslahti *et al.*, 2006; Mayer *et al.*, 2009; Kinnunen *et al.*, 2012), it can still reduce the PM concentration supplied to the main DPF while insuring an oxidation function (Vakkilainen & Lylykangas, 2004; Lehtoranta *et al.*, 2009; Bhatt *et al.*, 2013). This would eventually increase the DPF loading time and reduce the need for active regenerations (fuel economy). While the PFF has been extensively studied for different functions, its combination with a downstream filter and the effects on the DPF backpressure, soot mass accumulation and active regeneration events have never been investigated to the author's knowledge.

*2.3.4.2. Partial-Flow Filters*

Uncoated PM-Metalit

This filter from Emitec is composed of a thin stainless steel foil forming sinusoidal shaped channels. Along the length of the channel, the exhaust flow encounters metallic "shovels" forcing a change of direction of the flow and directing it towards a porous sintered metal fleece layer located on top of the channels (Figure 2-5). Part of the exhaust gas flows through the fleece, depositing medium and large particles through deep-bed filtration and reaches the top-neighbouring channel. Due to their higher momentum, the largest particulates are also trapped in this zone through inertial impaction. The majority of the exhaust gas by-passes the fleece and travels either along or within the fleece in the direction of the flow, as the channel is not totally blocked by the shovel structure. This portion of exhaust gas contains on average smaller particulates, depending on the medium-large PM filtration efficiency taking place in zone 1 (Figure 2-5). At that stage, the filtration occurs through diffusion mechanisms with the exhaust gas depositing small particulates along the fleece (zone 2 and 3 in Figure 2-5). Over the total length of the filter, the exhaust gas flows several times through the fleece (filtration stages), increasing the filtration efficiency.

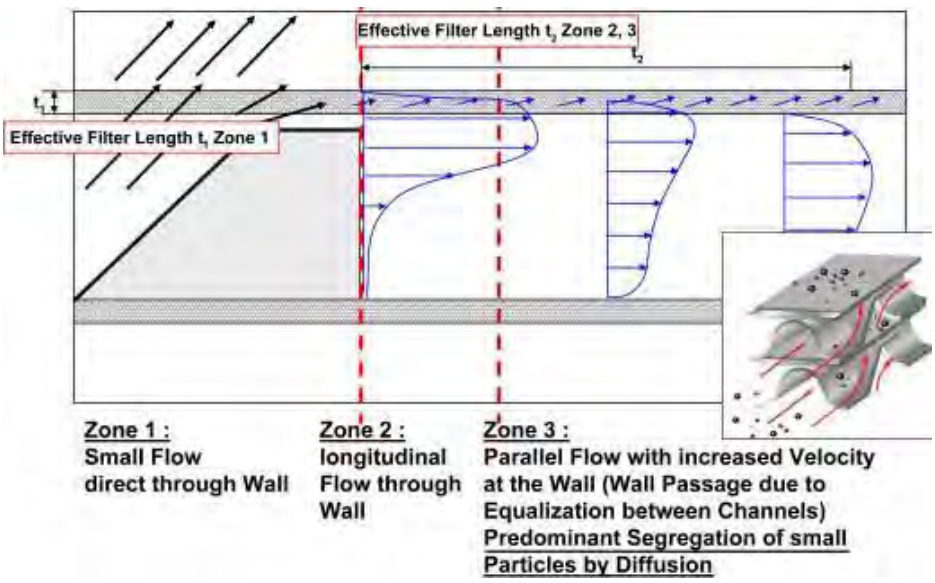


**Figure 2-5.** Schematic of the filtration mechanisms taking place within the PM-Metalit, reproduced by permission from Kramer *et al.* (2009)

Even though some investigations used a coated PM-Metalit, it was left uncoated in this study as it was considered that the washcoat could block the fleece layer, reducing its porosity and affecting the filtration efficiency (Pace *et al.*, 2005). While this uncoated PFF cannot replace the DOC due to the lack of oxidation function, this component was not dismissed due to the possible development of more suitable and effective coating techniques in the future.

Coated Partial Oxidation Catalyst (POC)

The POC, from EcoCat, is composed of corrugated fine metallic mesh screen layers welded together to form tortuous channels. When the exhaust gas enters the component, it can either flow straight through the substrate walls that trap some of the exhaust particulates or travel along the tortuous channels (preferential path when the filter becomes loaded with soot), as seen in Figure 2-6. Similarly to the PM-Metalit, as the exhaust gas flows through the filter, it can be submitted to several filtration stages which increase the filtration efficiency.

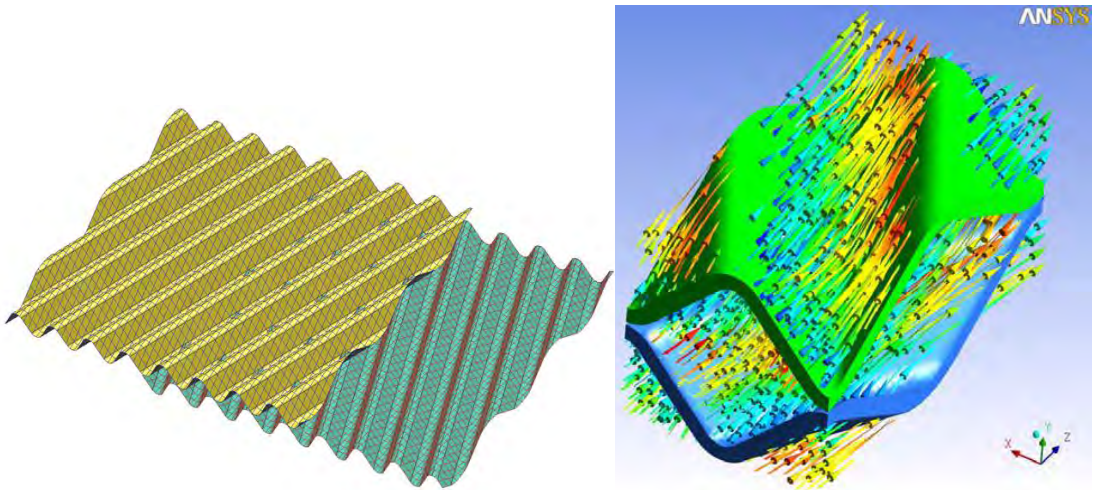


**Figure 2-6.** Layers arrangement in the POC (left) and flow path within the filter (right), from Lehtoranta *et al.* (2007)

Coated Longitudinal Structure (LS) Catalyst

This catalyst developed by Emitec can be considered as a flow-through catalyst (as opposed to the partial-flow filters) with particular channel shapes that create flow turbulence along the catalyst length (Figure 2-7), promoting mass and heat transfer between the exhaust gas and the coated walls of the substrate (Maus and Brück 2005; Dawson & Kramer, 2006; Presti *et al.* 2006; Cordiner *et al.*, 2009; Seifert *et al.*, 2011; Jayat *et al.*, 2015). The LS catalyst is not a straightforward filter as it does not physically trap the exhaust gas particulates. It was considered in this study as it is though that the flow turbulence in the channels could possibly enhance the oxidation of soot and soluble organic fraction (SOF) within the catalyst (Nohara & Komatsu, 2014), reducing the particulate concentration measured at the outlet of the component compared to a conventional flow-through oxidation catalyst.

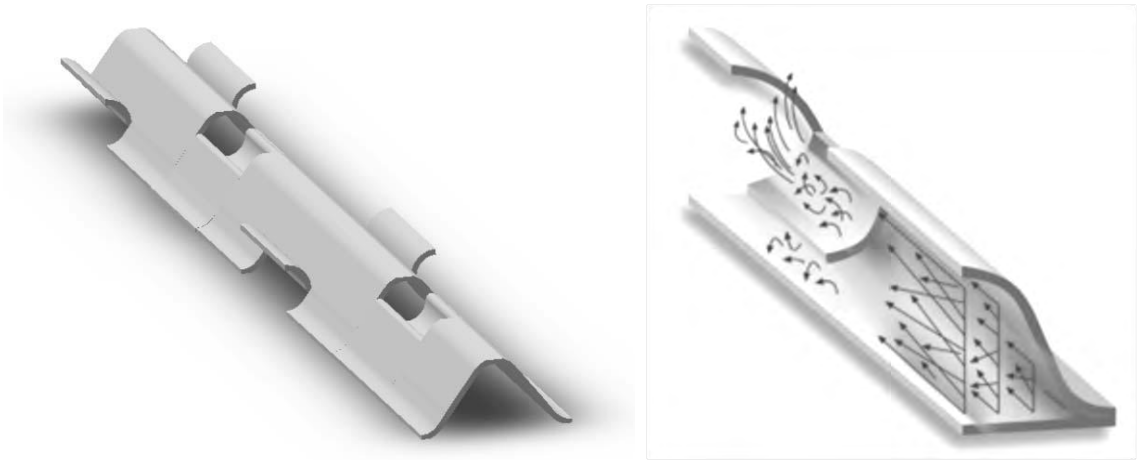

**Figure 2-7.** View from a single channel in the LS catalyst (left) from Cordiner *et al.* (2009) and schematic of the flow behaviour within the channel (right) from Jayat *et al.* (2015)

The development of thermally efficient diesel aftertreatment systems has been receiving a special attention over the years, as presented in this chapter. However, further research is still required, as emissions legislation tightens, to develop new aftertreatment technologies and catalyst design optimisation requiring experimental validation.

# 3. EXPERIMENTAL FACILITIES

This chapter describes the facilities, instrumentation and equipments used for the research work presented in this thesis.

## 3.1. ENGINE AND FUELS

### 3.1.1. Diesel Engine and Instrumentation

The engine used in this study is an air-cooled single cylinder, direct injection, naturally aspirated compression ignition engine, whose main specifications can be found in Table 3-1. This practical engine was selected as it is able to operate with various diesel-type fuels and propane.

**Table 3-1.** Engine characteristics

| **Cylinders** | 1 |
|---|---|
| **Displacement volume** | 773 $cm^3$ |
| **Bore** | 98.4 mm |
| **Stroke** | 101.6 mm |
| **Compression ratio** | 15.5:1 |
| **Peak power** | 8.6 kW @ 2500 rpm |
| **Peak torque** | 39.2 Nm @ 1800 rpm |
| **Pump-line-nozzle** | 3 holes |
| **Piston** | Bowl-in-piston |
| **Injection system diameter** | Ø 0.25 mm |
| **Injection opening pressure** | 180 bar |
| **Injection timing** | 22 CAD BTDC |

The engine is loaded and motored by an air-cooled thyristor-controlled Thrige Titan DC motor-generator machine dynamometer coupled to a load cell. The intake air flow is measured by a Romet G65 rotary airflow meter. The engine oil temperature, recorded using a K-type thermocouple, was used to check that the engine was fully warm as a means to reduce test-to-test variability. This engine was essentially used as an exhaust generator and operated at different conditions (engine speed, load, EGR rate, type of fuel) to vary the exhaust gas temperature, flow rate and composition. The exhaust system is fitted with a valve to manually control the quantity of externally cooled exhaust gas recirculation provided to the engine. The level of EGR was determined volumetrically as the percentage reduction in volume flow rate of inlet air at a fixed engine condition.

### 3.1.2. Liquid Fuels

The main fuel used in this research is ultra-low sulphur diesel (ULSD) but the engine was also operated with other liquid diesel-type fuels, such as gas to liquid (GTL) and rapeseed methyl ester (RME) in section 5.2. The engine injection system was not modified when operated with these alternative fuels as the requirement was to produce a variety of exhaust gases and not the optimisation of the combustion. The properties of each fuel, supplied by Shell Global Solutions UK, can be found in Table 3-2.

**Table 3-2.** Properties of the liquid fuels

| Properties | ULSD | GTL | RME |
|---|---|---|---|
| **Cetane number** | 53.9 | 80 | 54.7 |
| **Density at 15 °C (kg/m$^3$)** | 827.1 | 784.6 | 883.7 |
| **Viscosity at 40 °C (cSt)** | 2.5 | 3.5 | 4.5 |
| **50% Distillation (°C)** | 264 | 295 | 335 |
| **90% Distillation (°C)** | 329 | 342 | 342 |
| **LCV (low calorific value) (MJ/kg)** | 42.7 | 43.9 | 39 |
| **Sulphur (mg/kg)** | 46 | ~0 or <10 | 5 |
| **Total aromatics (wt %)** | 24.4 | 0.3 | ~0 |
| **C (wt %)** | 86.5 | 85 | 77.2 |
| **H (wt %)** | 13.5 | 15 | 12 |
| **O (wt%)** | ~0 | ~0 | 10.8 |
| **H/C ratio (Molar)** | 1.88 | 2.1 | 1.85 |

### 3.1.3. Gaseous Components Additions

To vary the exhaust gas composition for the study in section 5.2, the engine was also operated using dual-fuel combustion, with diesel as the pilot fuel and gaseous propane (properties in Table 3-3) injected in the intake manifold, at a percentage of 0.2% and 0.5% based on the volume of intake air replacement. These percentages were chosen in order to significantly increase and diversify the engine exhaust unburned hydrocarbon emissions, while maintaining combustion stability.

**Table 3-3.** Properties of the gaseous propane

| | |
|---|---|
| **Relative density (15.6°C, 1 atm)** | 1.5 |
| **Boiling point (°C)** | - 42.1 |
| **Latent heat of vaporisation at 15.6°C (kJ/kg)** | 358.2 |
| **Flammability range (%vol. in air)** | 2.2 - 9.5 |
| **Auto-ignition temperature (°C)** | 470 |
| **Sulphur (%wt)** | 0 - 0.02 |
| **LCV (MJ/kg)** | 46.3 |

Gaseous oxygen was also injected in the exhaust gas, to compensate for the oxygen decrease from the use of EGR in section 5.2 or vary the oxygen concentration at the DOC inlet, in section 5.3. In these cases, oxygen was injected from a gas cylinder of pure synthetic oxygen and the flow was adjusted based on the percentage of oxygen recorded in the exhaust gas using an AVL DiGas analyser.

To study the passive regeneration behaviour of the uncoated PM-Metalit (section 6.1.5.1), $NO_2$ from a gas cylinder, was added into the exhaust gas. The flow was calibrated to reach the required concentration of $NO_2$ at the filter inlet during steady-state engine operating conditions, as measured with the MultiGas 2030 Fourier Transform Infrared (FTIR) analyser.

## 3.2. ENGINE EXHAUST SYSTEM AND AFTERTREATMENT

### 3.2.1. Exhaust System and Instrumentation

The exhaust system is composed of two cans that can house full size aftertreatment components (118.4 mm diameter). Moreover, it is fitted with thermocouples and pressure sensors, as well as sampling points, to allow the measurement of exhaust gas properties at different positions along the exhaust line.

Throughout this research work, three different catalyst locations in the exhaust line were investigated (Figure 3-1), based on the temperature requirements and the dimensions of the aftertreatment components used.

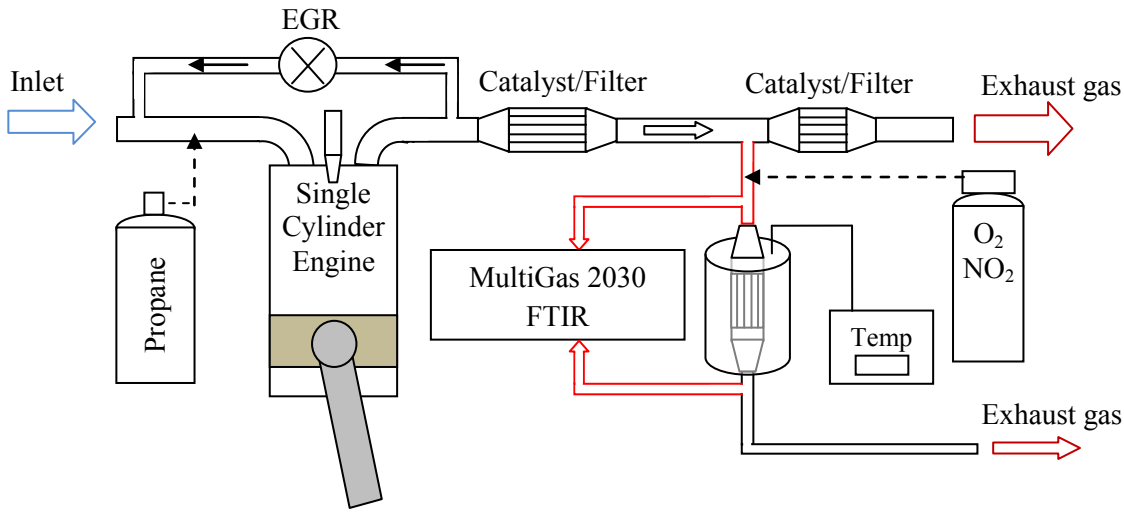


**Figure 3-1.** Schematic of the experimental set-up

In most of the investigations, full size catalysts were directly placed in the exhaust system. For the light-off experiments (section 5.2 and 5.3), the catalyst inlet temperature was varied while maintaining the exhaust gas flow rate and composition constant. In these cases, a one-inch-diameter catalyst was placed in a furnace for which the temperature was externally controlled. The engine was then operated at a steady-state condition and a portion of exhaust gas (35 L/min) was directed towards the catalyst which was heated at a temperature ramp of 2°C/min. Engine-out exhaust species concentrations were measured at the beginning and at the end of each experiment to compare any changes in the exhaust gas composition during the test. Throughout the experiments, the evolution of the DOC outlet exhaust gas concentration was continuously recorded to calculate the conversion efficiency based on the inlet concentration. Similarly, for the investigation of the PFF+DPF system, a one-inch diameter DPF was fitted in the same configuration system.

Each exhaust gas sampling (for emission measurement or to be directed towards another aftertreatment component) was made with the sampling line at a temperature of 200°C, to limit any water and hydrocarbon condensation, while preventing any reaction between exhaust gas species in the line.

To determine the space velocity within each catalyst, the exhaust gas flow rate was calculated using the inlet air and fuel flow rate, the exhaust temperature specific to the engine operating condition and the pressure measured in the exhaust system.

### 3.2.2. Diesel Oxidation Catalysts and Particulate Filters

A variety of coated and non-coated substrates were investigated (flow-through, partial-flow and wall-flow components), with different materials (ceramic and metallic), cell shapes (square and sinusoidal), wall thicknesses, cell densities and channel designs (Figure 3-2) selected based on their commercially available.

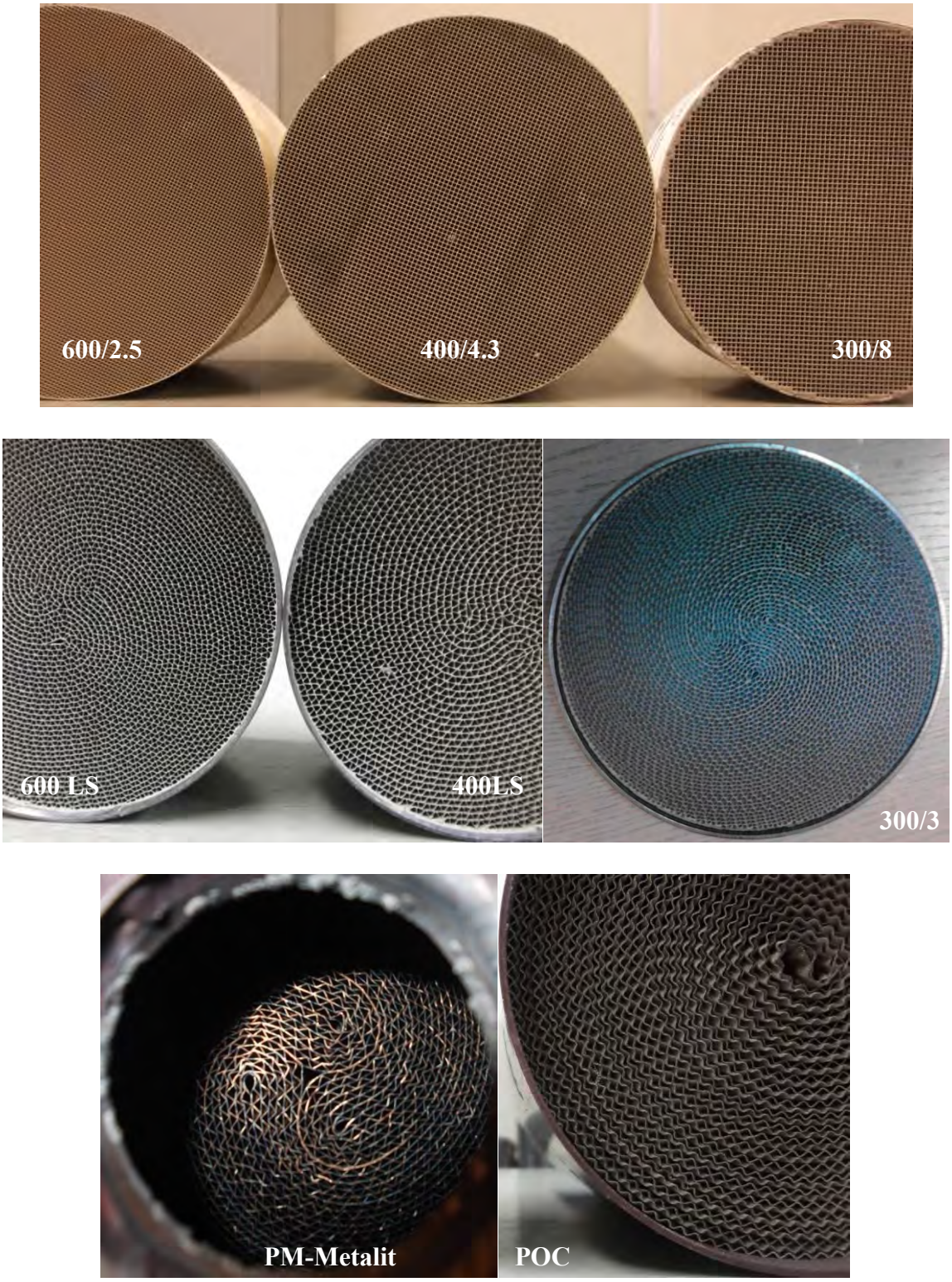


**Figure 3-2.** Pictures of the aftertreatment components studied (118.4 mm diameter)

When investigating the effects of the substrate properties on the conversion efficiency (Chapter 4), the catalytic coating (washcoat, PGM composition and loading) and ageing conditions (750°C for 10 hours) were kept the same, to allow fair comparison (components 2 to 8 in Table 3-4). Components 1 and 9 were coated with different catalytic formulations (as developed by the manufacturers) and received not aged. These differences, as well as the differences in volume, were taken into account when comparing their efficiency with each others.

**Table 3-4.** Oxidation catalysts and filters used in the experiments

| | **Name** | **Cell Density Wall Thickness (cpsi/mil)** | **Material** | **Diameter x Length (mm)** | **PGM Loading ($g/ft^3$)/ Pt:Pd Ratio** | **Supplier** | **Volume (L)** |
|---|---|---|---|---|---|---|---|
| **1** | DOC | 400/4.3 | Ceramic | 25.4 x 91.4 | 120/1:1 | Unknown | 0.05 |
| **2** | DOC | 400/4.3 | Ceramic | 118.4 x 150 | Pt-rich | NGK | 1.65 |
| **3** | DOC | 600/2.5 | Ceramic | 118.4 x 100 | Pt-rich | Corning | 1.10 |
| **4** | DOC | 600/2.5 | Ceramic | 118.4 x 75 | Pt-rich | Corning | 0.83 |
| **5** | DOC | 300/8 | Ceramic | 118.4 x 45 | Pt-rich | Corning | 0.50 |
| **6** | DOC | 300/3 | Metallic | 118.4 x 50.8 | Pt-rich | Emitec | 0.56 |
| **7** | DOC | 200/400 LS/2.6 | Metallic | 118.4 x 74.5 | Pt-rich | Emitec | 0.82 |
| **8** | LS | 300/600 LS/2.0 | Metallic | 118.4 x 74.5 | Pt-rich | Emitec | 0.82 |
| **9** | POC | 330/4.3 | Metallic | 118 x 150 | 21/1:0 | EcoCat | 1.64 |
| **10** | PM-Metalit | 200/2.6 | Metallic | 118.4 x 123 | Pt-rich | Emitec | 1.35 |
| **11** | DPF | 300/12 | Ceramic | 25.4 x 155 | None | Unknown | 0.08 |

Due to their specific design, the properties of the PM-Metalit and POC are presented in more detail in Table 3-5 and Table 3-6.

**Table 3-5.** Properties of the PM-Metalit

| **PM-Metalit Properties** | |
|---|---|
| **Flat/Corrugated foil thickness** | 0.3/0.065 mm |
| **Fleece Properties** | |
| **Thickness** | 0.5 mm |
| **Porosity** | 85% |

**Table 3-6.** Properties of the POC fleece

| | |
|---|---|
| **Foil thickness** | 0.11 mm |
| **Porosity** from Heikkilä *et al.* (2012) | 47% |

## 3.3. EXHAUST GAS EMISSION ANALYSIS

### 3.3.1. Fourier Transform Infrared Spectrometry (FTIR)

An MKS MultiGas 2030 FTIR analyser was used to measure gaseous exhaust emissions. This measurement technique relies on the relation between light absorption at a certain wavelength and species concentration. This apparatus was used here to measure the concentration of the following exhaust gas species: nitrogen oxides (NO, $NO_2$ and $N_2O$), water ($H_2O$), formaldehyde ($CH_2O$), carbon dioxide ($CO_2$), carbon monoxide (CO) and individual light-hydrocarbons such as methane ($CH_4$), ethane ($C_2H_6$), propane ($C_3H_8$), ethylene ($C_2H_4$), propylene ($C_3H_6$) and acetylene ($C_2H_2$). Due to spectrum interferences, medium and long-chain hydrocarbon concentrations were measured as a single exhaust gas group.

### 3.3.2. AVL DiGas

An AVL DiGas 440 was used to measure oxygen exhaust content, using an electrochemical oxygen sensor.

### 3.3.3. Scanning Mobility Particle Sizer (SMPS)

The measurement of total PM concentration and size distribution was made using a TSI SMPS (scanning mobility particle sizer) composed of an electrostatic classifier series 3080, a 3081 DMA (differential mobility analyser) and a 3775 TSI CPC (condensation particle counter). A portion of the exhaust gas was sampled and diluted with air using a TSI 379020A rotating disk thermodiluter to control the dilution ratio (1 part of exhaust to 36 parts of air) and temperature (150°C). The results presented in graphs were adjusted with the dilution ratio. The sampled particulates were then electronically charged and flown through the DMA that classified them by their electrical mobility size which is proportional to their aerodynamic diameter. The CPC eventually counted the number of particles for each size range. The particles distribution was measured using the following parameters:

Sheath Flow Rate: 6.00 L/min

Aerosol Flow Rate: 0.60 L/min

Lower Size: 10.4 nm

Upper Size: 378.6 nm

Scan Time: 120 sec

The particulate size distribution obtained for diesel exhaust gas is composed of different types of particulates, based on their size (Figure 3-3). For the studies investigating particulate removal, the particulates were divided into three groups, i.e. small, medium and large particulates.

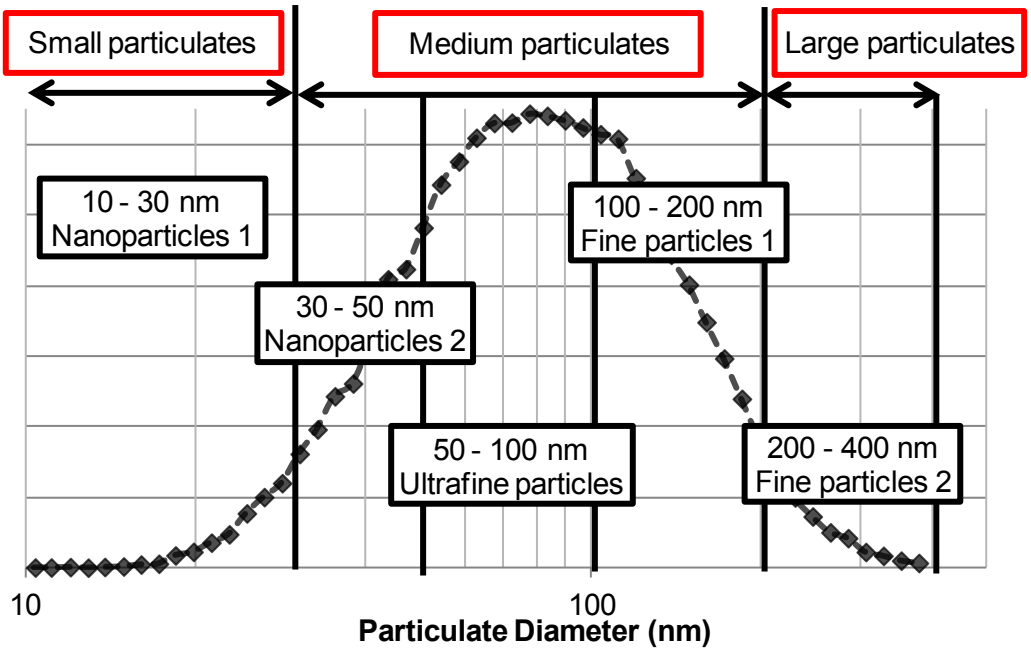


**Figure 3-3.** Typical particulate size distribution for the engine used in this study

The particulate mass was calculated using an estimation of the particulate density as developed in Lapuerta *et al*. (2003), relating the density with particulate diameter, in an equation developed based on experimental analysis.

### 3.3.4. Thermogravimetric Analysis (TGA)

Particulate matter was collected using an in-house developed Venturi nozzle diluter, mixing the exhaust gas sampled through a heated line (200°C) with ambient compressed air at 1 bar (dilution ratio of 1 part of exhaust to 8 parts of air). The PM was collected for 45 min at a flow of 9 L/min on 47 mm diameter glass micro-fibre filters (Whatman, without Teflon coating) fitted in a filter holding plate and stopper. A thermogravimetric analysis of the collected filters using a Perkin Elmer (Pyris 1 TGA) was used to investigate the soot reactivity.

The TGA was operated using the heating program presented below:

1. Initial atmosphere: nitrogen
2. Isothermal for 10 min at 40°C
3. Heating ramp 3°C/min from 40°C to 400°C
4. Isothermal for 30 min at 400°C
5. Cooling ramp from 400°C to 100°C at 3°C/min
6. Change of atmosphere to air
7. Heating ramp from 100°C to 650°C at 3°C/min
8. Isothermal for 60 min at 650°C
9. Cooling ramp from 650°C to 20°C at 50°C/min

The first 4 steps of the heating program allowed complete vaporisation of the volatile organic compounds and water condensed on the soot. The maximum temperature reached in air atmosphere to oxidise the soot was set to 650°C to limit the filter decomposition. The temperature ramp was set-up at 3°C/min to allow sufficient time to reach close to steady-state steps.

### 3.3.5. Transmission Electronic Microscope (TEM)

Particulate matter agglomerates from upstream and downstream of the partial-flow filters were collected on 3 mm diameter Formvar-coated copper grids. A high-resolution transmission electron microscopy (HR-TEM) Phillips CM-200 was used to obtain micrographs from the agglomerates and calculate their morphological and micro-structural parameters using a homemade Matlab software (digital image analysis software), as presented in Lapuerta *et al.* (2006) and Lapuerta *et al.* (2010). The conversion from pixels to nanometres was calibrated by comparison with standard latex spheres shadowed with gold.

## 3.4. EXPERIMENTAL ERRORS AND REPEATABILITY

During the experimental work carried-out in this thesis, care was taken to reduce the uncertainties and test-to-test variability derived from the use of the equipment and measurement techniques previously presented.

Before and after each measurement session, the FTIR as well as the measurement lines and sampling pump were flown with gaseous nitrogen to clean them from remaining condensed water and impurities. Additionally, the lines, pump and dilution system used to sample particulates from the exhaust were cleaned with propanol after each measurement session. In order to assure the consistency of the results, the baseline (zero level) of the equipment (FTIR and SMPS) was performed with the measurement of the ambient air through the sampling system (background data) before and after each test condition. Additionally, when a cold start was not required, the engine was operated at a specific steady-state condition with a known exhaust CO, HC, $NO_x$ and particulate concentration at the beginning and at the end of the tests, to compare the evolution of the exhaust concentration on a day-to-day basis and check repeatability. Finally, each measurement presented here is the average of at least three measurements, to account for measurement and engine variability. The measurements were additionally repeated when uncertain results were obtained and the erroneous samples were discarded.

## 3.5. SOFTWARE USED FOR THE MODELLING OF THE AFTERTREATMENT SYSTEM

The use of modelling and simulation tools in aftertreatment research and development allows a reduction in the number of experimental tests required to investigate the viability of a system. Modelling can aid in the definition of the requirements in terms of catalyst physical and chemical properties for a specific application in order to select the most appropriate component before manufacturing and testing. Moreover, it can help analysing and understanding the behaviour of a component during its use and predict the effects of different engine operating conditions on its activity, such as the use of various drive cycles, limiting the requirement for additional experiments or facilities. This translates into potential cost and time savings. The modelling of the aftertreatment system relies on a complex combination of fluid dynamics (to reproduce the harsh and continuously changing working environment due to the transient aspect of vehicle engine operation) and kinetic reactions (to understand the fundamentals of the parameters governing the catalytic reactions) to eventually reproduce the external and internal environment in which the system operates.

As this study is based on investigating strategies and designs to improve the catalyst activity, the focus was not given on developing an in-house model but rather use modelling as a tool to predict behaviours, assist in the choices to be made before any experiment and expand the study towards other conditions relevant to the application.

The modelling of the exhaust aftertreatment systems presented in this thesis uses Axisuite simulation software. This software, developed by Exothermia, allows simulating the performance of aftertreatment devices (e.g. flow-through catalysts, filters) on a range of exhaust gas conditions and compositions, using a time-based simulation. The inputs for the simulation are the properties of the exhaust gas (e.g. temperature, gas composition and flow rate) and those of the aftertreatment component (physical and chemical characteristics). The

material properties of the components used in this study were loaded from Axisuite standard library which offers a selection of the most typical substrate materials such as the regular cordierite ceramic or metallic substrate used in this study. The chemical properties of the catalysts, such as washcoat characteristics and kinetic coefficients, were obtained from an experimentally validated model developed by Jaguar Land Rover. The models and assumptions used by this software for the modelling of the oxidation catalyst are presented in Lafossas *et al.* (2011). The results of the simulation predict the time-based evolution of relevant properties such as temperature, pressure, exhaust gas composition and therefore, conversion efficiencies, among other parameters.

The modelling software was used for different purposes, as a tool to predict and estimate the thermal behaviour of various catalysts. Axisuite thermal predictions over an NEDC were first evaluated by comparing Axisuite-simulated temperature with the actual measurement on an engine test bench (Figure 3-4).

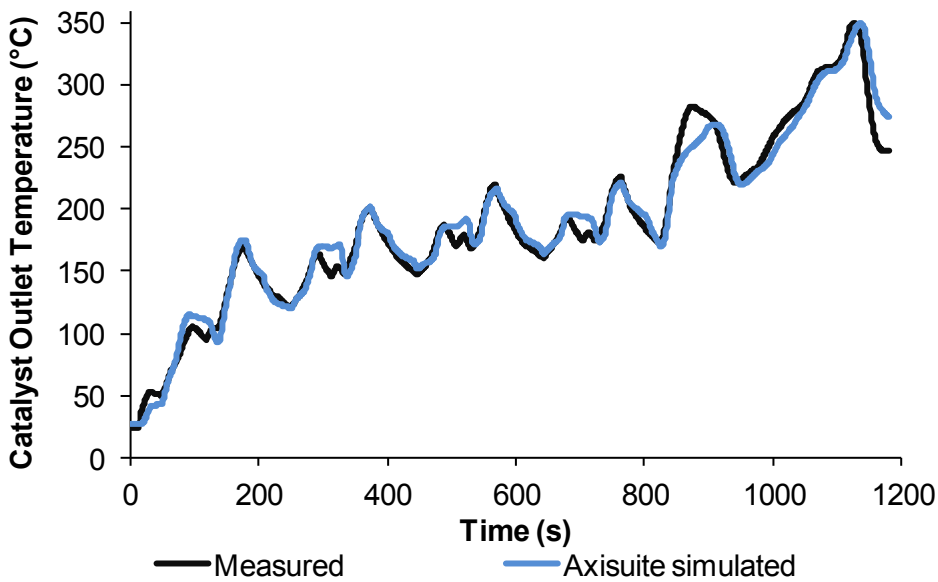


**Figure 3-4.** Comparison of the DOC outlet temperature as predicted by Axisuite, with the measured one from an engine over an NEDC

The main temperature ramps (increases and decreases) were well predicted by the software and matched the temperature profile observed at the outlet of the DOC. However, during quick changes of temperature, Axisuite predictions appeared less dynamic and showed a flatter profile of temperature when in reality peaks were recorded. These differences were considered when using Axisuite to predict the temperature profile of the different catalysts.

Axisuite was firstly used to evaluate and compare several catalysts from the point of view of thermal behaviour and activity (section 4.3), to eventually select the most suitable configurations before experimental tests. The second application of Axisuite, in section 4.5, focused on expanding the results from the experimental work (section 4.4) using the catalysts outlet temperature measured during the tests to validate the model from Axisuite. The study was then expanded towards alternative drive cycles (Paris cycle and urban part of the NEDC with stop/start strategy), to investigate the thermal behaviour of the catalysts configurations under more challenging and transient conditions.

This overview of the experimental facilities presents the aftertreatment components tested and the engine exhaust set-up used, as well as the methods and measurement techniques that allowed the investigations and results developed in the following chapters.

# 4. A THERMALLY EFFICIENT DOC CONFIGURATION TO IMPROVE LOW-TEMPERATURE ACTIVITY

The study presented in this chapter investigates the replacement of a reference oxidation catalyst (400 cpsi / 4 mil, equivalent to 62 cells per $cm^2$ and 0.1 mm thick) by monoliths with different cell densities and wall thicknesses, in order to promote the catalyst thermal behaviour and enhance its low-temperature activity. While numerous possibilities of substrate cell density and wall thickness combinations exist in the market, it is necessary to select the most relevant substrates for this application before any experiment. Therefore, a theoretical analysis, followed by a simulation study, was carried-out to select relevant catalysts substrates before experimental investigation of their thermal and oxidation behaviour with genuine diesel exhaust gas.

## 4.1. METHODOLOGY

### 4.1.1. Theoretical Study Assumptions

The theoretical study is carried-out for a non-coated ceramic cordierite substrate as it is currently the most widely used material in oxidation catalysts for automotive applications (Carty & Lednor, 1996). Both the length and diameter of the substrates were kept similar to a reference 400 cpsi /4 mil substrate, to maintain comparable space requirements. The cordierite porosity was kept at a typical value of 35%, low enough to ensure mechanical and thermal durability and high enough for the support of the washcoat and its adhesion during the coating process (Gulati, 2000).

### 4.1.2. Input Data for the Modelling and Simulation Study

The thermal behaviour of the substrates selected based on the outcomes of the theoretical study was investigated using Axisuite simulation, with a scenario based on the exhaust gas properties of an exhaust bank from an EU5 diesel engine operated following an NEDC. This cycle was chosen as it is currently used in the European light-duty vehicles emission legislation. The input data concerning the physical properties of the substrates were loaded from Axisuite standard library (material properties) and the dimensions were taken from a reference catalyst currently in production. To evaluate the catalytic activity, the substrates were modelled coated, as they would be if implemented into a vehicle exhaust system. The catalytic coating data used in Axisuite (washcoat properties, kinetic coefficients) came from an experimentally validated model developed by Jaguar Land Rover. In addition, a simulation of the substrate wall temperature distribution at certain phases of the NEDC was presented to compare the improved thermal behaviour of the selected substrates and combinations. These temperature distributions produced by Axisuite are based on equations modelling the heat release and heat transfer within the catalyst, during its use. This includes the axial and radial wall conductivity, the heat convection due to the exhaust gas flow, the heat release due to the exothermic character of CO and THC oxidation reactions and, to a lesser extent, the heat transfer due to radiation.

### 4.1.3. Set-Up and Methodology for the Experimental Study

In addition to the substrates selected based on the outcomes of the modelling study, other substrates were also investigated here, to extend the potential benefit of the two-brick configuration. The dimensions of the catalysts (length and diameter) were adjusted compared to the ones from the modelling study, as a smaller engine was used in the experimental investigation (Table 4-1).

**Table 4-1.** Catalysts combinations used in the experimental study

| Cell Density (cpsi)/Wall Thickness (mil) | Diameter (mm) x Length (mm) | Comments |
|---|---|---|
| 400/4 | 118.4 x 150 | Reference catalyst already used in the exhaust system of production vehicles. |
| 600/2.5 | 118.4 x 100 | First brick in the two-brick configurations.<br>Tested independently to provide a clearer understanding of its behaviour in the two-brick configuration (no sample point between the two bricks in the can). |
| 600/2.5<br>+ 300/8 | 118.4 x 100<br>+ 118.4 x 45 | Defined as 2BC in this study, uses a second ceramic brick with low cell density and thick walls. |
| 600/2.5<br>+ 300/3 | 118.4 x 100<br>+ 118.4 x 50 | Defined as 2BM in this study, uses a second metallic brick with low cell density. |
| 600/2.5<br>+ 400/2.5 LS | 118.4 x 75<br>+ 118.4 x 75 | Defined as 2B4LS in this study, composed of a shorter first brick compared to the previous configurations and a second metallic brick with a specific design to enhance turbulence within the channels. |
| 600/2.5<br>+ 600/2 LS | 118.4 x 75<br>+ 118.4 x 75 | Defined as 2B6LS in this study, similar to 2B4LS with a higher cell density substrate as second brick. |

Each catalyst had the same coating formulation and loading, and was aged under identical conditions to directly isolate the effects of material and cell density/wall thickness. The total length was kept comparable between the two-brick configurations with a gap of up to 5 mm between the two catalysts (2BC), to maintain similar package requirements for the whole system and total space velocity in the catalysts.

The thermal capacity of the tested configurations was calculated when possible (Table 4-2) and used to support the analysis of their thermal response during the experiment.

**Table 4-2.** Mass and thermal capacity of the catalysts configurations studied

| | **400/4** | **600/2.5** | **2BC** | **2BM** | **2B4LS** | **2B6LS** |
|---|---|---|---|---|---|---|
| **Total mass (kg)** | 0.844 | 0.506 | 0.834 (0.506 + 0.328) | 1.422 (0.506 + 0.916) | 1.436 (0.405 + 1.031) | 1.413 (0.405 + 1.008) |
| **Thermal capacity (J/K) at 150°C** | 810.8 | 486.1 | 801.2 | 876.6 | 937.8 | 925.6 |
| **Uncoated surface area available ($m^2$)** | 4.75 | 3.99 | 4.15 (3.99+1.16) | 4.60 (3.99+1.61) | (2.99+ - ) | (2.99+ - ) |

The 600/2.5 showed the lowest thermal capacity, due to its shorter dimensions and thin walls. The low cell density ceramic catalyst (2BC) also led to a low thermal mass due to the reduction in the number of walls and therefore material used in the substrate. The three last configurations, using a second metallic brick, showed the highest thermal masses, due to the thick mantle surrounding the catalysts adding weight to the system and the higher material density, despite the lower thermal capacity relative to mass of the metallic substrates compared to the ceramic ones. The highest thermal masses were measured for the 2B4LS and 2B6LS configurations, due to their longer second metallic brick.

During the experiment, the space velocity was more equally distributed between the two bricks in the LS configurations, while for the other combinations, the longer first brick led to an increase in exhaust gas residence time within the 600/2.5 catalyst (Table 4-3).

**Table 4-3.** Space velocity in the catalysts combinations (first and second catalysts) for the selected engine operating conditions

| Engine Operating Conditions (rpm/bar IMEP) – Exhaust Temperature | 400/4 | 600/2.5 | 2BC<br>1st brick<br>2nd brick | 2BM<br>1st brick<br>2nd brick | 2B4LS<br>1st brick<br>2nd brick | 2B6LS<br>1st brick<br>2nd brick |
|---|---|---|---|---|---|---|
| **750/0 – 80°C** | 12 000/h | 18 000/h | 18 000/h<br>39 900/h | 18 000/h<br>35 300/h | 23 900/h<br>24 100/h | 23 900/h<br>24 100/h |
| **1050/3 – 160°C** | 16 300/h | 24 500/h | 24 500/h<br>54 500/h | 24 500/h<br>48 300/h | 32 700/h<br>32 900/h | 32 700/h<br>32 900/h |
| **1500/4 – 255°C** | 33 300/h | 49 900/h | 49 900/h<br>111 000/h | 49 900/h<br>98 300/h | 66 600/h<br>67 000/h | 66 600/h<br>67 000/h |
| **1900/4 – 330°C** | 48 000/h | 72 100/h | 72 100/h<br>160 100/h | 72 100 /h<br>141 800/h | 96 100/h<br>96 700/h | 96 100/h<br>96 700/h |
| **1500/5 – 350°C** | 36 300/h | 54 500/h | 54 500/h<br>121 100/h | 54 500/h<br>107 300/h | 72 700/h<br>73 100/h | 72 700/h<br>73 100/h |

The engine operating conditions described in Table 4-3 were repeated in the same order for the six catalyst configurations and showed repeatable exhaust gas concentrations (Figure 4-1), allowing fair comparison of the activity between configurations.

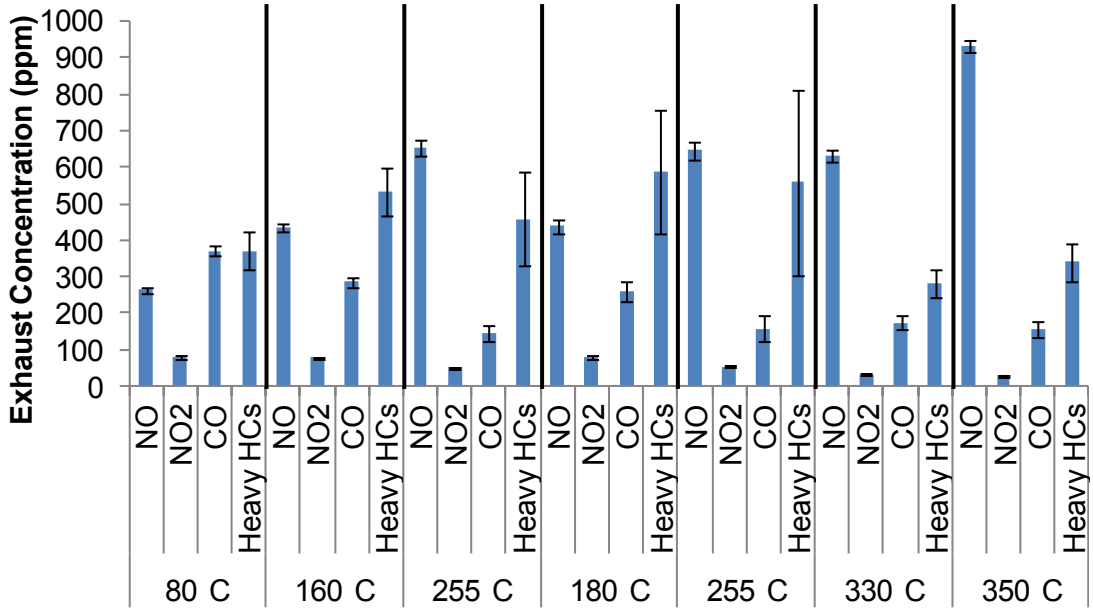


**Figure 4-1.** Variations (error bars) in the exhaust gas concentration during the repetition of the engine operating conditions for the different combinations of catalysts

However, during the investigation of the catalyst thermal response, test-to-test engine-out temperature variability was recorded from one configuration to another. To take into account these variations, a parameter representing the temperature losses over the catalysts was calculated, based on the difference between the inlet and outlet temperatures, to provide additional information for the thermal behaviour analysis.

After analysing the thermal behaviour of the catalyst configurations, their CO, HC and $NO_x$ conversion efficiencies were studied during the steady-state conditions of the experiment. The conversion efficiency was plotted against the inlet temperature to allow the analysis of the catalyst activity at a given temperature and to take into account the variations in terms of inlet temperature reproducibility from one configuration to another. In parallel, the conversion efficiency was also plotted against the configurations outlet temperatures, to take into account the differences in temperature losses over the configurations. The conversion efficiency of the short 600/2.5 brick was also presented to estimate the portion of the conversion efficiency accounted for by the first brick of the configurations.

### 4.1.4. Model Setup for the Alternative Driving Cycles Study

An additional Axisuite model was developed, based on the experimental data previously obtained, in order to expand the two-brick configuration study to additional drive cycles. The input exhaust gas scenario was created based on the engine operating conditions recorded during the experiment as presented in 4.1.3 (exhaust gas compositions, temperatures and mass flow rates). The model was tuned to reproduce the measured 400/4 catalyst outlet temperatures, and validated by comparing the simulated outlet temperatures with the actual measurements for the other catalysts (600/2.5, 2BC and 2BM). This Axisuite model was then used to investigate the thermal behaviour of the selected catalysts over alternative drive cycles, based on the data from the engine presented in 4.1.2 running a Paris cycle and the urban parts of an NEDC with stop/start function. Due to the larger engine used in this simulation, the catalysts dimensions were increased (same dimensions as in 4.1.2.) to allow a fair estimation. The modelling of the turbulent LS catalysts was not developed in this work, due to their complex channel design, requiring further and more specific tests to understand how to model their behaviour.

## 4.2. RESULTS OF THE THEORETICAL STUDY

This theoretical study is conducted to provide a first estimation of the effect of varying the substrate cell density and wall thickness on the main parameters considered when selecting an aftertreatment substrate (i.e. light-off capacity, conversion efficiency, pressure losses and durability). Theoretical equations derived from the literature are applied on a variety of cell density/wall thickness combinations to eventually select the most promising substrates for further modelling and simulation studies.

### 4.2.1. Presentation of the Equations

The parameters presented below estimate the catalyst capacity to warm-up (light-off factor), to efficiently convert CO and THCs (conversion efficiency factor), to generate undesirable backpressure and to be mechanically and thermally resistant. These properties related formulae (described below) were firstly developed in Gulati (2000) and (2001) and Gulati *et al.* (2001).

- Light-Off Factor (Equation 1) shows the substrate ability to quickly reach the temperature at which its catalytic activity starts. It relies on the thermal capacity of the substrate and the contact area between the walls and the exhaust gases and is expressed as:

$$\mathbf{LOF} = \frac{\mathbf{H.GSA}}{\mathbf{M^*}} \quad (°C/J) \qquad \textbf{Equation 1}$$

where

GSA: geometric surface area per volume of substrate ($m^2/m^3$)

M*: substrate thermal mass ($J/°C/m^{-3}$)

H: heat transfer factor (Equation 2) defined as:

$$\mathbf{H} = \frac{\mathbf{Nu.GSA}}{\mathbf{D_h}} \quad (m/m^3) \qquad \textbf{Equation 2}$$

where

Nu: Nusselt number depending on the cell shape and the condition state (here, transient state as the catalyst is warming-up)

$D_h$: hydraulic diameter (m)

- Conversion Efficiency Factor (Equation 3) estimates the conversion capacity of the catalyst once fully warmed, when the reactions are considered mass-transport limited. It takes into account the mass transfer and the contact area available for reaction between the exhaust gas and the substrate walls and is expressed as:

$$\mathbf{CEF = M.GSA} \quad (/m^3) \qquad \textbf{Equation 3}$$

where

M: Mass transfer factor (Equation 4), defined as:

$$\mathbf{M = \frac{Sh.GSA}{D_h}} \quad (m/m^3) \qquad \textbf{Equation 4}$$

where

Sh: Sherwood number depending on the cell shape and the condition state (here, steady-state as the catalyst is fully warmed)

- Pressure Losses (Equation 5) represents the losses due to friction with the walls as the exhaust gas flows inside the channels. The compression/expansion effect when the gas enters/exits the catalyst was neglected in this estimation of the pressure losses, as the friction losses can be considered dominating (Day, 1997). The pressure losses are expressed as:

$$\mathbf{\Delta P = 2\ {}_g fRe \frac{Q}{A.OFA} \frac{\lambda}{D_h{}^2}} \quad (Pa) \qquad \textbf{Equation 5}$$

where

$\mu_g$: dynamic viscosity of gas (Pa.s)

f: friction factor for square channels (14.2/Re)

Re: Reynolds number

Q: volumetric flow rate of gas ($m^3/s$)

A: cross sectional area ($m^2$)

OFA: Open frontal area

$\lambda$: channel length (m)

As the comparison is made for substrates of same length and diameter, at the same engine conditions, $\mu_g$, fRe, Q, A and $\lambda$ are constant and Equation 5 can be simplified to Equation 6:

$$\mathbf{\Delta P'} = \frac{\mathbf{1}}{\mathbf{OFA.D_h{}^2}} \quad (/m^2) \qquad \textbf{Equation 6}$$

- 2D Iso-static Strength (Equation 7) represents the strength of the substrate when a supposedly uniform pressure is applied around the substrate during the canning process and is defined as:

$$\boldsymbol{\sigma_{2D-iso}} = \mathbf{2.828}\ \boldsymbol{\sigma_w}\frac{\mathbf{t}}{\mathbf{L}} \quad (MPa) \qquad \textbf{Equation 7}$$

where

t: wall thickness (m)

L: cell pitch (m)

$\sigma_w$: Estimated tensile strength of the wall (Equation 8), defined as:

$$\boldsymbol{\sigma_w} = \boldsymbol{\sigma_o}.\mathbf{e}^{-\mathbf{4.9P}} \quad (MPa) \qquad \textbf{Equation 8}$$

where

P: fractional substrate wall porosity (0.35 for cordierite)

$\sigma_o = 117$ MPa tensile strength of non porous cordierite

- Average Shear Stress (Equation 9) represents the shear stress in the substrate created by a non-uniform pressure distribution during the canning process (misaligned substrate in the can for example) as defined below:

$$\boldsymbol{\tau_{AV}} = \frac{\mathbf{2}}{\mathbf{3}}\boldsymbol{\sigma_w}\left(\frac{\mathbf{t}}{\mathbf{L}}\right)^{\mathbf{2}} \quad (MPa) \qquad \textbf{Equation 9}$$

Other mechanical parameters can be defined, such as the axial crush strength (Gulati, 2001) or the modulus of rupture in the axial direction (Gulati, 2000). These properties show similar trends and dependence on cell density and wall thickness as the two previous parameters (Equation 7 and Equation 9) and were therefore dismissed to limit the number of parameters taken into account.

- Thermal Durability: Throughout its lifetime, a diesel exhaust substrate will have to withstand temperatures over 600°C when, for example, a filter active regeneration strategy is in use (Watanabe *et al.*, 2007; Kim *et al.*, 2014). Most of the time, it will be operating at lower temperatures than in gasoline engine exhaust, meaning lower thermal stresses will be applied on diesel substrates. A previous study on gasoline exhaust aftertreatment (Gulati *et al.*, 2002) emphasised a dependence of the thermal stresses to the substrate aspect ratio (length/diameter). It was highlighted that an aspect ratio between 1.2 and 1.4 is recommended in the case of an under-floor catalyst, meeting surface and centre temperatures of 600°C and 850°C, respectively. In the present study, the diesel substrates have an aspect ratio of 1.27 which assures their thermal durability, as the average temperature of a close-coupled diesel catalyst remains below 600°C.

### 4.2.2. Effect of Cell Density/Wall Thickness on the Catalyst Activity and Durability

In the previous section, Equation 1 to Equation 9 include some parameters others than the cell density and wall thickness. Each variable composing these equations can be expressed using only n, the cell density in cpsi and t, the wall thickness in mil, as, from Gulati (2001),

$$\mathbf{OFA} = \mathbf{n}\left(\frac{\mathbf{1}}{\sqrt{\mathbf{n}}} - \mathbf{t}\right)^{\mathbf{2}} \qquad \textbf{Equation 10}$$

$$\mathbf{GSA} = \mathbf{4n}\left(\frac{\mathbf{1}}{\sqrt{\mathbf{n}}} - \mathbf{t}\right) \qquad \textbf{Equation 11}$$

$$\mathbf{D_h} = \frac{1}{\sqrt{n}} - t \qquad \textbf{Equation 12}$$

Using Equations 10 to 12 and the assumptions made previously (same monolith volume and material used at the same engine conditions), Equations 1, 3, 6, 7 and 9 can be expressed as followed,

$$\mathbf{LOF}' = \frac{16n}{(\frac{1}{\sqrt{n}} - t)} \qquad \textbf{Equation 13}$$

$$\mathbf{CEF}' = 16n^2\left(\frac{1}{\sqrt{n}} - t\right) \qquad \textbf{Equation 14}$$

$$\mathbf{\Delta P}' = \frac{1}{n\,(\frac{1}{\sqrt{n}} - t)^4} \qquad \textbf{Equation 15}$$

$$\sigma_{2D-iso}{}' = 2.828\sigma_w t\sqrt{n} \qquad \textbf{Equation 16}$$

$$\tau_{AV}{}' = \frac{2}{3}\sigma_w t^2 n \qquad \textbf{Equation 17}$$

The range of cell densities studied was defined between 100 and 1200 cpsi. Under 100 cpsi, the reduced "contact area / hydraulic diameter" ratio would lead to highly reduced catalyst conversion efficiency. The upper limit of 1200 cpsi was chosen as it is the highest cell density currently available for ceramic substrates. In terms of wall thickness limits, 2 mil is the minimum currently made for ceramics, for mechanical durability reasons. The upper limit was set at 12 mil wall thickness as it is the thickest wall that can be found for flow-through substrates.

The results of Equation 13 to Equation 17 with varying cell densities and wall thicknesses can be presented in 3D surface graphs showing the improvement or degradation of the properties described above (light-off, conversion efficiency, pressure losses, and mechanical durability) compared to the reference 400/4 catalyst (Figure 4-2 to Figure 4-5).

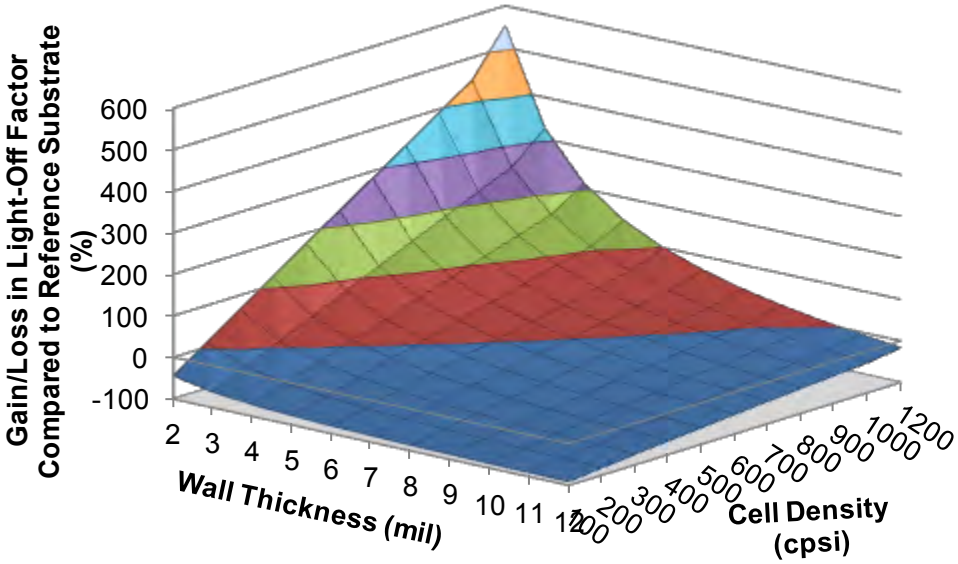


**Figure 4-2.** Effect of the cell density/wall thickness on the improvement or reduction in light-off factor compared to the reference substrate

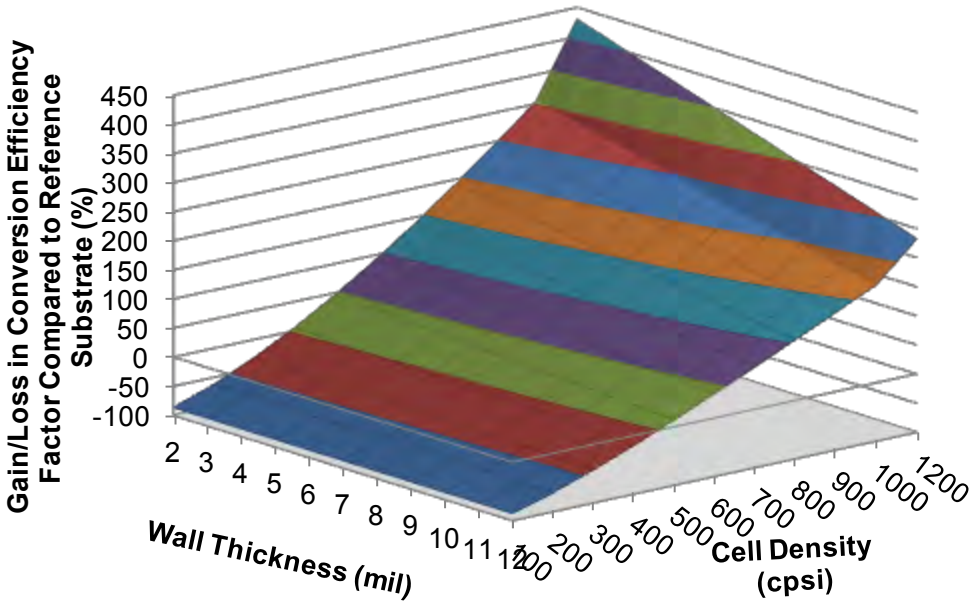


**Figure 4-3.** Effect of the cell density/wall thickness on the improvement or reduction in conversion efficiency factor compared to the reference substrate

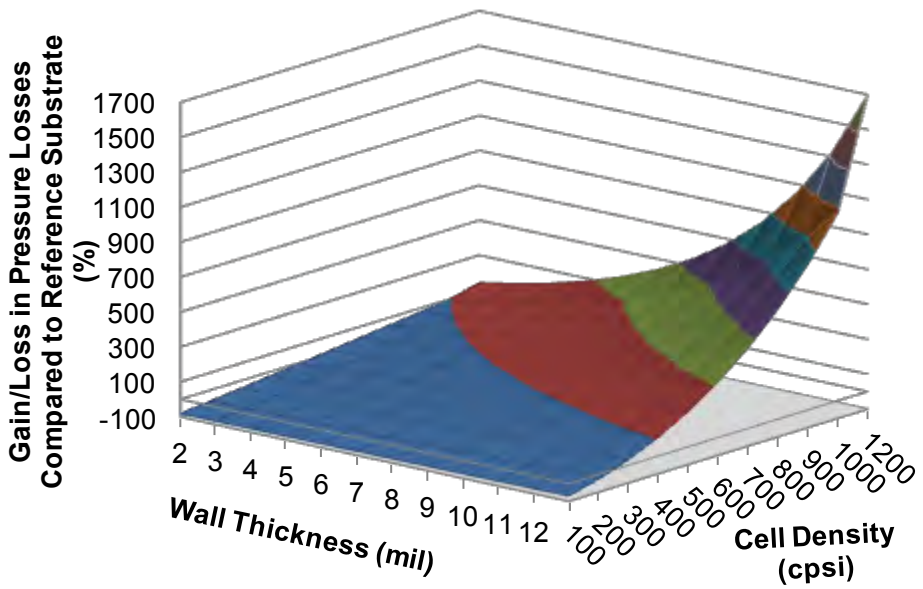


**Figure 4-4.** Effect of the cell density/wall thickness on the improvement or reduction in pressure losses compared to the reference substrate

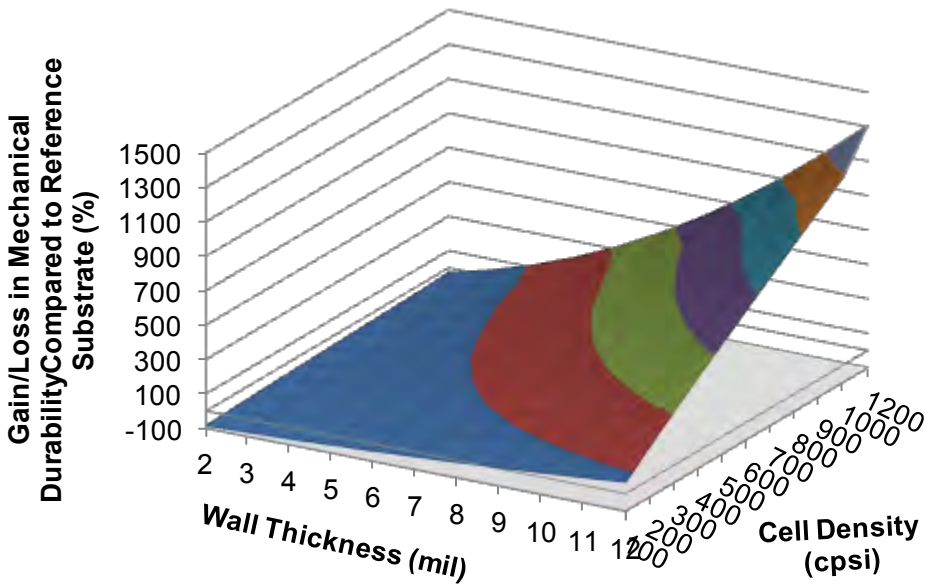


**Figure 4-5.** Effect of the cell density/wall thickness on the improvement or reduction in mechanical durability compared to the reference substrate

The results show that no substrate is the "ideal solution" meeting all the requirements simultaneously (i.e. high conversion efficiency, improved light-off and mechanical durability

with low pressure losses). A trade-off can be highlighted, as some factors such as light-off and conversion efficiency behave in an opposite way to pressure loss and mechanical durability, requiring some compromise. On one side, the priority can be given to a higher surface area for the conversion efficiency, with an improved light-off factor and insured mechanical strength with, however, increased pressure losses. Or, on the other side, the focus can be shifted on limiting the pressure losses and enhancing the mechanical strength while reducing the conversion efficiency and light-off performance.

Prior to choosing any substrate, the upper limit of the cell density was re-defined. Even though cell densities of up to 1200 cpsi are commercially available, the maximum cell density was intentionally limited to 600 cpsi. An increase in cell density reduces the cell hydraulic diameter, as shown in Figure 4-6, increasing the risk of soot plugging the channels. This would result in increased pressure losses and a reduced coated surface available for the conversion of the exhaust pollutants. This effect can be significant in our case as the oxidation catalyst is placed upstream of the particulate filter and receives untreated particulate emissions.

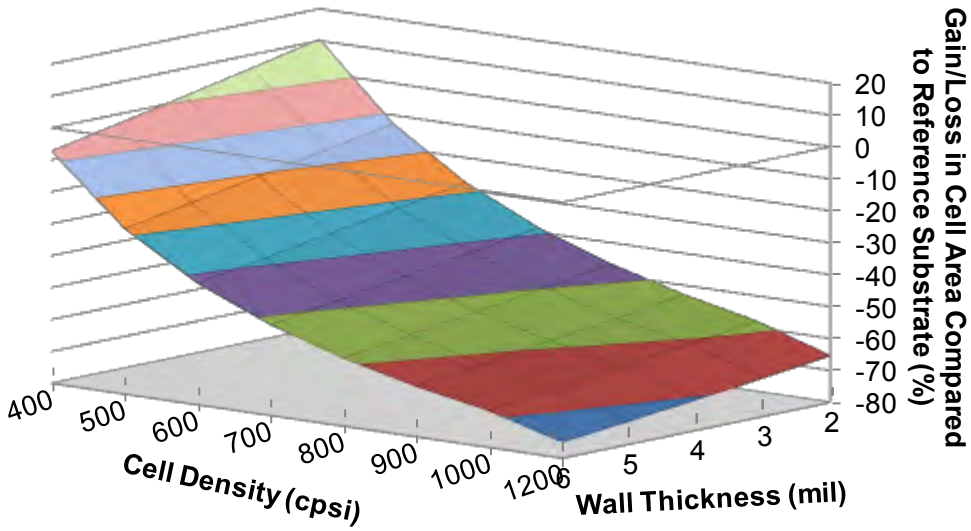


**Figure 4-6.** Effect of the cell density/wall thickness on the increase or decrease of the cell area compared to the 400/4 reference substrate

Table 4-4 summarises the cell density/wall thickness combinations that could be used to improve the catalysts properties previously developed, compared to the 400/4 substrate. For example, the 600/4 has an improved mechanical durability, conversion efficiency and light-off capacity compared to the reference 400/4 substrate but on the downside, leads to an increase in backpressure.

Based on the results of the theoretical study, several cell density/wall thickness configurations were chosen (Xs marked in Table 4-4) for their variety of enhanced properties and thermal behaviours, to be simulated during a driving cycle. To limit the manufacturing costs, the selected substrates were chosen among those commercially available. This also assures their durability as the manufacturer would have thoroughly tested that they can withstand the engineering constraints imposed during their use.

**Table 4-4.** Areas representing the improved properties (higher Conversion Efficiency Factor, Light-Off Factor, Mechanical Durability and lower Pressure losses) compared to the 400/4 substrate for different "cell density/wall thickness" configurations, with X marking the chosen substrates to be modelled

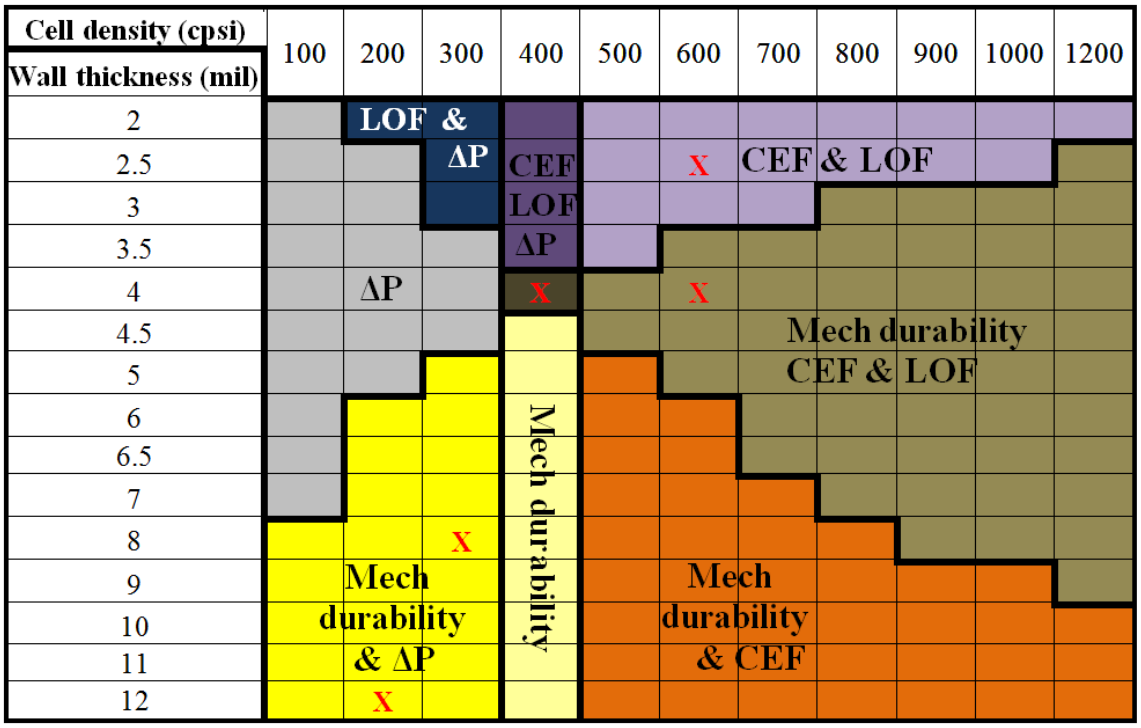

The properties of the selected substrates are summarised in Table 4-5.

**Table 4-5.** Chosen substrates with their improved or deteriorated properties compared to the reference 400/4 substrate, based on the theoretical equations results

| Substrate (cpsi/mil) | LOF | CEF | P loss | $\sigma_{2D\text{-}iso}$ | $\tau_{AV}$ | (1-OFA) |
|---|---|---|---|---|---|---|
| 200/12 | -83% | -68% | -27% | 97% | 289% | 88% |
| 300/8 | -61% | -39% | - 5 % | 61% | 160% | 56% |
| 400/4 | 0 % | 0 % | 0 % | 0 % | 0 % | 0 % |
| 600/4 | 60% | 81% | 58% | 14% | 30% | 13% |
| 600/2.5 | 162% | 89% | 35% | -29% | -50% | -28% |

To represent the thermal mass, the coefficient "1-Open Frontal Area" was introduced. The catalysts having the same substrate material and volume, the only aspect influencing their thermal mass is the quantity of material composing the substrate, which is directly proportional to the coefficient "1-OFA". It has to be noted that, in the case of the pressure losses and the "1-OFA" coefficient in Table 4-5, a negative value is preferred in order to limit the creation of non-desirable backpressure and limit the substrate thermal mass, respectively. For the remaining parameters, a positive value is desired. The selection of substrates includes high cell density catalysts (600/4 and 600/2.5) with expected good light-off and conversion factors. It also contains lower cell density catalysts with thicker walls (200/12 and 300/8) showing a reduced backpressure increase but deteriorated conversion and light-off properties.

These selected substrates were then modelled using Axisuite software to estimate their thermal behaviour, pressure and conversion efficiency under a diesel exhaust-type scenario (temperature, flow rate, emissions) and to eventually refine the catalysts selection before experimental investigation.

## 4.3. SIMULATION STUDY

### 4.3.1. Simulation of the Thermal Behaviour and Conversion Efficiency of the Selected Catalysts

#### *4.3.1.1. Cold Start – Warming Phases*

The high cell density/thin wall catalyst (600/2.5) provided good conversion efficiency for both CO and HCs emissions at the beginning of the simulated NEDC (lowest cumulative emissions of CO and THCs in Figure 4-7), as it reached its light-off temperature quicker than the other catalysts during peaks of engine CO emissions (Figure 4-8).

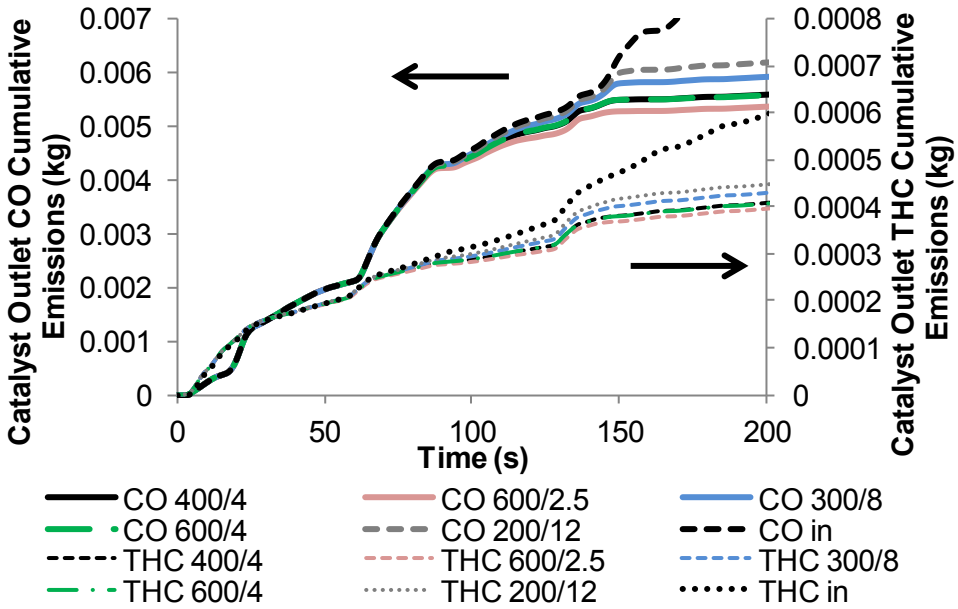


**Figure 4-7.** Effect of the cell density/wall thickness on the catalysts outlet CO and THC cumulative emissions during the first 200 seconds of the NEDC (light-off phase)

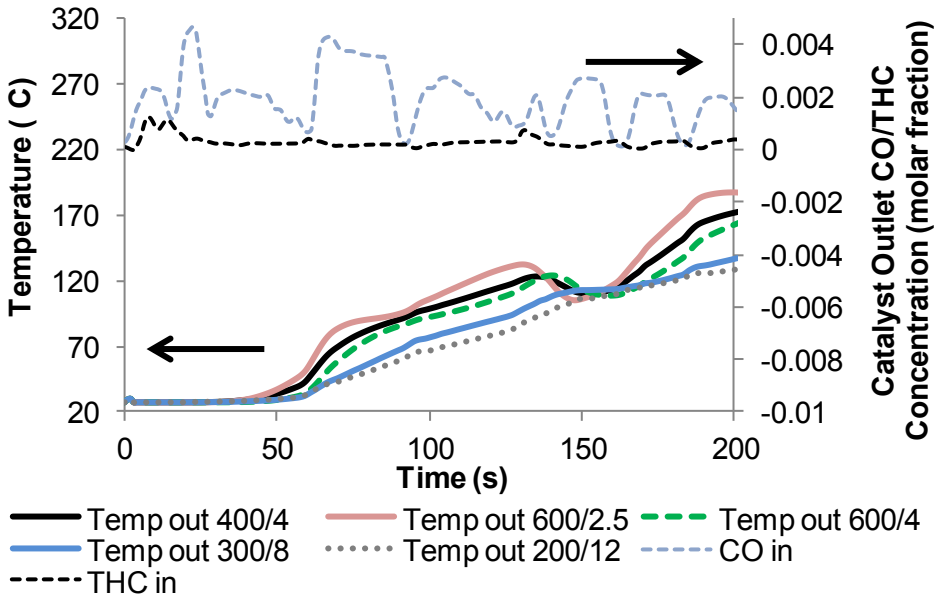


**Figure 4-8.** Effect of the cell density/wall thickness on the catalysts outlet temperature during the first 200 seconds of the NEDC (light-off phase) with the engine-out CO and HC emissions

On the contrary, as the wall thickness increased (comparison between 600/2.5 and 600/4), the conversion efficiency was slightly reduced as lower outlet temperatures were reached due to the increased thermal mass of the substrate. A reduction in the cell density while maintaining the same wall thickness (600/4 and 400/4) did not affect much the conversion efficiency of these catalysts. On the one hand, high cell densities promote the catalyst light-off by providing a greater "geometric surface area/hydraulic diameter" ratio, enhancing the mass and heat transfer for the conversion of CO and THCs. On the other hand, higher cell densities also translate also into a greater number of walls between the numerous cells, which can limit the catalyst warming capacity (Figure 4-8) due to the subsequent increase in material and therefore thermal mass (as illustrated with the "1-OFA" factor calculated in Table 4-5). These two effects seemed to compensate each other in this case, leading to comparable activity for 600/4 and 400/4 during the light-off phase. The 200/12 catalyst showed the highest CO and THC emissions due to its high thermal mass (low outlet temperature) and reduced surface of contact.

*4.3.1.2. Cooling Phases*

In a warmer part of the NEDC, between 225 and 275 seconds (Figure 4-9), the oxidation efficiency of the 600/2.5 was reduced as its cumulative CO and THC emissions increased and converged towards the ones from the other catalysts.

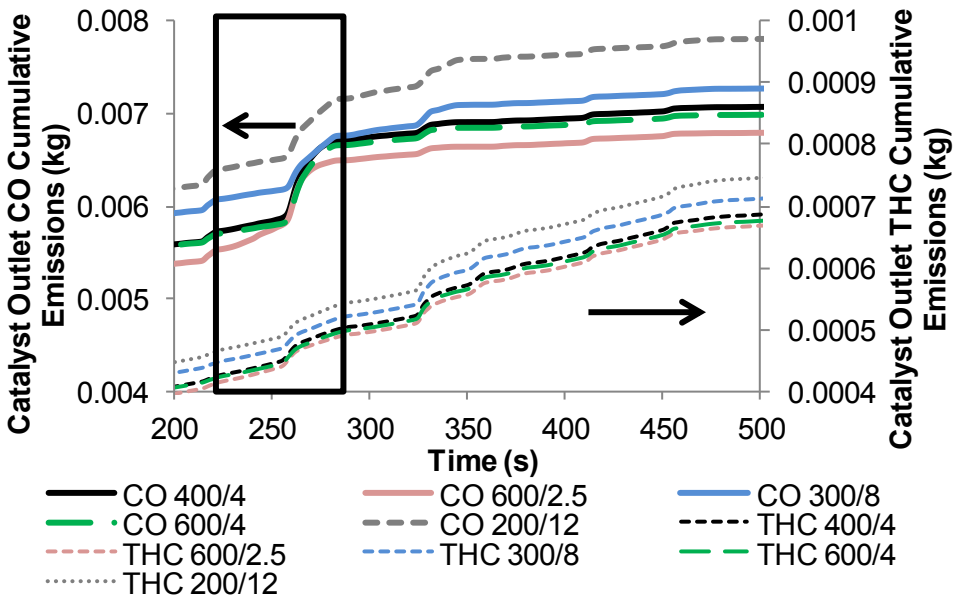


**Figure 4-9.** Effect of the cell density/wall thickness on the catalysts outlet CO and THC cumulative emissions during acceleration/deceleration phases of the NEDC

The catalyst outlet temperatures in Figure 4-10 showed that the 600/2.5 substrate cooled much quicker than the others, due to its lower thermal mass (thin walls) and increased surface area (high cell density), while peaks of CO emissions were produced.

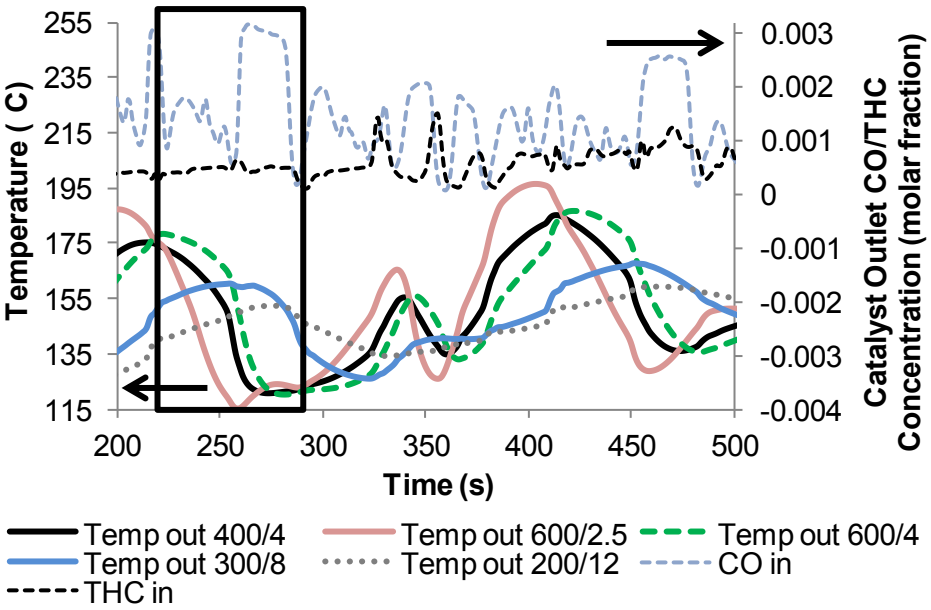


**Figure 4-10.** Effect of the cell density/wall thickness on the catalysts outlet temperature during acceleration/deceleration phases of the NEDC with the engine-out CO and HC emissions

Therefore, the quick light-off of this catalyst also led to a quick light-out (loss in activity) during deceleration phases, adversely affecting its conversion efficiency. This cooling effect can be even more pronounced in reality, as Axisuite thermal predictions were seen to behave in a less dynamic trend than the measured data (Figure 3-4). However, this loss in activity remained temporary as, beyond 275 seconds, the 600/2.5 catalyst conversion efficiency was ultimately restored, leading to the lowest level of CO and THCs at the end of the cycle.

Conversely, the thick walls of the 200/12 catalyst promoted thermal inertia and, during deceleration phases, maintained higher temperatures for longer compared to the other catalysts.

From these results, the 600/2.5 catalyst appeared to be the best candidate to replace the reference 400/4 from the conversion efficiency and thermal point of view. Unfortunately, as predicted in the theoretical study, the high cell density led to higher pressure loss (Table 4-6) that could degrade the engine power output and therefore increase the fuel consumption.

These Axisuite predicted pressure losses are in agreement with the estimations given in the theoretical study (Table 4-5). The Axisuite model uses the same assumptions as Equation 5 to estimate the friction losses, but it also takes into account the entrance/exit and the diffuser effects in its calculation of the total backpressure. This agreement shows that the assumptions used in Equation 15 (neglecting the entrance/exit effects) were acceptable for these conditions.

The results of the simulation showed that no substrate improved simultaneously all the properties of the 400/4 catalyst, similarly to the outcomes of the theoretical study. Table 4-6 provides an estimated gain in conversion efficiency over the NEDC for each catalyst, as predicted by the model.

**Table 4-6.** Summary of the conversion gain/loss and average backpressure increase over the NEDC for the alternative catalysts substrates compared to the reference 400/4 substrate

| | **600/2.5** | **600/4** | **300/8** | **200/12** |
|---|---|---|---|---|
| **CO/THC additional conversion (% of the reference 400/4)** | **4.6/2.2** | **2.1/2.8** | **-2.2/-3.4** | **-9.6/-10.9** |
| **mg of CO/THCs saved/km compared to reference** | 30.0/1.8 | 13.9/2.3 | **-14.1/-2.9** | **-63.3/-9.2** |
| **Average pressure increase (% of the reference 400/4 pressure)** | **32.5** | **59.1** | **-1.3** | **-21.6** |

Comparing the simulation results with the predictions from the theoretical study, the light-off factor seemed to particularly affect CO oxidation over the cycle, due to the high CO concentration recorded during the cold start (warming phase of the catalyst). THC emissions could be more related to the conversion efficiency factor. Most of these emissions were produced later during the cycle, when the available surface area became the limiting parameter (catalyst fully warm), as HC conversion can be affected by mass diffusion limitation (Johnson & Kittelson, 1994). This can be noticed with the comparable HC

emissions of the 600/2.5 and 600/4 and their similar CEF (Table 4-5). However, as THC oxidation is also dependent on CO oxidation completion, a reduction in CO oxidation could also directly affect THC conversion efficiency over the catalyst, as seen for 300/8 and 200/12.

To remedy the losses in temperature and activity during engine decelerations, the 600/2.5 catalyst could be combined with another catalyst that would compensate for these losses through heat storage. Moreover, this additional catalyst could also limit the pressure increase by reducing the length of the 600/2.5. The outcome would be a combination of two catalysts that would partially compensate for each other's drawbacks, increasing the conversion efficiency over a wider operating temperature window, while minimising the backpressure increase of the system.

### 4.3.2. Two-Catalyst Configurations

The second part of this study focuses on the use of two-catalyst configurations and compares their performance with the 400/4 reference catalyst, using Axisuite and the same input data as used in the previous single-catalyst study. The first catalyst of the configuration was selected with thin walls and a high cell density. This should promote the low-temperature activity due to the low thermal mass of the substrate (thin walls) enhancing its warming capacity, the increased surface of contact between the exhaust gas and the catalytic coating (high cell density) and the smaller channel hydraulic diameter promoting mass and heat transfer. The second brick was selected to store heat during the warming process and restore it during the cooling phases to reduce the possibility of catalyst light-out (loss of activity).

The aim of the two-catalyst configuration is to improve the overall conversion efficiency without modifying the external dimensions, i.e. diameter and total length. This allows a straightforward replacement of the reference catalyst and isolates the effect of varying the

cell density and wall thickness on the catalyst thermal behaviour. Shortening the length of the catalysts composing the two-brick configurations does not have a significant effect on their thermal durability. A shorter catalyst provides a more homogeneous axial temperature distribution and reduces the maximum temperature gradients recorded during the catalyst use. The new dimensions of the substrates led to a length/diameter ratio of 0.6, which is considered to be the minimum ratio required for a catalyst to withstand catalyst centre temperature of 950°C (Gulati *et al.*, 2002). Therefore, the thermal durability of the new configurations was still maintained. The mechanical durability of the shorter substrate would remain unchanged as it is essentially dependent on the cell density and wall thickness of the substrate, rather than its external dimensions (Equation 7 and Equation 9).

The first substrate was chosen to be a 600/2.5 substrate as it was the quickest to warm up and reached higher temperatures, showing the best CO emission reduction and a significant THC conversion over the NEDC in the first part of this study (Table 4-6). The 600/4 catalyst would have been more interesting for its higher THC conversion but it would have led to excessive backpressure. The rest of the study focuses on the choice of substrate for the second catalyst.

#### *4.3.2.1. Selection of the Second Catalyst*

The important characteristics of the second substrate are its higher thermal mass and limited backpressure increase while maintaining a significant activity. Following these design criteria, thick wall substrates with different cell densities were selected to find the best compromise. Once again, the selected substrates were chosen among those commercially available. In addition, a metallic substrate was also selected as a second catalyst. Metallic substrates are preferentially selected due to their capacity to provide higher cell densities and reduced wall thicknesses while maintaining a greater mechanical strength compared to their ceramic counterparts. While the metallic material shows high thermal conductivity, its higher

density also makes it a good candidate to store heat as a second brick. Different cell density and wall thickness configurations were investigated for the metallic substrate and the results presented here are for the most promising combination. The metallic catalyst was modelled in Axisuite using triangular cells, as the sinusoidal shape used in these substrates is not currently available in the software. The triangular cell shape is expected to lead to a reduced open channel area and coated surface, compared to the sinusoidal one, reducing the light-off capacity and the conversion efficiency.

The results of the simulation over the NEDC show that the two-catalyst configurations led to greater or similar conversion efficiencies, especially for CO, relatively to the 400/4 catalyst (Figure 4-11), with lower pressure increase compared to the 600/2.5 catalyst (Figure 4-12).

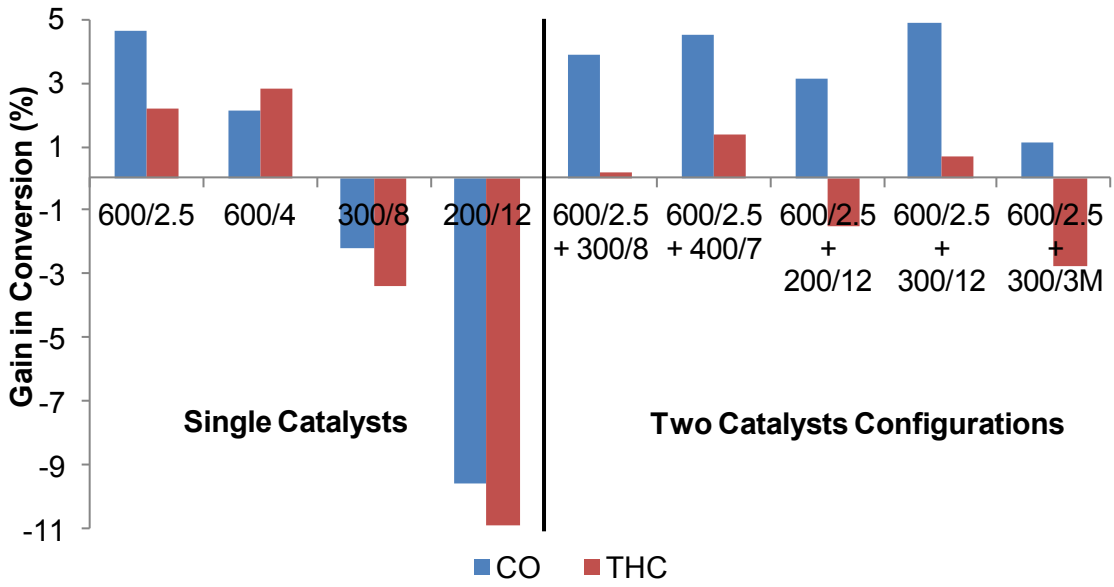


**Figure 4-11.** Comparison of the gain in total conversion efficiency when replacing the reference 400/4 catalyst by a single catalyst or a two-catalyst combination

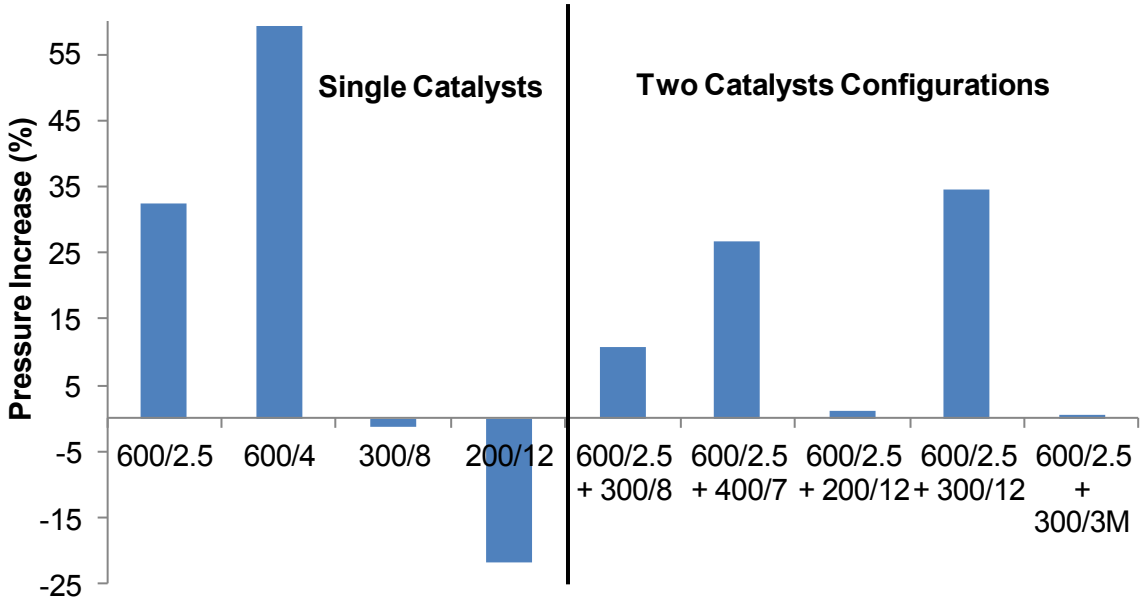


**Figure 4-12.** Comparison of the pressure increase when replacing the reference 400/4 catalyst by a single catalyst or a two-catalyst combination

The combinations that show the best compromise for the different parameters are the 600/2.5 + 300/8 and 600/2.5 + 200/12, the former leading to higher pressure losses but greater CO and THC conversion efficiency. The 600/2.5 + 400/7 and 600/2.5 + 300/12 showed higher CO and THC conversion but led to undesirably high pressure losses. The combination with a metallic catalyst (600/2.5 + 300/3M) showed limited conversion gains compared to the reference one. This required further assessment through the experimental tests as the approximation with the triangular cell shape could lead to erroneous estimations.

While the efficient warming capacity of the first brick was previously demonstrated, Figure 4-13 shows a cooling phase for the second catalysts from the chosen combinations. While the temperature of the 600/2.5 catalyst significantly dropped, the outlet temperature from the two-catalyst combinations remained higher during peaks of CO emissions (Figure 4-13), thanks to the higher thermal mass of the second catalyst. During warming phases, the two-brick configurations showed lower outlet temperatures, compared to the 600/2.5 catalyst

but higher local temperatures would still be expected in the first brick, maintaining a certain activity during these phases.

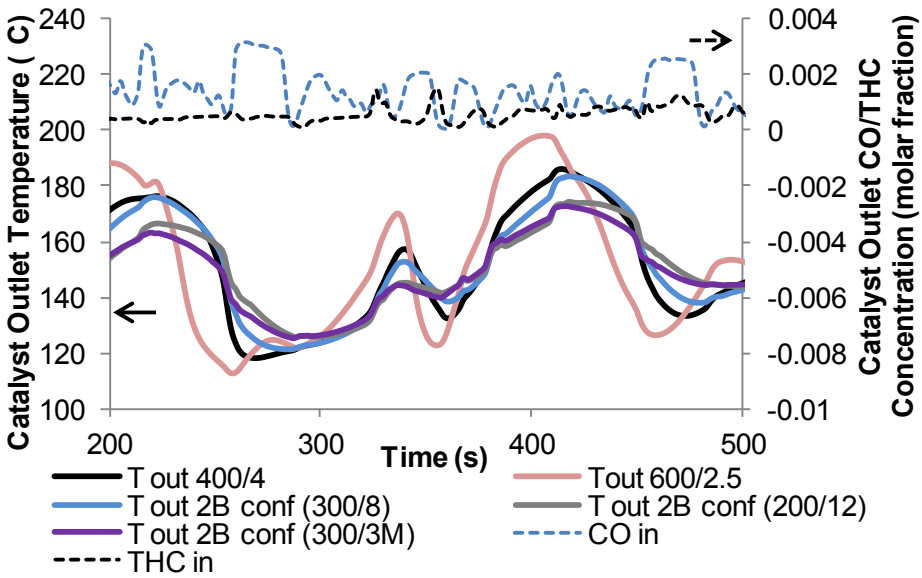


**Figure 4-13.** Effect of the two-brick configurations (2B) on the catalysts outlet temperature during acceleration/deceleration phases of the NEDC, compared to the 400/4 and 600/2.5 single catalysts, with engine-out CO and HC emissions

The enhanced thermal behaviour of the two-catalyst configurations can be directly seen on the cumulative CO and THC emissions (Figure 4-14).

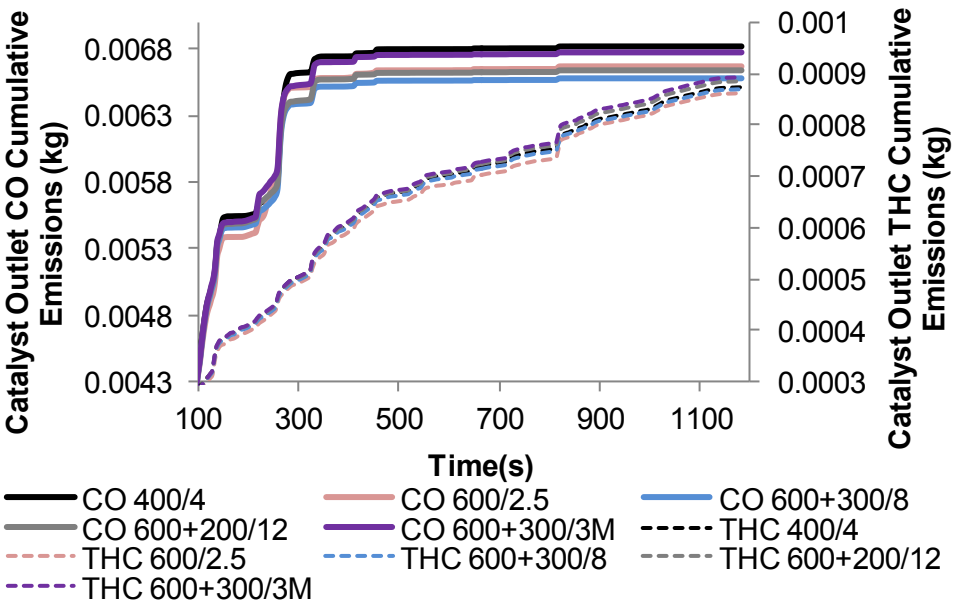


**Figure 4-14.** Effect of the two-brick configurations on the catalyst outlet CO and THC cumulative emissions compared to the 400/4 and 600/2.5 single catalysts over an NEDC

Between 150 and 200 seconds, the outlet level of CO from the two-catalyst configurations was lower than that for the 400/4 catalyst, due to an improved light-off capacity (first brick). Between 200 and 300 seconds, the significant CO emission increase noticed for the 600/2.5 (due to the quick cooling), was now replaced by a gentler increase for the two-catalyst configurations, ultimately resulting in lower CO cumulative emissions.

Compared to CO, the gain in THC conversion was less obvious. From Figure 4-14, the two-catalyst configurations showed limited improvement in the conversion efficiency compared to the reference 400/4 catalyst. The reduced surface area due to the triangular cells of the metallic substrate in the 600 + 300/3M led to the THC emissions to be slightly higher than the reference catalyst. As the catalysts became warmer, the differences in THC emissions with the 600/2.5 reduced, due to a greater geometric surface area readily available for oxidation, at the end of the cycle. The differences in CO and THC conversion efficiency between the use of the 200/12 and 300/8 as a second catalyst are primarily due to the higher contact area and lower hydraulic diameter in the 300/8 substrate. Another factor is the higher thermal mass of the 200/12 substrate, as it tended to reach lower temperatures. It also required more time to warm again, decreasing the conversion efficiency during re-acceleration phases. The thermal mass required for the second catalyst needs to be defined with a compromise between the heat storage necessary during deceleration phases and the light-off performance and contact area available for hydrocarbon conversion.

To fully illustrate the improved thermal behaviour of the two-catalyst configurations during the cooling phases (compared to the 600/2.5) and warming periods (compared to the 400/4), the wall temperature distribution within the substrates was generated using Axisuite.

Figure 4-15 and Figure 4-16 show the improvement in the warming and cooling capacity respectively, of the two brick configuration compared to a single catalyst, with the bottom of

the plot representing the centre line and the top, the periphery of the monolith (only half of the catalyst diameter is shown as an axial symmetry of the temperature profile was assumed).

During the warming phase (Figure 4-15), the first substrate being smaller and composed of thin walls (lower thermal mass) reached higher local temperatures compared to the reference 400/4 catalyst.

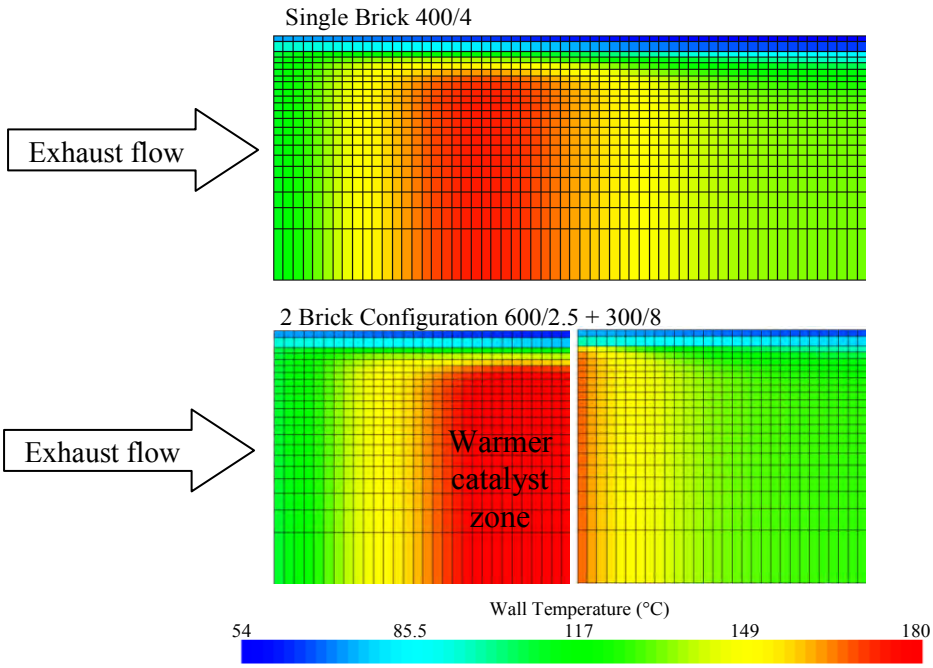


**Figure 4-15.** Temperature distribution in the catalysts (400/4 reference catalyst versus two-brick configuration) at the 290$^{th}$ second of the NEDC (warming phase)

During the cooling phase (Figure 4-16), the second catalyst retained more heat and reached higher temperatures compared to the 600/2.5 single part. This second aspect can be useful during deceleration phases and at idle, when cooler exhaust gas flows through the catalyst. To a lesser extent, it can also be effective when the car is stopped and restarted after some time as the higher thermal mass of the second catalyst would allow it to remain warmer for longer.

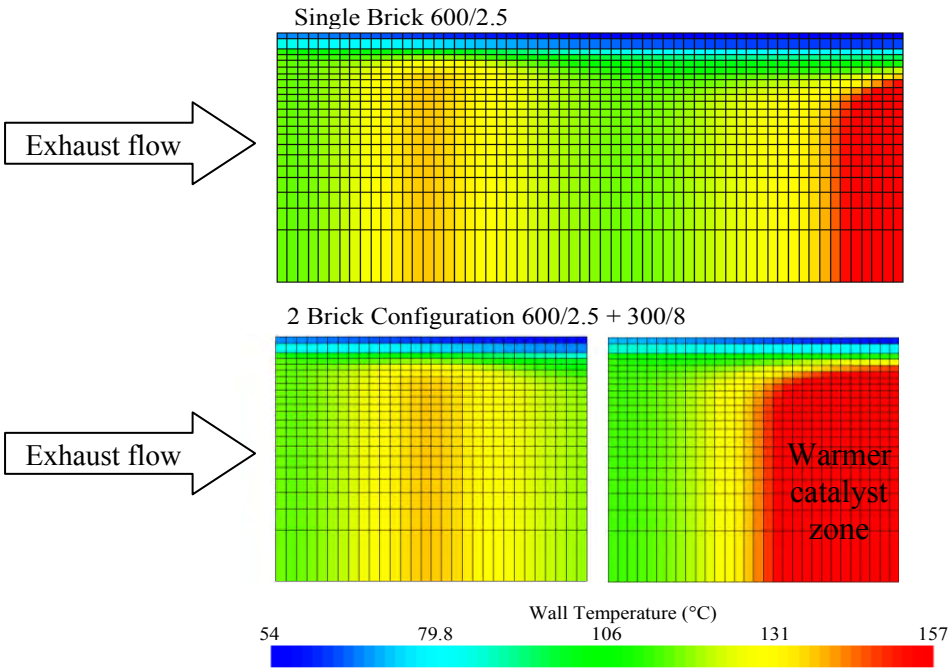


**Figure 4-16.** Temperature distribution in the catalysts (600/2.5 versus two-brick configuration) at the 230$^{th}$ second of the NEDC (cooling phase)

The two-catalyst configurations show the potential for lower CO and THC emissions without modifications of the external dimensions. The final choice of combination is motivated by either the priority to reduce the emissions or focus on limiting the increase in backpressure. It has yet to be determined, as part of the aftertreatment system requirements, if it is worth increasing the pressure loss by 11% to allow a further reduction of 3.9% in CO and 0.2% in THC emissions over the NEDC (choice of the 300/8 substrate as a second brick) or limiting at any cost the backpressure increase while reducing the gain in conversion efficiency (choice of the 200/12 substrate). From this perspective, the 400/4 substrate seemed to remain a good compromise in terms of conversion efficiency and pressure losses.

Finally, in order to optimise the dimensions, the simulation was repeated with a reduction of the original gap between the two catalysts from 10 mm to 5 mm, increasing the length of the second substrate by 5 mm. According to the results presented in Table 4-7, this allowed further improvements in the conversion efficiency with a slight increase in the pressure losses (longer second catalyst) compared to the reference substrate.

**Table 4-7.** Summary of the conversion gain/loss and average backpressure increase over the NEDC for the two-catalyst configurations with a 5 mm gap compared to the reference 400/4 substrate

| | **600/2.5 + 300/8** | **600/2.5 + 400/7** | **600/2.5 + 200/12** | **600/2.5 + 300/12** | **600/2.5 + 300/3M** |
|---|---|---|---|---|---|
| **CO/THC additional conversion (% of the reference 400/4)** | **4.5/1.0** | **5.1/2.1** | **3.7/-0.8** | **5.7/1.3** | **1.8/-2.0** |
| **mg of CO/THCs saved/km compared to reference** | 27.8/0.8 | 31.5/1.6 | 23.3/-0.7 | **35.2/1.0** | **11.3/-1.6** |
| **Average pressure increase (% of the reference 400/4 pressure)** | **+ 14.1** | **+ 30.2** | **+4.6** | **+ 37.9** | **+2.6** |

*4.3.2.2. $NO_2$ Production from the Two-Brick Configuration*

Having established the potential gain in terms of CO and THC conversion efficiency, another aspect of the DOC that needs investigating is its capacity to oxidise NO to produce $NO_2$ which can be used for passive continuous regeneration of the downstream DPF or promote the fast-SCR reaction. The behaviour regarding $NO_2$ production was studied for the optimal configuration 600/2.5 + 300/8 and compared to the reference catalyst 400/4. The model used in Axisuite took into account NO to $NO_2$ oxidation as well as hydrocarbons selective reduction of $NO_2$ to NO (Lafossas *et al.*, 2011).

The higher temperatures reached in the two-brick configuration and the improved "geometric surface area/hydraulic diameter" ratio from the first catalyst promoted NO oxidation (Figure 4-17), leading to a 12 % increase in $NO_2$ production over the cycle.

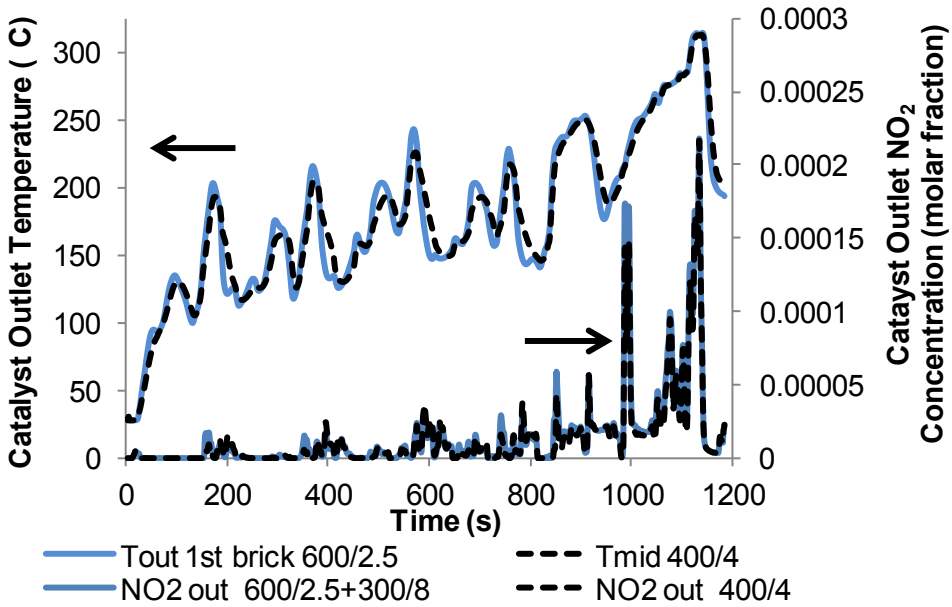


**Figure 4-17.** Effect of the two-brick configuration 600/2.5 + 300/8 on $NO_2$ production, compared to the reference 400/4 catalyst, during an NEDC

The results of the Axisuite simulation allowed the selection of promising catalysts to be used in the two-brick configurations (600/2.5, 300/8 ceramic and 300/3 metallic). The combinations created were submitted to experimental tests with genuine diesel exhaust gas to investigate their thermal behaviour and activity at various engine operating conditions.

## 4.4. EXPERIMENTAL STUDY OF THE TWO-BRICK CONFIGURATIONS

### 4.4.1. Thermal Behaviour of the Two-Brick Configurations with Genuine Diesel Exhaust Gas

Engine Start and Warming Phases

During the cold-start (Figure 4-18), the 600/2.5 catalyst showed a quick thermal response due to its low thermal mass and remained on average 5°C warmer at the end of the warming phase, compared to the other combinations.

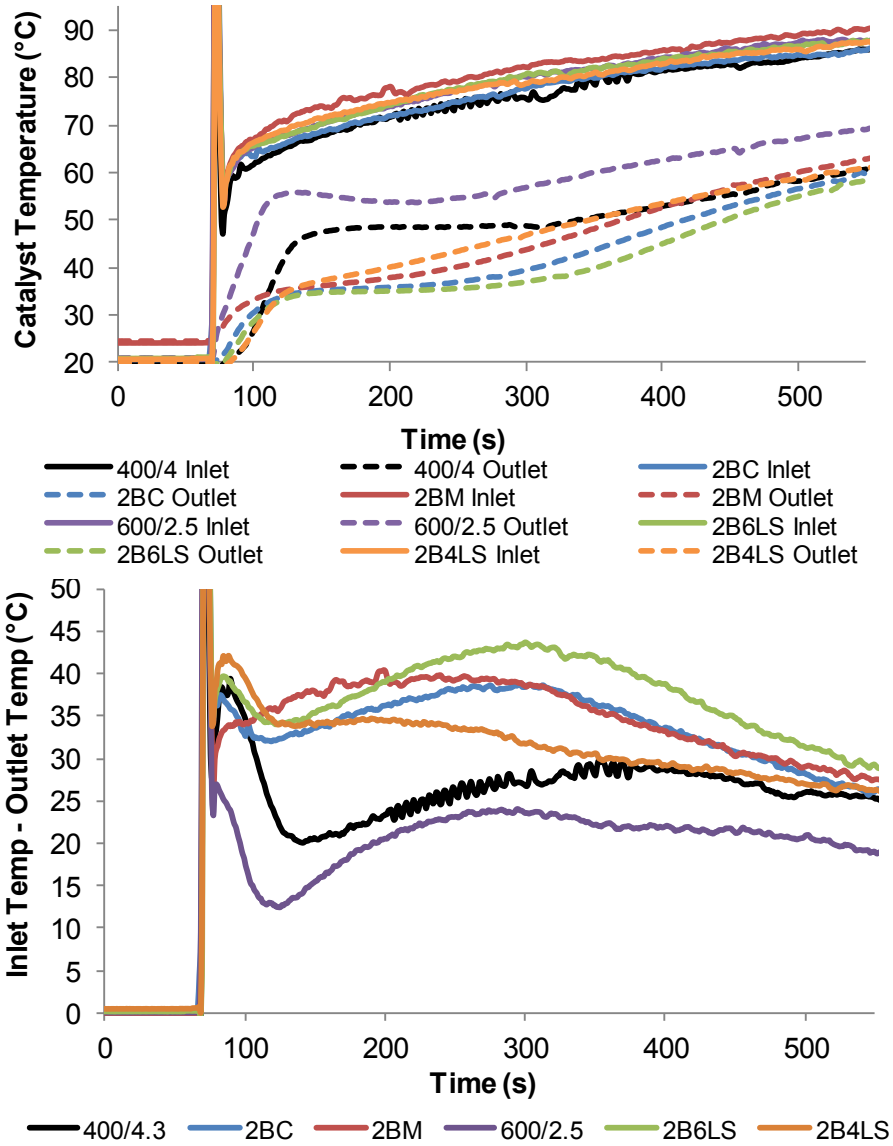


**Figure 4-18.** Catalysts inlet and outlet temperatures (top) and temperature losses (bottom) for the different combinations, during the warming phase of the experiment

The warming-up delay and lower temperatures recorded at the outlet of the two-brick combinations showed the effect of the second brick storing heat. This is especially noticeable for the 2B6LS, as its higher thermal mass led to greater temperature losses over the catalyst. The temperature losses over 2BM and 2BC were similar, which showed that not only a lower thermal mass (2BC) but also higher material heat conductivity (2BM) could promote the catalyst warm-up. On average, the two-brick configurations showed greater temperatures losses during the warming phase compared to the reference catalyst.

For the other warming phases of the experiment, the temperature losses for the 400/4 and the two-brick configurations were similar, with the configurations with a second metallic brick showing slightly higher temperature losses (up to an additional 5°C), as a direct effect of their higher thermal mass. Moreover, at higher temperatures, the greater thermal conductivity of the metallic substrate could spread the exhaust heat to the whole catalyst while the ceramic substrate would confine the heat within the centre, where most of the exhaust gases are concentrated and therefore reach locally higher temperatures (Jasper *et al.*, 1991). Despite the low temperatures recorded at the outlet of the two-brick configurations, the first catalyst (600/2.5) would still be reaching higher local temperatures than the reference one, due to its lower thermal mass.

Exothermic Events

When the exhaust gas temperature increased from 160°C to 255°C (Table 4-3), the outlet temperature of the catalyst configurations rose rapidly, reaching higher temperatures than at the inlet. These events occurred twice during the experiment, each time when the inlet temperature was reaching over 250°C (catalyst inlet temperature increase from 160°C to 255°C and from 180°C to 255°C).

*First Exothermic Event*

During the first exothermic event, the measurement of the exhaust gas concentration at the outlet of the 400/4 catalyst showed the release of hydrocarbons presumably condensed or stored in the zeolites composing the washcoat (Figure 4-19). Their release was followed by a significant increase in the catalyst outlet temperature, which exceeded the inlet temperature. This production of heat within the catalyst was accounted for by the exothermic oxidation reaction of the high concentration of released hydrocarbons.

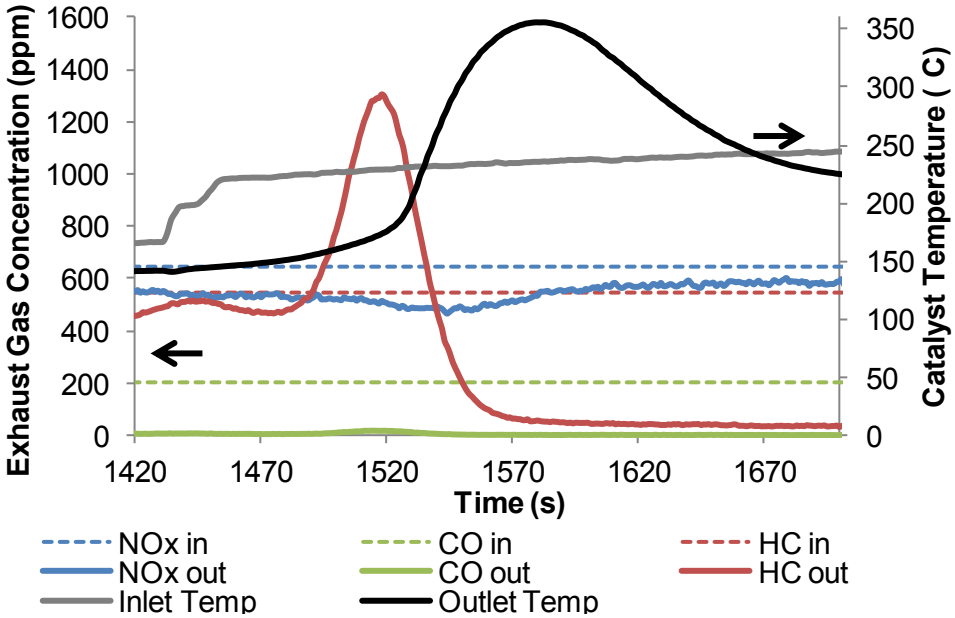


**Figure 4-19.** Evolution of the exhaust gas concentration and catalyst temperature during the release of the stored hydrocarbons in the 400/4 catalyst

Simultaneously, a slight reduction in $NO_x$ emissions was recorded while $N_2O$ increased at the catalyst outlet. This appeared to be caused by some released hydrocarbons momentarily reducing $NO_2$ (Figure 4-20), until they start oxidising using exhaust oxygen, at which point $NO_2$ outlet concentration increased again.

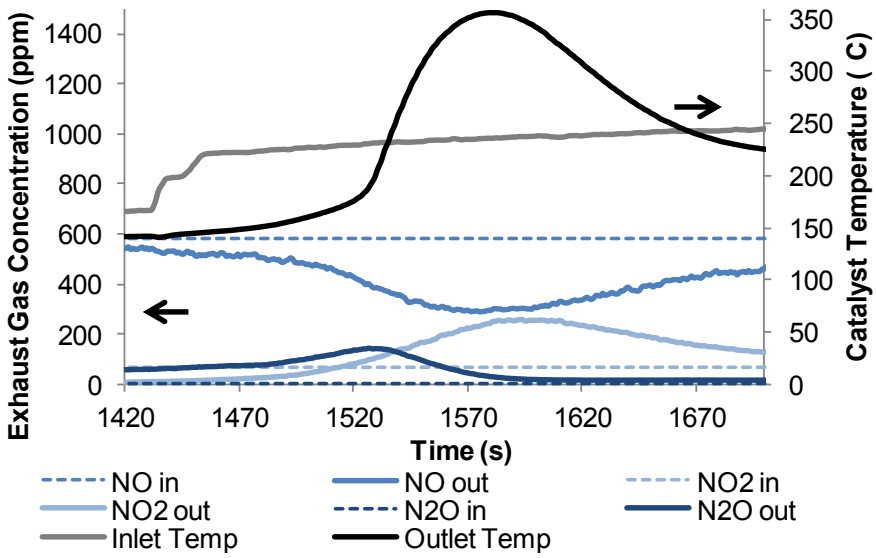


**Figure 4-20.** Evolution of the $NO_x$ exhaust concentration and catalyst temperature during the release of the stored hydrocarbons in the 400/4 catalyst

In terms of thermal behaviour during this event (Figure 4-21), the lower temperature peak reached by the 600/2.5 short catalyst compared to the reference 400/4 showed that the heat production was more promoted by an increased surface of contact (longer 400/4) than by a reduced thermal mass (600/2.5). A larger coated surface area could allow the storage and oxidation of a greater concentration of hydrocarbons, which, once released and oxidised, lead to a greater heat production.

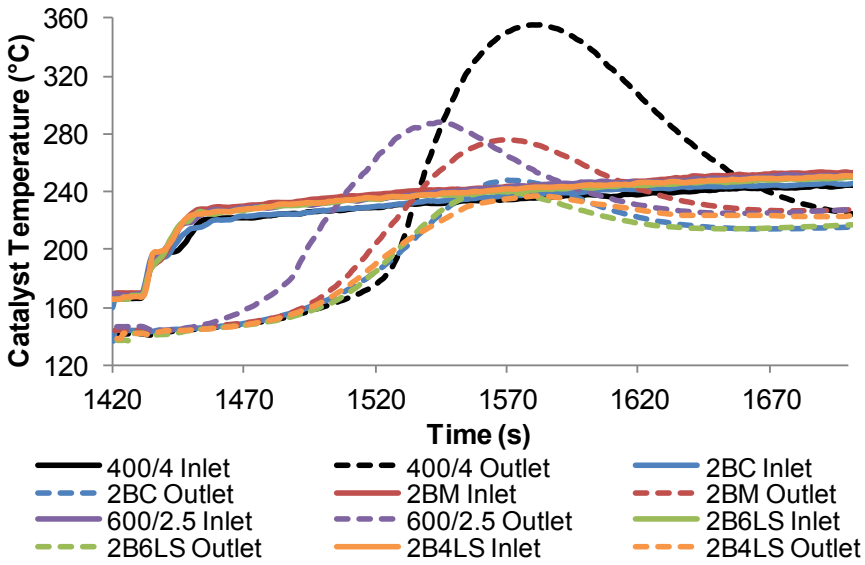


**Figure 4-21.** Catalyst inlet and outlet temperatures for the different combinations during the first exothermic event

Regarding the two-brick configurations, they reached lower peaks of temperature and showed a delay in the temperature increase. This is due to the higher thermal mass of the second brick combined with a lower cell density (reduced coated area), limiting the heat released at the catalyst outlet. It could be hypothesised that the second brick would benefit from the exothermic event created within the first brick to accumulate and store some of the heat produced. The higher thermal mass of the two-brick configuration with a metallic second brick (2BM) seemed to be compensated by its greater surface of contact (Table 4-2), as it reached the third highest peak of temperature and remained warmer for longer compared to the other two-catalyst configurations. Regarding the other configurations (2BC, 2B4LS and 2B6LS), their peaks of temperature remained limited and, as a consequence, they quickly cooled. While the lower cell density of the second brick in the 2BC configuration could explain the limited exothermic event, the LS configurations are expected to show a greater coated surface due to their advanced channel design. However, their higher thermal mass and the turbulence enhancing heat transfers between the walls and the cooler exhaust gases in the channels could have limited the local production of heat within the LS catalysts.

*Second Exothermic Event*

During the second exothermic event, no temperature peak was recorded for the 400/4 catalyst, while some peaks were still recorded for the other catalysts (Figure 4-22).

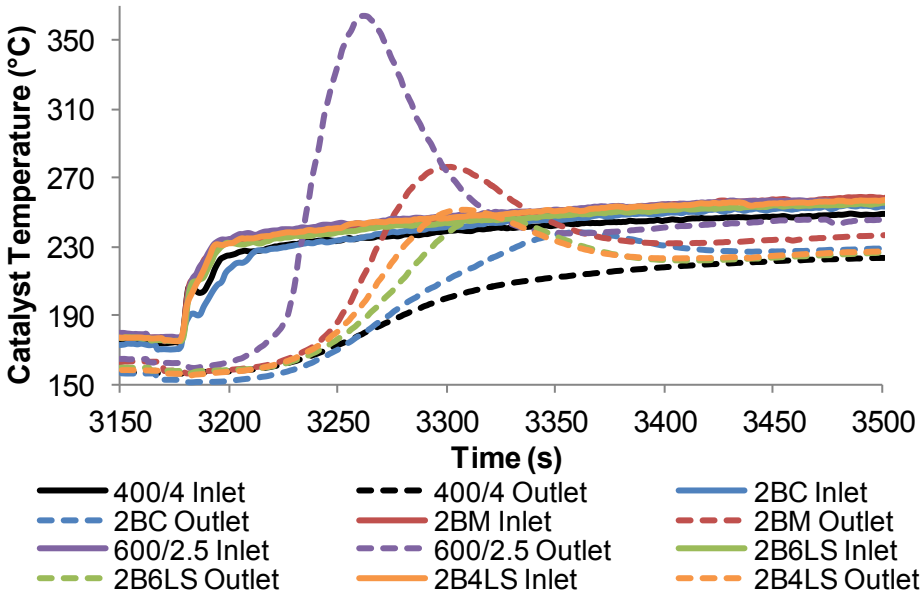


**Figure 4-22.** Catalyst inlet and outlet temperatures for the different combinations during the second exothermic event

This could be due to the 400/4 catalyst retaining more heat during the cooling between the two exothermic events (higher thermal mass compared to the first brick 600/2.5) and therefore sustaining the hydrocarbon oxidation. In contrast, the 600/2.5 greater peak of temperature during this second exothermic event shows that its lower thermal mass and higher surface of contact led to a cooling of the catalyst, allowing hydrocarbons storage to take place again before it reached the temperature required for their release. The slight temperature increases recorded for the two-brick configurations would therefore be due to the activity of the first brick. The higher peaks of temperature reached by the 600/2.5 and LS configurations compared to the first event could be due to the whole catalysts being on average warmer at the beginning of this second event which would promote greater exothermic reaction rates and heat production once the hydrocarbons are released. On the

opposite, the limited peak of temperature recorded for the 2BC could be explained by the lower surface of contact and heat conductivity of the second brick, reducing the cooling effect from the exhaust gas and preventing its light-out, similarly to the 400/4 catalyst.

The analysis of these phenomena provides an insight into the catalyst thermal behaviour in case of a sudden temperature increase, comparable to a lower extent, to those encountered in the DOC during DPF active regeneration events, when a high concentration of hydrocarbons is fed to the catalyst through post-injection to raise the exhaust gas temperature supplied to the downstream DPF.

These exothermic events took place in this experiment due to a long low-temperature period during which it is assumed that a significant quantity of HCs were stored in the zeolites. The accumulation of hydrocarbons in the zeolites would be more limited during genuine driving conditions as the exhaust gas would reach more often and quickly the threshold temperature required for the release of HCs, limiting the heat produced by their oxidation.

Cooling Phases

During the cooling phases (Figure 4-23), similarly to the simulations, the 600/2.5 showed a quick decrease in temperature. This is in agreement with the hypothesis that, between the two exothermic events, the temperature in the 600/2.5 catalyst decreased below the threshold required for the release of hydrocarbons, promoting their storage and release again later, as suggested in the exothermic event analysis. The configurations using metallic bricks had the lowest temperature losses during the cooling phases. The higher thermal mass of their second bricks efficiently retained the heat, compensating for the cooling of the first brick and maintaining higher outlet temperatures for longer. Despite its lower thermal mass, the cooling

behaviour of the 2BC was similar to the others, possibly due to the lower contact surface area, thicker walls and lower ceramic heat conductivity, reducing the cooling effect from the exhaust gas.

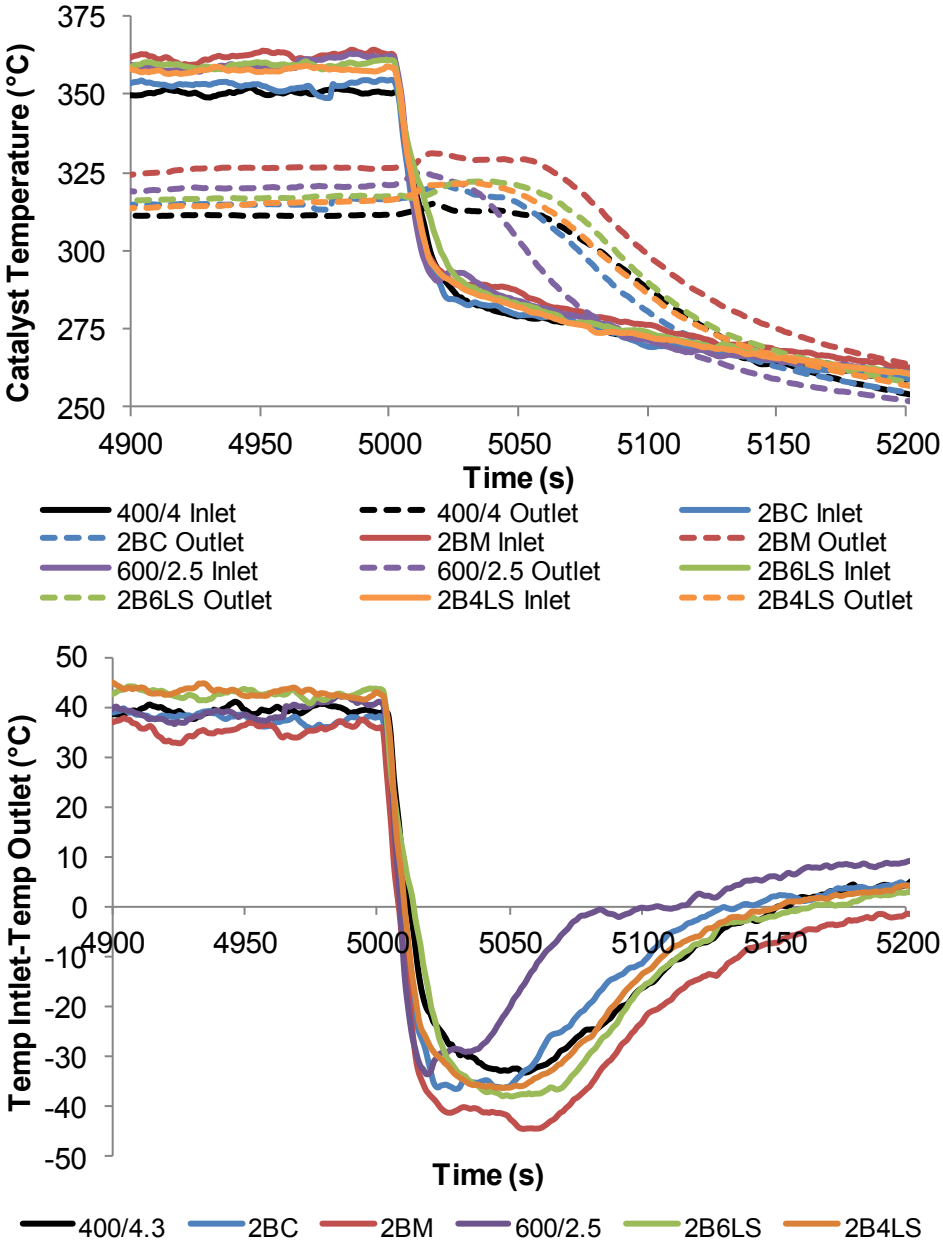


**Figure 4-23.** Catalyst inlet and outlet temperatures (top) and temperature losses (bottom) for the different combinations during a cooling event

Once the engine was stopped, the catalyst outlet temperatures were still monitored to investigate the cooling behaviour of the configurations at rest, with no exhaust gas flow (Figure 4-24).

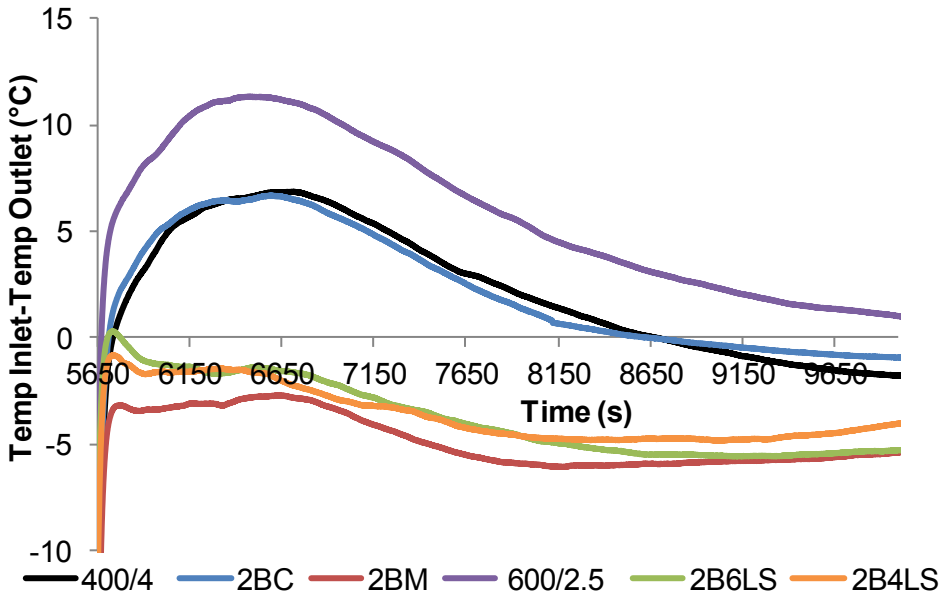


**Figure 4-24.** Temperature losses over the combinations of catalysts during a cooling at rest (no exhaust flow)

The outlet temperatures of the configurations with a metallic brick remained few degrees higher than their inlet temperatures for over three hours. This highlights the efficiency of the second brick in restoring the heat previously stored, as well as the higher heat conductivity of the metallic substrate which allowed a more homogeneous temperature distribution over the full length and diameter of the substrate. While the outlet temperature was only few degrees higher than the inlet, it can be assumed that the local temperature inside the catalysts would remain greater (slower cooling in the catalyst). This could be useful during stop/start periods, when the engine is automatically shut-down for few minutes at a traffic light. At the restart, these two-brick configurations could reach a greater oxidation activity from locally higher temperatures.

Steady-State Conditions

The variations in catalyst inlet temperatures during the steady-state engine operating phases were comparable for all the configurations (maximum of +/-1.5°C for temperatures below 300°C and up to +/-3.5°C at higher temperatures). The temperature losses over the catalyst combinations during these steady-state conditions (Figure 4-25) varied depending on the previous phase (cooling or warming).

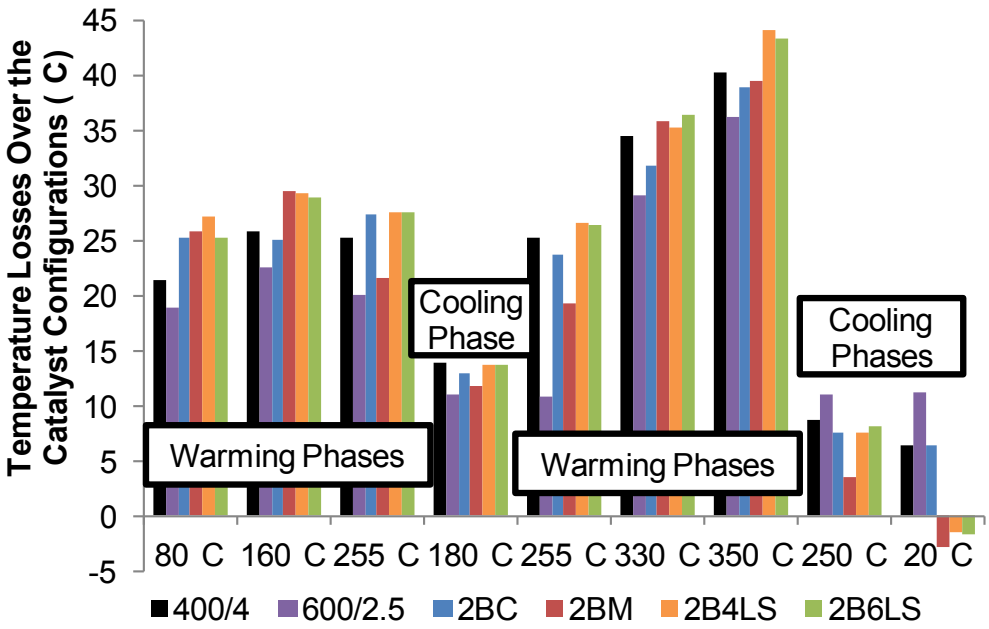


**Figure 4-25.** Temperature losses over the various combinations of catalysts during the steady-state phases of the experiment

After warming phases, at higher temperatures (250-350°C), the temperature losses were similar over the different configurations as the whole catalyst would eventually be more homogeneously warm, making the thermal and physical properties of the substrates less critical for their thermal behaviour. Moreover, the engine operating conditions used to reach these high temperatures required an increase in the exhaust flow rate that would promote a more even distribution of the exhaust heat over the full catalyst and therefore homogenise its temperature.

During the steady-state phase after the cooling from 255°C to 180°C, similar temperature losses were recorded over the configurations, showing a limited effect from the second brick restoring heat at this condition. However, after the cooling from 350°C to 250°C, at the end of the experiment, lower temperature losses were recorded for the two-brick configurations. This demonstrates that the second brick requires a certain period of heating and temperature level to accumulate and restore enough heat during a subsequent cooling phase.

### 4.4.2. Conversion Efficiency

#### *4.4.2.1. Carbon Monoxide (CO)*

The CO oxidation efficiency of the different catalysts was measured at similar inlet temperatures (Figure 4-26), which is critical for the comparison of the activity as it is kinetically limited at low temperatures and can be easily influenced by a variation in the exhaust gas temperature.

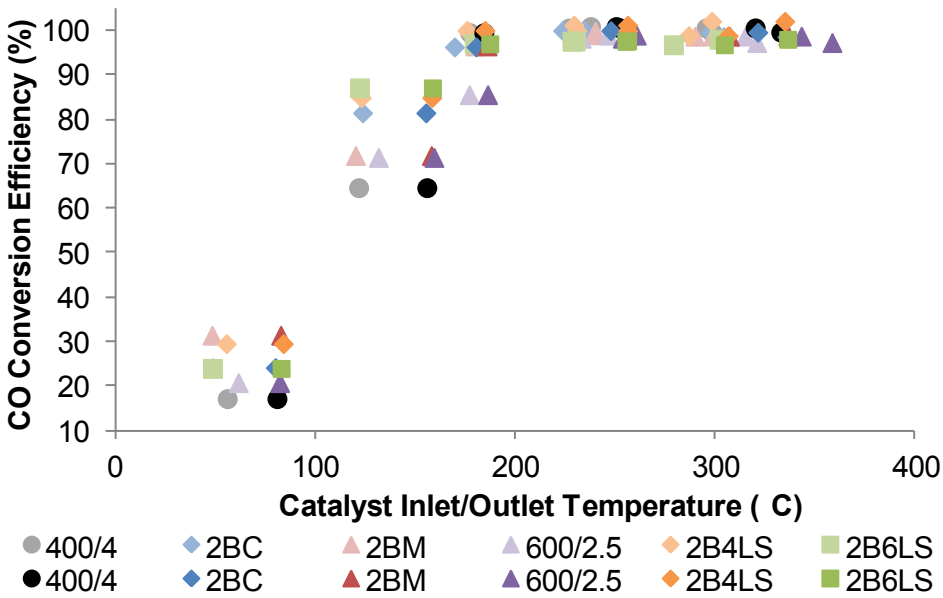


**Figure 4-26.** CO conversion efficiency for the combinations of catalysts based on their inlet (bright symbols) and outlet temperatures (faded symbols)

The first brick (600/2.5) accounted for the majority of the greater conversion efficiency recorded for the two-brick configurations (Figure 4-26), due to its warming capacity and higher surface area. Moreover, it had been previously demonstrated that most of the catalytic oxidation activity during warming phases is supposed to happen in the front of the catalyst which is on average warmer (McCullough & Douglas, 1996; Umehara *et al.*, 2000; Jeong & Kim, 2001), taking advantage, in that case, of the greater coated surface of the 600/2.5. The second brick also contributed in enhancing the conversion efficiency at low temperatures, even though its first purpose was to maintain the activity during cooling phases. The same PGM loading was coated on each catalyst and, due to the lower surface of contact in the second brick of the 2BC and 2BM configurations (low cell density), the same coating was concentrated over a smaller area which could promote the light-off from the closer proximity between active sites (Jasper *et al.*, 1991). The 2BC conversion efficiency could also be promoted by its lower thermal mass, associated with low heat conductivity and thicker walls that could concentrate the heat from the exhaust towards the centre of the catalyst and locally reach higher temperatures (Jasper *et al.*, 1991). Regarding the conversion efficiency based on the outlet temperature (faded symbols in Figure 4-26), the higher temperature losses over the two-brick configurations during the warming phase (Figure 4-25) were not directly representative of a reduced activity in the catalyst, as they reached higher conversion efficiency than the 400/4 at similar or even lower outlet temperatures. The catalytic activity below 200°C does not appear to rely solely on the catalyst temperature but on other parameters such as the surface area and heat and mass transfer. In the case of the 2BM, the second metallic brick brought a limited improvement in the activity at 155°C (opposite to its behaviour at 80°C), due to its reduced surface of contact and higher thermal conductivity spreading the heat over the whole catalyst and limiting local temperatures. The higher thermal mass of the LS catalysts which was reducing their warming capacity did not affect

much the conversion efficiency as, once these catalysts were warm, the promoting effect from the channel design and the greater surface of contact enhanced CO oxidation.

The conversion efficiency presented at 180°C was recorded after a cooling from 255°C. At this temperature, the substrate thermal properties were not critical anymore (similar conversion efficiency close to maximum for most of the configurations). This is due to the catalysts being fully warm and the efficiency only limited by a reduced surface of contact (600/2.5). Moreover, higher efficiencies are expected to be reached for the same temperature during a cooling process compared to a warming phase, due to the active sites remaining locally warmer (hysteresis) and maintaining a greater activity (Salomons *et al.*, 2007).

#### *4.4.2.2. Long-Chain Hydrocarbons (HC)*

The removal of long-chain hydrocarbons (up to C16), recorded at over 90% efficiency at 80°C exhaust gas temperature (Figure 4-27) was accounted for by HC condensation in the aftertreatment components, as well as the zeolites' trapping effect.

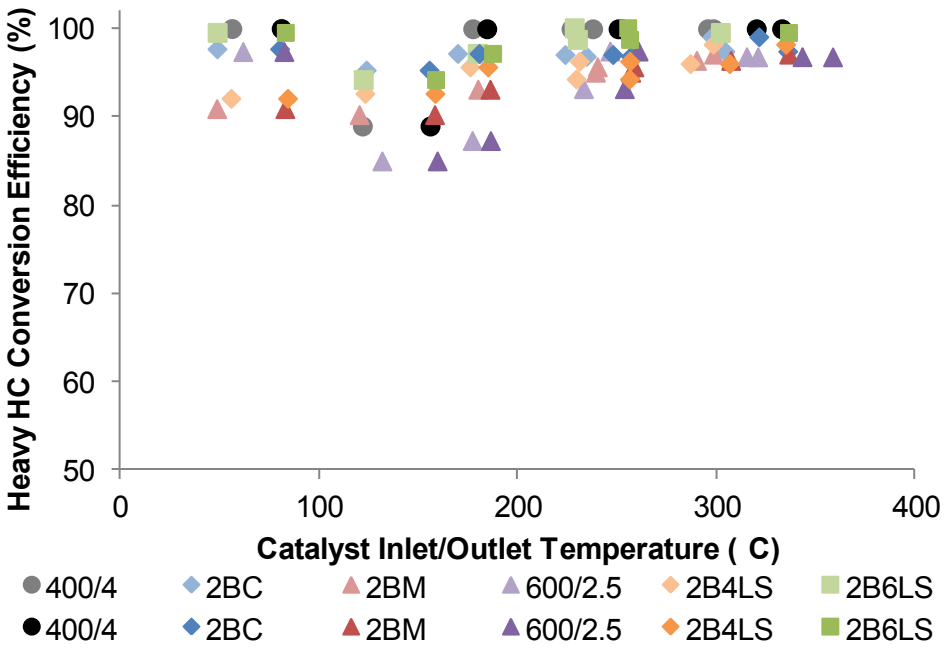


**Figure 4-27.** Heavy-hydrocarbons conversion efficiency for the combinations of catalysts based on their inlet (bright symbols) and outlet temperatures (faded symbols)

At 150°C, the decrease in conversion efficiency showed the release of some HCs from the zeolites while the catalyst became active for their oxidation. At this temperature, the two-brick configurations showed slightly higher conversion efficiency compared to the reference 400/4 catalyst, especially the 2BC and the LS configurations, similarly to CO oxidation. Hydrocarbon oxidation is thought to be influenced by CO conversion (adsorption competition) as, once CO oxidation starts, more catalytic sites become available for HC to adsorb onto and be oxidised (Patterson *et al.*, 2000). From 150°C, 100% conversion was reached by the reference catalyst while the 2BM configurations and the 600/2.5 catalyst remained at 96% efficiency. At higher temperatures, mass diffusion could become the limiting parameter for the oxidation of long-chain hydrocarbons. Therefore, the lower cell density/higher wall thickness characteristics of some of the second bricks would become critical as it reduces the surface of contact available and limit the mass diffusion of hydrocarbons towards the active sites. The 2B6LS showed the best activity out of the two-brick configurations as a direct effect of the enhanced mass transfer from a higher "surface area/hydraulic diameter" ratio and the specific cell design.

*4.4.2.3. Nitrogen Oxides ($NO_x$)*

Figure 4-28 shows that some $NO_x$ conversion (i.e. both NO and $NO_2$) was recorded even though the catalysts used in this study were not purposely designed to promote $NO_x$ reduction.

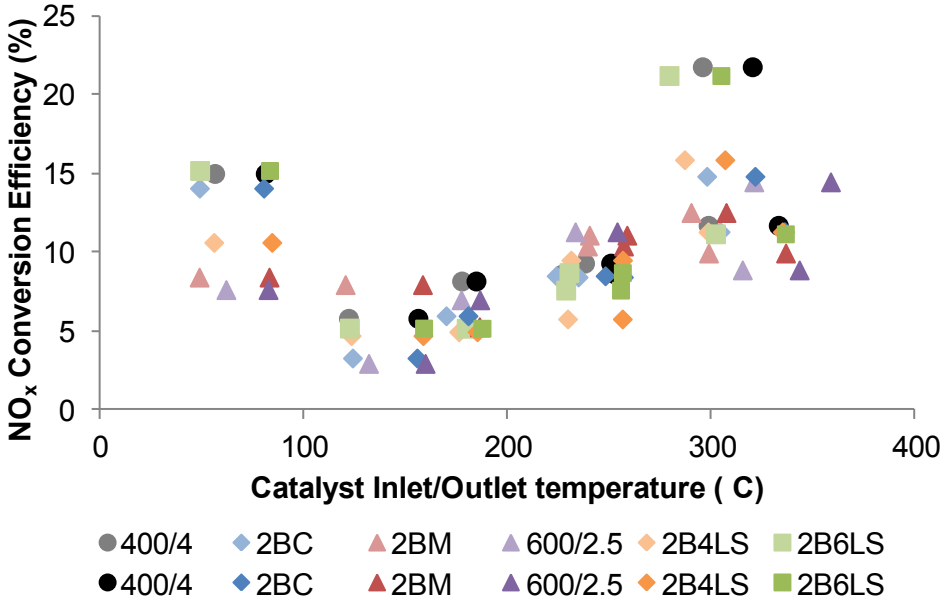


**Figure 4-28.** $NO_x$ conversion efficiency for the combinations of catalysts based on their inlet (bright symbols) and outlet temperatures (faded symbols)

The $NO_x$ conversion was comparable for the different configurations at medium temperatures but appeared more dissimilar at low and high temperatures, with the reference 400/4 catalyst and 2B6LS showing higher conversions. This low-temperature $NO_x$ concentration reduction could come from the use of $NO_2$ as an oxidant by hydrocarbons and CO, reducing it to either NO or $N_2$. As $NO_x$ conversion efficiency reflects the reduction of NO and $NO_2$, it provides an indication to the selectivity of the reduction of $NO_2$ to $N_2$. The comparisons between Figure 4-26 to Figure 4-28 show that the configurations with the greatest CO and heavy HC conversions were also the ones with the highest $NO_x$ reduction, illustrating the relations between these exhaust species. Between 100°C and 200°C, $NO_x$ reduction decreased due to less $NO_2$ being consumed as CO and HC used molecular oxygen.

Another source of $NO_x$ concentration reduction at the catalyst outlet could be $NO_x$ storage within the catalyst but this is expected to remain limited to surface area effects (no tailored oxygen carrier contained in the washcoat).

From 200°C, CO and HC complete oxidation allowed the catalytic sites to become accessible for NO, leading to an increase in $NO_2$ outlet concentration (Figure 4-29).

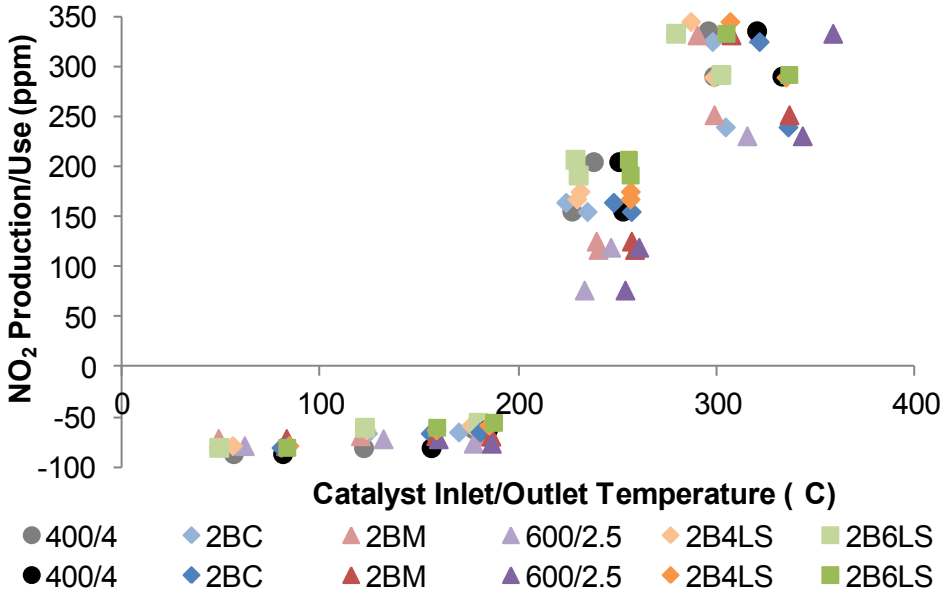


**Figure 4-29.** $NO_2$ production/consumption in the combinations of catalysts based on their inlet (bright symbols) and outlet temperatures (faded symbols)

The LS configurations showed similar $NO_2$ production compared to the reference catalyst, due to their mass and heat transfer promoted by their channel design, as well as the high surface of contact with the exhaust gas. Lower outlet $NO_2$ was recorded for the other configurations, due to their reduced surface of contact (low cell density for 2BM and 2BC and shorter dimension for 600/2.5). Due to NO oxidation taking place at higher temperatures, when most of the catalysts are warm, the critical parameter that influences the reaction becomes the surface of contact available, rather than the thermal mass of the substrate.

At temperatures over 300°C, close to 60% of NO was converted (Figure 4-30), either to $NO_2$ (Figure 4-29) but also to $N_2$ (HC reduction) as $NO_x$ conversion remained between 15% and 23% for the different configurations (Figure 4-30).

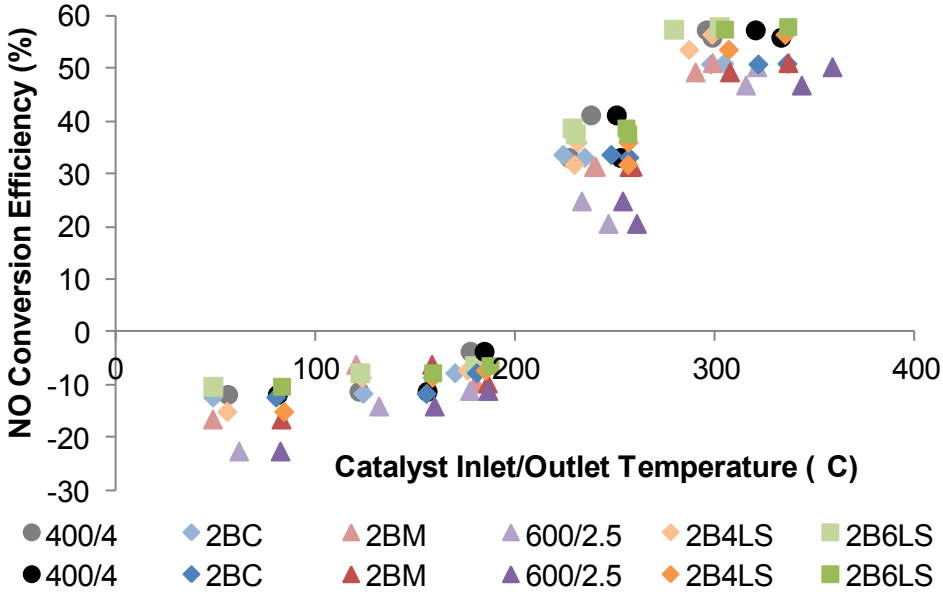


**Figure 4-30.** NO conversion efficiency for the combinations of catalysts based on their inlet (bright symbols) and outlet temperatures (faded symbols)

In terms of $N_2O$, a maximum of 17 ppm were produced at 250°C by the 2BM while for the remaining temperatures and configurations, fewer than 10 ppm were produced, showing a reasonable selectivity of the catalysts towards $NO_2$ and $N_2$ production, possibly due to the presence of palladium limiting platinum higher selectivity towards $N_2O$ (Glover *et al.*, 2011).

The results of this study outlined that the conversion efficiency is not solely governed by the thermal behaviour of a catalyst but that other parameters (surface of contact, mass transfer) should also be considered for the reactions taking place both at low and high temperatures. Moreover, the results in conversion efficiency proved that the metallic substrates showed similar or greater conversion efficiency compared to the ceramic ones. The results from the simulation were, therefore, erroneous due to the use of the triangular shapes,

reducing the surface area available for reaction. Additionally, the possible loss over time of the washcoat adhesion on metallic walls did not have any significant effects on the conversion efficiency of an aged catalyst in this study.

While the engine operating conditions used in this experimental study allowed the investigation of the transient thermal behaviour of the catalyst configurations, the study of highly transient and low loads conditions such as those encountered in urban area remained limited. Therefore, an additional simulation study was carried out to complete the two-brick configuration investigation and examine their behaviour at more critical conditions.

## 4.5. SIMULATIONS OF ALTERNATIVE DRIVING CYCLES

The evolution of the drive cycles for emission legislation focuses on their reproducibility of city driving patterns, with transient, low loads and idle phases. Therefore, it is useful to study the thermal behaviour and response of the two-brick configurations in the scope of alternative drive cycles, under conditions that can challenge their activity.

### 4.5.1. Validation of the Axisuite Model

Figure 4-31 shows that the trend of the temperature recorded at the outlet of the catalysts configurations during the experiment was well reproduced by the Axisuite model despite some slight differences.

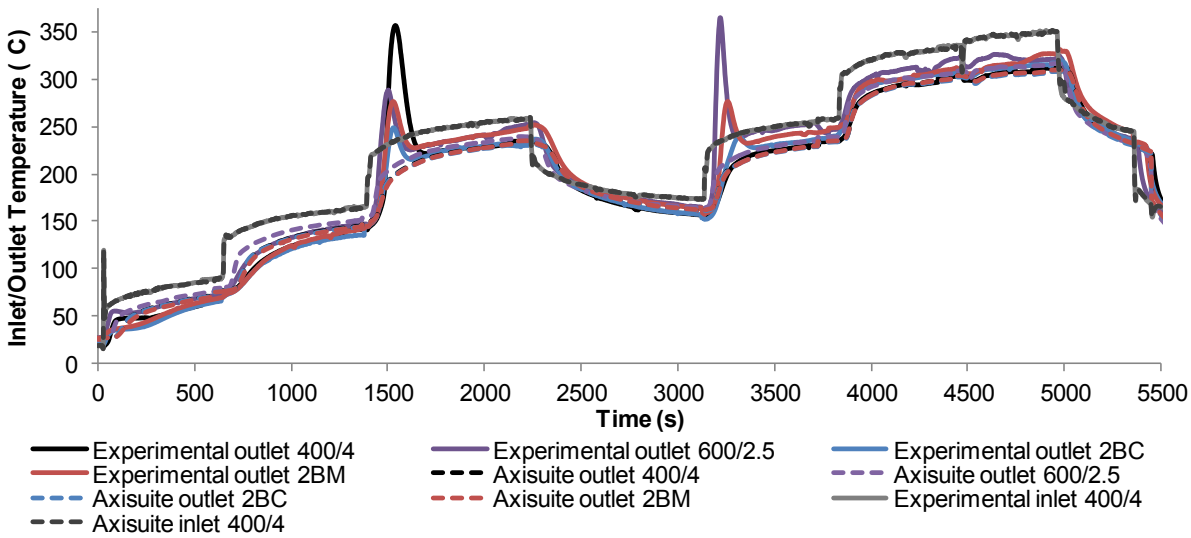


**Figure 4-31.** Catalyst inlet and outlet temperature profile measured (solid lines) and modelled (dash lines) during the experiment for the configurations studied

At the cold start, the model showed a slight delay in warming up and greater increase in temperature afterwards for each configuration. However, it reproduced the earlier warming capacity of the 600/2.5 relatively to the other configurations. The exothermic events leading to a sharp increase of the outlet temperatures were not reproduced by Axisuite. This phenomenon was caused by the specific conditions used in the experimental procedure (exhaust gas temperature remaining below 200°C for 20 min), which was not considered representative of genuine engine operating conditions. At higher temperatures, the predictions were lower than the measurements (especially for the 2BC), due to a possible underestimation of the heat produced by the exothermic reaction. The model was later used to predict the catalysts thermal behaviour at low temperatures, over urban cycles and during stop/start phases, when the conversion efficiency could remain limited. Therefore, the prediction accuracy at higher temperatures was less critical.

In terms of conversion efficiency, the model did not show good predictions of the experimental measurements, with a limited low-temperature oxidation activity for the

catalysts at 80°C. It seemed to underestimate the reduction reaction between $NO_2$ and CO/HC at low temperatures as some $NO_2$ was predicted at the catalyst outlet over the simulation while it was close to zero during the experiment. Moreover, the conversion efficiency was then overestimated at 160°C. This could be due to an underestimation of the effect of the inhibitions caused by the presence of other species on the active sites affecting the catalyst activity. Finally, the kinetic model predicted comparable conversion efficiency for the 400/4 and 600/2.5 catalysts on one side and for the 2BC and 2BM configurations on the other side. It appeared to be giving much more importance to the catalyst temperature, and reduces the effect of a higher surface area available for reaction, which is not in agreement with the measured data. For this reason, the model developed was only used to predict the thermal behaviour of the configurations, for which it showed comparable predictions with the experimental results.

Axisuite was also used to estimate the pressure increase over the different catalyst configurations (Table 4-8), as it was not possible to measure it during the experiment.

**Table 4-8.** Pressure increase calculated for the Axisuite model

| | **600/2.5** | **2BC** | **2BM** |
|---|---|---|---|
| **Average pressure increase over the experiment (%)** | -10.7 | 19.2 | 16.1 |

As expected, the two-brick configurations led to an average pressure increase that remained below 20% over the experimental cycle compared to the reference catalyst. The shorter dimension of the 600/2.5 and its greater open frontal area seemed to compensate for the increase in pressure losses caused by friction in the channels (reduced cell hydraulic diameter), which led to an overall reduction in the component backpressure compared to the reference catalyst.

Once the model was validated, the thermal behaviour of the configurations was studied with two other exhaust gas input scenarios, based on the data from an engine operating a Paris cycle on one side and the urban parts of an NEDC with stop/start strategy on the other side.

### 4.5.2. Thermal Behaviour during Alternative Driving Cycles

#### *4.5.2.1. Paris Cycle*

The Paris cycle was developed by the ADEME (Agence de l'Environnement et de la Maîtrise de l'Energie) and RATP (Régie Autonome des Transports Parisiens) to reproduce a typical driving pattern as encountered in Paris (Figure 4-32). This driving cycle was chosen here as it represents genuine urban driving conditions (low average speed, idle and highly transient phases with rapid accelerations/decelerations) where the catalyst activity can remain limited due to the low exhaust gas temperatures produced during these conditions.

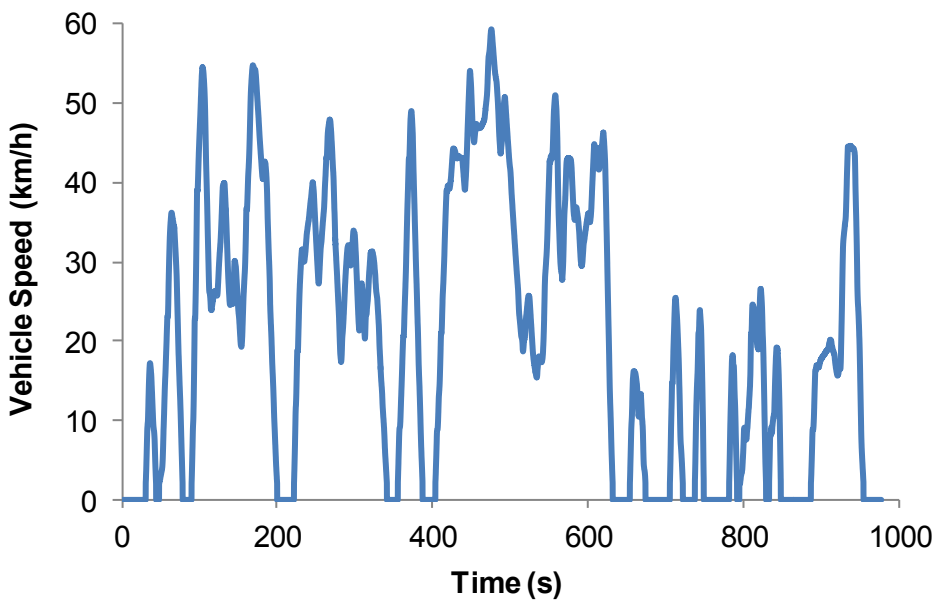


**Figure 4-32.** Vehicle speed during the Paris cycle

From the results predicted by the model and plotted in Figure 4-33, the two-brick configurations showed comparable thermal behaviour to the reference brick.

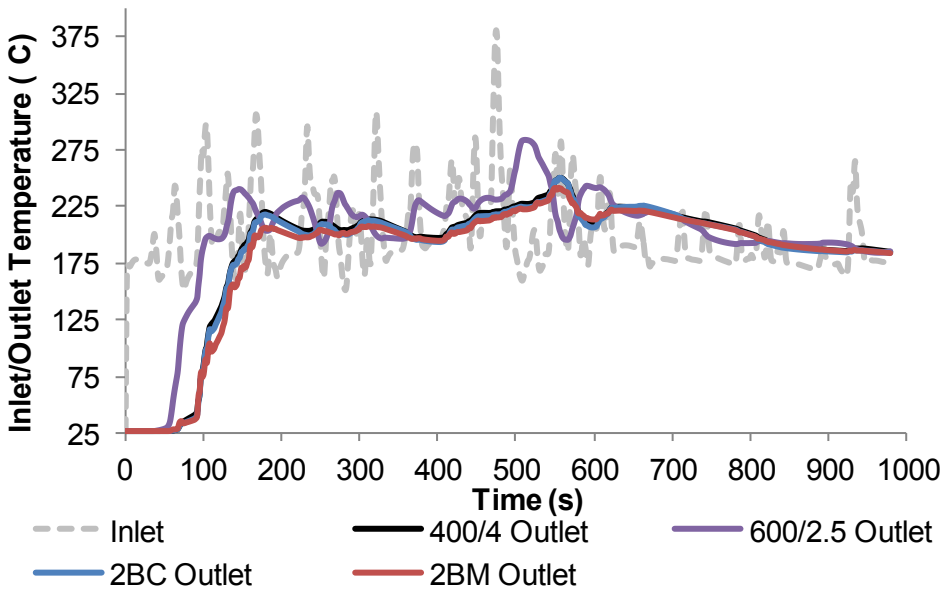


**Figure 4-33.** Temperature profiles for the catalysts configurations during the Paris cycle

Similar delays in warming-up can be noticed at the beginning of this cycle for the 400/4, 2BC and 2BM configurations, which makes the use of the short 600/2.5 brick interesting to allow earlier oxidation activity and compensate for this delay. Moreover, due to the highly transient characteristic of this cycle, the use of the two-brick configurations led to a low average temperature, as the warming time was limited between two accelerations. For this specific application, the second brick did not maintain a greater temperature during the deceleration phases due to the short warming phases. Most of the activity would therefore originate from the first brick. Thus, the 600/2.5 catalyst could be considered as an interesting replacement on its own due to its greater warming capacity at the beginning of the cycle, where more CO and HC were produced, while it remained most of the time at greater temperatures than the other configurations due to its lower thermal mass.

*4.5.2.2. Urban Parts of the NEDC with Stop/Start Strategy*

The thermal behaviour of the configurations was also investigated over the urban parts of the NEDC (Figure 4-34), where the exhaust gas temperature is at its lowest during this cycle.

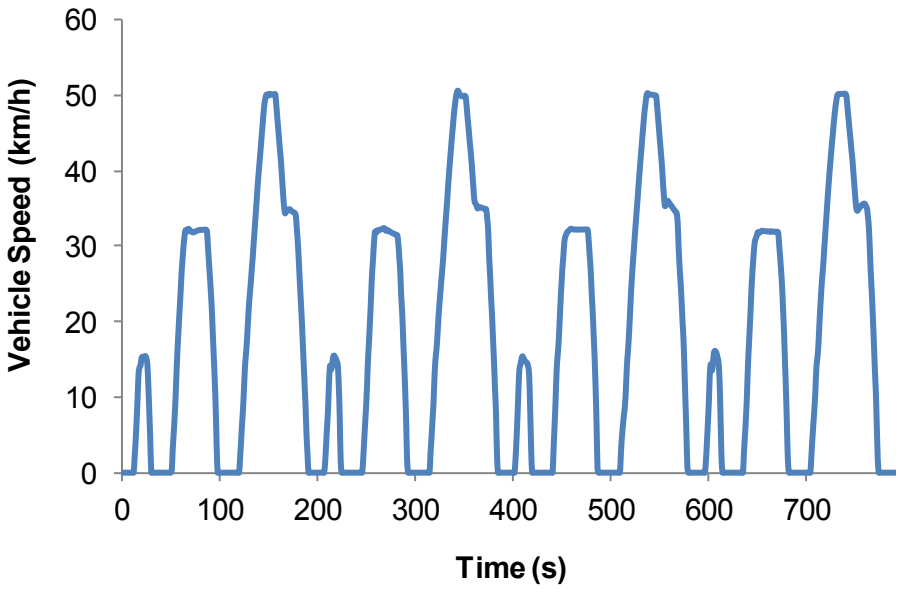


**Figure 4-34.** Vehicle speed during the urban part of the NEDC

In addition, the input scenario used for the simulation reproduces the behaviour of a vehicle fitted with a stop/start function, when the engine is stopped at idle and re-started at the next acceleration, to study the effect of this strategy on the thermal behaviour of the catalysts configurations.

Figure 4-35 highlights again the quick warming capacity of the short 600/2.5 catalyst, reaching higher temperatures more quickly at the beginning of the test, while the three other configurations showed similar thermal behaviour.

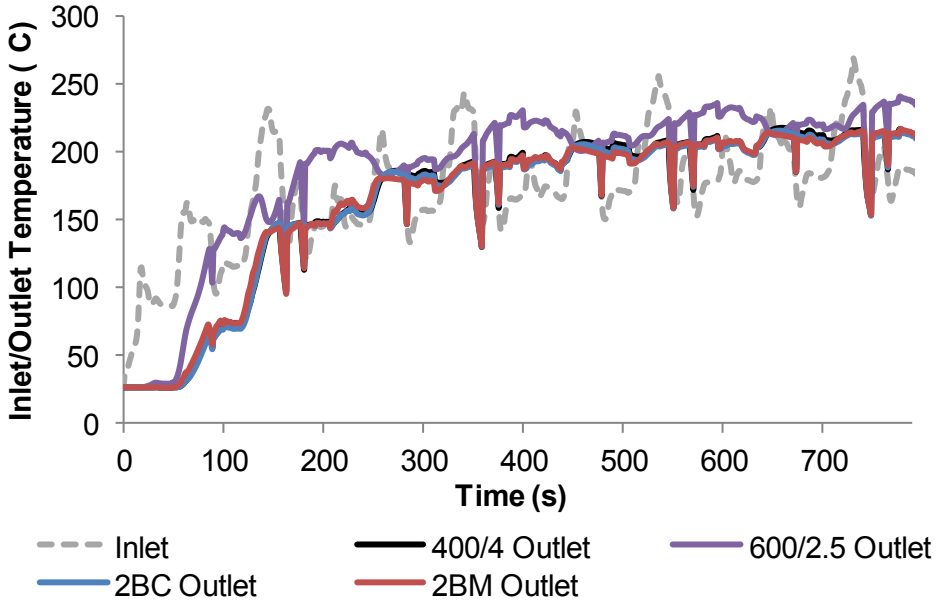


**Figure 4-35.** Catalyst temperature profiles during the urban parts of the NEDC with a Stop/Start strategy

While engine idle phases lead to a reduced exhaust flow rate, the stop/start strategy translates into an absence of flow through the exhaust system. During this phase, the share of heat transfer through forced convection is highly reduced and heat transfers through conduction and radiation become more important. Despite its higher temperatures during the engine operating phases, the thermal behaviour of the 600/2.5 was similar to the other catalysts during the stop phases (sharp cooling). This is due to the sudden changes in flow rates when the engine shutdown and restart, resulting in similar temperature ramp (decrease or increase) for the configurations, despite their different thermal characteristics. Nevertheless, during re-accelerations, the thin walls/high cell density of the 600/2.5 catalyst allowed a quicker warming, reaching again higher temperatures. As the cycle continued, the differences in outlet temperatures between catalysts were reduced but the 600/2.5 remained much warmer than the others, showing a limited effect from the second brick.

For these specific applications (highly transient, low-load phases) , the full length of the catalyst might not reach the light-off temperature over the duration of the cycle. Therefore, the use of a shorter catalyst (600/2.5) could be interesting due to its quicker thermal response during rapid changes in exhaust gas conditions, allowing the catalyst to become active earlier and remain on average warmer over the cycles. Additionally, the shorter length of the 600/2.5 could provide a reduction in the space required in the exhaust to house the catalyst. Finally, the 400/4 reference catalyst appeared to be also a reasonable compromise in terms of conversion efficiency, pressure loss, manufacturing and cost.

## 4.6. SUMMARY AND CONCLUSIONS

This chapter presented a complete catalyst design study aiming at enhancing the catalyst thermal behaviour. The use of theoretical equations provided an understanding of the relationships between some catalyst properties affecting the oxidation activity and its substrate cell density and wall thickness. The use of modelling tools then allowed the selection of thermally efficient catalyst configurations composed of two catalysts with different thermal masses that widen the operating temperature window. Finally, the selected catalyst configurations were tested on an engine with actual diesel exhaust gas, which proved the increased oxidation efficiency of the two-brick configurations compared to the reference catalyst. While this optimisation process focused solely on the substrate design, the catalyst activity can also be affected by the environment in which it has to operate, and more especially by the presence of certain species in the exhaust gas.

# 5. EFFECT OF THE EXHAUST GAS COMPOSITION ON THE DOC ACTIVITY

During its use, the DOC has to operate under varying exhaust gas compositions which have some effects on its activity. Understanding the exhaust gas conditions and species promoting or inhibiting the oxidation can assist in setting-up strategies and design that promote the low-temperature activity. First, the study focused on some interactions within the catalyst between exhaust gas pollutant species (CO, HCs and $NO_x$) that affect the oxidation activity. Then, the oxygen exhaust concentration, the main parameter promoting the oxidation, was investigated as a way of enhancing the DOC activity. Finally, the potential risk of soot accumulation within the catalyst channels was also investigated as it can, at certain conditions, deteriorate the activity.

## 5.1. METHODOLOGY

### 5.1.1. Exhaust Species Interaction Study

For this study, the engine was operated at a steady-state point (40% load at 1500 rpm) and fuelled with diesel and alternative fuels (rapeseed methyl ester (RME) and gas-to-liquid (GTL)), as well as operated with advanced combustion modes (dual-fuel propane/diesel combustion), to produce a variety of exhaust gas compositions for which the efficiency of the DOC was investigated. Exhaust gas recirculation was also used in most of the experiments, as it is a well known engine calibration strategy currently applied to reduce $NO_x$. Due to the reduction in oxygen exhaust concentration caused by the use of EGR (Ladommatos *et al.*, 2000), additional oxygen was injected upstream of the DOC, to maintain comparable oxygen concentration at the catalyst inlet for each type of exhaust gas (with and without EGR). For each engine operating condition, the DOC (Component 1 in Table 3-4) was placed in a

furnace and its light-off and activity monitored during a heating temperature ramp (around 2°C/min) and at an exhaust gas space velocity of 35 000/h. The exhaust gas concentration at the catalyst outlet was continuously recorded to calculate the conversion efficiency based on the inlet concentration.

### 5.1.2. Oxygen Study

To study the effect of oxygen on the low-temperature activity of the oxidation catalyst, the engine was operated at a steady-state condition (40% load at 1500 rpm) with EGR strategy to reduce the oxygen content in the exhaust to 12% (volume). Pure synthetic oxygen was added to the exhaust flow throughout the experiment, to reach two additional oxygen concentrations at the catalyst inlet (e.g. 15% and 20% in volume). The addition of oxygen was studied at several catalyst inlet temperatures between 100 and 200°C and space velocities (from 30 000 to 80 000/h by increasing the flow rate diverted from the engine), to reproduce engine low loads operating conditions, using Catalyst 1 in Table 3-4 in the experimental set-up described in section 3.2.1. The different temperatures were selected based on the CO light-off curve obtained at the baseline condition (dots on Figure 5-1).

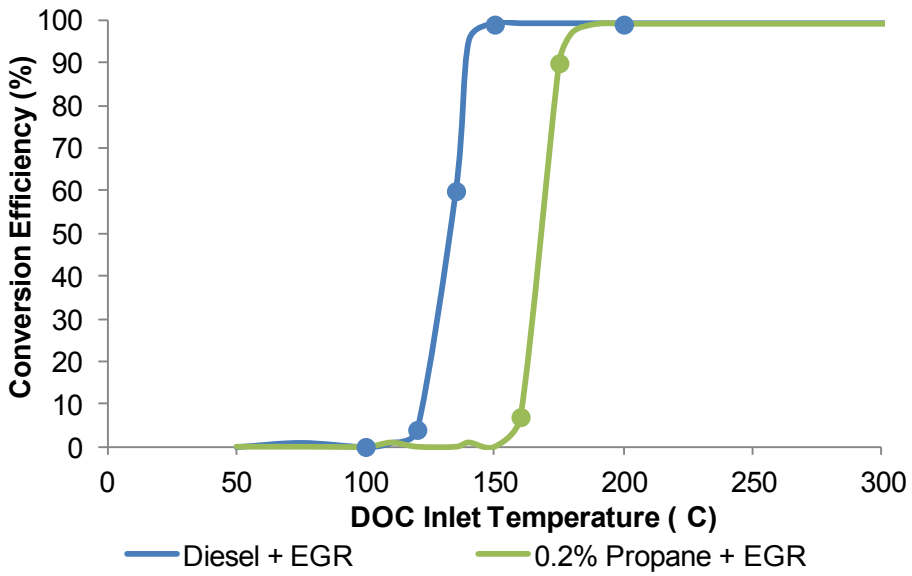


**Figure 5-1.** Typical CO light-off curves at 30 000/h with 12% oxygen under diesel and dual-fuel combustion exhaust gases with the use of EGR

A low temperature (100°C) was firstly chosen when no CO conversion is taking place, in order to define if the addition of oxygen could trigger the oxidation reaction. The next experiment was performed at 120°C, when CO oxidation starts. A higher temperature was chosen when CO conversion is in process (135°C) to study the effect of oxygen addition coupled with different space velocities. Finally, the last two points of study were at 150°C and 200°C when CO is almost fully oxidised.

In the second part, the engine was operated with dual-fuel combustion (diesel-propane). Gaseous propane was injected in the intake of the engine as a percentage of the volume of inlet air (0.2%). This combustion mode enabled the study of the effect of oxygen addition on the catalytic activity at higher concentrations of CO and hydrocarbons and especially its effect on some hydrocarbon individual species oxidation (medium-heavy hydrocarbons, propylene and ethylene). As this investigation focuses on enhancing the low-temperature oxidation (below 200°C), hydrocarbon species that require higher temperatures to be oxidised were not studied here. The catalyst activity under dual-fuel combustion exhaust gas is shifted towards higher temperatures compared to the diesel one, due to the greater CO and hydrocarbon concentrations increasing the inhibition and adsorption competition between species (Figure 5-1). Therefore, for the second part of this study, oxygen injection was studied between 160°C and 175°C which are the most relevant temperatures for this application.

### 5.1.3. PM Effect on the DOC Activity Study

For the experiment regarding PM accumulation effect on the catalyst activity and potential soot plugging, the engine was operated using a high EGR condition which produces a significant concentration of exhaust particulate matter (1500 rpm at 40% load with 30% EGR) to accelerate the sooting process.

The 600/2.5 catalyst (component 4 in Table 3-4) was used for this experiment as it is the catalyst that would suffer most from soot accumulation in the two-brick configuration study (Chapter 4), due to its higher cell density. CO, HC and $NO_x$ concentrations were recorded at the catalyst inlet and outlet to investigate the changes in conversion efficiency during an 8 hour test, to allow significant exposure to exhaust particulate matter. Particulate sizes and concentrations were also recorded to understand the evolution of the PM removal in the DOC. At this condition, the potential passive regeneration was considered limited due to the low engine-out $NO_2$ concentration (c.a. 40 ppm) and catalyst inlet temperature (280°C) as well as the loose contact between the particulates and the catalyst (flow-through channels).

While NO and CO concentrations were considered repeatable (Figure 5-2) over the experiment, hydrocarbon measurement was less stable.

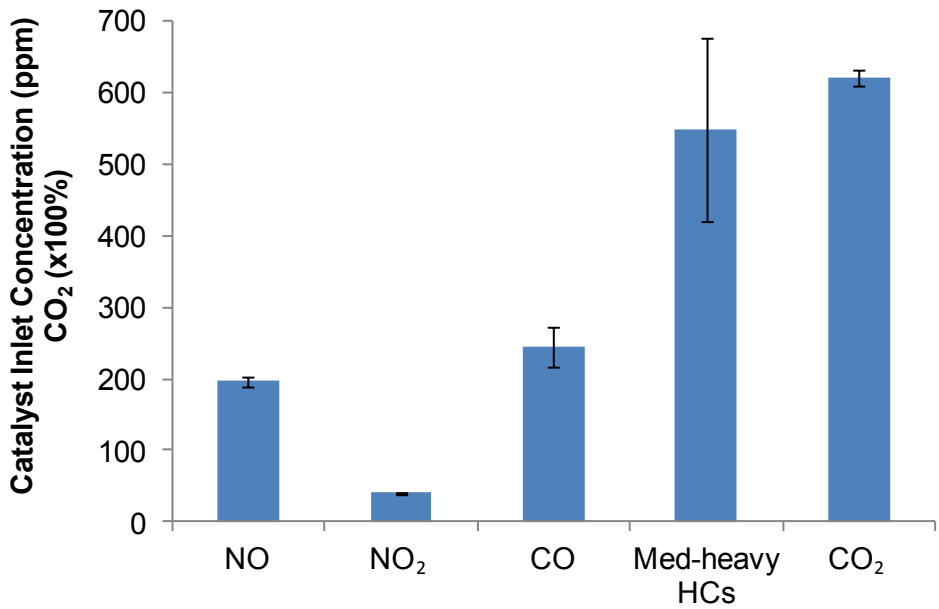


**Figure 5-2.** Variations in the catalyst inlet exhaust gas concentration during the 8 hour experiment

$CO_2$ concentration, which is a good indicator of the consistency of the engine operation, fluctuated between 6% and 6.3%, showing a stable engine condition during the experimental tests. The variations in the hydrocarbon level were therefore considered to be due to the

apparatus and sampling system measurement sensitivity. The results in terms of conversion efficiency were calculated based on the catalyst inlet and outlet exhaust concentrations, taking into account this emission variability. Similarly, the filtration efficiency was calculated based on the PM inlet and outlet concentration for each measurement session.

## 5.2. RESULTS AND DISCUSSION ON THE STUDY ON INTERACTIONS BETWEEN EXHAUST GAS POLLUTANTS

The presence and concentrations of some exhaust gas species (CO, HCs and $NO_x$) and their interactions with each other can affect the catalyst oxidation behaviour, promoting or inhibiting the reactions. A better understanding of these interactions and their effects could eventually support the design of the aftertreatment system to enhance the removal of pollutants, most especially at low temperatures. This study investigates the correlation between species concentrations in genuine exhaust gases and the subsequent changes in the oxidation activity, to define the diversity and priority among these species interactions.

### 5.2.1. Exhaust Gas Composition

The composition of the exhaust gases used to study the DOC activity is shown in Figure 5-3.

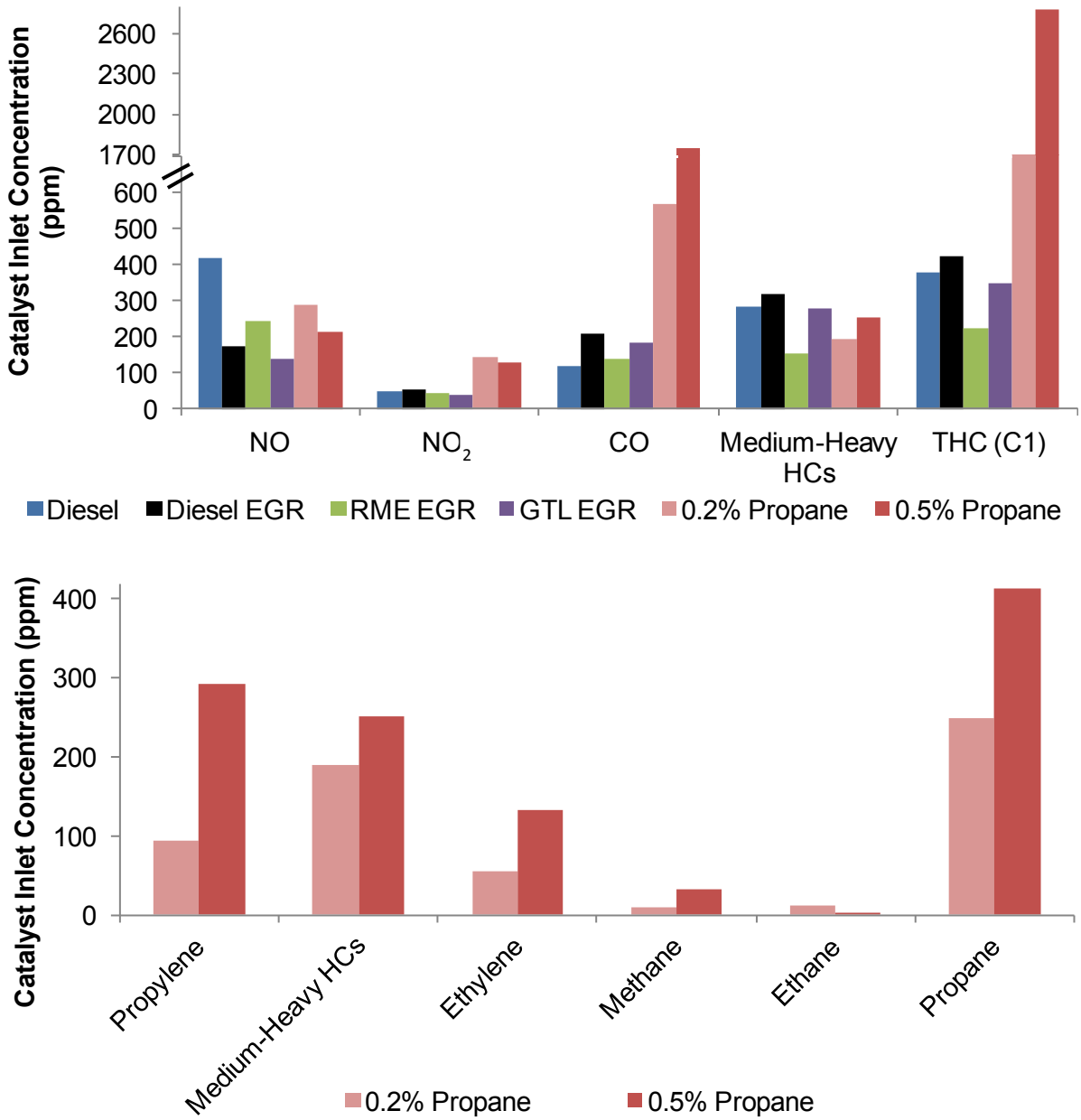


**Figure 5-3.** Engine exhaust gas compositions from the combustion of alternative fuels (top) and exhaust hydrocarbon species concentrations from the engine operation on dual-fuelling (bottom)

The different exhaust compositions were obtained from the following fuels and operating conditions:

- Diesel without EGR (reference fuel) produced the lowest level of CO and greatest level of NO.
- Diesel with EGR showed a significant reduction in NO emissions, while CO and THC concentrations were higher compared to diesel without EGR.
- RME with EGR produced a similar level of CO compared to diesel without EGR with a lower THC concentration. It is assumed that its aromatic hydrocarbons exhaust content is lower (absence of aromatics in the fuel) but that the hydrocarbons produced are on average heavier than those emitted using conventional diesel (Ballesteros *et al.*, 2008; Ballesteros *et al.*, 2010).
- GTL with EGR produced a higher level of CO and a level of THCs similar to the reference fuel. However, these hydrocarbons are expected to contain less aromatic hydrocarbons than those emitted using conventional diesel, similarly to RME, as GTL does not contain aromatics. This condition also produced the lowest $NO_x$ emissions recorded during this experiment.
- Dual-fuel combustion showed a rather different exhaust gas composition compared to the single fuel combustions, with a significant increase in CO and THC concentrations. It also produced higher concentrations of light hydrocarbon species and especially light alkanes (propane) and alkenes (ethylene and propylene). Medium-heavy hydrocarbons concentration (products from the combustion of diesel fuel) was similar to the single fuel combustions. The use of propane also produced a lower level of NO but an increased level of $NO_2$ compared to the other types of exhaust gases.

For the single fuel combustions used in this study, medium-heavy hydrocarbons represented around 80% of the total hydrocarbon exhaust concentration. Diesel/propane dual-

fuel combustion produced a more varied spectrum of hydrocarbon species as can be seen in Figure 5-3, which allowed the study of individual hydrocarbon interactions.

### 5.2.2. CO Oxidation

The start of CO oxidation in the DOC appeared to be dependent on its concentration in the exhaust gas (Figure 5-4). As CO concentration increased in the exhaust gas, its light-off was delayed towards higher temperatures (except for diesel combustion without EGR). CO can strongly adsorb onto active sites at low temperatures and cover the majority of the catalyst surface (Voltz *et al.*, 1973; Yao, 1984; Watling *et al.*, 2012). This, in return, limits oxygen access to the catalytic sites, preventing the start of CO oxidation. This self-inhibition was reduced at lower concentration of CO, as can be seen in the case of RME exhaust gas.

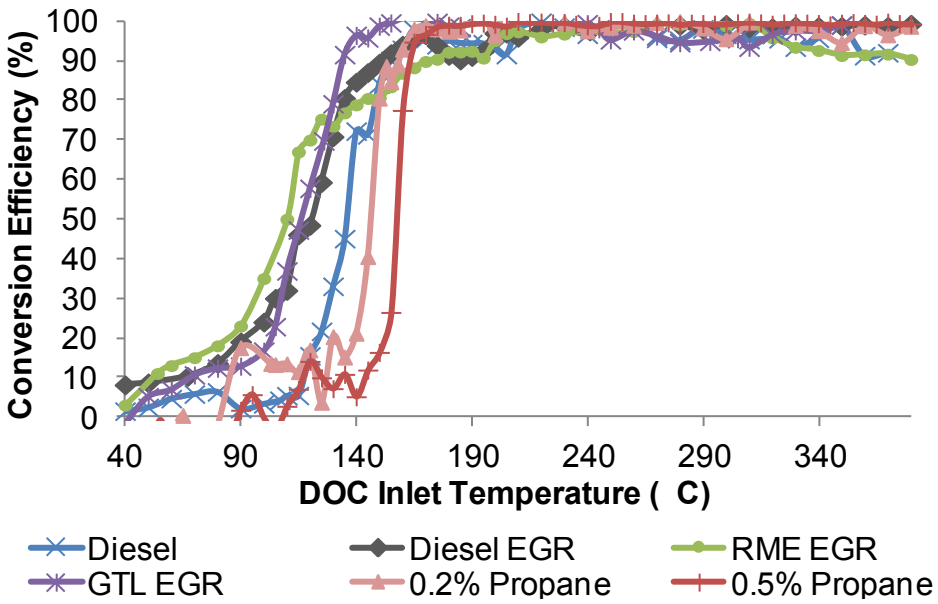


**Figure 5-4.** CO light-off curves for the different exhaust gas compositions

The presence of hydrocarbons can also affect CO oxidation by competing for the same active sites. This inhibition can be altered as some of the hydrocarbons were trapped in the coated zeolites, to limit the quantity of tailpipe hydrocarbons emitted at low temperature. The lower HC concentration recorded in the exhaust gas from RME combustion (Figure 5-3)

could also reduce the potential inhibition from CO and HC competition and allow earlier CO light-off.

In dual-fuel combustion, at 130°C-140°C, both CO and light alkenes (Figure 5-4 and Figure 5-5) showed some limited conversion (up to 15% efficiency) which could highlight mutual inhibition as, similarly to CO, light alkenes strongly adsorb on active sites, due to their double bonds (Mittendorfer *et al.*, 2003; Diehl *et al.*, 2010). The greater light alkene concentration recorded in dual-fuel combustion (Figure 5-3) would therefore strongly affect CO light-off, as noticed in Figure 5-4. It is unlikely that propane had any influence on CO light-off as light alkanes adsorb poorly on metallic PGM surfaces (Yao, 1980) and therefore are not supposed to compete to a large extent with respect to CO strong adsorption.

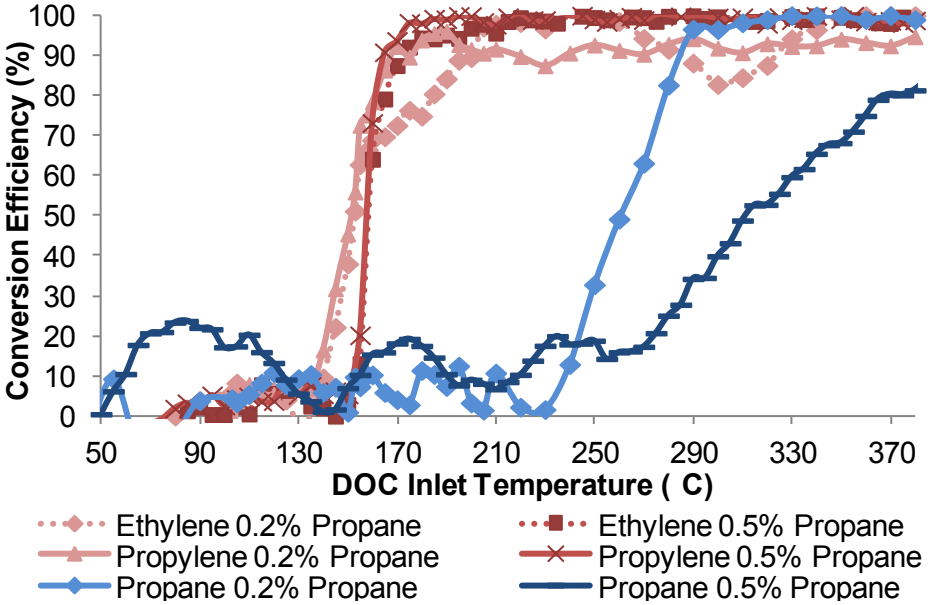


**Figure 5-5.** Light-off curves for light alkene (ethylene and propylene) and alkane (propane) hydrocarbons for the dual-fuel combustion modes

$NO_x$ species can also compete with CO for adsorption and potentially inhibit CO oxidation (Voltz *et al.*, 1973; Al-Harbi *et al.*, 2012; Watling *et al.*, 2012). It can be noticed that the exhaust gases containing the lowest NO concentrations were the ones showing an earlier CO light-off (RME, GTL and diesel combustion with EGR). On the contrary, the exhaust gas

from the combustion of diesel without EGR contained the highest level of NO and the lowest level of CO while showing a rather delayed start in CO oxidation. The inhibition of CO oxidation by NO was especially visible for this exhaust gas as CO presented some limited conversion between 50°C and 110°C (5% oxidation) before the reaction rate increased (Figure 5-4). Even though CO oxidation from diesel without EGR exhaust gas started at similar temperatures compared to the others, it remained limited to few percentages of conversion efficiency for some time before increasing again. The comparison of CO oxidation from diesel combustion with and without EGR confirms that a higher level of NO (diesel without EGR) seemed to be more detrimental on CO light-off than a higher level of CO and HC (with zeolites present) for these ranges of exhaust concentrations. It has been observed (Parker *et al.*, 1989; Zheng & Altman, 2000; Watling *et al.*, 2012) that NO and $NO_2$ can easily adsorb onto Pt and Pd active sites and efficiently dissociate, producing a high coverage of adsorbed nitrogen species and oxygen atoms on the active sites that limits other species adsorption (e.g. CO). This could be particularly enhanced in the diesel without EGR exhaust gas, due to its higher NO concentration.

The competitive adsorption at low temperatures between CO, light alkene and $NO_x$ species only happened once CO oxidation had started as, before that, CO was strongly covering most of the active sites. Once the temperature allowed CO oxidation reaction to start, its products desorbed, freeing some active sites on which CO, as well as NO and alkenes tried to adsorb (Al-Harbi *et al.*, 2012). These adsorption competitions eventually reduced CO access to the catalytic sites and limited its oxidation (5-10% conversion efficiency) over a certain range of temperatures until the other adsorbed species reacted and desorbed, freeing the active sites for more CO to adsorb again, allowing the oxidation rate to increase.

While CO oxidation in the DOC was essentially limited by low temperatures before the reaction rates increased (RME, GTL and diesel with EGR exhaust gases), for the exhaust

gases from diesel without EGR and dual-fuel combustion, the limiting factor was CO access to the active sites. Thus, once CO overcame the inhibitions and adsorbed on the active sites at higher temperatures, its oxidation showed greater reaction rates as most of the catalytic sites were already kinetically active for CO oxidation. Another reason for the sharp increase in CO conversion efficiency noticed in dual-fuel combustion exhaust gas is that the CO oxidation reaction is exothermic. As CO concentration in dual-fuel combustion was much higher than in the other exhaust gases, it involved a greater heat release during the reaction. This increased the catalyst local temperature once the oxidation started and especially promoted the activity of the catalytic sites, which translated into greater reaction rates. As a result, despite its late light-off, the maximum CO conversion efficiency in dual-fuel combustion was reached at similar temperatures to that of the other exhaust gases. In this experiment, the more delayed the start of oxidation was, the greater the reaction rate. Figure 5-6 shows that the exhaust gases with an early start in CO oxidation were not necessarily the ones that reached their maximum conversion efficiency first, as the reaction rates of the oxidation could still be affected after the start, by competition with other exhaust species.

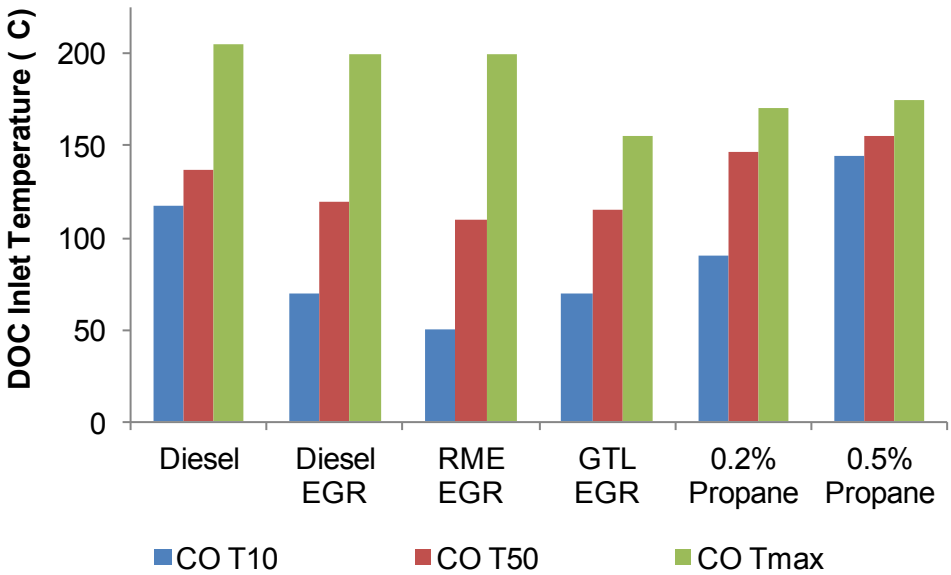


**Figure 5-6.** Effect of the different exhaust gas compositions on the required catalyst inlet temperature to reach 10% (T10), 50% (T50) and 100% (Tmax) CO conversion efficiency

After CO oxidation had started (Figure 5-4), some inflections could be noticed in the conversion efficiency of CO from RME exhaust gas at 120°C, similarly to what had been noticed in other studies (Al-Harbi *et al.*, 2012). These changes in CO oxidation rate can be related to an increase in medium-heavy hydrocarbon conversion happening at the same temperature (Figure 5-7).

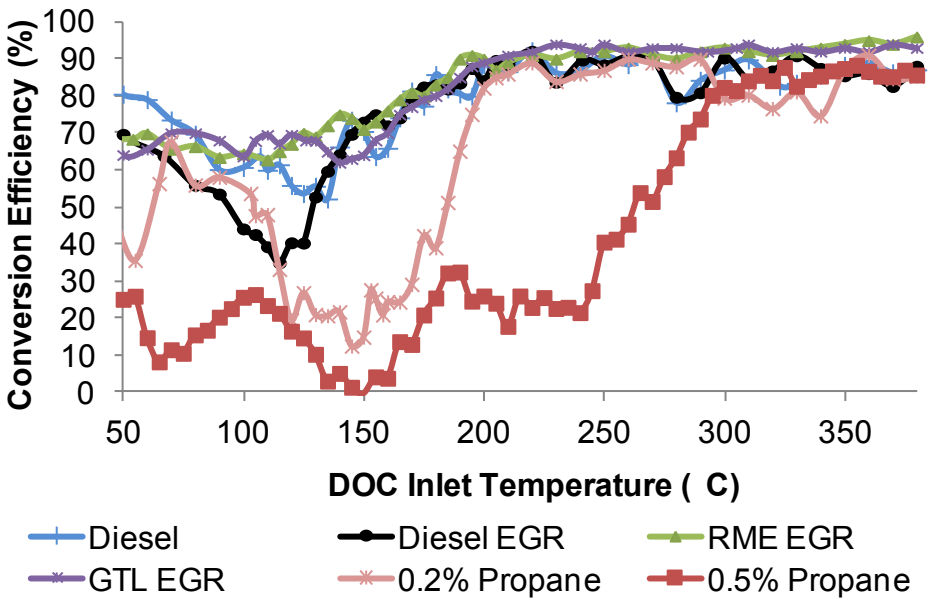


**Figure 5-7.** Medium-heavy hydrocarbon light-off curves for the different exhaust gas compositions

Once hydrocarbons were released from the zeolites and became active for oxidation, they competed for the same sites as CO, limiting its oxidation. This was particularly seen in the case of RME exhaust gas as its hydrocarbon oxidation started at lower temperatures and the hydrocarbons produced were on average heavier compared to the other exhaust gases, possibly affecting CO accessibility to the active sites. Due to this competition taking place when the catalyst was not yet able to fully oxidise CO (only 55% conversion efficiency), it more strongly affected CO conversion. This inflection in the light-off curve could also be noticed for diesel with EGR. However, the effect was less since hydrocarbons oxidised at higher temperatures (130°C), when more catalytic sites were available and active for both CO

and HC oxidation, reducing the inhibition effect on CO. A minor slowdown in CO conversion efficiency increase could also be noticed at 135°C for diesel without EGR and 150°C for 0.2% propane, when hydrocarbon oxidation started to increase. This effect could not be noticed for the other exhaust gases due to either lower hydrocarbon concentrations or HC oxidation starting at higher temperatures when a greater proportion of catalytic sites were already active for CO oxidation.

Figure 5-8 is a schematic summarising the exhaust species interactions affecting CO oxidation as presented above. Before the oxidation starts, the catalyst is covered by carbonaceous species from CO, strongly adsorbed onto the active sites, restricting oxygen access and limiting CO oxidation. Later, once CO starts desorbing, other species adsorb onto the free active sites (light alkenes and nitrogen oxides) limiting CO adsorption and oxidation. Finally, when the oxidation is developing, medium-heavy hydrocarbons can also start adsorbing on the active sites and competing with CO, affecting the reaction rate of CO oxidation (inflection on the light-off curve at higher temperatures).

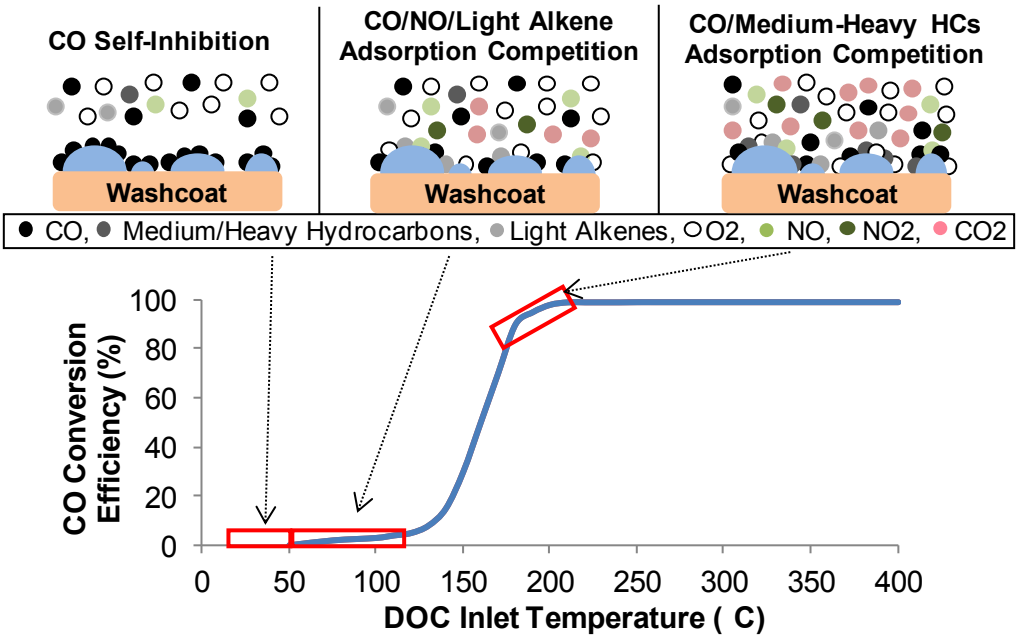


**Figure 5-8.** Mechanisms affecting CO oxidation (light-off curve and state of the catalyst surface)

### 5.2.3. HC Oxidation

#### *5.2.3.1. Medium-Heavy Hydrocarbons*

The low-temperature conversion recorded for the long-chain hydrocarbons was considered to be due to the zeolites coated onto the catalyst that momentarily removed and stored hydrocarbons before their release and oxidation (Phillips *et al.*, 1999), as well as possible hydrocarbon condensation within the catalyst.

Figure 5-7 shows that the zeolites behaved similarly for most of the exhaust gases used in the study, with 60% - 75% hydrocarbon removal at 70°C. The light-off curve from the 0.5% propane dual-fuel combustion behaved differently even though it contained a similar concentration of medium-heavy hydrocarbons. This highlights some strong inhibition effects potentially from different hydrocarbons species from the combustion of 0.5% propane, as the zeolite trapping efficiency was greatly reduced. A comparison between the exhaust composition from the combustion of 0.2% and 0.5% propane in the engine showed higher CO and light HC species concentration for 0.5% propane (Figure 5-3). Nevertheless, these exhaust species would not have a direct deactivation effect on the zeolites activity as they are short hydrocarbon chains and therefore less efficiently trapped by zeolites. Further investigations are required in that case, in order to understand what would cause such a great inhibition in the zeolite trapping.

Once the trapped hydrocarbons were released from the zeolites, different oxidation behaviours were recorded for the various exhaust gas compositions as the activation energy and rate of the reaction depend on the nature of the hydrocarbons, their molecular structure (saturated, unsaturated, cyclic, aromatics, etc.) and chain length which influence their adsorption strength (Mabilon *et al.*, 1995). The light-off curves of HC from the combustion of RME and GTL showed a plateau in the conversion at 70% efficiency before it started increasing while the rest of the exhaust gases showed a drop in their HC conversion

efficiency. This drop can be explained by the higher concentration of aromatic hydrocarbons in comparison to RME and GTL. Aromatic hydrocarbons require on average higher temperatures to oxidise as they are more weakly adsorbed due to their ring shape and their oxidation can suffer inhibitions from other species (Patterson *et al.*, 2000; Mittendorfer *et al.*, 2003; Grbic *et al.*, 2004). The depth of the loss in HC conversion efficiency depends on how efficiently these hydrocarbons were oxidised as they were released from the zeolites. The greatest drop in conversion efficiency was recorded for the dual-fuel combustion exhaust gas which could be due to the presence of more numerous short-chain hydrocarbons limiting the oxidation of the released hydrocarbons (Diehl *et al.*, 2010).

It has been previously reported that NO could compete with hydrocarbons for adsorption on the catalytic sites and limit their oxidation (Voltz *et al.*, 1973; Burch & Millington, 1995; Irani *et al.*, 2009). Nevertheless, several studies have also investigated the capacity of hydrocarbons to partially or completely reduce $NO_2$, depending on the type of hydrocarbon used (Burch & Millington, 1995; Burch *et al.*, 2002; Katare *et al.*, 2007; Al-Harbi *et al.*, 2012). Thus, the availability of $NO_2$ within the catalyst should be considered. It can be noticed on Figure 5-9 that no $NO_2$ was recorded at the catalyst outlet, despite its presence in the feed gas.

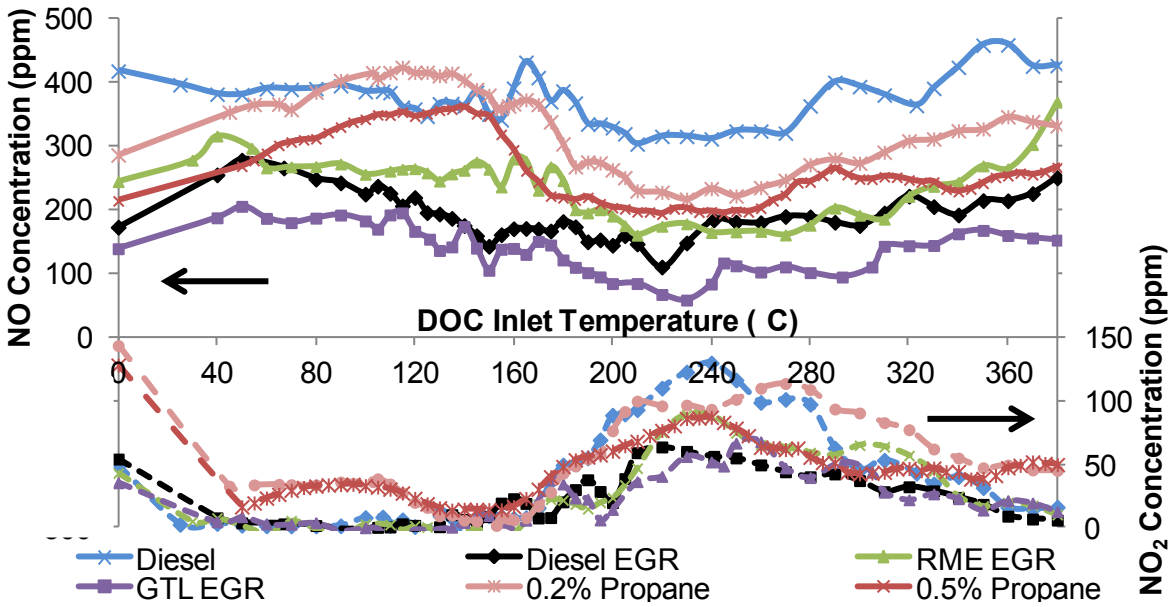


**Figure 5-9.** NO and $NO_2$ catalyst outlet concentration during the temperature ramp for the different exhaust gas compositions (0°C representing the catalyst inlet concentrations)

At low temperature, hydrocarbons are preferentially oxidised by $NO_2$, producing NO at the catalyst outlet (as noticed in Figure 5-9) and $N_2$. As the temperature increases, they start reacting preferentially with molecular oxygen from $O_2$ rather than $NO_2$, allowing $NO_2$ concentration to increase again at the catalyst outlet and NO level reducing to its inlet value. However, based on the stoichiometric ratio required for hydrocarbon oxidation with $NO_2$, this reaction would account for the oxidation of only a limited quantity of hydrocarbons. This mechanism could explain the opposite behaviour of CO and HC light-off for diesel combustion with and without EGR, as diesel with EGR showed a greater drop in hydrocarbon conversion while having an early CO light-off compared to diesel without EGR. Therefore, the higher NO concentration which was detrimental for CO light-off could be promoting low-temperature hydrocarbon oxidation through $NO_2$ production. NO and $NO_2$ can also be stored on the alumina washcoat and form nitrites or nitrates which hydrocarbons can react with (Burch *et al.*, 1998; Oh *et al.*, 2011). This could also explain the greater hydrocarbon

conversion at low temperature and the lower NO concentration recorded at the catalyst outlet for diesel combustion without EGR.

CO has also been considered as an inhibitor for the oxidation of other species, as previously mentioned. From CO and HC light-off graphs (Figure 5-4 and Figure 5-7), it seems that the start of hydrocarbon oxidation happened when a portion of CO had already been oxidised, around 50% of the inlet CO, for most of the exhaust gases (Figure 5-10).

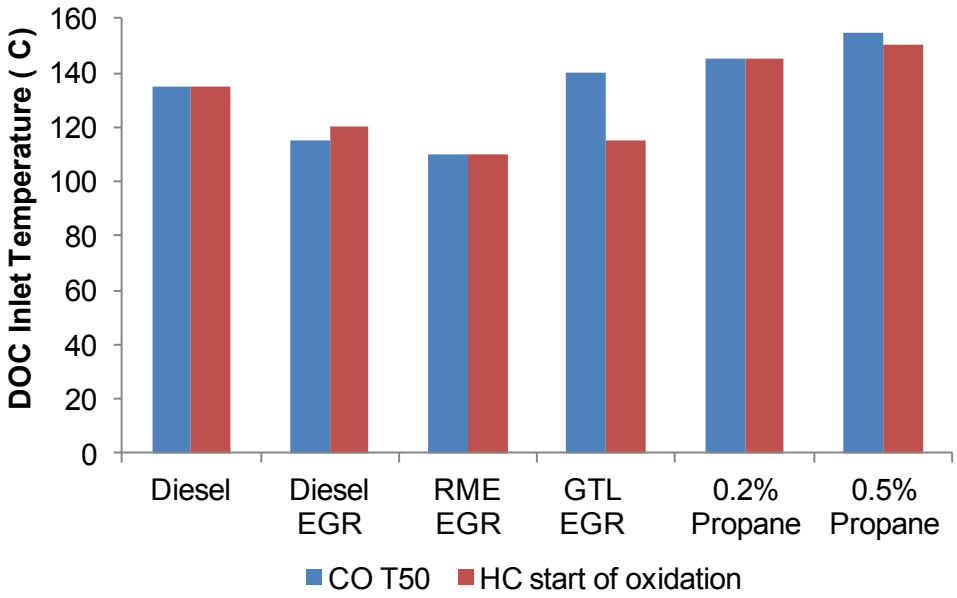


**Figure 5-10.** Catalyst inlet temperature required to reach 50% CO oxidation and for medium-heavy hydrocarbon oxidation to start, for the different exhaust gas compositions

Catalytic sites become available for hydrocarbons only after CO oxidation is already well developed (Patterson *et al.*, 2000). As CO conversion efficiency increases, its concentration along the catalyst length decreases. This reduces CO inhibition effect on hydrocarbon oxidation by allowing HC to adsorb on available catalytic sites at the rear of the catalyst brick. Therefore, before this threshold, as hydrocarbons are released from zeolites, most of the active sites can already be occupied by strongly adsorbed CO, covering the catalyst and limiting the ability of released hydrocarbons to adsorb and be oxidised.

#### *5.2.3.2. Light Hydrocarbons*

From propane, propylene and ethylene light-off curves, it can be observed that zeolites only selectively trap medium-long chain hydrocarbons at low temperature (Figure 5-5).

Propylene and ethylene oxidation started at lower temperatures than medium-heavy hydrocarbons and followed a steady increase until reaching the maximum conversion efficiency, in a similar trend to CO light-off curve. Light alkenes are short-chains of unsaturated hydrocarbons and therefore are more easily oxidised at lower temperatures than other hydrocarbons. Moreover, their oxidation does not suffer from competitive adsorption with other hydrocarbons but it can still be inhibited by a high light alkene concentration at low temperatures due to their strong adsorption onto the active sites (Mittendorfer *et al.*, 2003; Diehl *et al.*, 2010), similarly to CO. Light alkenes can also suffer from adsorption competition with CO at low temperatures, as previously mentioned, and it can be noticed that their oxidation commenced shortly after CO oxidation had started, as more active sites became available for them to adsorb. The fact that they are less affected by competitive adsorption with other exhaust species justifies why the general trend of the light alkenes light-off curve was not much altered when changing from 0.2% to 0.5% propane exhaust composition. The slightly delayed start of oxidation for the light alkene in the exhaust from 0.5% propane combustion (around 20°C) can be justified by its higher alkene and CO content. Nevertheless, similarly to CO, once the oxidation started, a greater reaction rate was recorded for the oxidation of the light alkenes in the combustion using 0.5% propane, leading both dual-fuel combustion exhaust gases to reach their maximum conversion efficiency at similar temperatures.

Propane, an alkane hydrocarbon, is a stable component due to its carbon atom being saturated by hydrogen, requiring more energy to be broken down and therefore greater temperatures to be oxidised. As previously mentioned, light alkanes poorly adsorb on active

sites and their oxidation can be affected by the presence of other exhaust species. Therefore, their oxidation can only start when most of the other exhaust components are already oxidised, especially strongly adsorbed CO and light alkenes. This is the reason why propane light-off and reaction rate were greatly affected by the change of exhaust composition (increase in CO and hydrocarbon concentration) from the use of 0.2% to 0.5% propane in dual-fuel combustion.

### 5.2.4. Evolution of the Distribution of Hydrocarbon Species during Light-Off

Figure 5-11 shows the evolution of the emissions of hydrocarbons in terms of individual species, during the catalyst light-off, with the exhaust gas from diesel combustion. As previously highlighted, the majority of the hydrocarbons in diesel exhaust gas are medium-heavy ones, due to the incomplete combustion of the long-chain hydrocarbons composing diesel fuel. The decrease in HC concentration at 100°C followed by a slight increase at 200°C was accounted for by the zeolites momentarily trapping and releasing hydrocarbons at higher temperatures. With increasing exhaust temperatures, heavy HCs were more efficiently oxidised than the other types of hydrocarbons. At 380°C, the majority of the HCs remaining at the catalyst outlet were alkane types (methane, ethane and propane) representing 70% of the catalyst outlet THCs (compared to 8% of the THCs in the feedgas) due to their saturated structures. Heavy HCs were still representing 27% of the catalyst outlet THCs due to mass diffusion limitation for the heaviest hydrocarbons.

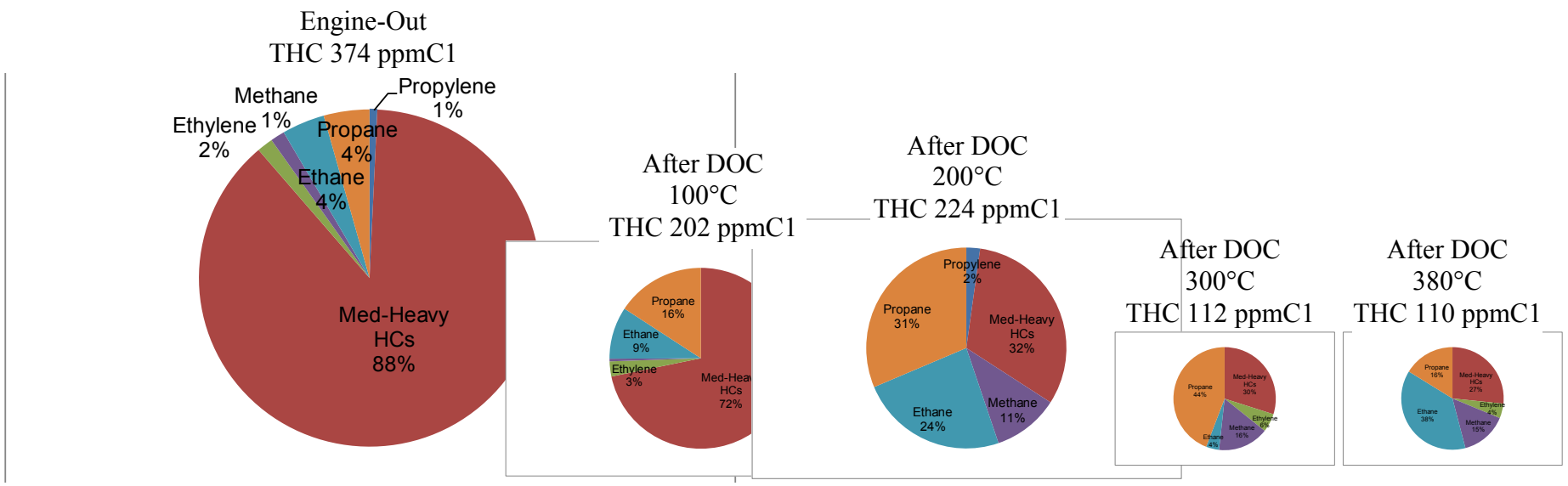


**Figure 5-11.** Hydrocarbon speciation and distribution for diesel exhaust gas

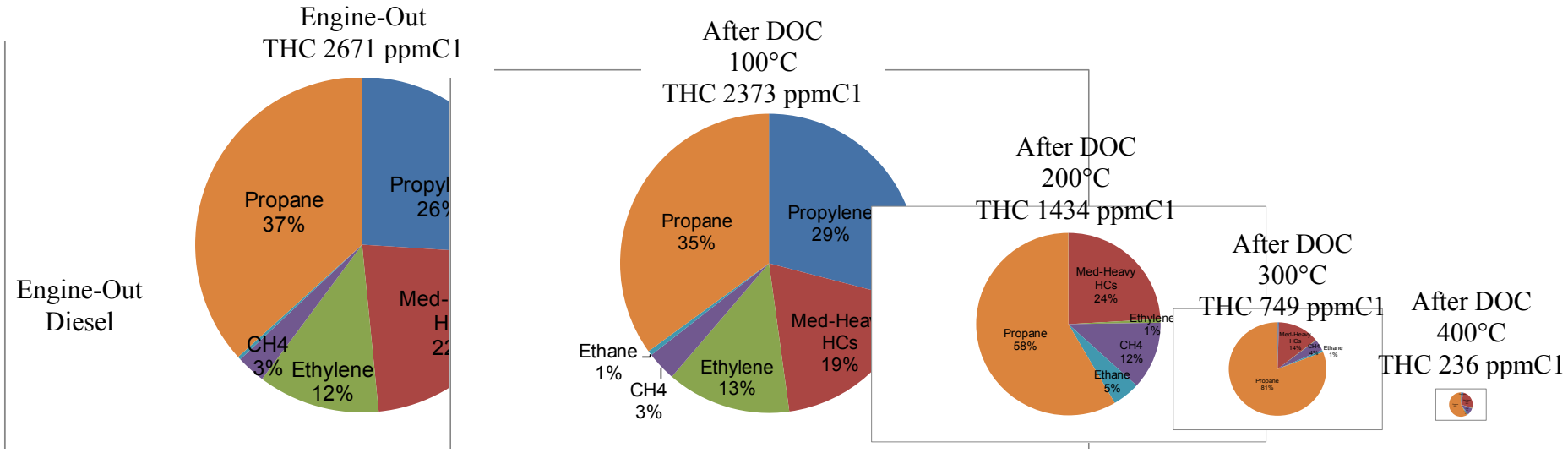


**Figure 5-12.** Hydrocarbon speciation and distribution for dual-fuel combustion exhaust gas and comparison with diesel hydrocarbon concentration

The comparison between engine-out hydrocarbons from dual-fuel combustion (0.5% propane) with the ones scaled for diesel (Figure 5-12) emphasises the much greater HC concentration found in the exhaust when using gaseous propane as an additional fuel. The reduction in THC emissions was more gradual for the exhaust gas from dual-fuel combustion compared to diesel ones, due to the lack of effect of zeolites on the short-chain hydrocarbons, representing the majority of the THC emissions for the dual-fuel combustion mode. From 200°C, the alkenes were completely oxidised and propane represented the main hydrocarbon remaining at the DOC outlet until 400°C. At 400°C, propane was selectively oxidised (representing 68% of THCs at the outlet at 400°C compared to 92% at 300°C) while the proportion of heavy hydrocarbons increased again (from 5% to 25% of THCs) due to the previously mentioned mass diffusion limitation.

### 5.2.5. Strategies to Reduce Exhaust Gas Interactions and Promote Low-Temperature Activity

While some interactions between gaseous pollutants exist within the DOC (adsorption competition), it is possible to take advantage of them to design an efficient aftertreatment system at low exhaust temperatures. To promote low-temperature CO oxidation, NO should be temporarily removed from the exhaust gas to reduce CO-$NO_x$ competition. The use of EGR strategy allows an improvement in CO light-off, by reducing NO engine-out concentration, but care should be taken to limit possible fouling of the EGR cooler at low temperatures (use of high-pressure loop or temporarily by-pass the cooler). Higher CO concentrations can inhibit CO start of oxidation but can also increase its reaction rate once the oxidation has started, due to the heat produced by the exothermic reaction. Moreover, trapping medium-heavy hydrocarbons through the use of zeolites can reduce the competition for active sites between hydrocarbons and CO, affecting CO oxidation rates (inflection in CO

light-off curve) and delaying hydrocarbons start of oxidation. It is proposed in this study that promoting CO oxidation at lower temperature would allow more active sites to be available for adsorption, when hydrocarbons are released from the zeolites. In the meantime, hydrocarbons can react with stored $NO_x$ and partially reduce them at low-medium temperatures. Light alkene hydrocarbons show early light-off and are not much affected by competition with other species apart from themselves and CO. Favouring their production in the combustion instead of producing other hydrocarbons (use of specific fuel or engine calibration without affecting the combustion efficiency), would therefore allow a greater THC oxidation efficiency at low temperature. Light alkanes on the contrary require higher temperatures to be oxidised. They do not affect other species oxidation but suffer from other species stronger adsorption. Due to their short carbon chains, they are not efficiently trapped in zeolites and therefore are released into the atmosphere until the temperature is high enough to allow their oxidation. This study did not find any strategies directly promoting their oxidation, but the oxidation of other species at lower temperatures (e.g. CO, light alkenes, etc.) can reduce the competitive adsorption and increase active site availability and local temperatures which can indirectly promote light alkanes oxidation.

While the catalyst activity can be affected by gaseous pollutant interactions on the catalytic sites, the concentration of oxygen in the exhaust, required for the oxidation reactions, could also influence the conversion efficiency in the DOC.

## 5.3. OXYGEN EXHAUST GAS CONCENTRATION

### 5.3.1. Background Study

The study of the activity of an Axisuite simulated catalyst operating during an NEDC (Figure 5-13) shows that some losses in the oxidation efficiency can be noticed at the beginning of the cycle.

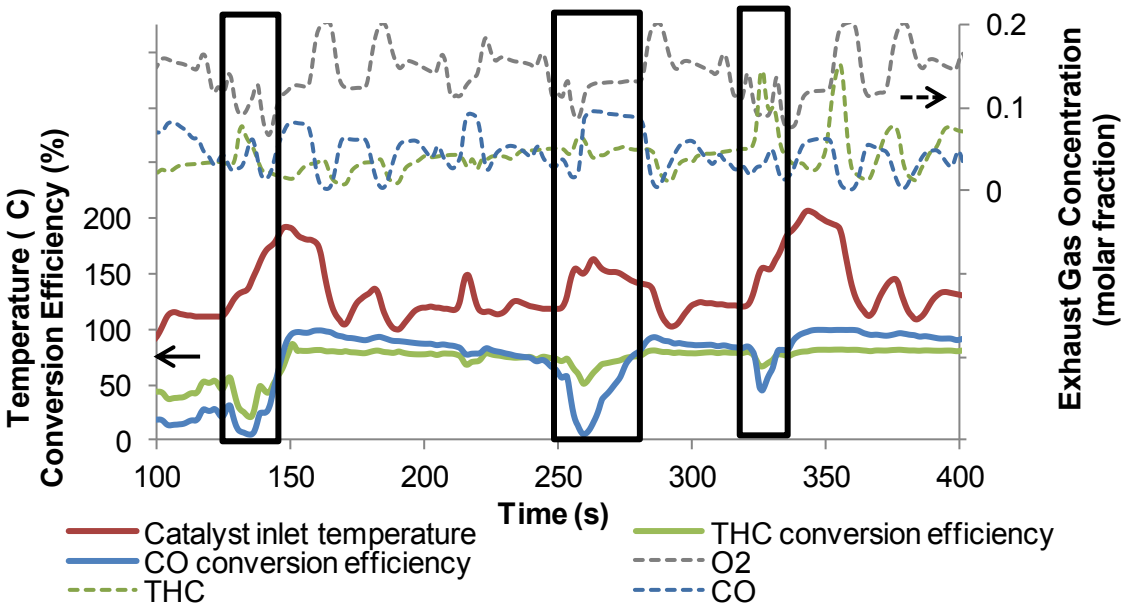


**Figure 5-13.** Simulation of the exhaust composition, DOC temperature and conversion efficiency of a diesel engine over an NEDC

These losses take place during warming phases when peaks of CO and HC emissions and decreases in oxygen exhaust concentration are simultaneously recorded. These trends are representative of a vehicle acceleration phase during the driving cycle. While this acceleration also leads to an increase in the catalyst space velocity which can affect its oxidation efficiency (reduction of the exhaust gas residence time), the comparison with other points of the cycle with similar space velocities shows that this parameter is not solely responsible for the loss in activity. On the contrary, it is thought that the decrease in oxygen, from operating the engine at lower air-fuel ratios during the acceleration phases, could be degrading the catalyst activity. The air-fuel ratio, and subsequently oxygen exhaust

concentration, is carefully controlled by the engine calibration strategies to promote the combustion efficiency while limiting the production of exhaust gas pollutants without sacrificing the power output. The injection of additional oxygen, upstream of the oxidation catalyst, could be a solution to compensate for the decrease in oxygen exhaust concentration during acceleration phases. This could limit the loss or even promote the oxidation activity, especially at low temperature, without affecting the optimum air-fuel ratio required for the combustion.

This study investigates the potential of the addition of oxygen upstream of the DOC, coupled with various space velocities and exhaust gas temperatures, to understand and define the conditions under which it could efficiently promote CO oxidation, especially at low temperatures. The second part of the study investigates the same injection strategy but with exhaust gas produced from propane/diesel dual-fuel combustion, to investigate the effect on the oxidation of specific individual hydrocarbon species.

### 5.3.2. Results and Discussions from the Oxygen Concentration Study

#### *5.3.2.1. Exhaust Gas Composition*

The use of propane in dual-fuel combustion led to an increase in CO and total hydrocarbon concentration compared to diesel exhaust gas (Figure 5-14), with a decrease in NO and slight increase in $NO_2$. The level of medium-heavy hydrocarbons remained similar for both types of combustion as they are formed from the combustion of diesel. Light hydrocarbon concentration significantly increased with dual-fuel combustion (Figure 5-15) which allowed the study of the effect of oxygen addition on the oxidation of light alkene hydrocarbon species.

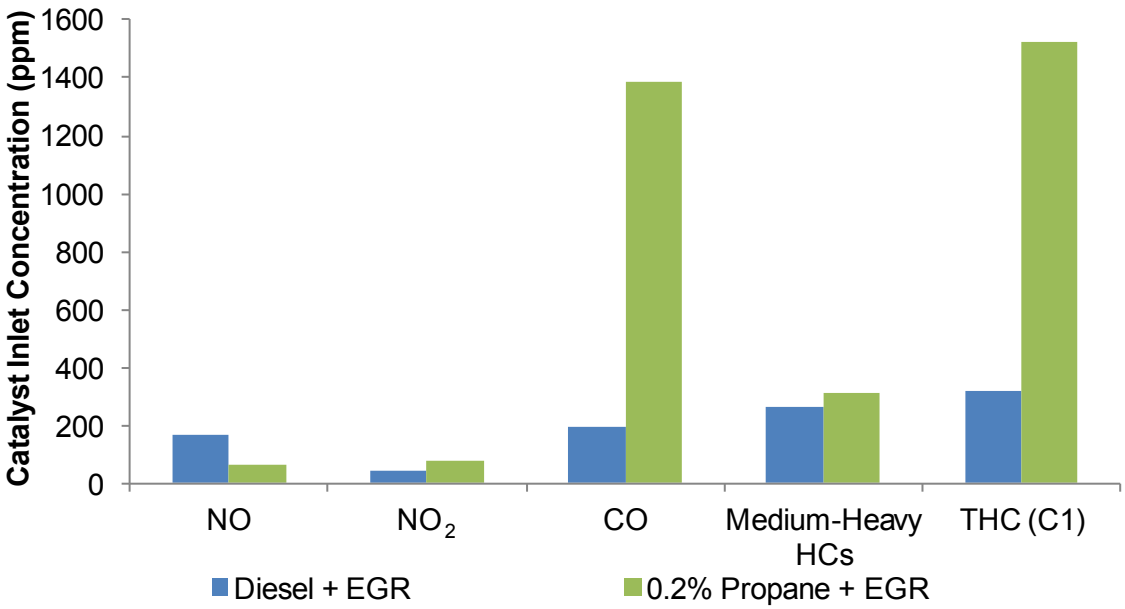


**Figure 5-14.** Concentrations at the catalyst inlet for the single diesel fuel combustion and dual-fuel combustion with propane, both using EGR strategy

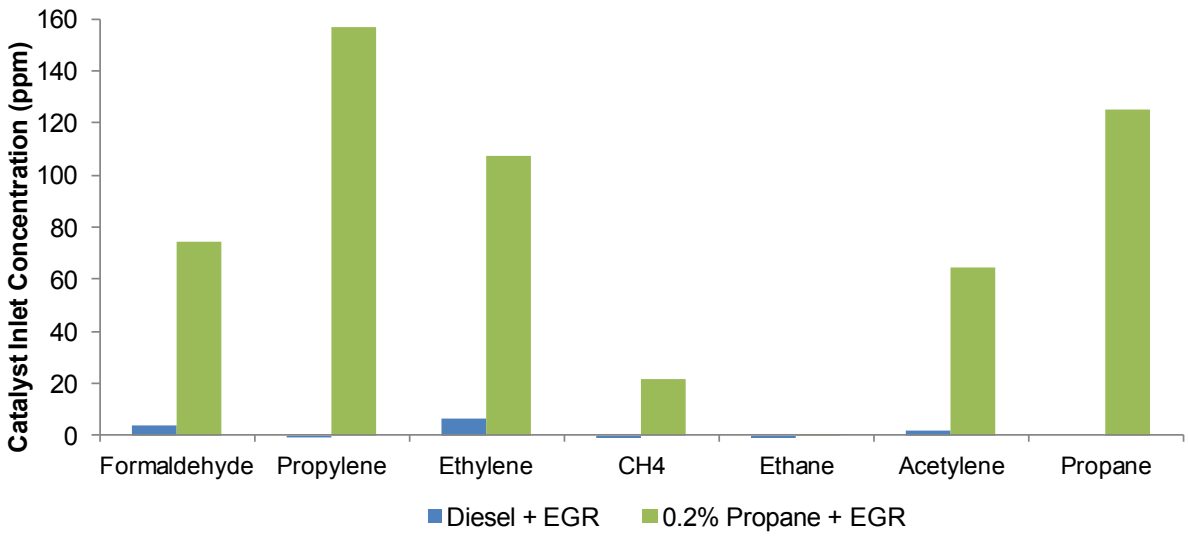


**Figure 5-15.** Concentrations at the catalyst inlet of individual hydrocarbon species for single diesel fuel combustion and dual-fuel combustion with propane, both using EGR strategy

*5.3.2.2. Oxygen Effect on CO from Diesel Fuel Combustion*

The addition of oxygen at a catalyst inlet temperature of 100°C did not show any effect on CO conversion efficiency (Figure 5-16). The parameter limiting the activity at this temperature is not oxygen availability but primarily the low temperature that prevents the catalytic sites to be active for CO oxidation. Moreover, at low temperatures, CO is considered to self-inhibit its oxidation by strongly adsorbing on the active sites, restricting oxygen access which in return limits the reaction (Voltz *et al.*, 1973; Yao, 1984; Watling *et al.*, 2012), as presented in section 5.2. The additional oxygen injected in the exhaust gas was not able to access the active sites and therefore did not show any promotion of CO oxidation.

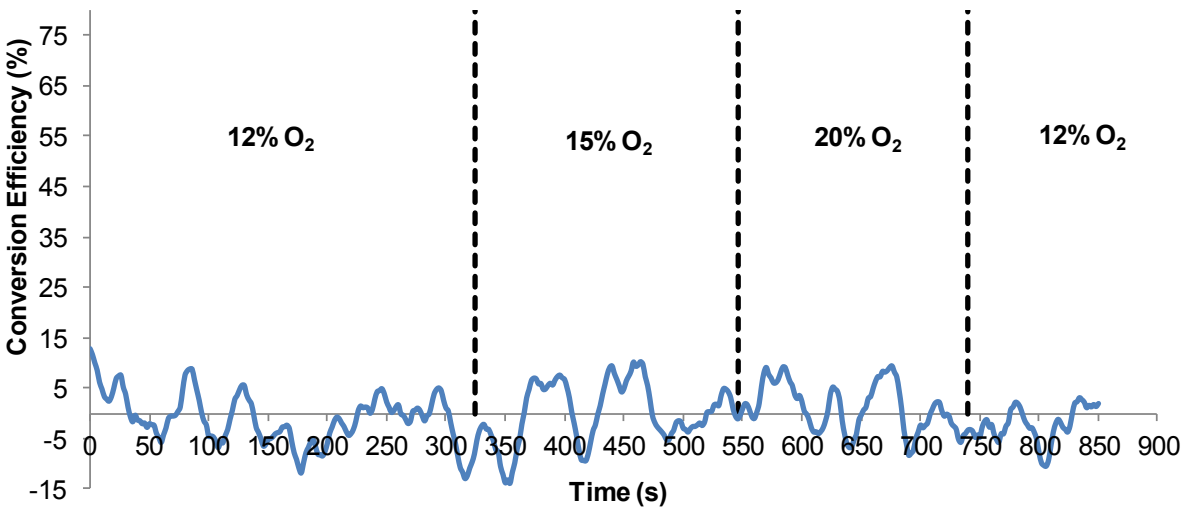


**Figure 5-16.** Effect of oxygen exhaust concentration on CO conversion efficiency at 100°C and 30 000/h space velocity

At 120°C (Figure 5-17), the addition of oxygen was showing a more noticeable effect on CO conversion efficiency than at 100°C. This could be due to the oxidation being triggered at 120°C (Figure 5-1). Therefore, any addition of oxygen can enhance the conversion as some active sites are physically available for oxygen adsorption and kinetically ready for the oxidation reaction to take place. When oxygen exhaust concentration was reduced back to 12%, a certain hysteresis was noticeable as the conversion efficiency did not directly decrease

back to its initial value. The addition of oxygen can promote the production of heat due to the exothermic character of CO oxidation. Once the oxygen injection was stopped, the catalytic sites remained warm for some time, maintaining a higher activity, even when the level of oxygen was back to its initial value. The exhaust gas then cooled the catalyst, reducing this "post-injection effect" and decreasing the CO conversion efficiency to a level remaining greater than the initial value.

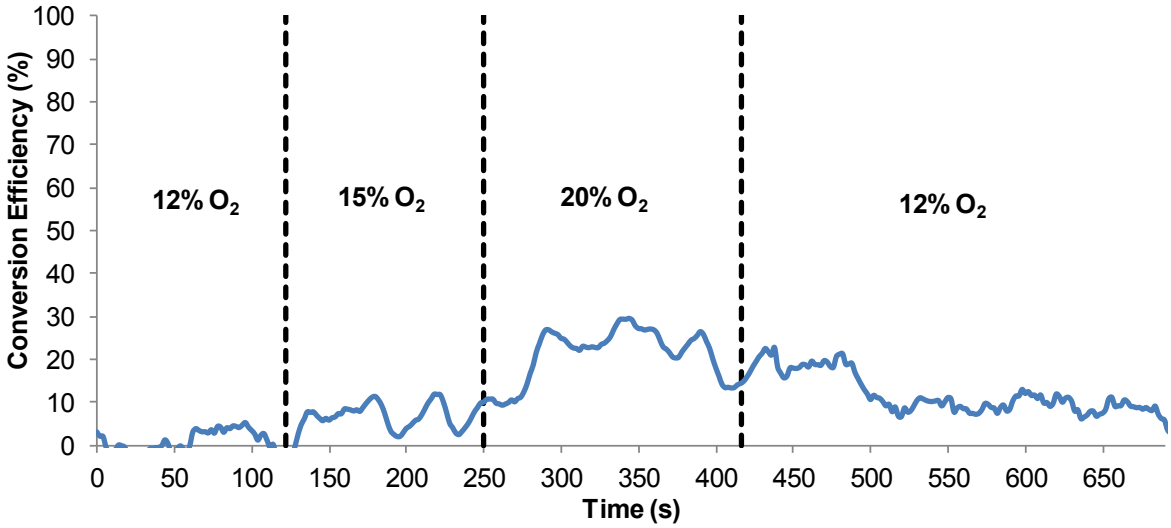


**Figure 5-17.** Effect of oxygen exhaust concentration on CO conversion efficiency at 120°C and 30 000/h space velocity

From 135°C onwards, the addition of oxygen was investigated at different space velocities to study how temperature and exhaust flow rate can be coupled to enhance CO conversion efficiency. The space velocity was not increased for the previous temperatures as the conversion was already limited at low space velocity.

Oxygen addition promoted the activity at 135°C and 30 000/h space velocity as it increased CO conversion from 60% with 12% $O_2$ to 80% with 20% $O_2$ (Figure 5-18). The oxygen "post-injection" effect was also noticeable at this temperature, as the conversion efficiency obtained at 20% oxygen concentration was maintained when the concentration was decreased back to 12%.

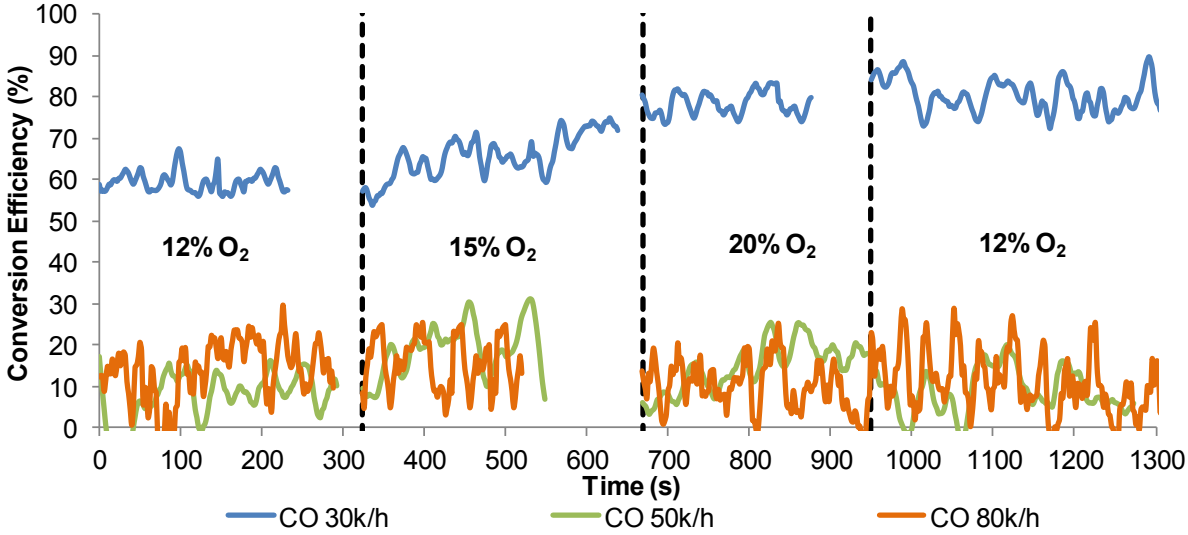


**Figure 5-18.** Effect of oxygen exhaust concentration and space velocity on CO conversion efficiency at 135°C

This effect was more pronounced at 135°C than at 120°C, due to the exhaust gas being warmer and requiring more time to cool the catalyst. Moreover, small increases in temperature can enhance dramatically the conversion efficiency as the reaction rates are considerably increasing in this range of temperature (Figure 5-1). As the space velocity increased (50 000/h and 80 000/h), the conversion efficiency remained limited due to the reduced exhaust gas residence time. At 50 000/h, the increase to 15% and 20% oxygen concentration seemed to promote the oxidation to a limited extent, while at 80 000/h, the oxygen injection did not affect the conversion efficiency at all. These limited improvements show that, at higher space velocities, the parameter mainly affecting the oxidation is the reduced exhaust gas residence time in the catalyst, and that it cannot be counteracted by an increase in oxygen availability. Moreover, high space velocities limit the local heating effect from the addition of oxygen, as there is a competition between the production of heat from the exothermic reaction and the high exhaust gas flow rate, evacuating the heat produced and cooling the catalyst.

At 150°C (Figure 5-19), CO conversion at low and medium space velocities was at its maximum efficiency (95%-100%). Therefore the possibility for further increase remained limited. A slight decrease in efficiency was noticed with 20% oxygen concentration at 30 000/h and 50 000/h. In this experiment, as the compressed oxygen exits the gas cylinder, the oxygen temperature would decrease and could cool the warm catalyst when injected in the exhaust.

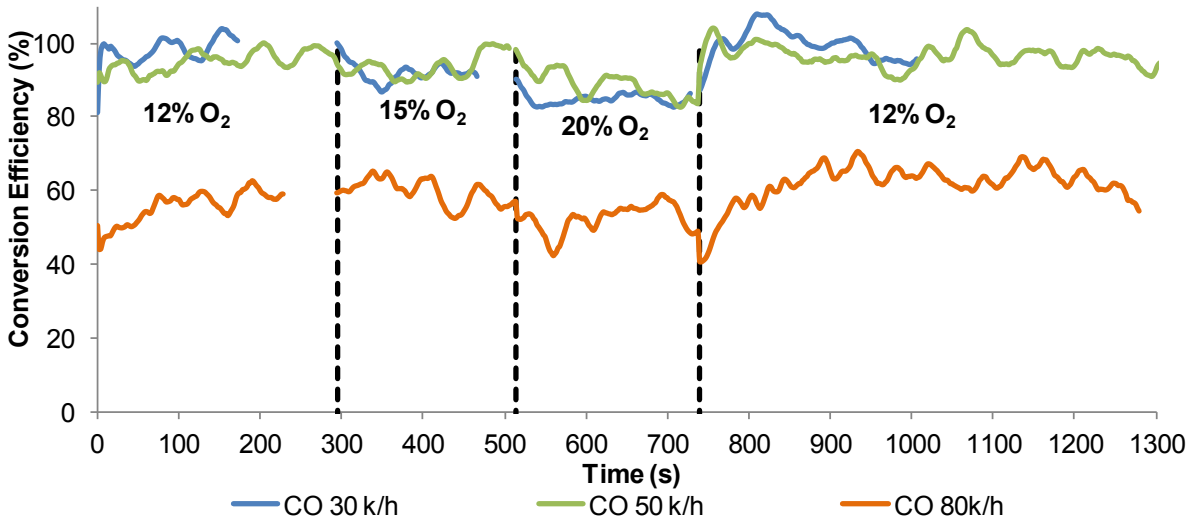


**Figure 5-19.** Effect of oxygen exhaust concentration and space velocity on CO conversion efficiency at 150°C

While at low temperatures (120-135°C) oxygen promoted the catalyst activity through heat production, at higher exhaust gas temperatures, it could have the opposite effect and reduce the oxidation efficiency through the cooling of some parts of the catalyst that could not be compensated by the heat produced from the exothermic reaction. During a cooling process, some of the catalytic sites can remain warm enough to promote a certain activity (hysteresis). Therefore, even if the catalyst temperature decreased due to the cooler oxygen, the conversion efficiency losses remained limited. Moreover, this reduction in the activity seemed to be only momentarily as the efficiency went back to its initial value when the oxygen injection was stopped. At higher space velocity (80 000/h), changes in oxygen concentration did not show any effect on the activity and the loss in conversion from the

oxygen cooling effect was more limited than for the lower space velocities. This was due to the conversion being already affected by the reduced residence time and the effect of a greater space velocity limiting, this time, the cooling caused by the injection of oxygen.

The injections of oxygen at 200°C showed similar effects to those at 150°C (losses in conversion when oxygen reached 20% concentration) and were therefore not presented here. These losses were lower than at 150°C as more active sites were warmer and already active to allow most of the conversion to take place. The high space velocity 80 000/h was again less affected by the cooling effect of oxygen at this temperature, due to the high flow rate at 200°C limiting the cooling.

The results from this first part (summarised in Figure 5-20) suggest that the addition of oxygen can enhance the DOC activity at low and medium space velocities and at temperatures where the catalyst is ready for oxidation.

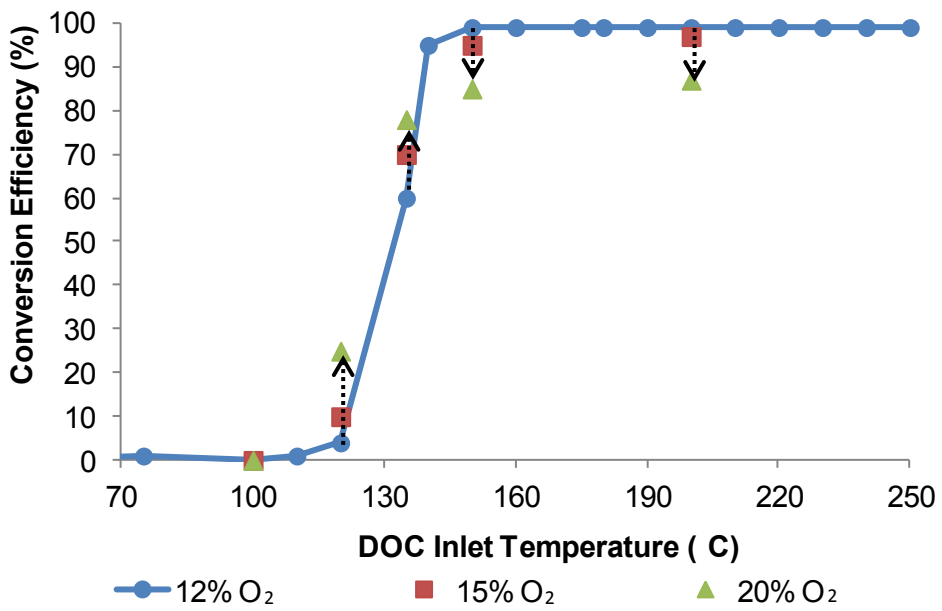


**Figure 5-20.** Summary of the effect of oxygen exhaust concentration on CO conversion efficiency in the DOC, at 30 000/h space velocity

Based on these outcomes, the effect of oxygen addition on the oxidation of CO and hydrocarbon species using exhaust gas from dual-fuel combustion was studied at the most relevant temperatures, close to the light-off, and at medium space velocity, in the following part.

### *5.3.2.3. Oxygen Effect on CO and HCs from Dual-Fuel Combustion*

At 160°C, the exhaust species (CO and light alkene) showed limited oxidation with 12% oxygen exhaust concentration (Figure 5-21).

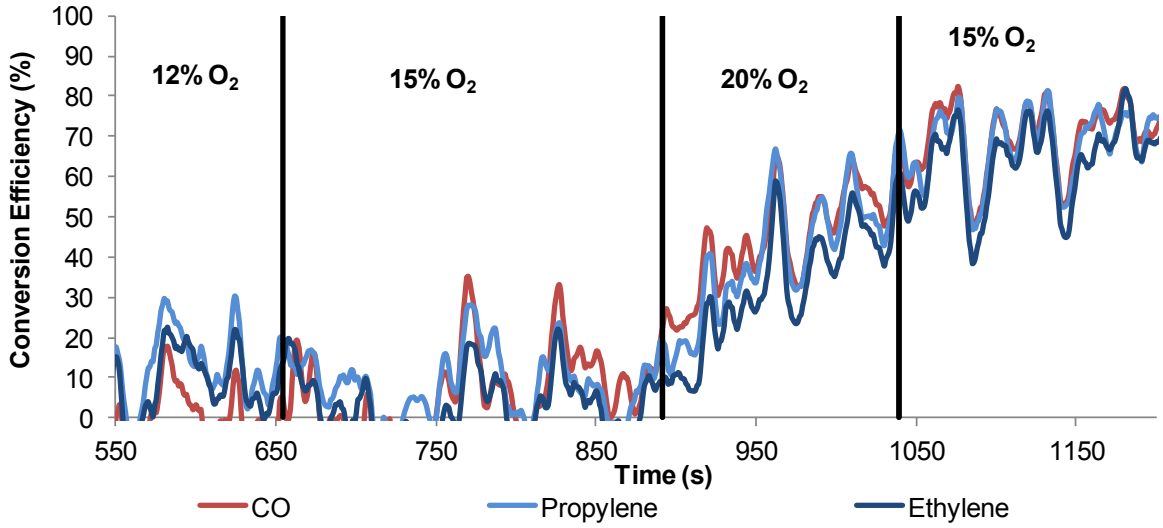


**Figure 5-21.** Effect of oxygen exhaust concentration on CO, propylene and ethylene conversion efficiency at 40 000/h space velocity

While increasing the oxygen content to 15% did not affect much the activity, with a 20% oxygen concentration, the oxidation reaction was suddenly triggered for both CO and the light alkenes. The exothermic oxidation of this high concentration of CO and alkenes is expected to have locally produced heat within the catalyst, which, in return, enhanced the activity, explaining the sharp increase in oxidation efficiency due to this chain reaction. At these conditions, no cooling effect and losses in conversion efficiency were recorded when reaching 20% oxygen concentration. The higher quantity of heat produced (greater CO and

alkene concentrations), was able to counteract the cooling from the ambient oxygen, compared to the diesel conditions. When oxygen content was reduced from 20% to 15%, the conversion formed a plateau at around 70% efficiency, showing that the catalytic sites remained active for CO and alkene oxidation despite the reduction in oxygen concentration. While at 20% concentration, the activity was promoted by the heat produced from the exothermic reaction, the reduction to 15% oxygen concentration led to a balance between heat production and cooling from the injected oxygen forming a plateau in the conversion efficiency.

From the medium-heavy hydrocarbons point of view, the increase in oxygen concentration from 15% to 20% did not show any promotion of the oxidation. Their conversion efficiency only increased after strongly-adsorbed CO and light alkenes had started oxidising and, by desorbing, freed some active sites which then became available for hydrocarbons to adsorb onto.

While the catalyst activity can be affected by gaseous species interactions, as previously presented, the presence of solid species in the exhaust gas (soot) and their accumulation over the catalysts walls also need assessing as part of this investigation on the effect of the exhaust gas composition on the catalyst activity.

## 5.4. EFFECT OF THE EXHAUST PM ON THE DIESEL OXIDATION CATALYST ACTIVITY

The location of the DOC, conventionally upstream of the particulate filter, results in a high concentration of particulate matter entering the catalyst. While its flow-through channels are not designed to trap exhaust particulates, the reduction in channel hydraulic diameter (increase in cell density) can lead to particulate accumulation on the walls and possible plugging of some channels. This could result in a reduction of the coated surface area available for the reaction, and therefore affect the long-term catalyst activity. This potential risk was assessed over the following experiment.

### 5.4.1. Effect of EGR Strategy on the DOC Activity

#### *5.4.1.1. Gaseous Exhaust Species*

The use of EGR strategy to increase the particulate concentration entering the catalyst and its subsequent increase in CO engine-out concentration did not affect significantly CO and HC oxidation at this steady-state condition (Figure 5-22). Conversely, the reduction in NO exhaust concentration due to EGR greatly lowered the production of $NO_2$ from NO oxidation in the DOC. It was shown before that NO oxidation efficiency can be influenced by the concentration of NO available in the feed gas, as NO is positive order for its oxidation reaction (Mulla *et al.*, 2005; Mulla *et al.*, 2006).

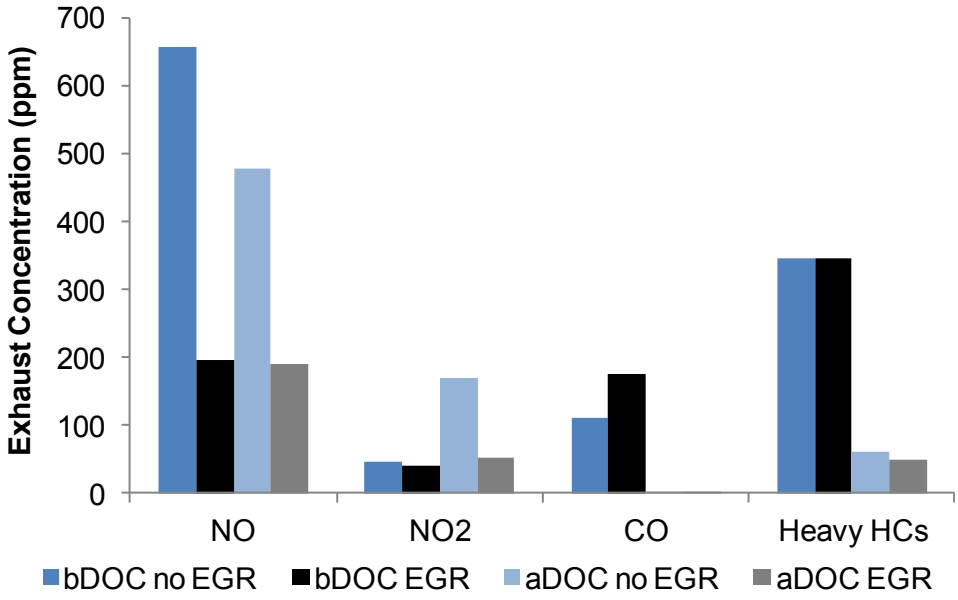


**Figure 5-22.** Effect of EGR on the exhaust gas concentration at the catalyst inlet and outlet

*5.4.1.2. Effect of EGR on the Soot Profile and PM Removal in the DOC*

Figure 5-23 shows that the use of EGR especially increased PM concentration in the medium-large particulate size range, shifting the particulate geometric mean diameter from 86.5 nm to 102.4 nm. The reduction in oxygen caused by the re-circulation of a portion of exhaust gas in the combustion chamber reduces the efficiency of the soot oxidation process taking place during the late combustion/expansion stroke a well as promotes the formation of fuel-rich zones where soot is created. Moreover, the use of EGR slightly reduced the small particulate concentration (below 30 nm), possibly due to an agglomeration and growth of these re-circulated particulates in the engine (Gill *et al.*, 2011).

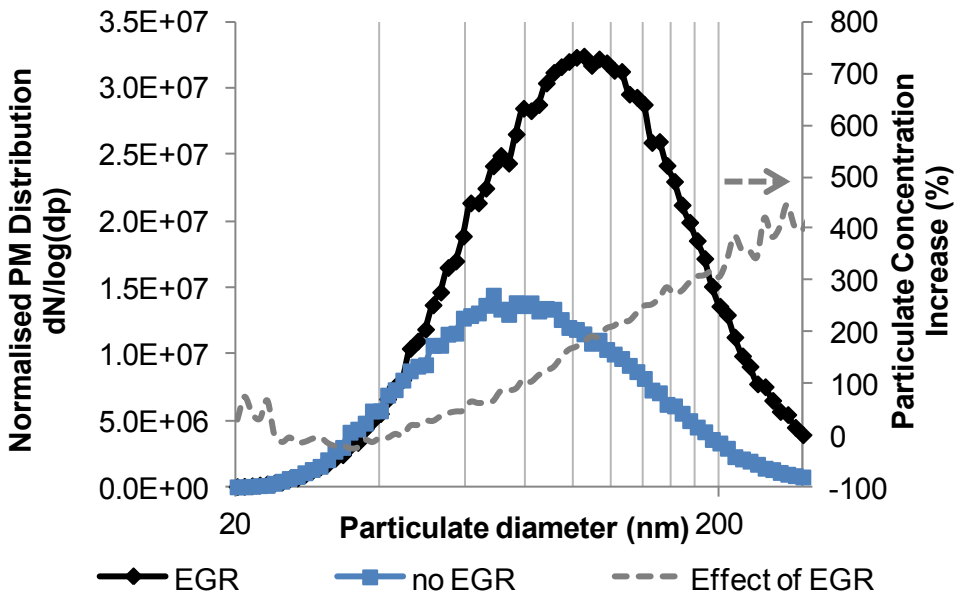


**Figure 5-23.** Effect of EGR on the engine-out particulate profile and concentration

These changes in PM profile and concentration from the use of EGR could also affect the particulate removal efficiency of the DOC. As the soot oxidation is particularly reduced in the combustion chamber, the re-circulation of exhaust gas (and therefore particulates) tends to increase more specifically the soot concentrations compared to the volatiles. This would translate into a reduction in PM removal over the DOC with the use of EGR, as the DOC is much less efficient in trapping soot compared to oxidising the volatile compounds (Johnson & Kittelson, 1996).

### 5.4.2. Effect of Particulate Matter on the DOC Activity

#### *5.4.2.1. Gaseous Exhaust Species Oxidation*

CO conversion efficiency did not show any degradation effect from the 8 hour exposure to the high engine-out PM concentration, while HCs presented little reduction in conversion efficiency (Figure 5-24). On the contrary, the production of $NO_2$ (recorded here as a negative conversion efficiency) decreased over time, showing a reduction in NO oxidation efficiency.

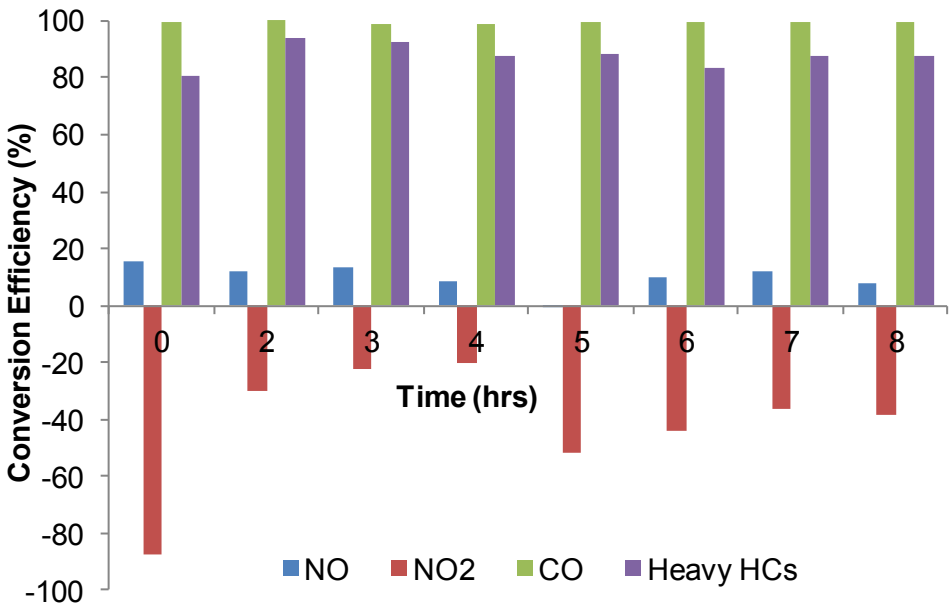


**Figure 5-24.** Effect of the duration of the test on the conversion efficiency over the DOC for NO, $NO_2$, CO and HCs

The measurement of $NO_2$ concentration at the catalyst outlet (Figure 5-25) showed a steady decrease over time before increasing at 5 hours and eventually decreasing again.

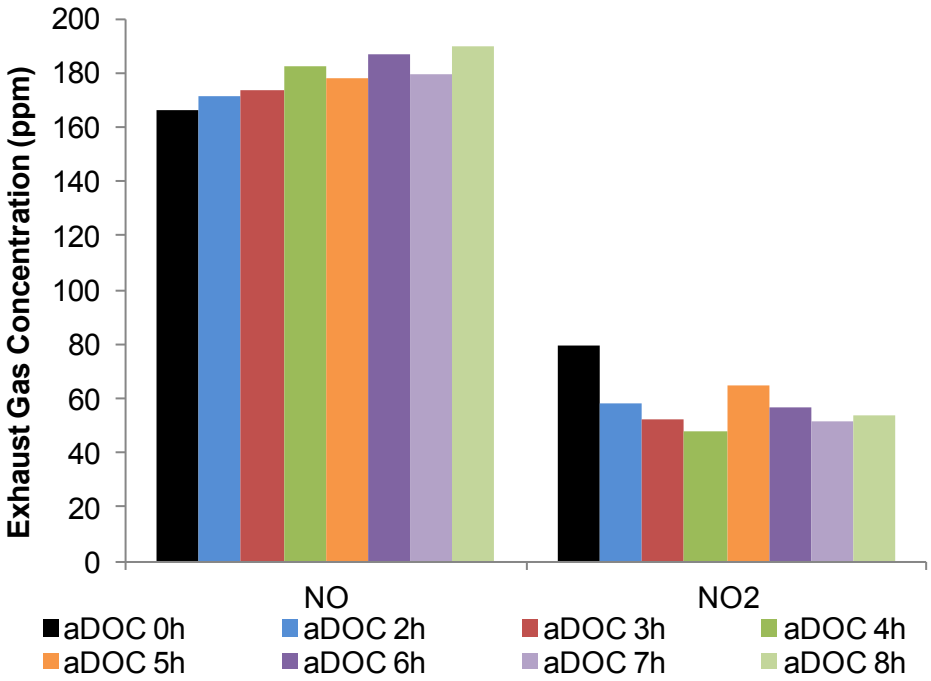


**Figure 5-25.** Effect of the duration of the test on NO and $NO_2$ catalyst outlet concentrations

Small changes in NO inlet concentration, as presented in Figure 5-22 could not be solely accounted for this $NO_2$ behaviour. Some studies have highlighted the deactivation of the catalyst by the oxidation of platinum particles in rich-oxygen environment (Hauff *et al.*, 2012). While the presence of reductant species such as CO and hydrocarbons can assist in reducing back PtO and promote the reactivation of the catalyst, it is proposed that, after a certain time, the accumulated particulates could also act as a reductant for some of the platinum oxides, partially restoring the catalyst NO oxidation activity. Moreover, it is hypothesised that NO limited oxidation could also be more affected by a reduction in the coated surface available for reaction (due to the soot accumulation). In that case, the increase in $NO_2$ production noticed after five hours could be due to a possible removal of some of the accumulated particulates (blow-off), slightly restoring the catalyst activity before the soot accumulation started again.

While these PM effects on NO oxidation remained limited over time, they could deteriorate to a greater extent the activity of specific catalysts (flow-through or wall-flow types) designed to produce $NO_2$, such as the SCRF.

The last part of this study on the soot interactions with the oxidation catalyst concentrates on the evolution of the PM removal efficiency within the DOC over time.

#### *5.4.2.2. Particulate Matter Removal*

Figure 5-26 shows a 14% reduction in the particulate number over the DOC at the beginning of the experiment which decreased to 7% after 7 hours, before increasing again at the end.

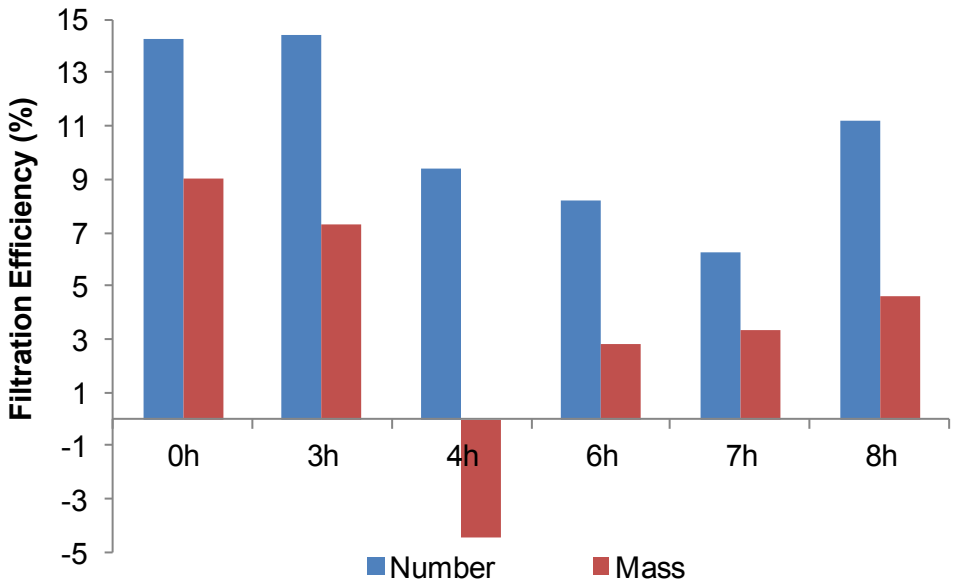


**Figure 5-26.** Effect of the duration of the test on the particulate removal (number and mass) over the DOC

This evolution shows a particulate saturation of the catalyst after some time. The smaller hydraulic diameter of the substrate cells would be expected to reduce the soot path length, promoting soot agglomeration within the channels. The filtration in terms of mass remained more limited, as presented in Johnson & Kittelson (1996) and even showed a negative efficiency value at 4 hours. The low sulphur content in the fuel (below 50 ppm) and the temperature range considered here (280°C) limited the possibility of sulphate oxidation in the DOC, which would increase the concentration of small particulates at the catalyst outlet (McDonald *et al.*, 1995). This loss in mass filtration while maintaining a 10% filtration efficiency in terms of number could highlight a blow-off event of previously accumulated small particulates that would agglomerate before being released, increasing the particulate geometric mean diameter at the catalyst outlet (Figure 5-27) .

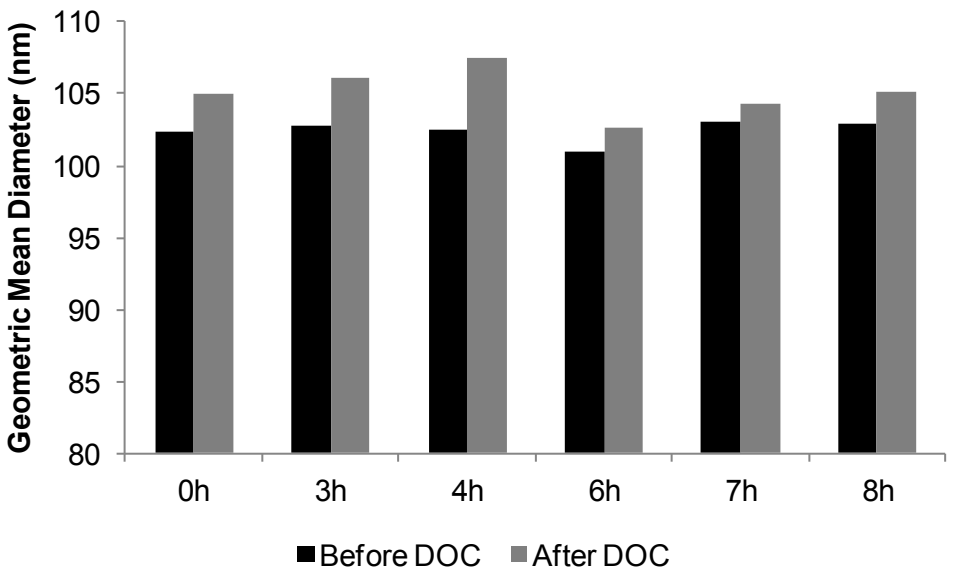


**Figure 5-27.** Evolution of the particulate geometric mean diameter at the catalyst inlet and outlet, over the duration of the experiment

The re-increase in mass filtration after 4 hours shows that the blow-off event allowed a certain regeneration of the catalyst, promoting again particulate removal, simultaneously to the re-gain in NO oxidation efficiency noticed in Figure 5-25. Nevertheless, this "regeneration" did not allow a promotion of the filtration efficiency in terms of particulate number which continued to decrease over time.

The study of the filtration efficiency for different particulate sizes (Figure 5-28) promotes the previous hypothesis about soot agglomeration blow-off. The number of small and medium particulates (20-50 nm) was reduced by 10-20% within the catalyst, from the oxidation of condensed hydrocarbons and possible particulate trapping through diffusion. A decrease in the efficiency was recorded as the particulate diameter increased, eventually reaching negative values for PM diameter larger than 200 nm. In addition to the blow-off of agglomerated small particulates, the inertia of the largest particulates, following the exhaust gas stream in the flow-through catalyst would have promoted this negative filtration efficiency noticed after 4 hours, due to a release of particulates at the catalyst outlet. The

evolution of the filtration efficiency with time showed a decrease by half of the filtration for the 20-60 nm PM while, for the largest particulates, the efficiency plunged below zero, with an increasing number of particulates being released to the atmosphere.

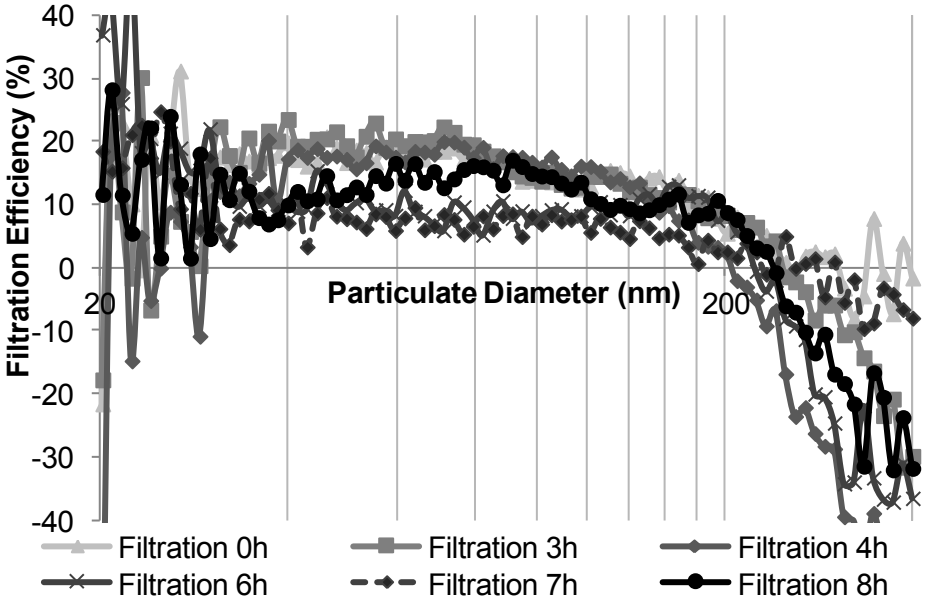


**Figure 5-28.** Effect of the duration of the test on the DOC filtration efficiency in terms of particulate size

Experiments at different engine operating conditions (modification of the engine-out PM distribution/concentration and exhaust flow rate) could lead to different results in terms of particulate removal over the DOC, i.e. a greater flow rate could reduce the PM deposition and volatile oxidation while increasing blow-off phenomena. Nevertheless, it can be noticed that the oxidation catalyst tended to "regenerate itself" after some time, limiting the long-term effect of soot accumulation on the oxidation efficiency of gaseous species. No significant pressure increase was recorded over time, showing a negligible effect of the soot accumulation on the backpressure.

After its removal from the exhaust system, the catalyst was noticeably black and some accumulated elements were visible in the centre of the inlet face (Figure 5-29). Some of these elements were fragments originating from the Interam® material used to wrap the catalyst, as

well as soot cake accumulation deposits. While some parts of the front face and channels were plugged, the affected area remained limited compared to the total frontal surface. Therefore, it is expected that the major contributor to the changes in filtration and oxidation noticed in this experiment would have been accounted for by some soot accumulation within the channels rather than on the front face.

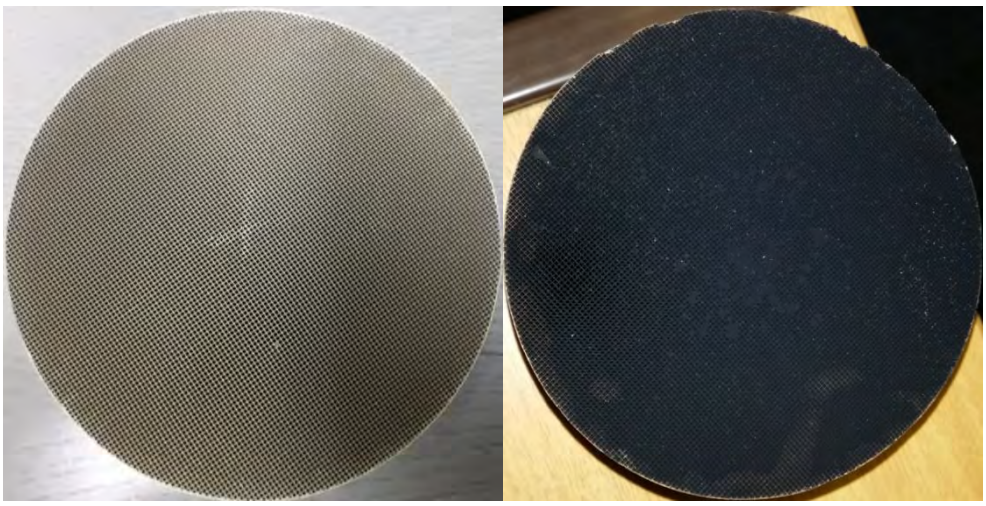

**Figure 5-29.** DOC front face before the experiment (left) and once removed from the exhaust system after the 8 hour test (right)

## 5.5. SUMMARY AND CONCLUSIONS

This chapter presented some strategies to enhance the catalyst activity through the understanding of the effects of the exhaust gas composition on the catalyst activity. Some interactions between exhaust gas species (CO, HC, $NO_x$ and $O_2$) were shown to affect the oxidation, either promoting it (momentary removal of gaseous species, addition of oxygen) or inhibiting it (adsorption competition on active sites). One aspect also highlighted was the limited removal efficiency of PM over the DOC. The use of an alternative substrate to replace the flow-through catalyst, designed to combine oxidation and filtration functions could enhance this limited particulate removal and assist the downstream DPF. This concept is developed in the following chapter, through the study of partial-flow filters.

# 6. COMBINATION OF FILTRATION AND OXIDATION FUNCTIONS TO IMPROVE THE DPF THERMAL MANAGEMENT

This study investigates the potential of using a partial-flow filter (PFF) as a replacement for an oxidation catalyst, to combine both filtration and oxidation functions within one aftertreatment component. The ultimate aim is to reduce the frequency and/or duration of the DPF active regeneration, whilst promoting efficient particulate removal. This combination of functions also takes advantage of the close-coupled position (higher temperature profiles) to promote more frequent passive regeneration of the PFF. The filtration mechanisms and efficiency, oxidation activity, as well as the long-term activity of the potential partial-flow filter candidates (PM-Metalit and POC) and flow-through catalysts (LS and conventional 400/4 DOC) were investigated and compared to allow the selection of the most relevant components to be used finally in a PFF+DPF configuration.

## 6.1. METHODOLOGY

### 6.1.1. Filtration and Oxidation Mechanisms and Efficiencies

The engine was operated at various conditions to study the filtration mechanisms and compare the filtration, oxidation, pressure and temperature behaviours of the different components, i.e. PM-Metalit, POC, LS and DOC (Components 10, 9, 8 and 2 respectively in Table 3-4). These conditions were selected to vary the exhaust gas properties, in terms of particulate matter profile (using different percentages of exhaust gas recirculation and engine load) and space velocity (varying the engine flow rate) to estimate if the components could maintain a significant PM removal under changing engine conditions.

When comparing the particulate filtration efficiency of the PM-Metalit, POC, LS and DOC, similar engine conditions (PM concentration and profile, space velocity and exhaust gas temperature) were used to isolate the effect of the aftertreatment component. Due to its shorter length, the space velocity in the PM-Metalit was slightly higher compared to the other catalysts, at the same engine conditions.

While the PM-Metalit was left uncoated, the POC, LS and conventional DOC were coated with a catalytic formulation promoting the oxidation of exhaust gas pollutants. When investigating the PM removal for these components, not only the physical trapping of particulates but also the oxidation of the volatile fraction needed to be considered. Additionally to the space velocity and PM profile, the temperature and particulate composition (volatile hydrocarbons and solid carbon) were additional parameters that could affect the filtration efficiency. The nature of the particulates can be altered by a change of engine load (i.e. higher loads producing a greater fraction of solid particulates with less condensed hydrocarbons) and by the use of EGR (increase in soot particulates compared to volatile compounds). The analysis of the PM removal for these coated components is therefore more complex as, for example, an increase in load reduces the contribution of volatiles to total PM while increasing, at the same time, the exhaust gas temperature that would promote volatile hydrocarbon oxidation. Moreover, the coating can also promote the formation of sulphate compounds from the oxidation of the sulphur present in the fuel at high exhaust gas temperature. Nevertheless, this mechanism was expected to remain limited due to the low sulphur content of the diesel fuel used in this study (below 50 ppm).

For the comparison at idle engine operating condition, the low engine speed (750 rpm) greatly reduced the space velocity within the aftertreatment component to 15 000/h. The particulate size distribution was also shifted towards smaller particulates and lower total concentration due to a reduction in the quantity of fuel injected in the combustion chamber.

Furthermore, at this condition, the low exhaust gas temperature allowed water and some hydrocarbons to condense in the exhaust. Due to the low soot concentration, these condensates could not easily adsorb onto solid particulates and therefore formed small liquid droplets on their own, constituting most of the nuclei particulates measured in the engine exhaust gas at this condition. At this condition, the majority of the particulate number is located in the small PM size range (10 nm to 40 nm) while the mass weighting is still more dominant in the PM diameter range over 50 nm, despite the presence of fewer particulates of this size (Figure 6-1). This PM distribution profile, composed of a higher portion of nuclei particulates and fewer accumulated ones, made idle a relevant additional condition to study the filtration efficiency of the investigated aftertreatment components.

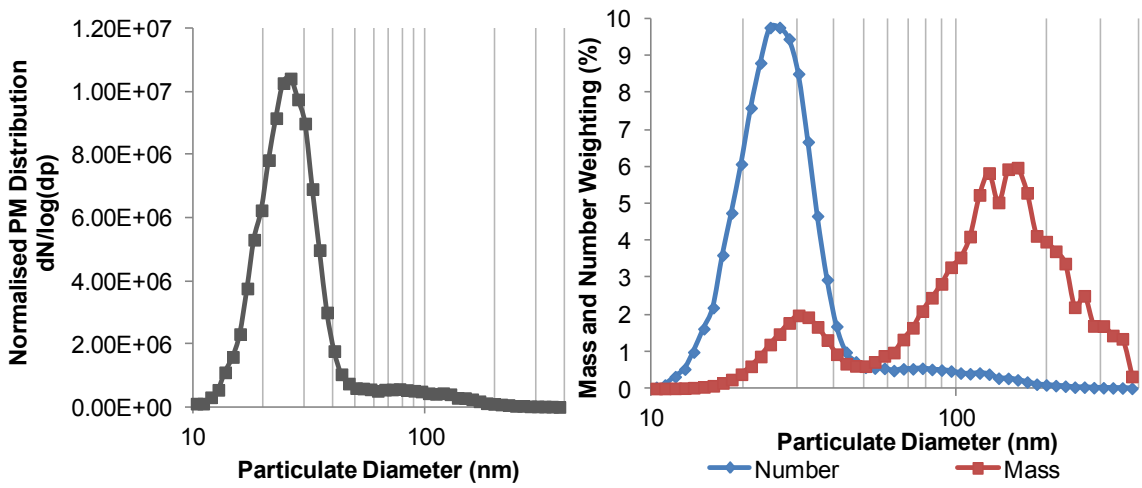


**Figure 6-1.** Engine-out PM profile (left) and mass and number weighting over the particulate diameter (right) for the idle engine condition

### 6.1.2. Long-Term Filtration and Oxidation Activity

The long-term activity was investigated by exposing the aftertreatment components to the exhaust gas from a steady-state engine operating condition (1500 rpm, 4 bar IMEP) and record the evolution of their filtration and oxidation efficiency over time.

Over the experiment, the mass of soot accumulated in the PFFs, in grams of soot per litre of filter, was estimated based on the engine-out soot mass emissions, the average mass

filtration of the filter and the duration of the test. This approach neglected any passive regeneration that would oxidise the particulates into CO and $CO_2$. It was assumed that the passive regeneration of the PM-Metalit would be reduced due to the absence of catalytic coating while for the POC, the temperatures reached during this experiment (250°C) would limit any regeneration. The filters were loaded over a period of 8.5h.

The flow-through channel design of the LS substrate and DOC limits the soot accumulation in these catalysts, leading to a limited PM removal, especially in mass. Moreover, as previously presented in sections 5.4 and 6.2, these catalysts appeared to "self-regenerate" and clean themselves through frequent and uncontrolled particulate blow-off events. This unsteady filtration efficiency makes the mass of soot accumulated within these catalysts difficult to estimate. Therefore, their long-term filtration efficiency was investigated in terms of duration, rather than soot loading within the component.

### 6.1.3. Partial-Flow Filters Passive Regeneration Study

#### *6.1.3.1. Passive Regeneration of the PM-Metalit*

For the investigation of the behaviour of the PM-Metalit during passive regeneration, two sources of $NO_2$ were used. First, specific engine operating conditions were selected to produce average exhaust gas temperatures over 250°C, as this is expected to be the minimum temperature required for the soot oxidation with $NO_2$ (Okawara *et al.*, 2005). At these conditions, the engine produced up to 56 ppm of $NO_2$ and this concentration decreased as the exhaust gas temperature increased, due to the changes in load. However, due to the limited engine-out $NO_2$ concentrations recorded at these conditions, the second part of the study adds external $NO_2$ to the system to further investigate the promotion of the regeneration efficiency. $NO_2$ inlet concentration was varied from 100 ppm to 400 ppm and CO, HC and $NO_x$ outlet

concentrations were recorded at an engine operating conditions producing an exhaust gas temperature of 420°C.

#### *6.1.3.2. Passive Regeneration of the POC*

For this experiment, a DOC was placed upstream of the POC to remove CO from the exhaust gas and allow the measurement of any CO produced in the POC from the partial oxidation of soot. Due to the high concentration of $CO_2$ in the feed gas, it was not possible to measure the eventual production of $CO_2$ from complete soot oxidation. For this experiment, the engine operating condition was selected to produce an exhaust gas temperature of 360°C.

### 6.1.4. Combined PFF+DPF System

To investigate the interest of a PFF+DPF system, the PM filtration efficiency, soot loading and pressure increase of a DPF fitted with an upstream PM-Metalit and then POC was recorded and compared to a standalone DPF during a 7 hour experiment. The steady-state engine operating condition for this experiment (1500 rpm, 5 bar IMEP with 15% EGR) was selected to allow the production of a significant concentration of engine-out particulates to study the evolution of the DPF loading.

## 6.2. STUDY OF THE FILTRATION MECHANISMS

As part of the PFF investigation, it is necessary to understand the filtration mechanisms within these aftertreatment components as they are different from the conventional wall-flow filters, due to their specific channel design.

### 6.2.1. Partial-Flow Filters

#### *6.2.1.1. PM-Metalit*

Effect of the Particulate Matter Profile on the PM-Metalit Filtration Efficiency

For both sets of space velocities (Figure 6-2 and Figure 6-3), the effect of an increase in PM concentration was different depending on their diameter. The higher concentration of medium-large particulates at the filter inlet (48 000/h 30EGR condition) could lead to an increase proportion of these larger particulates in the flow by-passing the membrane and limit the filtration of small PM, as they could affect the access of small particulates to the filtering medium in zone 2 and 3 (Figure 2-5). At moderate PM levels this decrease in filtration efficiency was compensated as higher concentration of small PM promoted their removal through diffusion mechanisms (relying on particulate concentration gradients) compensating the previous effect. On the contrary, changes in the PM concentration profiles did not affect medium-large PM filtration efficiency. Their filtration mainly relies on the portion of flow diverted towards the fleece which is not much affected by the concentration of exhaust PM but rather by a change in space velocity.

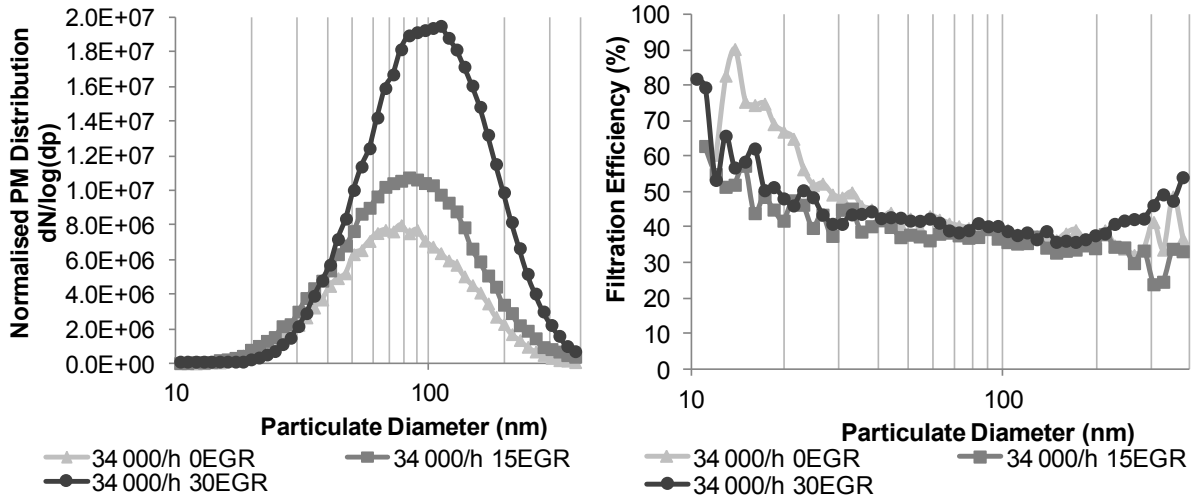


**Figure 6-2.** PM-Metalit filtration efficiency (right) for different PM profiles (left) at 34 000/h space velocity

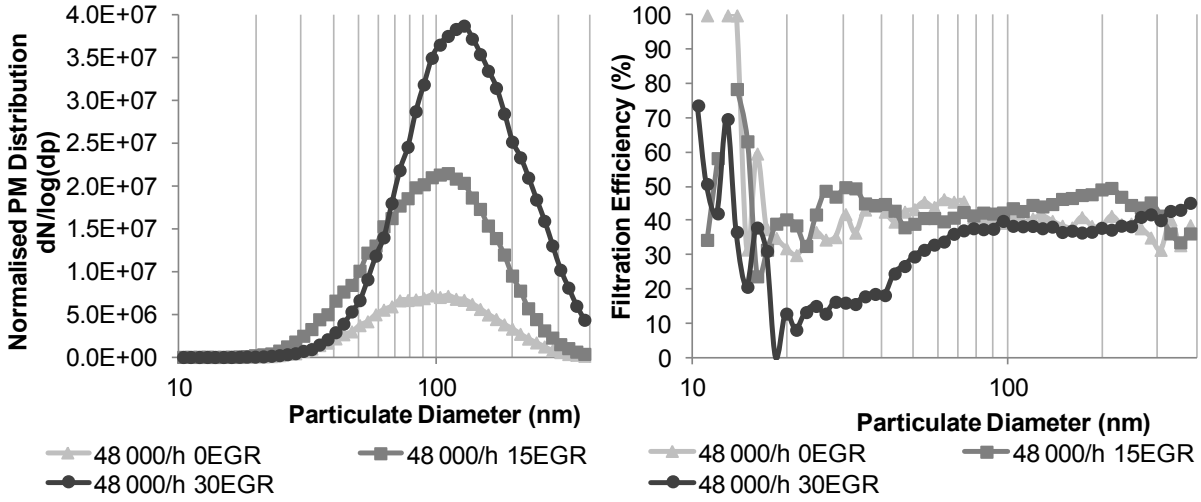


**Figure 6-3.** PM-Metalit filtration efficiency (right) for different PM profiles (left) at 48 000/h space velocity

Figure 6-4 shows that the PFF was able to maintain its filtration efficiency over 25%, in terms of mass and number, for the different engine operating conditions, despite the changes in PM profiles and flow rates.

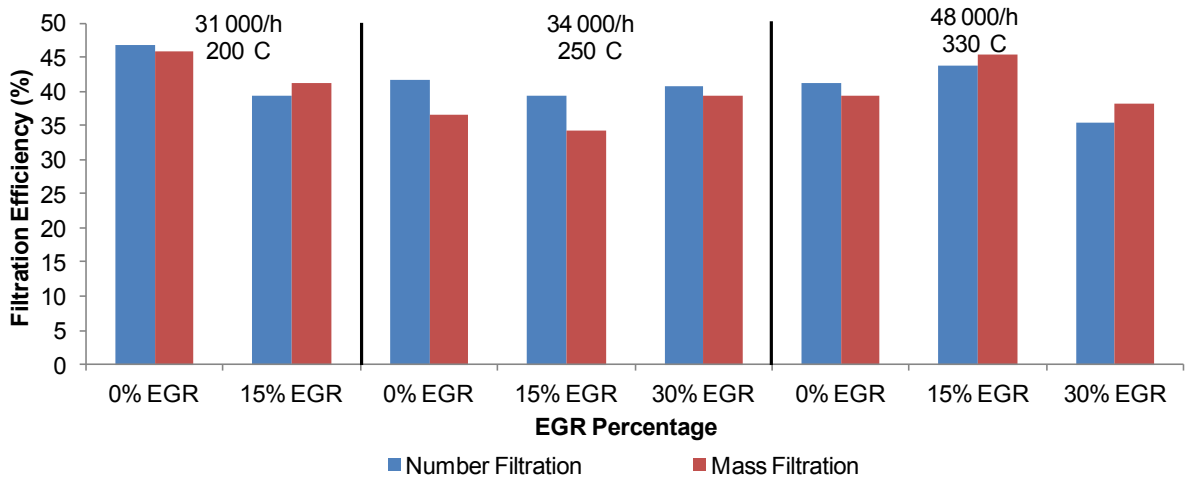


**Figure 6-4.** PM number and mass filtration efficiency over the PM-Metalit for the different space velocities and PM profiles

Effect of Space Velocity on the PM-Metalit Filtration Efficiency

The main effect of increasing the exhaust flow rate on the filtration mechanisms within the PM-Metalit is that a greater portion of exhaust gas can be pushed through the membrane, in zone 1 (Figure 2-5), leading to two conflicting effects on the removal of small PM. On one hand, the greater portion of exhaust gas flowing through zone 1 (Figure 2-5) reduces the quantity of small particulates being treated in zone 2 and 3 (smaller portion of exhaust gas), which could reduce their removal. On the other hand, the exhaust gas velocity in these zones (2 and 3) is reduced, which can promote the filtration of small particulates in this zone.

The results presented in Figure 6-5 show that changes in space velocity at a limited flow rate did not affect the removal of small PM. Further increase of the space velocity could eventually affect the exhaust gas residence time within the filter (increased velocity in zone 2 and 3) and therefore reduce the filtration efficiency for this range of particulate size, especially at conditions combining high space velocities with high inlet PM concentration (48k/h 30EGR and 54k/h 0EGR in Figure 6-6). The two-side effects of increasing the exhaust gas flow rate (reduced velocity in zone 2 & 3 but increased overall flow rate) needs to be further assessed to define where the balance between the two effects is.

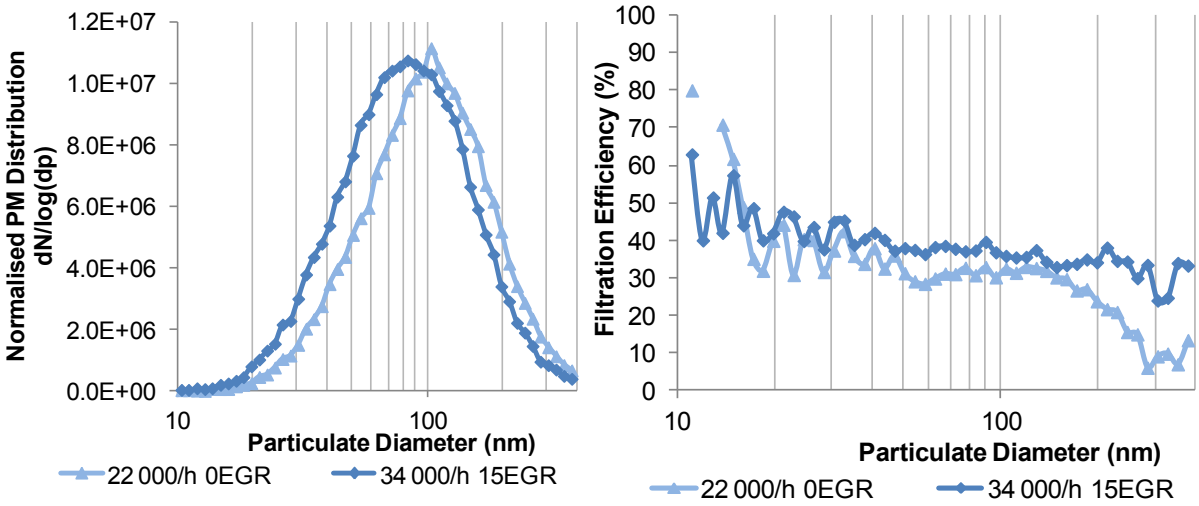


**Figure 6-5.** PM-Metalit filtration efficiency (right) at comparable PM profiles (left) for two different space velocities

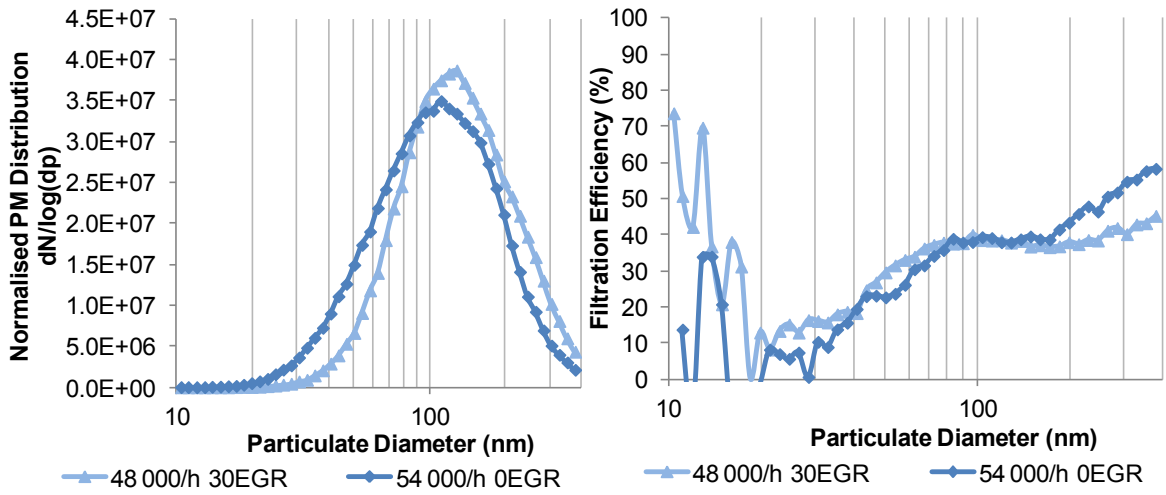


**Figure 6-6.** PM-Metalit filtration efficiency (right) at comparable PM profiles (left) for two different space velocities

In the case of medium-large particulates, the filtration was promoted by an increase in space velocity, due to the greater portion of exhaust gas diverted towards the fleece, where the filtration for medium-large PM takes place. Nevertheless, as the exhaust flow rate further increases, the residence time within the filter would also be reduced, which could eventually affect the filtration at greater space velocities.

For the different sets of conditions, the filtration in terms of mass and number (Figure 6-7) was always greater at higher space velocity, independently of the inlet PM concentrations. Moreover, as the space velocity increased, the mass filtration seemed more promoted than the number filtration due to the greater removal of medium-large particulates accounting for most of the total PM mass.

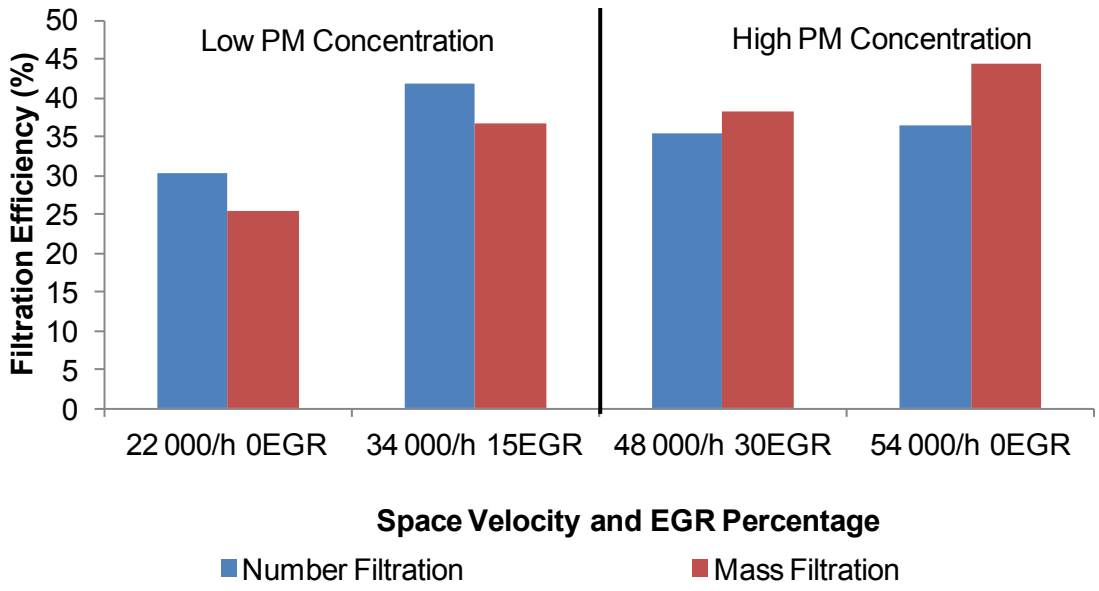


**Figure 6-7.** Effect of the space velocity on PM number and mass filtration efficiency over the PM-Metalit for comparable PM profiles

The PM-Metalit showed significant filtration efficiency (over 30% and 25% for particulate number and mass filtration efficiency respectively) despite changing engine conditions, with slight losses in efficiency at conditions with high space velocity and PM concentration.

*6.2.1.2. POC*

Effect of the Particulate Matter Profile on the POC Filtration Efficiency

At low space velocity (Figure 6-8), only the highest PM concentration (28 000/h 30EGR) showed a decrease in the filtration efficiency over the whole diameter range. This could be caused by a saturation of the coated membrane by particulates, limiting the filtration and allowing the exhaust gas to by-pass the filtration medium. As the space velocity increased (Figure 6-9), the increase in PM concentration showed a limited effect on the POC filtration. The saturation of the membrane by particulates seemed to be counteracted by an increase in space velocity, possibly as a greater portion of exhaust gas was pushed through the membrane, overcoming the PM accumulation. Changes in PM composition caused by the use

of EGR (reduced volatile fraction in PM) could also affect to a limited extent the removal of small particulates from the oxidation of volatile compounds.

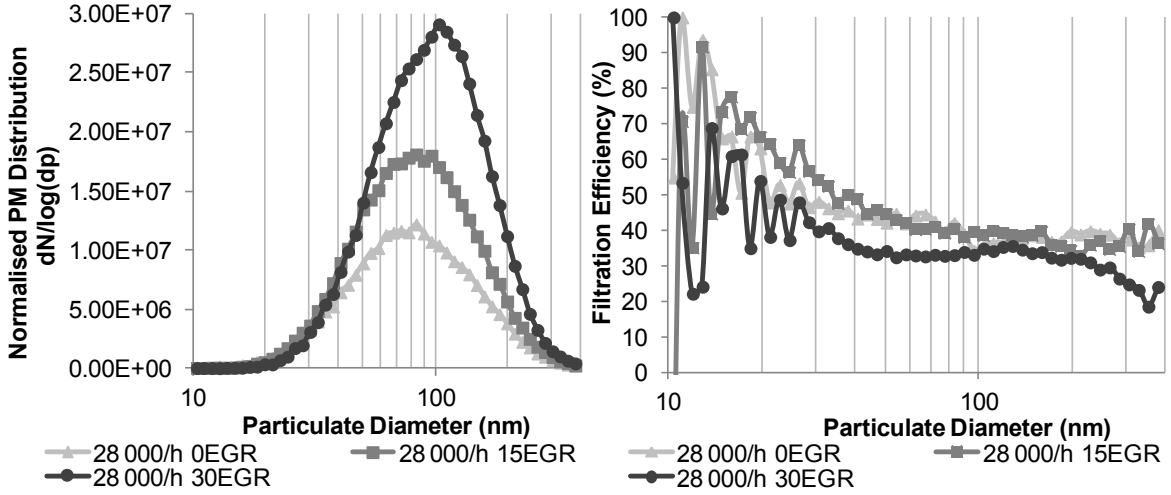


**Figure 6-8.** POC filtration efficiency (right) for different PM profiles (left) at 28 000/h space velocity

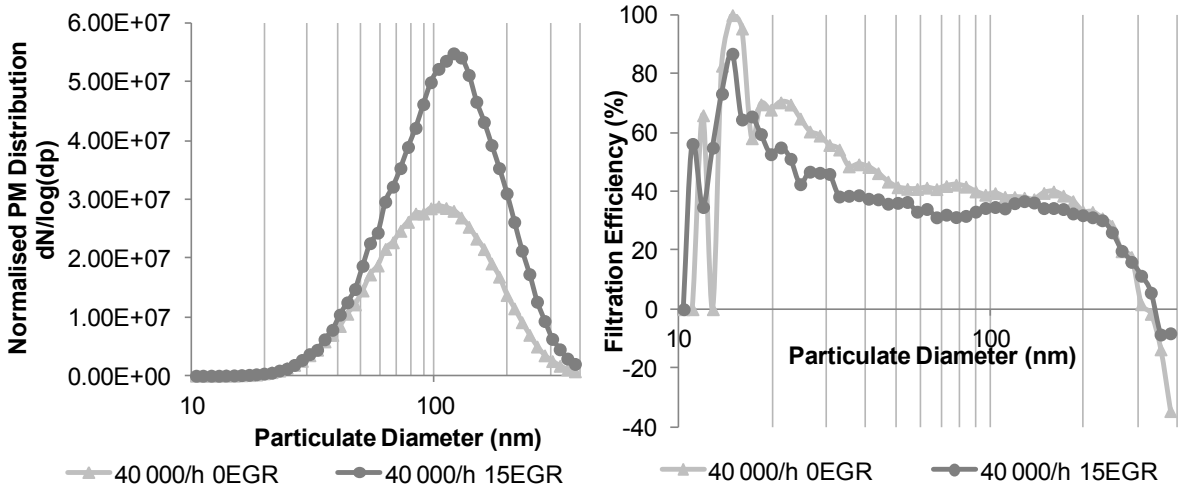


**Figure 6-9.** POC filtration efficiency (right) for different PM profiles (left) at 40 000/h space velocity

This resulted in a constant decrease in mass and number filtration efficiency with an increase in the PM concentration for low and medium space velocity (Figure 6-10) while it remained unchanged for the highest space velocities (40 000/h and 44 000/h).

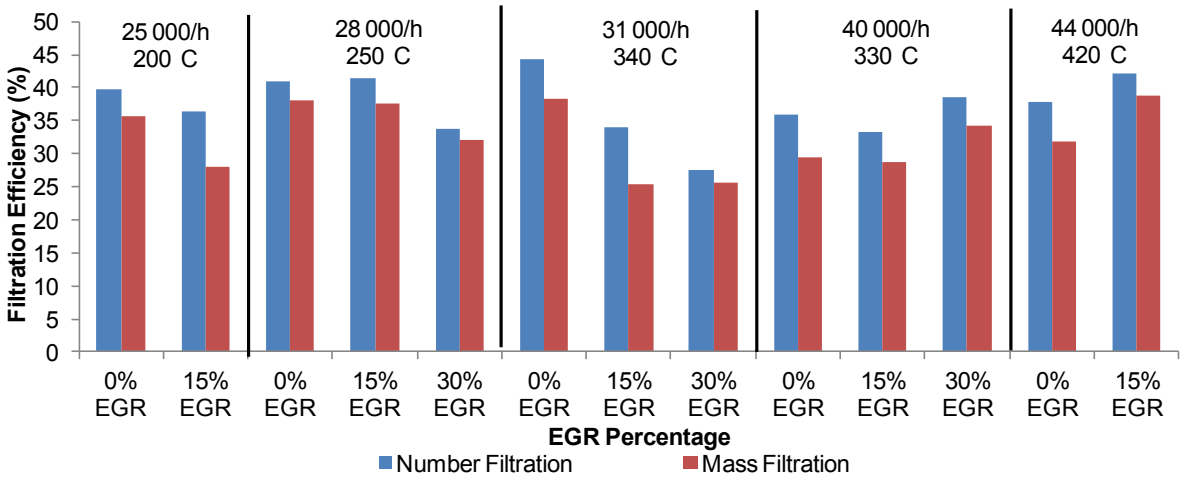


**Figure 6-10.** PM number and mass filtration efficiency over the POC for the different space velocities and PM profiles

Effect of Space Velocity on the POC Filtration Efficiency

The effect of increasing the space velocity for comparable PM profiles led to an improvement in the filtration efficiency of small and medium particulates but a decrease in filtration for the largest ones (Figure 6-11 and Figure 6-12). This decrease was especially noticeable at high space velocity, where the filtration became negative (44 000/h 0EGR). On one hand, an increase in the flow rate would lead to a greater portion of exhaust gas being pushed through the membrane, enhancing the PM filtration. On the other hand, as the flow further increases, and due to the membrane being coated (reduced porosity), more exhaust could by-pass the filtration stages, reducing the removal of the largest particulates. The fact that these particulates were less efficiently removed and that their concentration was even increased at the filter outlet (negative filtration, Figure 6-12), could be also due to a release of previously accumulated particulates (blow-off), carried away by the passing high flow. As the space velocity further increased, the gain in filtration lowered, due a reduction in the residence time. The higher exhaust gas temperatures reached for the high space velocity conditions could also promote the oxidation of PM volatile compounds, accounting for some

of the removal recorded for small and medium PM, counteracting the reduction in the residence time from higher flow rates.

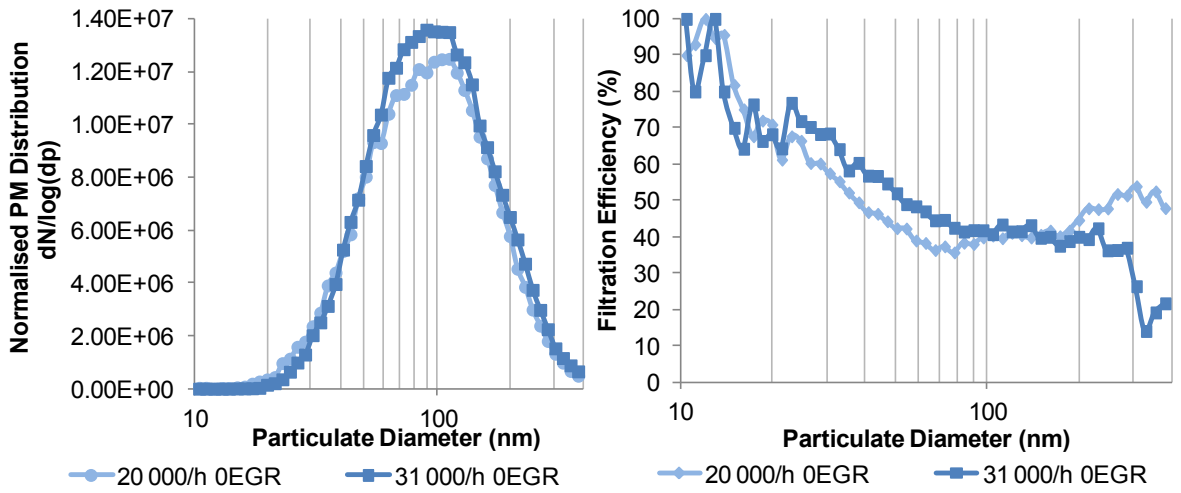


**Figure 6-11.** POC filtration efficiency (right) at comparable PM profiles (left) for two different space velocities

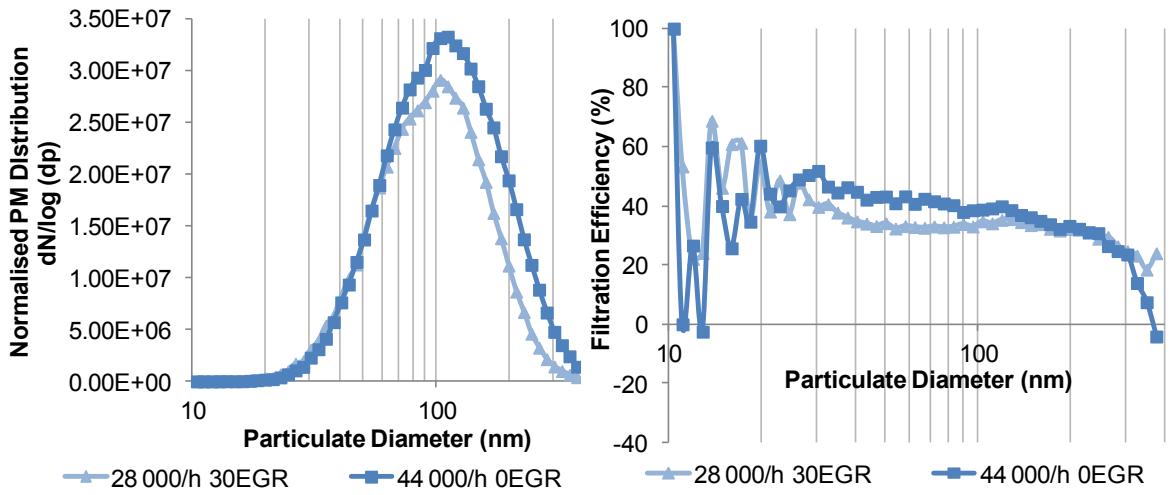


**Figure 6-12.** POC filtration efficiency (right) at comparable PM profiles (left) for two different space velocities

The limited filtration efficiency of the POC (Figure 6-13) at low PM concentration was enhanced by an increase in space velocity promoting medium size PM removal. For greater space velocities at high PM concentrations, the gain in filtration from an increased flow rate was reduced (shorter residence time), leading to comparable filtration efficiency at 28 000/h and 44 000/h.

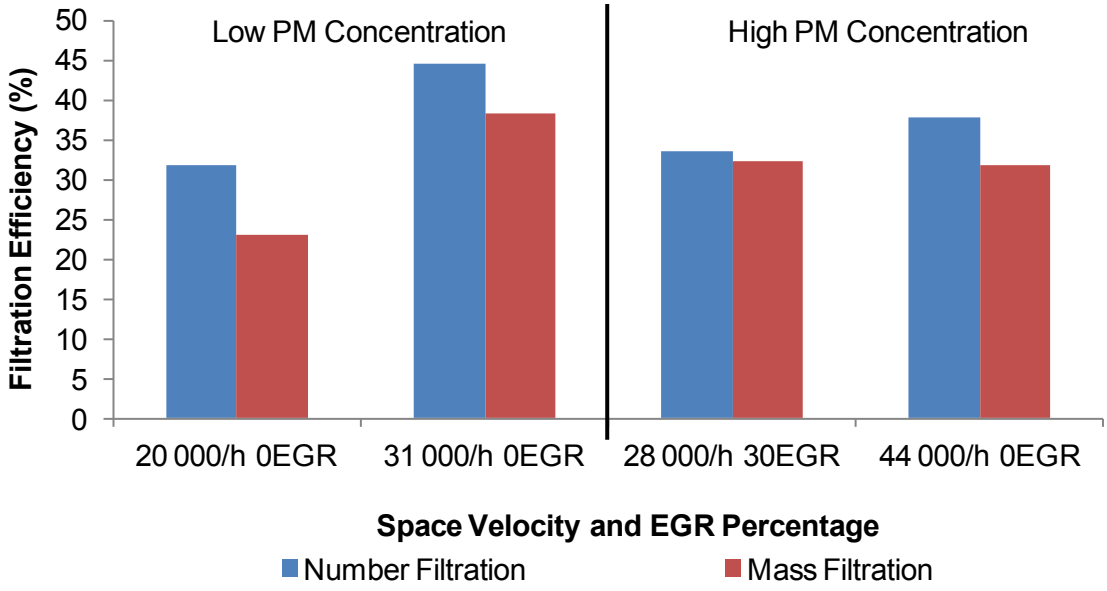


**Figure 6-13.** Effect of the space velocity on PM number and mass filtration efficiency over the POC for comparable PM profiles

While the filtration was affected by changes in the engine operating conditions, the POC showed that it could maintain a mass and number filtration over 25% and 27% efficiency, respectively.

The two previous components (PM-Metalit and POC) are partial-flow filters types with a filtering medium allowing a PM removal over 25% efficiency, while the following components are flow-through catalysts (LS and conventional DOC) which are studied to obtain a broader view of the filtration mechanisms taking place within different substrate technologies.

### 6.2.2. Flow-Through Catalysts

The removal of particulates within flow-through catalysts, such as the LS catalyst or the conventional DOC tested here, relies heavily on the oxidation of the volatile fraction composing the particulate matter (condensed and adsorbed hydrocarbons), and remains limited towards physical particulate trapping (Johnson & Kittelson, 1996).

*6.2.2.1. LS Catalyst*

Effect of the Particulate Matter Profile on the PM Removal in the LS Catalyst

At low space velocity (Figure 6-14), with an exhaust gas temperature of 220°C, an increase in inlet particulate concentration did not affect the removal of the small-medium size PM but degraded the trapping of the large particulates. The removal of the small-medium size particulates could be mostly accounted for by diffusion losses enhanced by the presence of the catalyst. The sharper decrease towards negative filtration for the largest particulates shows the release to the atmosphere of particulates over 200 nm diameter, formed by previously accumulated and aggregated particulates within the catalyst. The changes in particulate composition from using EGR could also explain the losses in filtration for the largest particulates, as the volatile fraction that can be oxidised within the coated catalyst is reduced during the exhaust gas re-circulation process.

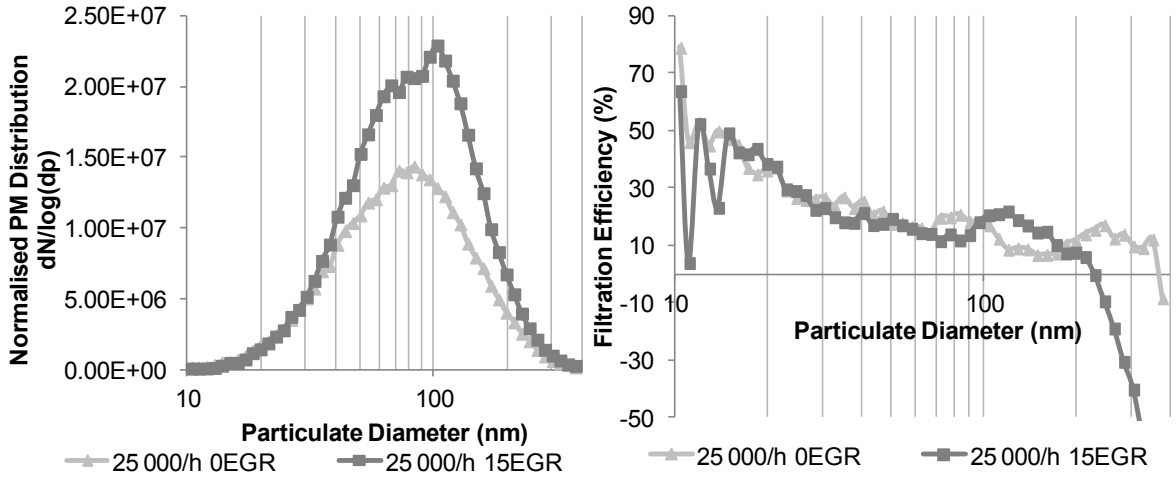


**Figure 6-14.** LS filtration efficiency (right) for different PM profiles (left) at 25 000/h space velocity

For higher PM concentrations and space velocities (Figure 6-15), the loss in removal caused by an increase in the catalyst inlet particulate concentration affected a wider range of particulate sizes (medium-large PM), reducing the overall efficiency. The LS catalyst was not able to maintain the PM removal at these conditions, as the reduced exhaust gas residence time became critical and its negative effect on the removal could not be counteracted by the higher exhaust gas temperature (390°C) promoting the oxidation.

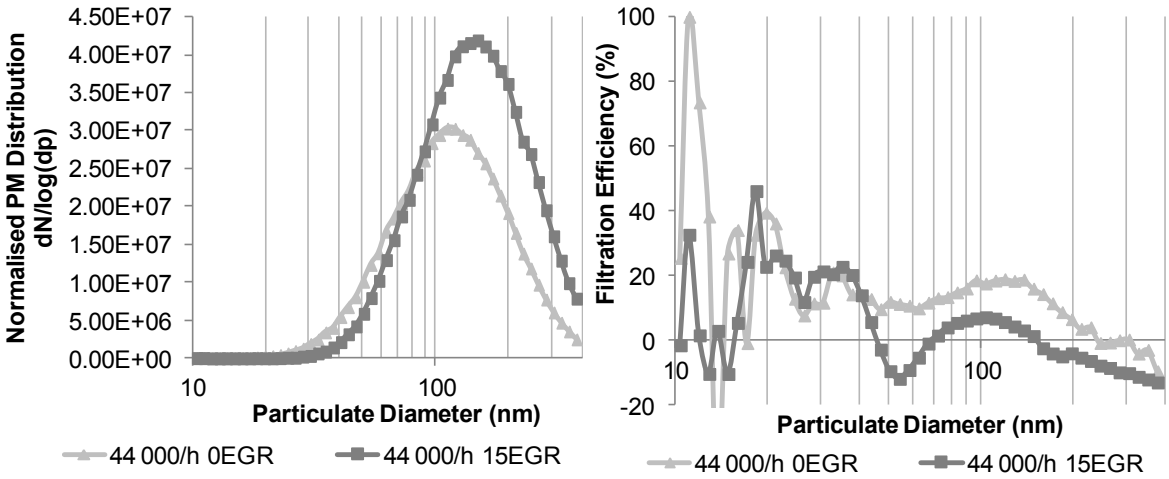


**Figure 6-15.** LS filtration efficiency (right) for different PM profiles (left) at 44 000/h space velocity

The LS catalyst mass and number filtration efficiencies (Figure 6-16) were much lower compared to the two previous partial-flow filters due to its flow-through type channels. The mass filtration was especially affected by increased inlet PM concentrations compared to the number filtration, at low space velocity. The LS showed an average filtration of 10-15% in number and 5-10% in mass but this filtration was not maintained at every condition and became less consistent at higher space velocities, especially in terms of mass (particulate blow-off). The greater particulate removal noticeable at the 40 000/h condition could have been promoted by a "cleaning" of the channels caused by a particulate blow-off during the previous condition, allowing more particulates to accumulate again, similarly to the self-regeneration effect noticed for the 600/2.5 catalyst in section 5.4.

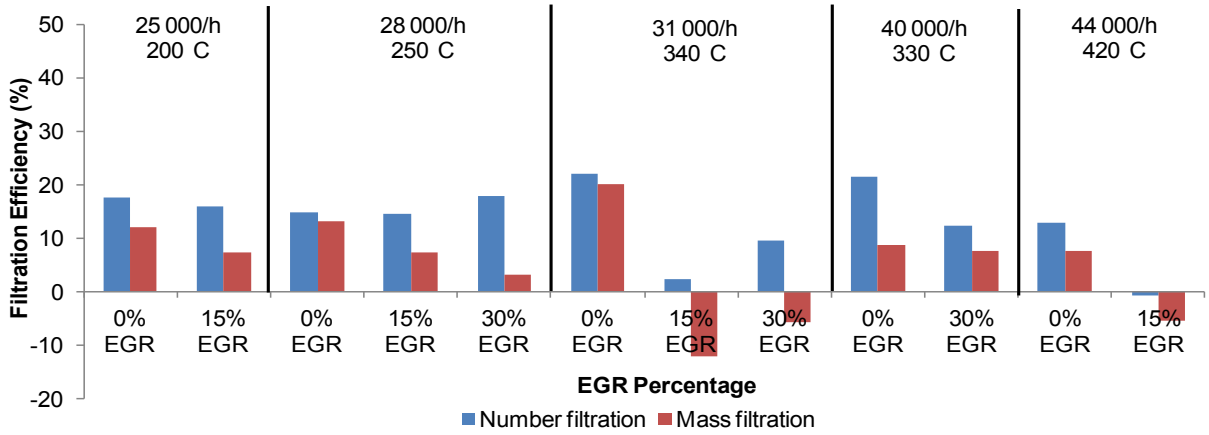


**Figure 6-16.** PM number and mass filtration efficiency over the LS catalyst for the various space velocities and PM profiles

Effect of Space Velocity on the PM Removal in the LS Catalyst

The effect of space velocity on the particulate removal in the LS catalyst is less straightforward as, in this experiment, the engine conditions showing the higher space velocities were also the ones that produced the highest exhaust gas temperature. Therefore, while an increase in space velocity could degrade the removal efficiency (reduction of the exhaust residence time), a higher temperature would on the contrary promote the oxidation of the volatile compounds. Both effects seemed to counteract each other as the general trend in particulate removal was not much altered by an increase in space velocity (Figure 6-17), as only a slight decrease in the removal of the smallest particulates was recorded. While the space velocities presented here are in the lower range, at higher space velocities, the filtration was especially affected in the largest particulate size (blow-off). In addition to the space velocity, the state of the catalyst (cleaned or being loaded) also affected the efficiency, as greater particulate removals were recorded after a "self-regeneration" of the catalyst (negative filtration efficiency due to particulates blow-off cleaning the channels as proposed in section 5.4), independently of the space velocity.

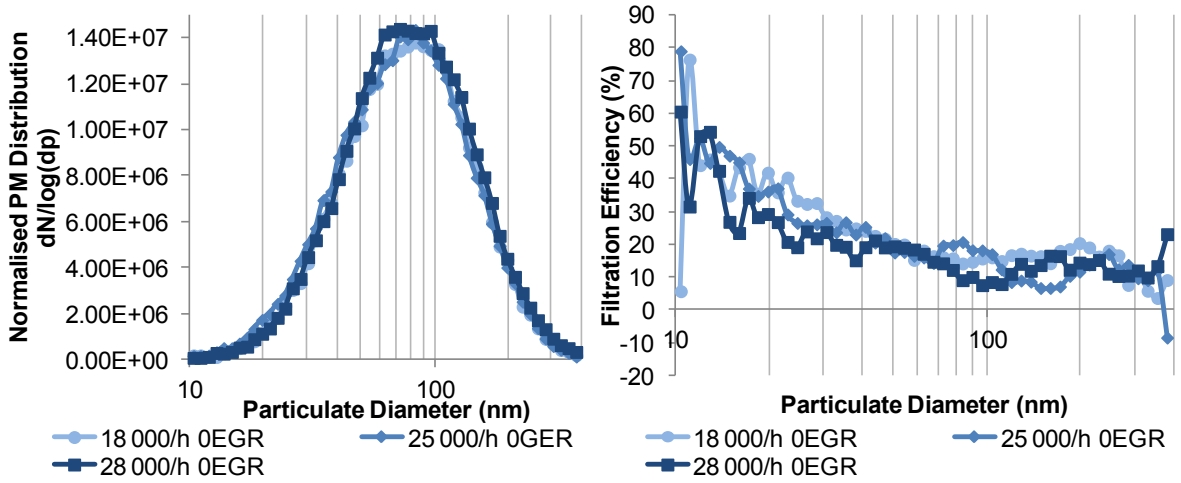


**Figure 6-17.** LS filtration efficiency (right) at comparable PM profiles (left) for three different space velocities

In Figure 6-18, the increase in space velocity resulted in a continuous but limited decrease of the removal efficiency, in terms of mass and number, over the different conditions.

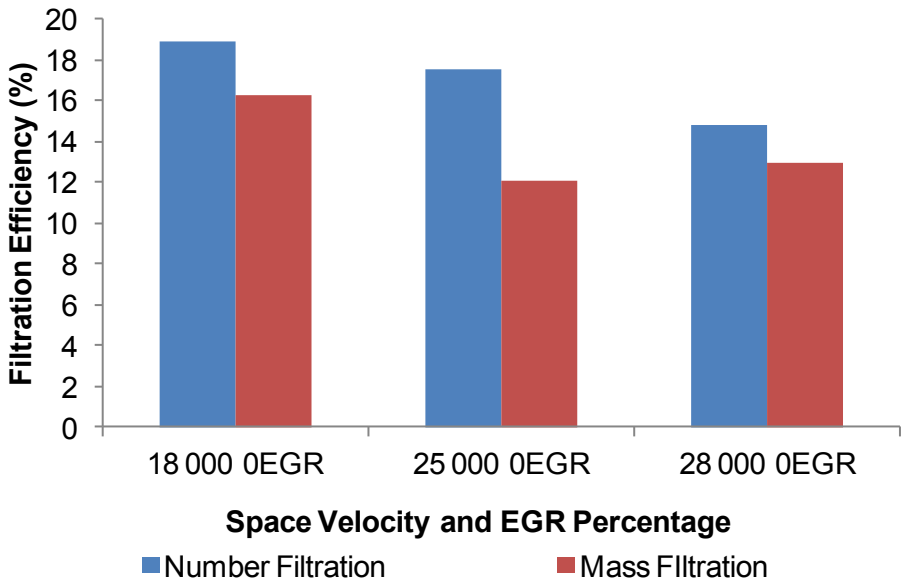


**Figure 6-18.** Effect of the space velocity on PM number and mass filtration efficiency over the LS catalyst for comparable PM profiles

*6.2.2.2. Conventional Flow-Through DOC*

Effect of the Particulate Matter Profile on the PM Removal in the DOC

Similarly to the LS catalyst, at low space velocity (Figure 6-19), comparable removal efficiencies were recorded when the PM concentration increased at the DOC inlet. A slightly greater removal was noticeable for the medium-size particulates under higher inlet PM concentration, which could be accounted for by more particulates accumulating on the walls through interception. This also led to a greater blow-off phenomenon for the largest particulates (negative filtration efficiency). As the inlet PM concentration increased (at greater PM concentration, higher space velocity and temperature), the removal seemed promoted over the whole size range of particulates (Figure 6-20). The deposition rate through interception could be enhanced again by larger and more numerous particulates that would aggregate before being blown-off.

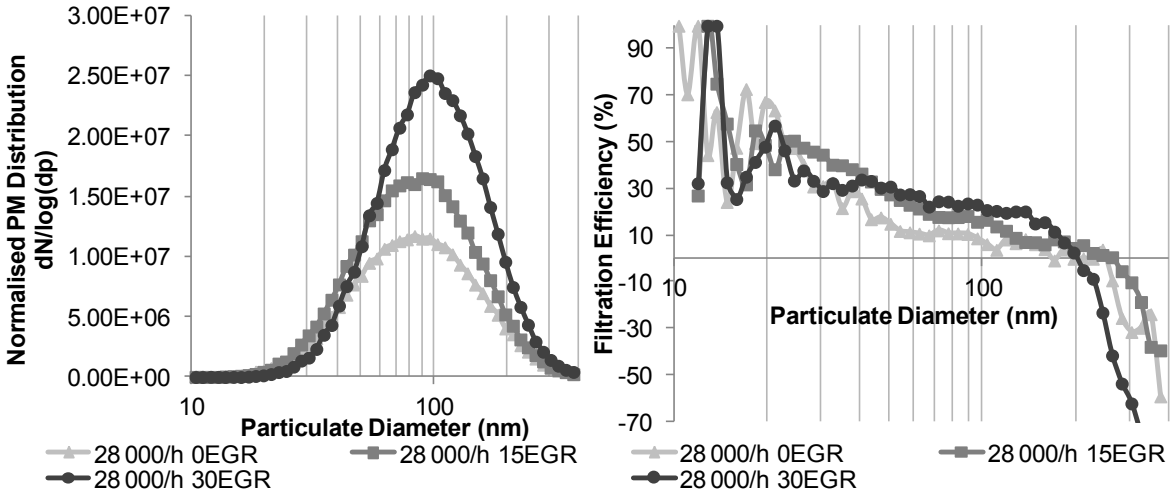


**Figure 6-19.** DOC filtration efficiency (right) for different PM profiles (left) at 28 000/h space velocity

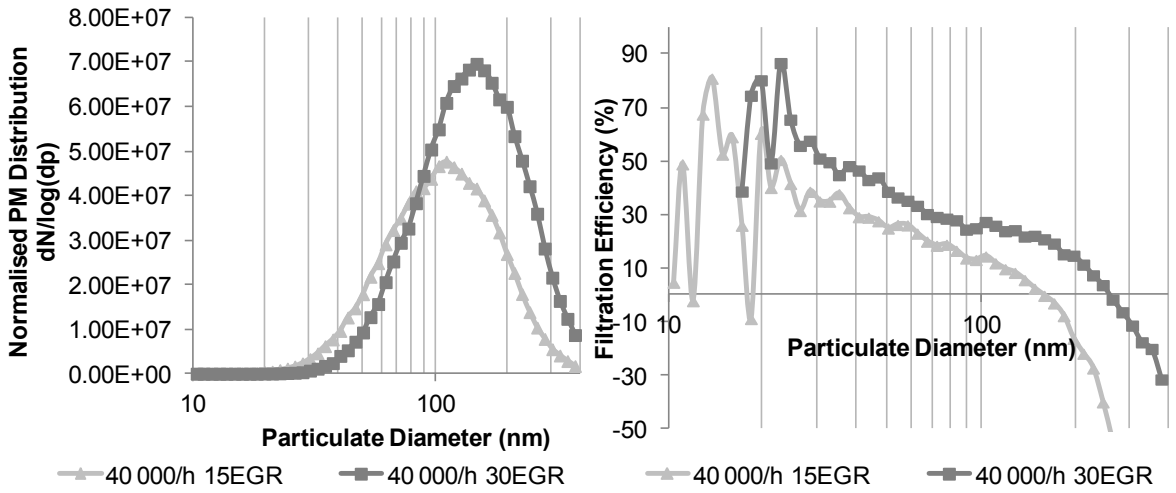


**Figure 6-20.** DOC filtration efficiency (right) for different PM profiles (left) at 40 000/h space velocity

The DOC filtration efficiency did not show great consistency (Figure 6-21) at the different engine conditions. The particulate removal in terms of number was recorded between 10% and 20% (mostly accounted for by diffusion losses) while the mass filtration efficiency remained limited (below 7%) and even negative at some conditions.

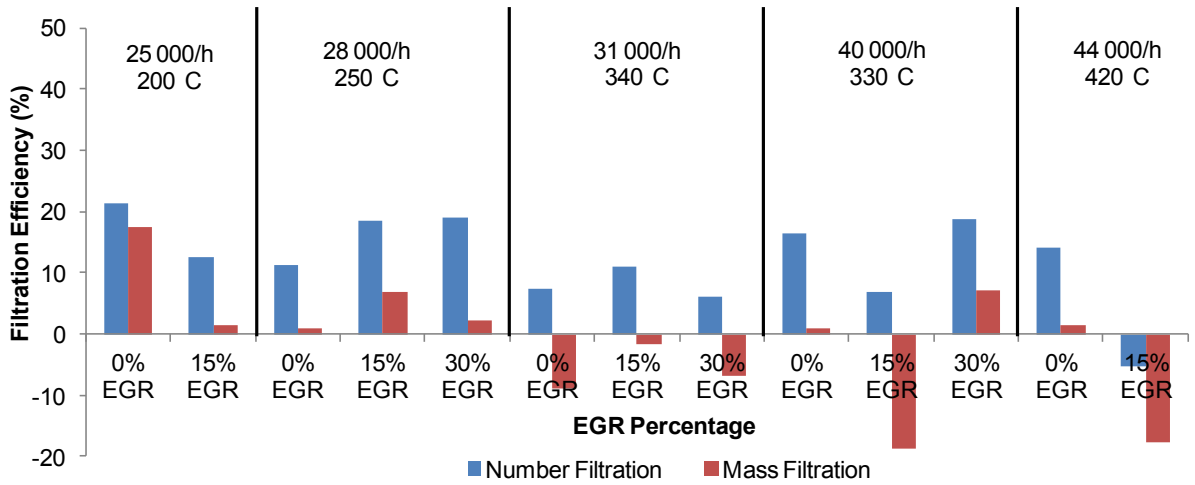


**Figure 6-21.** PM number and mass filtration efficiency over the DOC catalyst for the various space velocities and PM profiles

Effect of Space Velocity on the PM Removal in the DOC

An increase in space velocity (Figure 6-22) led, on average, to a general decrease in the removal efficiency over the whole range of particulate sizes.

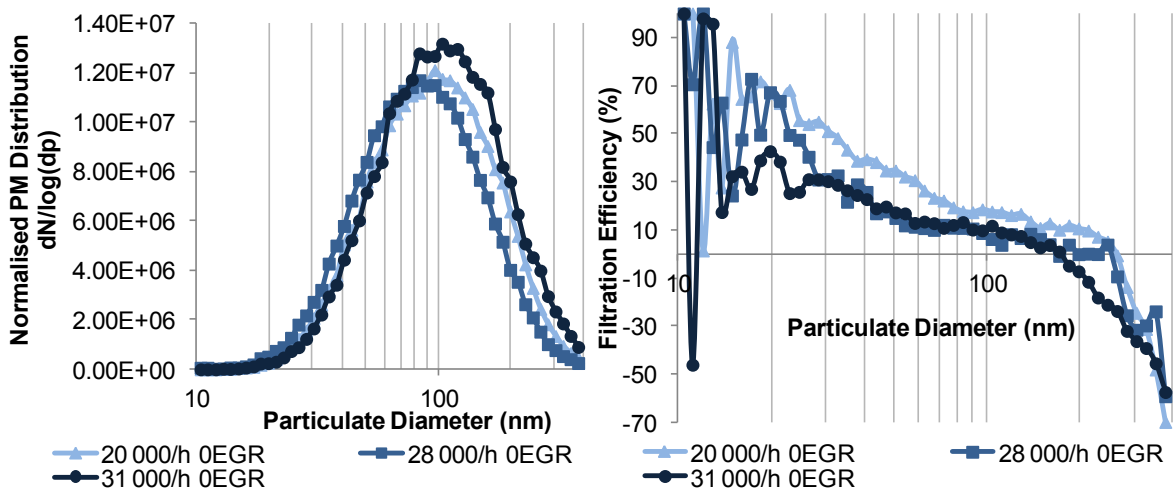


**Figure 6-22.** DOC filtration efficiency (right) at comparable PM profiles (left) for three different space velocities

This translated into a constant decrease in PM removal efficiency (number and mass) over the DOC, leading to an apparent negative mass removal (Figure 6-23), i.e. an increase in the particulate mass at the DOC outlet compared to the inlet. The effect of the space velocity on the removal of the largest particulates seemed less straightforward as some increases in SV led to a reduction of the filtration while others promoted it. The removal of large particulates appeared to be more influenced by the filter loading state, as a condition following a blow-off event showed better PM removal and less particulate release.

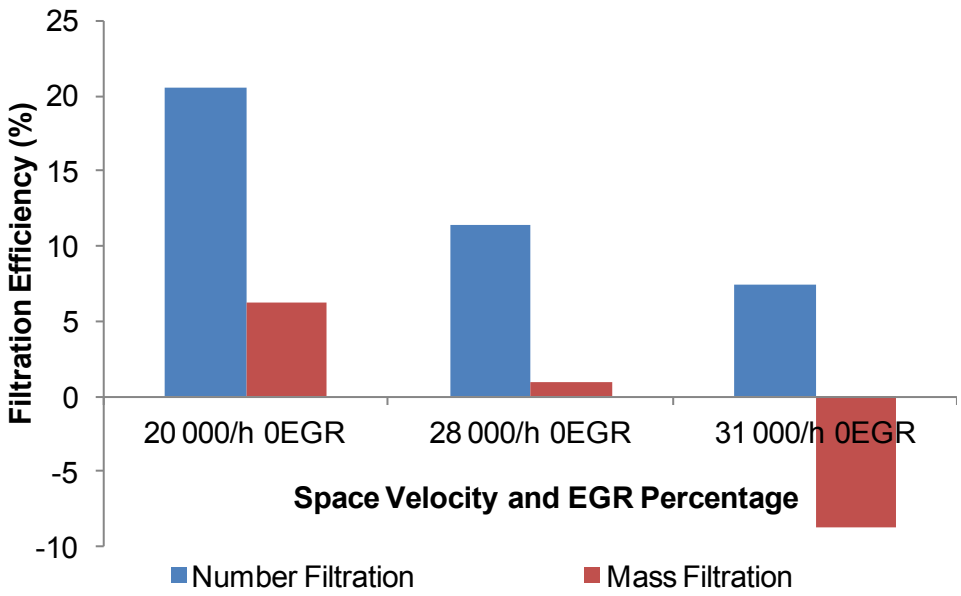


**Figure 6-23.** Effect of the space velocity on PM number and mass filtration efficiency over the DOC catalyst for comparable PM profiles

The flow-through catalysts (LS and DOC) showed limited PM removal, especially in terms of mass. While the LS showed a more steady removal pattern, the particulate removal in the DOC remained generally low and unsteady over the engine conditions, with a constant increase of large PM concentration at the catalyst outlet compared to the inlet.

After assessing the filtration efficiency at various engine operating conditions and understanding the particulate removal mechanisms within the different aftertreatment components, a direct comparison of their activity (filtration and oxidation efficiency) at equivalent exhaust conditions is necessary to select the most relevant system.

## 6.3. COMPARISONS BETWEEN THE PFFS AND FLOW-THROUGH CATALYSTS

### 6.3.1. Filtration Efficiency

#### *6.3.1.1. Study of the Filtration Efficiency at 25 000/h SV – 200°C*

At this engine condition, a clear difference in filtration efficiency was recorded between the partial-flow filters on the one hand and the flow-through catalysts on the other hand (Figure 6-24). The POC showed slightly lower filtration efficiency compared to the PM-Metalit which could be due to their differences in channel design and filtration mechanisms, limiting the POC filtration at low flow rate compared to the PM-Metalit. Moreover, the coating on the membrane of the POC, reducing its porosity, could also limit the portion of exhaust gas flowing through it and being filtered. The filtration efficiency of the flow-through catalysts was less than half that of the filters, due to their straight channel design and absence of membrane.

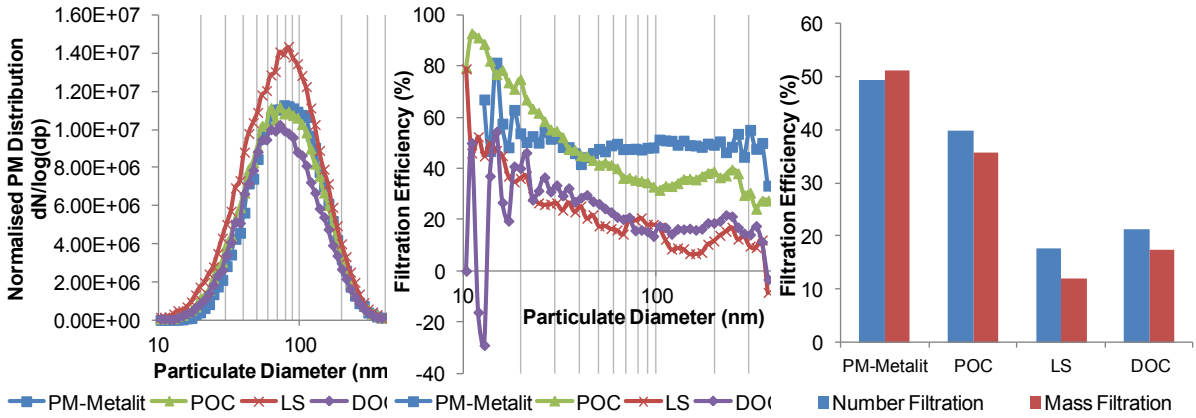


**Figure 6-24.** PM filtration efficiency per particulate size (middle) and in terms of mass and number (right) for comparable engine-out particulate profiles (left) at 25 000/h space velocity

#### *6.3.1.2. Study of the Filtration Efficiency at 28 000/h SV – 250°C*

As the space velocity and temperature increased, the differences in filtration between partial-flow filters and flow-through catalysts increased (Figure 6-25). This is due to the

beneficial effect of a higher flow rate pushing a greater portion of exhaust gas through the membrane, promoting the particulate filtration in the filters. On the contrary, the higher space velocity reduced the exhaust gas residence time in the flow-through catalysts which affected the PM deposition rate and promoted blow-off phenomena (especially in the DOC). At this condition, the POC and PM-Metalit showed comparable filtration, as the POC coating also became active for the oxidation of volatiles. Moreover, the accumulation of particulates in the membrane of the PM-Metalit could reduce the filtration efficiency compared to the clean membrane (previous results), similarly to the effect of the coating on the POC membrane. This would explain the comparable filtration efficiency recorded for the coated membrane in the POC and the PM-Metalit membrane starting to accumulate soot. At this condition, the LS catalyst showed a reduced tendency to large particulate blow-off, compared to the DOC, leading to a greater number and mass filtration efficiency. However, the LS catalyst also showed a lower efficiency for the removal of particulates below 40 nm diameter, which could be due to a reduction in the small particulate accumulation and aggregation over the channels (due to the turbulent flow), preventing the build-up of larger particulates on the wall, and would be more inclined to be re-entrained in the exhaust (negative filtration efficiency).

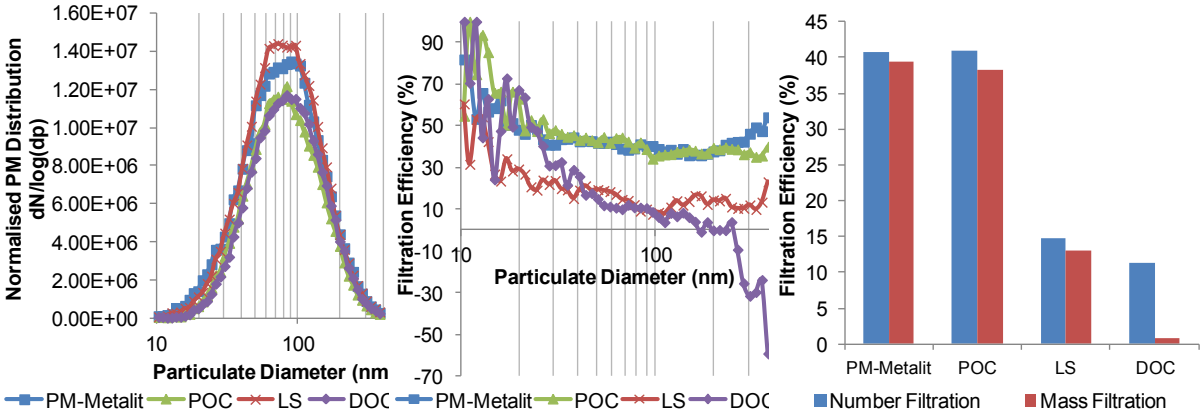


**Figure 6-25.** PM filtration efficiency per particulate size (middle) and in terms of mass and number (right) for comparable engine-out particulate profiles (left) at 28 000/h space velocity

*6.3.1.3. Study of the Filtration Efficiency at 40 000/h SV – 330°C*

At this condition, the inlet PM concentration of the DOC was not comparable to the ones of the other aftertreatment components and therefore was dismissed from the comparison. At this greater flow rate, the filtration was reduced for both filters (Figure 6-26). The negative efficiency recorded for the large particulates in the POC (blow-off event) seemed to be counteracted by a greater removal of the particulates in the small-medium size range, showing comparable overall filtration efficiency to the PM-Metalit. At this higher space velocity condition, the PM-Metalit maintained greater filtration efficiency for the large particulates compared to the POC, due to their filtration in zone 1 (Figure 2-5) being promoted by the higher exhaust flow rate. The LS catalyst showed high particulate number filtration efficiency, due to a greater filtration of the small-medium particulates but a limited mass filtration efficiency due to large particulate blowing-off, as PM kept accumulating over the channels.

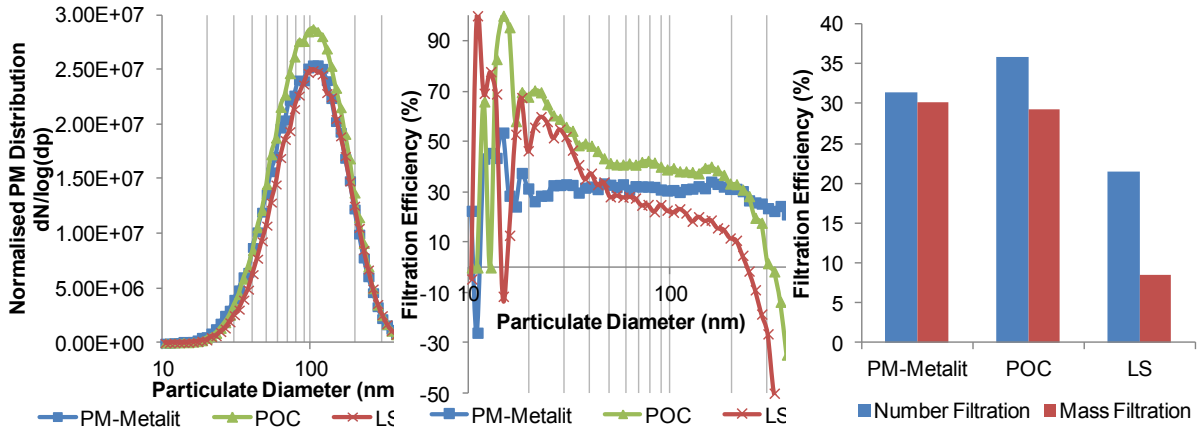


**Figure 6-26.** PM filtration efficiency per particulate size (middle) and in terms of mass and number (right) for comparable engine-out particulate profiles (left) at 40 000/h space velocity

*6.3.1.4. Study of the Filtration Efficiency at 44 000/h SV – 420°C*

As the engine-out PM profile shifted towards higher diameters, the measurement of small particulate emissions became less reliable due to the reduced concentrations at diameters below 30 nm, and no specific trend was obtained for the filtration of particulates for this size range (Figure 6-27). Nevertheless, each component showed the negative effect of high space velocity on the removal of the largest particulates. The filtration efficiency for both filters was maintained at this high flow rate condition (greater flow diverted towards the filtrating medium) despite slight losses in the removal of PM over 300 nm diameter. In the case of the flow-through catalysts, the reduced residence time greatly deteriorated the PM removal, promoting blow-off phenomena, while some small-medium size particulates were still removed from the exhaust gas.

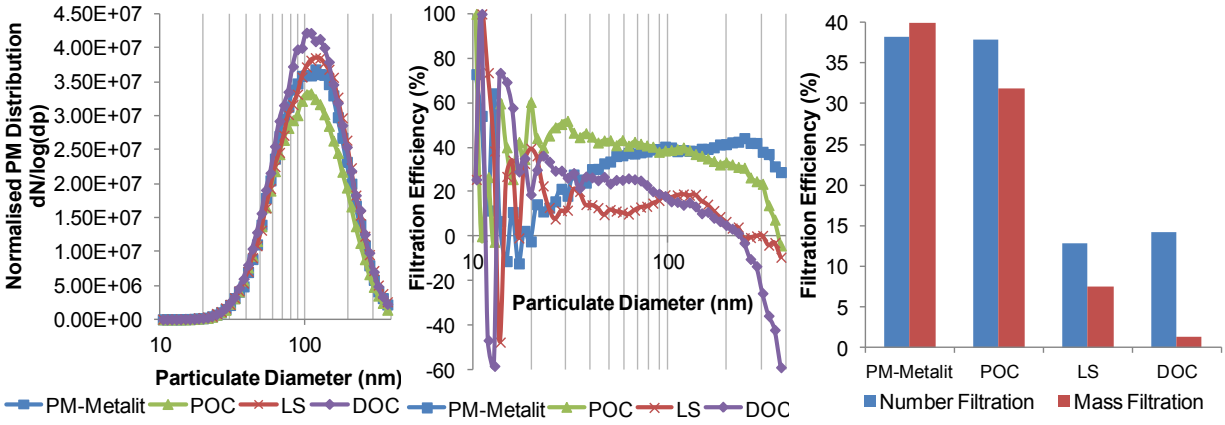


**Figure 6-27.** PM filtration efficiency per particulate size (middle) and in terms of mass and number (right) for comparable engine-out particulate profiles (left) at 44 000/h space velocity

Due to their different substrate designs and filtration mechanisms, the partial-flow filters (PM-Metalit and POC) and the flow-through catalysts (LS and DOC) showed considerably different PM removal, in terms of mass and number, at equivalent exhaust conditions. Both partial-flow filters maintained significant and comparable filtration efficiency over the changing engine conditions, despite their differences in filtration mechanisms. In contrast, the

flow-through catalysts showed unsteady and variable particulate removal. The LS catalyst showed comparable PM removal in terms of number to the DOC, but greater particulate mass removal, as less blow-off events were recorded in this catalyst. It was expected that the oxidation would be enhanced in the LS catalyst through the promotion of heat and mass transfer (turbulent flow). This would in return enhance some soot and volatile oxidation with the use of $NO_2$ and $O_2$, translating into a greater but limited particulate removal, compared to the conventional DOC.

The PM removal in these components was investigated here for particulates largely contained in the accumulation mode, typical of conventional diesel exhaust gas (Figure 1-2). Due to the more harmful effect of the small particulates on health, it is also necessary to investigate the removal of particulates with a size below 50 nm diameter, such as the particulates produced when the engine is at idle.

### 6.3.2. Filtration Efficiency at Idle Engine Condition

At this engine condition, the PM-Metalit and POC showed greater filtration efficiency in terms of number but most especially in terms of mass, compared to the flow-through catalysts, due to their enhanced particulate removal in the medium-large diameter range (Figure 6-28). For the non-coated PM-Metalit, this filtration is expected to rely mostly on the physical trapping of particulates, which suggests that, at idle condition, not only condensed hydrocarbons but also solid soot are produced during the combustion, despite the low-temperature environment. On the contrary, the POC filtration is the result of a combination of oxidation (coated membrane) and physical trapping of particulates, which previously appeared more limited at low space velocities compared to the PM-Metalit.

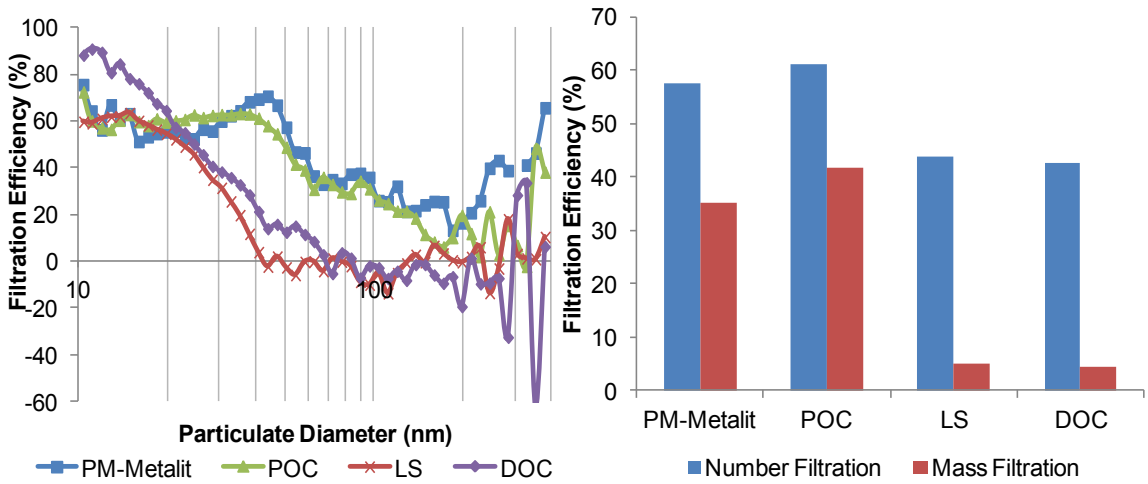


**Figure 6-28.** PM removal over the different components at idle conditions, in terms of filtration per diameter and PM number and mass filtration

The comparable overall filtration efficiency recorded for both partial-flow filters could be due to the promotion of the oxidation over the POC (greater residence time), enhancing the removal of PM, composed of a greater fraction of volatile hydrocarbons at this condition. The analysis of the changes in PM composition (section 6.4.1.1) provides a greater understanding of the extent to which the oxidation of volatile compounds took place in the POC. In the flow-through catalysts, only particulates smaller than 50 nm diameter (volatiles) were removed, similarly to the results of other studies (Johnson & Kittelson, 1996). This removal pattern is representative of droplets condensation and diffusion losses promoted by the low exhaust gas flow rate. While these phenomena could also have taken place in the partial-flow filters, especially enhanced by the presence of the membrane, the mass filtration efficiency obtained for the PM-Metalit and POC was over 30% while for the flow-through catalysts, it remained below 10%. This shows that the partial-flow filters were still able to physically remove some solid particulates from the exhaust, accounting for the mass removed, despite the particulate reduced size. This was especially promoted by the longer residence time (low exhaust gas flow rate), which on the contrary reduced the largest PM removal (smaller portion of flow pushed through the membrane) in the partial-flow filters.

The purpose of this study being to replace the DOC by another component, the different catalysts capacity to oxidise diesel exhaust pollutants (CO, HC and NO) needs also to be investigated and compared with the conventional oxidation catalyst activity to select the most relevant technology as a possible replacement for the DOC.

### 6.3.3. Catalyst Oxidation Efficiency

As the PM-Metalit was not coated, it was left aside for this investigation. However, exhaust composition measurements showed that $NO_2$ was fully consumed over this component, especially at high temperature, mostly from the oxidation of hydrocarbons, as a reduction in HC concentration was recorded (5% to 20% efficiency), with a simultaneous increase in CO concentration at the outlet (HC partial oxidation). $NO_x$ concentration was slightly reduced over the filter (data not presented here), showing some selectivity of $NO_2$ reduction towards $N_2$ formation. Nevertheless, these efficiencies remained limited due to the absence of coating.

The LS catalyst showed the greatest CO oxidation activity at low temperature (Figure 6-29), due to its channel design enhancing the mass and heat transfer, despite its higher thermal mass (metallic substrate).

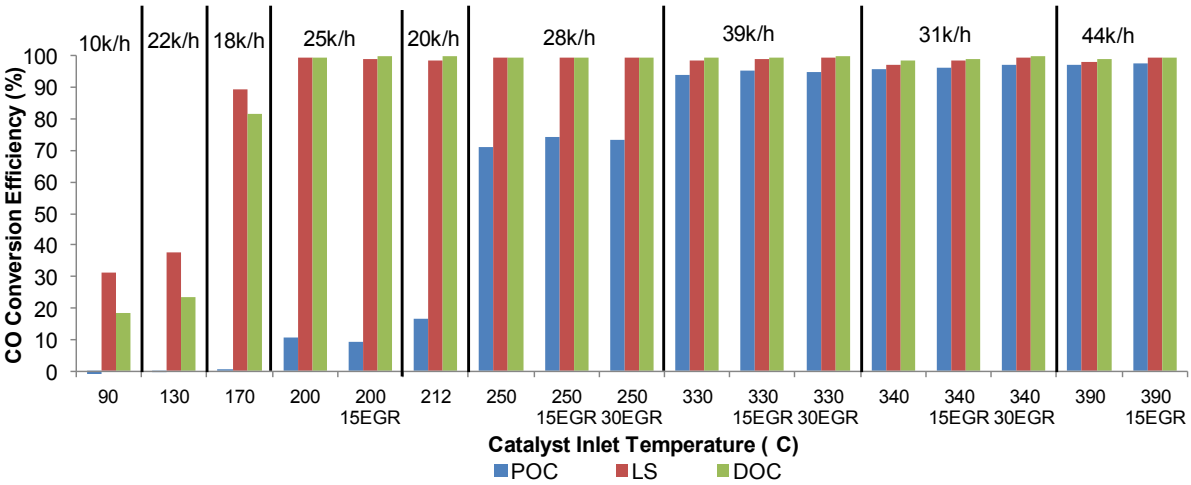


**Figure 6-29.** CO conversion efficiency at various engine operating conditions for the three catalysts (POC, LS catalyst and DOC)

On the opposite, the POC oxidation started at higher temperatures and reached lower efficiency. This could be due to the differences in coating formulation and loading (four times lower than for the two other catalysts) used in this component. Moreover, the coated surface area could be reduced due to the presence of the membrane and the accumulation of particulates.

In terms of hydrocarbons (Figure 6-30), the presence of zeolites accounted for the high removal efficiency recorded for the LS and DOC catalysts at low temperatures. As expected, the POC also showed the lowest hydrocarbon removal at low temperatures due to the absence of zeolite, limiting the trapping functionality, and the lower catalytic loading used. Moreover, the limited CO conversion efficiency recorded in the POC could also affect its hydrocarbons oxidation activity as it relies on CO oxidation completion, to limit the interactions and allow hydrocarbons to adsorb onto the free catalytic sites.

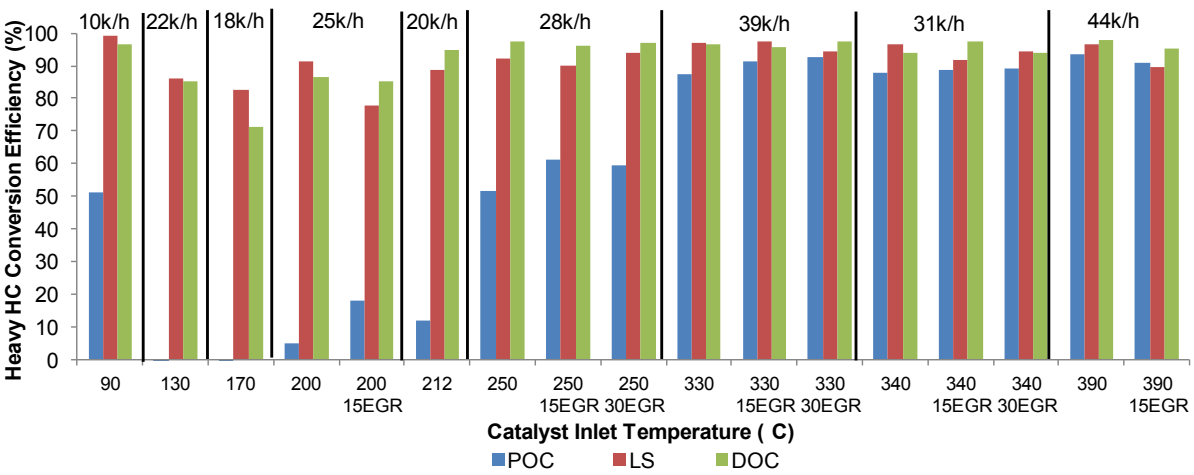


**Figure 6-30.** Heavy hydrocarbons conversion efficiency at various engine operating conditions for the three catalysts (POC, LS catalyst and DOC)

Finally, from $NO_x$ point of view, the three catalysts showed comparable $NO_x$ reduction at temperatures below 250°C, starting from 12% due to the reduction of $NO_2$ by hydrocarbons.

As hydrocarbons used molecular oxygen from $O_2$ from 250°C onwards, $NO_x$ reduction efficiency decreased with an increase in temperatures and remained below 5%.

Special attention was given to the capacity of the catalysts to produce $NO_2$, as it can be used by the downstream DPF and SCR components. The recording of $NO_2$ outlet concentration can also provide an insight into the POC behaviour regarding passive regeneration. While $NO_2$ was completely reduced by hydrocarbons at low temperatures in the LS catalyst and DOC, some $NO_2$ was still recorded at the POC outlet (Figure 6-31) despite hydrocarbons not being fully oxidised (Figure 6-30).

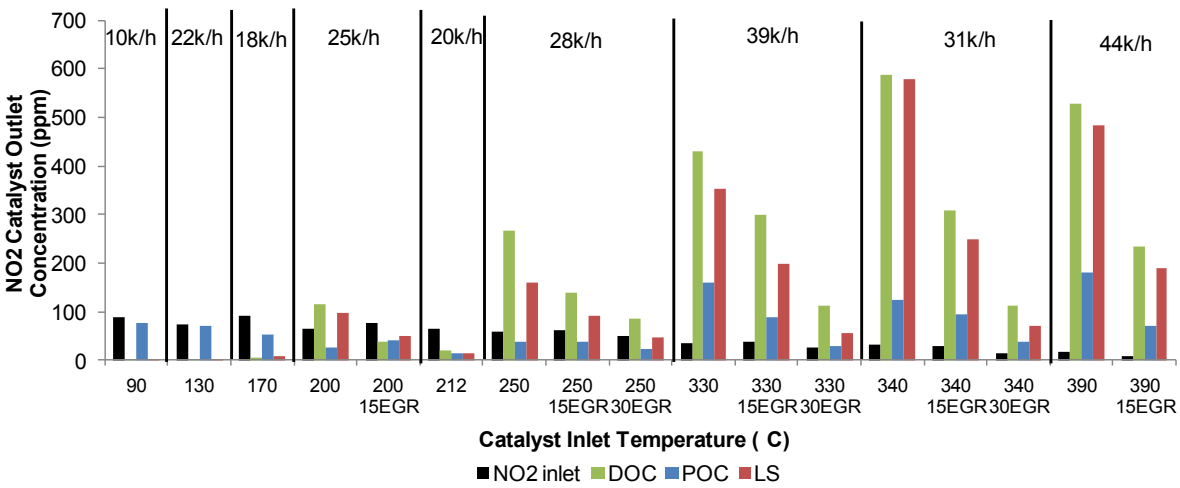


**Figure 6-31.** $NO_2$ concentration at the outlet of the three catalysts (POC, LS and DOC) at various engine conditions

The POC specific channel design, limiting the conversion efficiency and reducing the surface area, could also affect the use of $NO_2$ by hydrocarbons over the catalyst. Conversely, for the LS catalyst and DOC, $NO_2$ appeared at the outlet only once hydrocarbons were oxidised using $O_2$, from 200°C. As the temperature increased, the POC showed a limited production of $NO_2$, up to an additional 150 ppm at the catalyst outlet. For the DOC and LS catalyst, up to 550 ppm of additional $NO_2$ was recorded at the outlet. While the LS advanced channel design was thought to enhance the production of $NO_2$ compared to the conventional

flow-through oxidation catalyst, it did not show greater NO oxidation compared to the DOC used in this application.

To complete the study of the catalysts oxidation and filtration efficiency, their activity was assessed over an extensive operating duration to estimate their durability in terms of exposure to the exhaust gas environment and especially the effect of particulate matter accumulation on their activity. The passive regeneration of the partial-flow filters (PM-Metalit and POC) was also investigated as a means to recover the loss in filtration due to the accumulation of particulates.

### 6.3.4. Comparison of the Long-Term Activity

#### *6.3.4.1. Long-Term Filtration Efficiency*

Partial-Flow Filters (PM-Metalit and POC)

Both filters showed a degradation of their filtration efficiency over the extensive operating period (Figure 6-32 and Figure 6-33). The POC had a more steady decrease in filtration efficiency in terms of number as it maintained a greater removal of small-medium size particulates, possibly due to its catalytic coating allowing some condensed hydrocarbons oxidation, compared to the bare PM-Metalit. Comparable mass filtration losses were recorded, due to the same decrease in removal efficiency for the largest, heavier PM (blow-off phenomena). The long-term activity, leading to a particulate saturation of the membrane, affected to a different extent the removal of the small-medium particulates compared to the larger ones. In the long term, the soot accumulation over the filter can result in a blocked membrane, allowing a greater portion of exhaust gas to by-pass the filtration medium. Eventually, the complete saturation of the filtering membrane would result in the filter behaving like a flow-through catalyst, with greatly diminished particulate removal efficiency. Due to the configuration investigated in this study, the DPF active regenerations could also

promote some regeneration in the upstream partial-flow filter. This would reduce the period for which the partial-flow filter is fully loaded, depending on the regeneration strategy (frequency and duration).

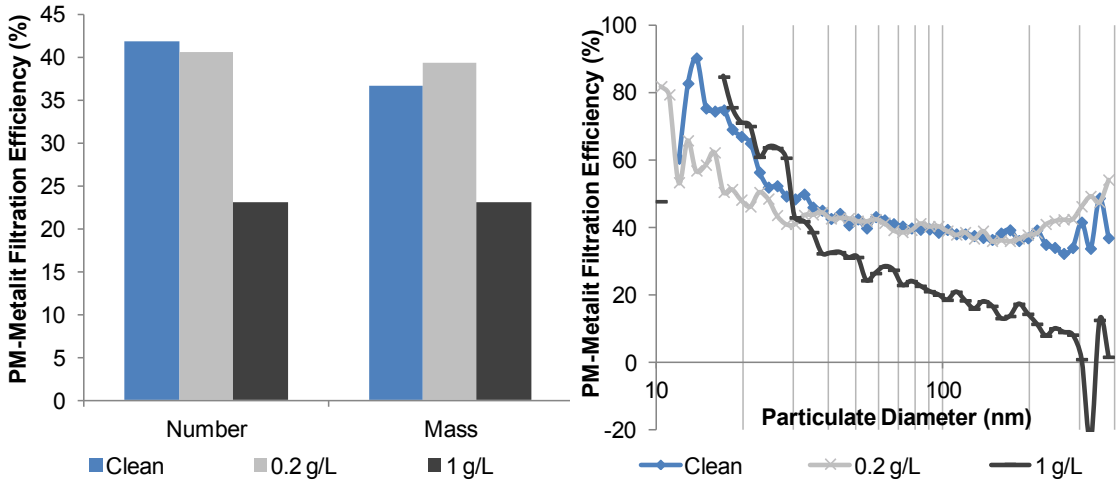


**Figure 6-32.** PM number and mass filtration efficiency of the PM-Metalit based on particulate diameters at different soot loadings

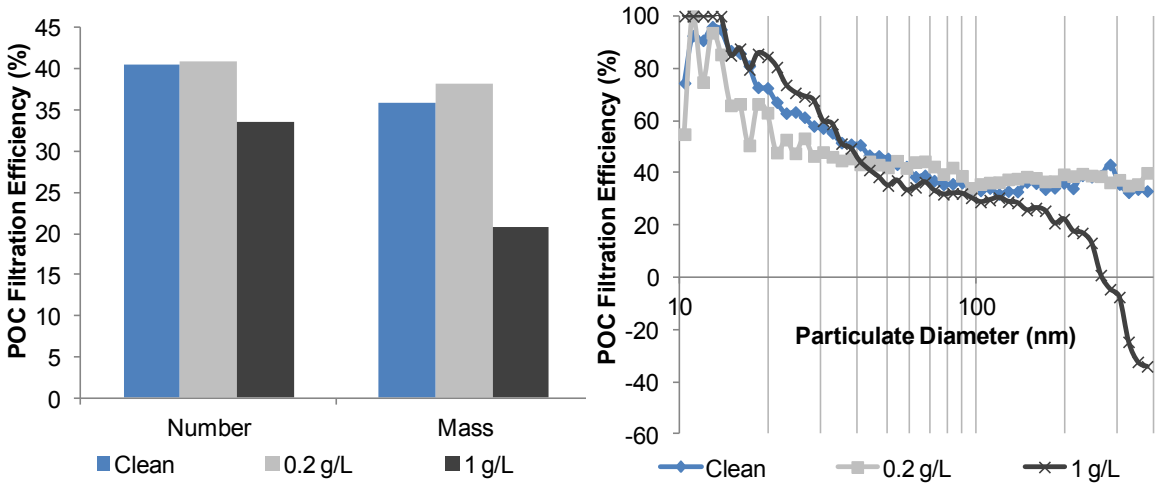


**Figure 6-33.** PM number and mass filtration efficiency of the POC based on particulate diameters for different soot loadings

Flow-Through Catalysts (LS and DOC)

After several hours of operation, both catalysts showed an improvement in particulate removal (Figure 6-34 and Figure 6-35).

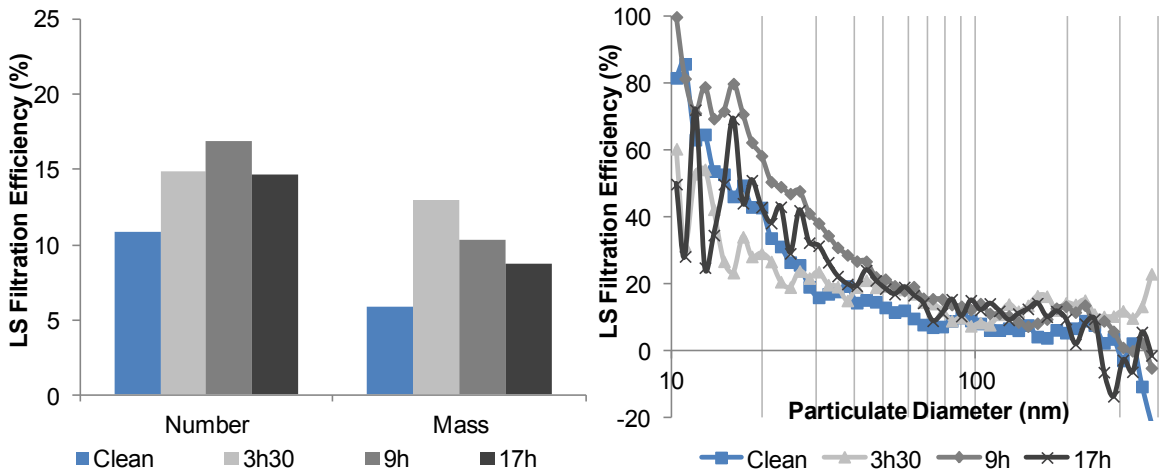


**Figure 6-34.** PM number and mass filtration efficiency (left) and filtration efficiency based on particulate diameters (right) during the loading period for the LS catalyst

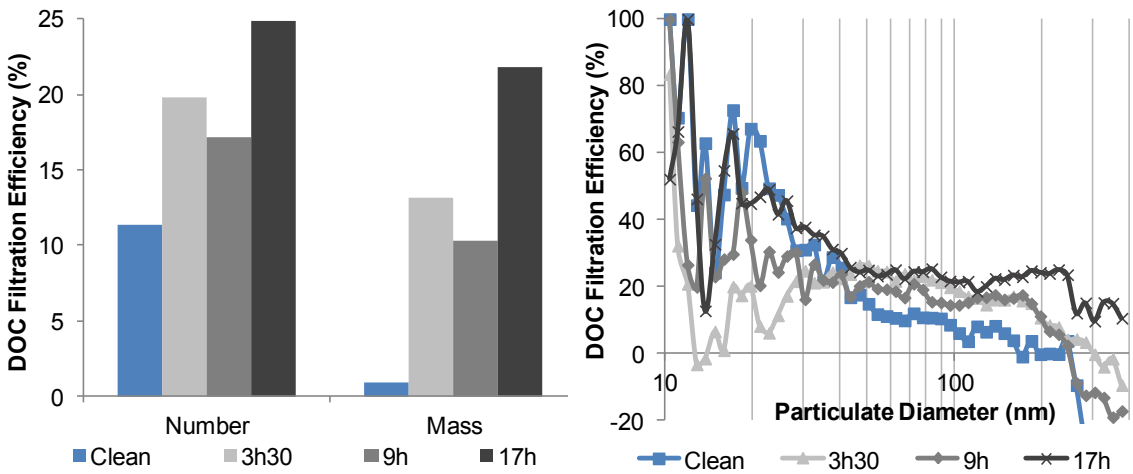


**Figure 6-35.** PM number and mass filtration efficiency (left) and filtration efficiency based on particulate diameters (right) during the loading period for the conventional DOC

The accumulation of soot on the walls could promote PM removal through interception (reduced channel hydraulic diameter) and diffusion mechanisms. The increase in filtration efficiency was noticeable in terms of number, as well as mass, from an improved removal of

large particulates. While the total efficiency was fluctuating during the loading period, the trend of the filtration efficiency according to particulate size appeared unaffected by the soot accumulation. This could be due to the main PM filtration mechanism being diffusion in the flow-through catalysts, especially targeting the removal of small particulates. The LS catalyst showed more consistent filtration efficiency, especially for the medium-large particulate size range, compared to the DOC. The specific channel design of the LS catalyst can promote radial flow distribution, which would allow a more even distribution of the soot accumulation within the catalyst and reduce potential particulate blow-off events. However, the turbulence created within the LS channels could explain the reduced overall particulate removal compared to the DOC, as their adhesion to the wall could be more limited.

#### *6.3.4.2. Long-Term Oxidation Efficiency of the POC, LS and DOC*

The effect of a low-temperature extensive operating duration on the catalyst oxidation efficiency would be primarily some soot accumulation on the catalyst channels that could obstruct or cover the catalytic sites. These accumulated materials could be removed through oxidation at high temperature but this was avoided here to investigate the long-term activity at conditions where the clean-up process would remain limited.

Over time, the POC showed a greater degradation of its oxidation capacity as CO and HC concentrations increased at the catalyst outlet (Figure 6-36) compared to the LS and DOC (over 99% and 95% conversion efficiency for CO and HC respectively). The conversion efficiency in the POC dropped from 91% to 43% for CO oxidation while for HC it decreased from 75% to 20%. NO oxidation also appeared affected by the long test duration as NO outlet concentration increased and $NO_2$ decreased over time, with this trend being noticeable for the three components.

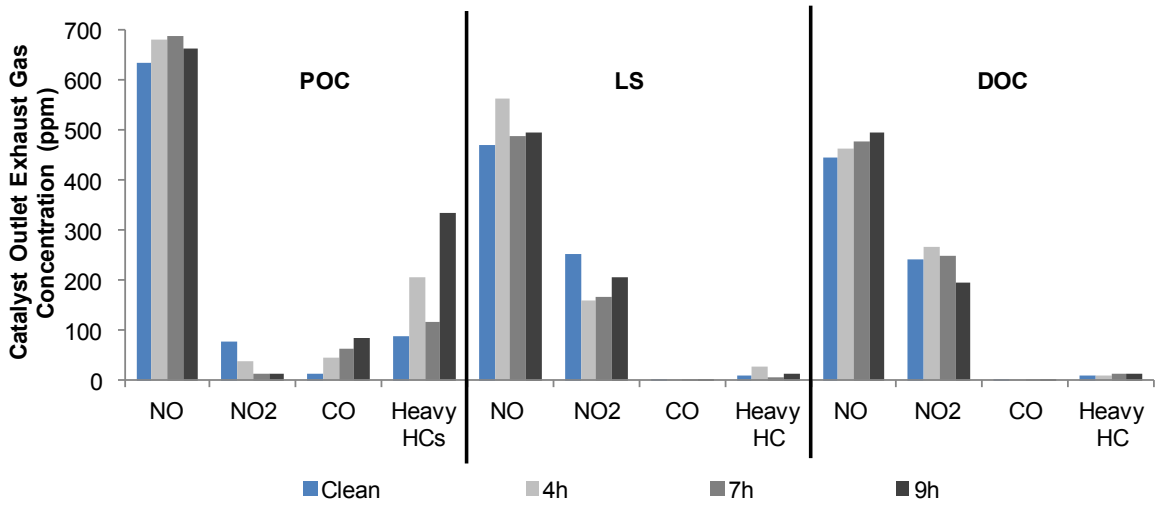


**Figure 6-36.** Effect of the duration of the experiment on the catalyst outlet exhaust gas concentration (NO, $NO_2$, CO and HC)

The significant concentration of $NO_2$ recorded at the catalysts outlet and the limited temperature at this condition (250°C) show that the oxidation of the accumulated particulates would not be accounted for this reduction in $NO_2$ for the LS and DOC. In the case of the POC, the closer contact between the accumulated soot and the coating in the membrane could have promoted particulate oxidation but this would still remain limited at this temperature. The accumulation of soot over the catalytic coating could decrease the surface available for the reaction, primarily affecting NO oxidation efficiency. Due to the POC being especially designed to physically trap particulates, the effect of their accumulation over the coated channels and membrane would be even greater within this component, affecting CO and HC oxidation as well.

To reduce the negative effects of soot accumulation on the filtration and oxidation efficiencies, the partial-flow filters (PM-Metalit and POC) have to be able to regenerate without an active strategy, to limit any increase in fuel consumption and additional system

complexity. Therefore, it is necessary to investigate their behaviour regarding passive regeneration and the requirements to allow a recovery of their activity.

### 6.3.5. Passive Regeneration

#### *6.3.5.1. Passive Regeneration of the PM-Metalit*

In the PM-Metalit, the production of $NO_2$ was not catalytically promoted and therefore remained limited at the temperatures used in this experiment. Moreover, the absence of coating tends to increase the temperature required to promote soot oxidation within the catalyst (Görsmann, 2005; Johansen *et al.*, 2007; Schejbal *et al.*, 2010; Kotrba *et al.*, 2013). Passive regeneration would remain limited for this component (lack of $NO_2$ and low temperature), without the assistance of an upstream DOC.

First, the passive regeneration of the filter was studied using $NO_2$ as produced by the engine. Then, additional $NO_2$ from a gas cylinder was provided to investigate the requirements in terms of $NO_2$ concentration for an effective regeneration.

<u>Study of the PM-Metalit Passive Regeneration using Engine-Out $NO_2$</u>

The measurements of the exhaust gas concentrations (Figure 6-37) showed an almost complete consumption of engine-out $NO_2$ in the filter (inlet $NO_2$ consumption increasing from 63% at 250°C to 94% at 420°C). In addition to soot, $NO_2$ could also react with the HCs present in the exhaust (slight decrease in concentration at 420°C), for which the oxidation using molecular oxygen would happen at much greater temperatures (absence of catalytic coating). A slight increase in CO outlet concentration was recorded, from possible soot oxidation and hydrocarbons partial oxidation. The decrease in $NO_x$ concentration at the filter outlet while $N_2O$ concentration remained unchanged (below 1 ppm) shows that some of the

$NO_2$ was completely reduced to $N_2$. No $NO_2$ consumption was recorded in the empty can, confirming that this reaction only took place in the presence of the filter.

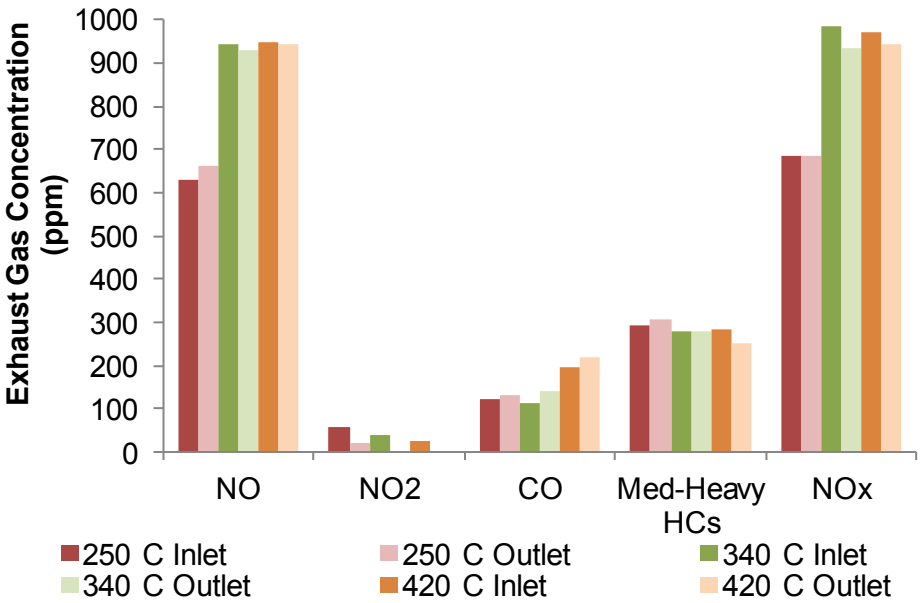


**Figure 6-37.** Inlet and outlet exhaust gas emissions for the engines conditions selected to study the passive regeneration of the PM-Metalit

Due to the limited engine-out $NO_2$ concentrations recorded at these conditions, additional $NO_2$ was provided to the system to further investigate the promotion of the regeneration efficiency.

Study of the PM-Metalit Passive Regeneration with Additional $NO_2$

At low $NO_2$ inlet concentrations (23 ppm from the engine-out and 100 ppm), $NO_2$ was fully consumed in the filter with a subsequent decrease in HC and increase in CO outlet concentrations (Figure 6-38), similarly to the results obtained with $NO_2$ from the engine (HC partial oxidation). As the $NO_2$ inlet concentration further increased (200 ppm to 400 ppm), the outlet concentration increased too, while HC concentration at the filter outlet kept decreasing. This shows a saturation of the reaction between $NO_2$ and HC, with excess $NO_2$ not being consumed by other species, particularly soot. The parameter limiting the soot

oxidation in that case appeared to be the temperature (due to the absence of catalytic coating) as $NO_2$ was present in sufficient concentration.

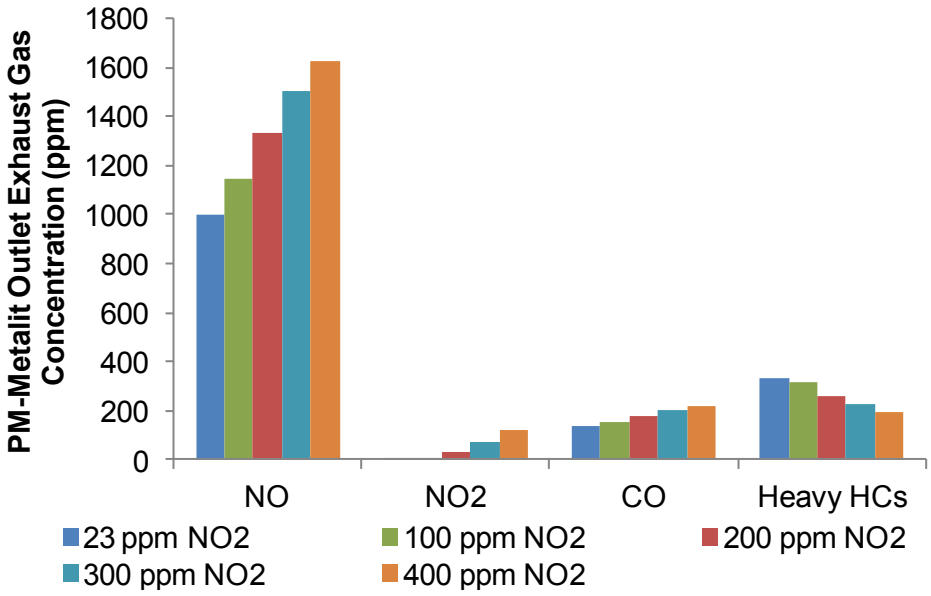


**Figure 6-38.** The influence of $NO_2$ concentration on the other exhaust gas emissions at the PM-Metalit outlet, at 420°C

Despite no direct evidence of the filter regeneration from the recordings of the exhaust gas concentrations, the filtration efficiency was partially restored, especially in terms of mass, from an improvement in the removal of large particulates (Figure 6-39). This could also be due to possible particulate blow-off, as the engine conditions used during the regeneration tests required high exhaust flow rates. The removal of the large particulates during these blow-off events would have cleaned the membrane and restored its trapping capacity, especially for this particulate size range.

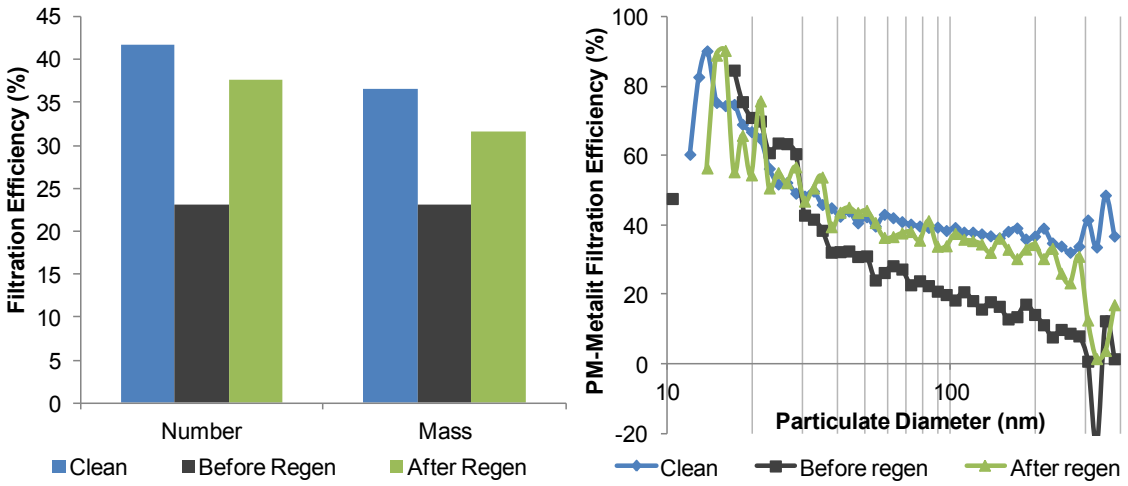


**Figure 6-39.** Effect of the regeneration on the PM number and mass filtration efficiency (left) and filtration per particulate diameter (right) for the PM-Metalit

### *6.3.5.2. Passive Regeneration of the POC*

The use of the upstream DOC to allow the recording of potential CO production over the filter (from incomplete soot oxidation) increased the $NO_2$ concentration fed to the POC compared to the engine-out concentration. However, the POC did not consume $NO_2$ entirely as 150 ppm remained at the filter outlet (Figure 6-40). This had already been previously noticed (section 6.3.3), when, despite the low engine-out $NO_2$ concentration, some $NO_2$ was still recorded at the filter outlet. As CO and HC were already oxidised by the DOC and POC, the $NO_2$ consumed in the POC was considered to be used to oxidise the soot. The coating of the POC can also produce in-situ $NO_2$ that could assist the local oxidation of the nearby particulates, which would not be noticeable through these measurements. The products of the soot reaction could either be $CO_2$ (complete soot oxidation) or CO which, due to the absence of CO at the filter outlet, could be directly oxidised in the POC to $CO_2$ at this temperature (Figure 6-29).

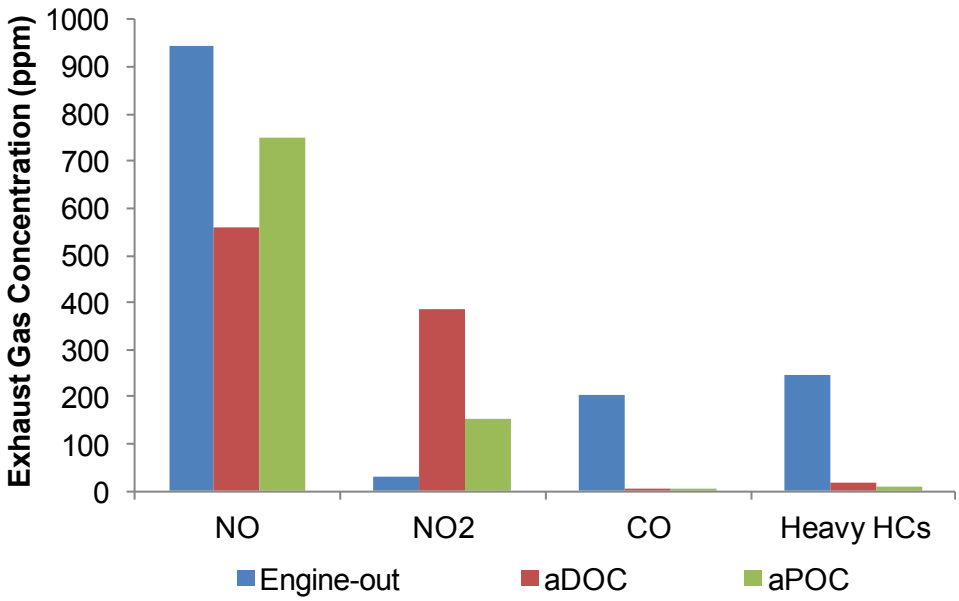


**Figure 6-40.** Exhaust gas concentration (inlet and DOC and POC outlet) during the regeneration process, at 360°C

Changes in the POC filtration pattern before and after the regeneration study were recorded (Figure 6-41), showing that some regeneration still took place within the filter at an exhaust gas temperature of 360°C, with a consumption of 230 ppm of $NO_2$ in the coated partial-flow filter.

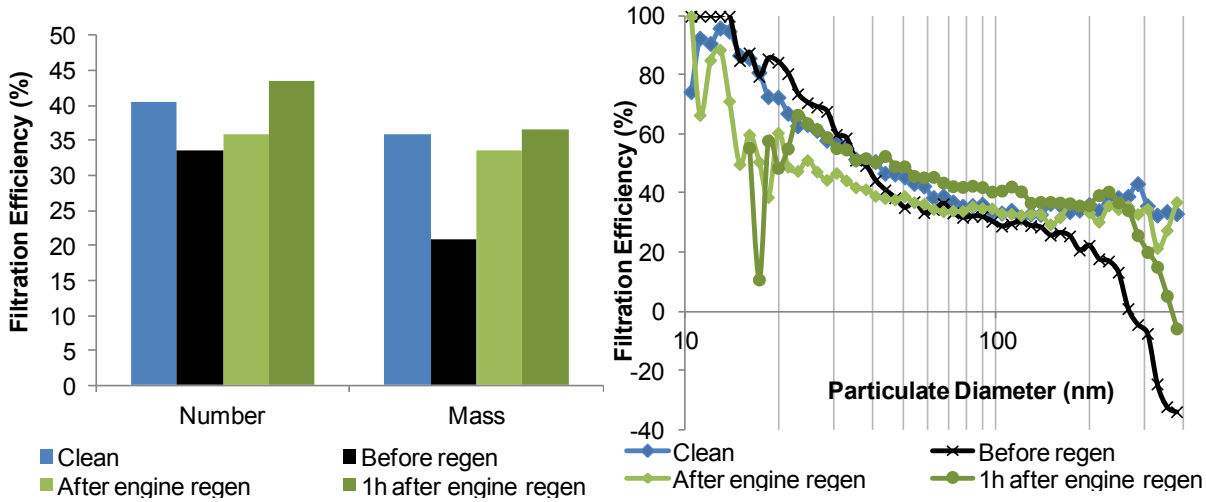


**Figure 6-41.** Effect of the regeneration on the PM number and mass filtration efficiency (left) and filtration per particulate diameter (right) for the POC

After the regeneration, the mass and number filtration efficiencies reached similar levels to the initial values, once clean. The recovery of the POC filtration comes from an increase in medium and especially large particulate removal which had been affected by the soot accumulation. Nevertheless, the filtration for the largest particulates remained lower than for the clean state, similarly to the PM-Metalit. It can be noticed that the measurement an hour after the regeneration showed greater filtration efficiency, possibly due to a soot layer accumulating on the wall, increasing the filtration effect (reduced porosity) of the component.

### 6.3.6. Temperature and Pressure Comparison Between PFF and Flow-Through Catalysts

The partial-flow filter, located upstream of the DPF, will affect the temperature profile fed to the downstream components, depending on its thermal behaviour.

While the POC, LS and DOC components were located in the same can in the exhaust system during the experiments, the PM-Metalit was already canned and had to be installed in a different location of the exhaust system, closer to the exhaust manifold. Therefore, the temperature losses over this component were greater (Figure 6-42) due to the higher inlet temperature profile.

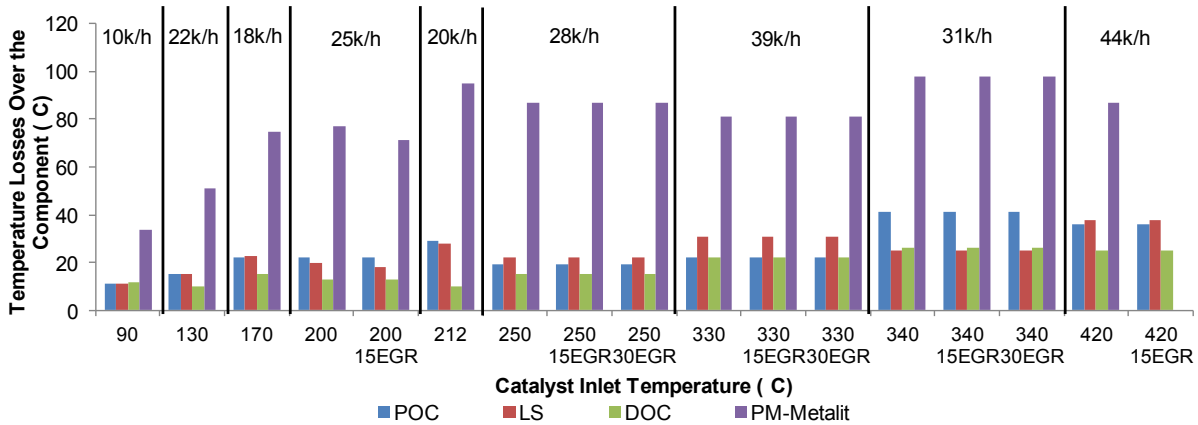


**Figure 6-42.** Temperature reduction over the different components for various engine operating conditions

Moreover, differences in canning (material, configurations) could also have caused these greater temperature losses recorded over the PM-Metalit. When comparing the other three components, the ceramic DOC showed the lowest temperature losses, due to its lighter substrate (lower material density). The differences in temperature losses between the LS and POC remained similar for the different conditions, apart from the 31 000/h and 39 000/h conditions for which they showed opposite results. Higher temperature losses would therefore be expected when replacing a ceramic DOC by a metallic partial-flow filter, due to its specific substrate design and material properties. It was not possible to investigate the behaviour of the components during an active regeneration event, at much higher temperatures, but this would be necessary to provide a fuller understanding of their thermal behaviour.

In terms of pressure, the components showed in general greater backpressure than the DOC. The LS catalyst, due to its channel design creating obstacles to the exhaust flow, showed a slightly higher backpressure relatively to the DOC (straight channels). As expected, the PM-Metalit and the POC showed the greatest pressure increase due to their specific design including filtering membrane and tortuous flow path. When clean, the pressure losses were triple compared to the DOC and, as they became soot loaded, their backpressure increased but still remained limited compared to wall-flow filters, which was in agreement with other studies (Brück *et al.*, 2001b; Jacobs *et al.*, 2006; Babu *et al.*, 2008). Under clean conditions, the use of a PFF upstream of the DPF would lead to a greater overall backpressure compared to a DOC+DPF combination. However, as the PFF accumulates soot, the pressure drop across the DPF would build-up more slowly than with the use of a DOC. This would reduce the total backpressure increase over time, until the PFF saturates with soot. The choices in PFF dimensions and DPF regeneration strategy (requirements to trigger

an active regeneration) could both influence the maximum exhaust backpressure, and should therefore be carefully selected to produce an appropriate system with limited backpressure increase.

From the outcomes of this study, the PM-Metalit and POC showed promising PM removal efficiency (Figure 6-43) compared to the flow-through catalysts. The LS catalyst showed a greater particulate mass removal and a steadier filtration compared to the conventional DOC, as well as greater low-temperature oxidation capacity.

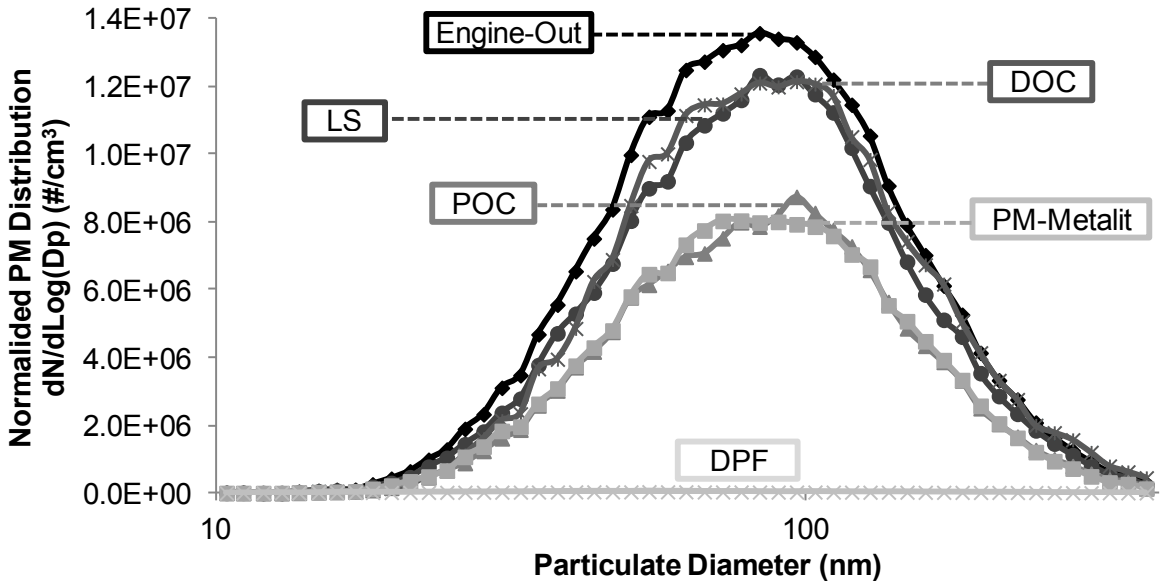


**Figure 6-43.** PM size distribution in the engine-out and at the outlet of the LS catalyst, conventional DOC, POC, PM-Metalit and DPF

In the scope of promoting PM removal to assist the main DPF, the PM-Metalit and POC were selected to be each studied in the following part with a downstream DPF, to investigate their interactions and effects on the filter loading.

## 6.4. INVESTIGATION OF A PFF + DPF SYSTEM

### 6.4.1. Effect of the PFF on the Particulates Supplied to the DPF

The use of an upstream filtering component such as the PFF (PM-Metalit or POC) will affect, to a certain extent, the concentration, size, composition, morphology and reactivity of the particulates reaching the DPF.

#### *6.4.1.1. Particulate Concentration, Size and Composition*

The fraction of PM removed by the partial-flow filter varied depending on the engine operating condition, with a filtration between 25% and 50% efficiency. On average, the filtration was greater in terms of particulate number compared to mass due to some limitations in the removal of the largest particulates within the filters. This fraction of particulates removed from the exhaust gas can affect the soot accumulation in the DPF and especially reduce the formation of a soot cake over the walls that would promote the filtration efficiency in the main filter (cake acting as an additional filtering medium).

In terms of size, a constant increase in the particulate geometric mean diameter was recorded over the PFFs (greater filtration efficiency for the small particulates compared to the larger ones). Additionally, during particulate blow-off (e.g. when the filter became loaded), the particulates released were over 100 nm diameter. This increase in particulate size over the PFF would not be of a great concern as large particulates are less harmful than the small ones and they would be removed by the downstream DPF that shows greater filtration efficiency for these ranges of particulate diameter.

Finally, the PFF could also modify the composition of the particulate matter, especially affecting the fraction of volatile and solid material. This was especially noticeable for the coated POC, where some of the volatile material was oxidised. A thermodenuder, removing the volatile compounds through condensation on active carbons, was used to study the

filtration efficiency of the PM solid fraction only over the PFFs. This was investigated at idle engine condition, where low exhaust gas and combustion temperatures led to a greater portion of condensed hydrocarbons and volatiles in the particulate matter. A reduction of the POC filtration efficiency (Figure 6-44) was recorded, especially in terms of mass, while the particulate removal in the uncoated PM-Metalit remained similar. This shows the influence of the oxidation mechanism on the particulate removal in the POC at this condition (high volatile fraction), especially promoted in the small-medium particulate size range.

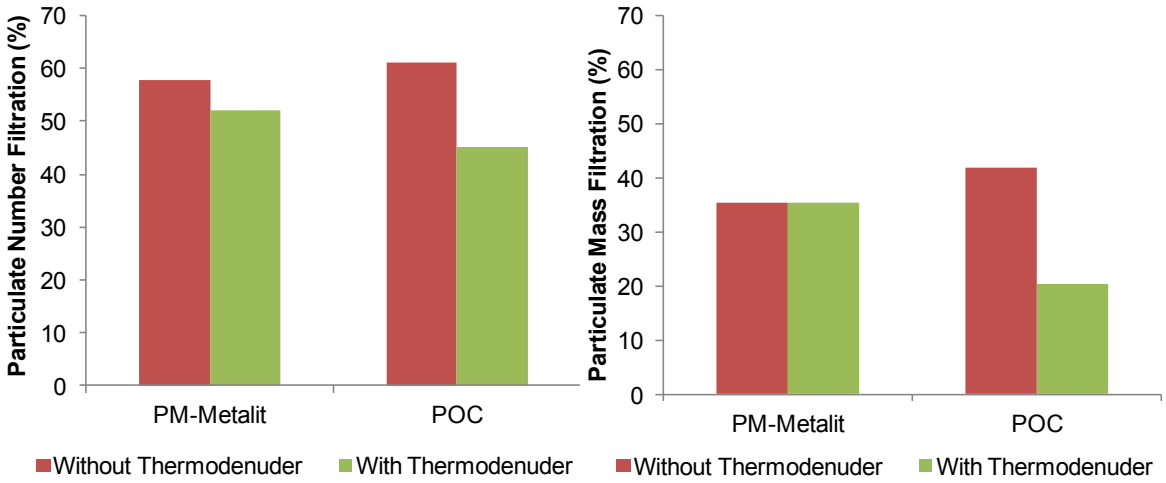


**Figure 6-44.** Effect of the removal of the particulate volatile fraction on the POC and PM-Metalit number (left) and mass filtration efficiency (right), at idle, with thermodenuder (particulate solid fraction only) and without the thermodenuder (solid + volatile)

These changes in the nature of particulates need also to be assessed from the morphology and particulate structure point of view.

#### *6.4.1.2. Particulate Morphology and Microstructure*

Particulate matter agglomerates were collected upstream and downstream of the partial-flow filter in order to quantify the effect of the POC on the morphological and micro-structural parameters of the PM. The radius of gyration results confirmed the increase of the average agglomerate size at the POC outlet, as previously seen with the mobility diameter. This is due to the collision and agglomeration between aggregates taking place in the partial-flow filter resulting in agglomerates composed of a higher number of primary particulates (Figure 6-45 (a) and (b)).

The shape of the agglomerates (quantified by their fractal dimension) remained constant both upstream and downstream of the POC. As a result, the agglomerate filtration characteristics in the downstream DPF will not be affected.

Particulate matter microstructure was quantified by the average interlayer spacing (d002) and average thickness of the graphene layer which composed the soot primary particulates. It is shown that there are no significant statistical differences between the interlayer spacing and the average thicknesses of the graphene layer of the primary particles collected upstream and downstream of the POC (Figure 6-45 (c)). This confirms that the non-filtered particulates (found downstream of the POC) were not oxidised over the POC at this condition. It is suggested that the limited parameters for the soot oxidation in this component were the low exhaust temperature (250°C), as well as the limited residence time between the soot and the catalysed active sites.

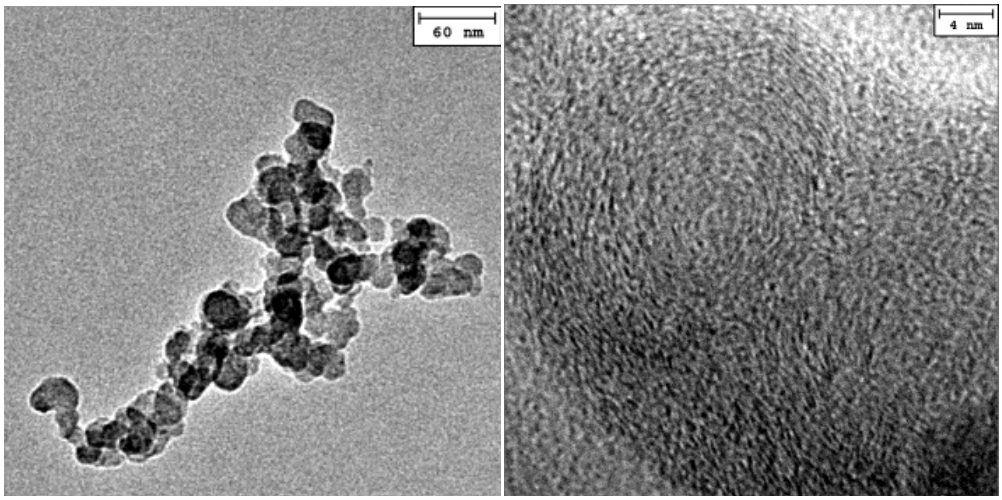


(a) (b)

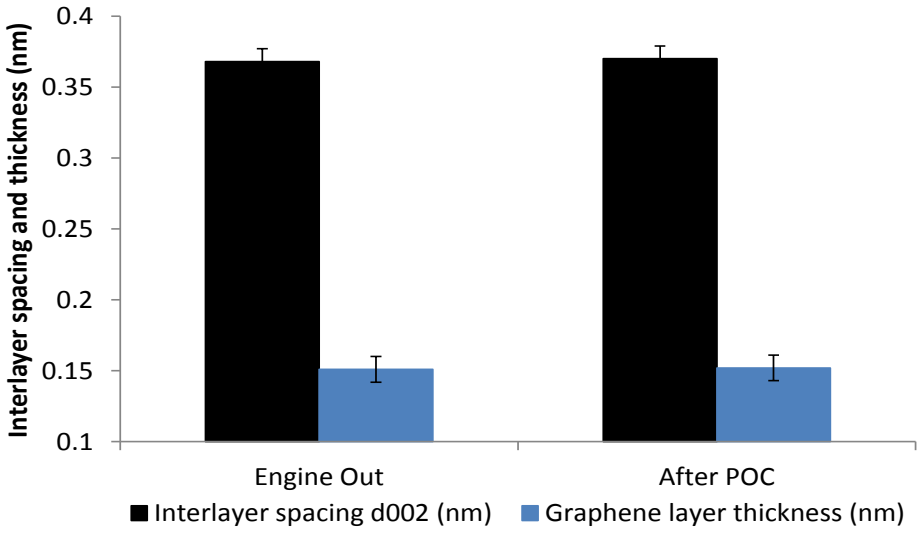


(c)

**Figure 6-45.** Particulate matter characteristics after the POC: (a) morphology, (b) micro-structure and (c) microstructural parameters (Courtesy of Professor F. Martos)

*6.4.1.3. Particulate Reactivity*

The particulate reactivity was investigated through thermogravimetric analysis (TGA) using the experimental protocol defined in section 3.3. The soot reactivity is representative of its capacity to oxidise and defines the temperature required for the reaction, which can influence the DPF regeneration efficiency and subsequent fuel penalty. In the DOC, the soot contact with the coating is expected to remain too loose and time-limited (absence of filtering medium trapping the particulates) to affect the soot reactivity. For the study with the partial-flow filters, the particulates were collected upstream and downstream of both filters (PM-Metalit and POC) at the same engine condition (1500 rpm, 5 bar IMEP). The comparison of the soot reactivity, using the soot weight derivative (Figure 6-46), showed a slight shift towards lower temperatures for the soot sampled downstream of the POC while no changes were noticed for the samples collected upstream and downstream of the PM-Metalit. As the PM-Metalit was left uncoated, little effect on the soot reactivity was expected from this component. The effect of the POC on the soot reactivity remained limited and was not expected to affect the DPF regeneration efficiency.

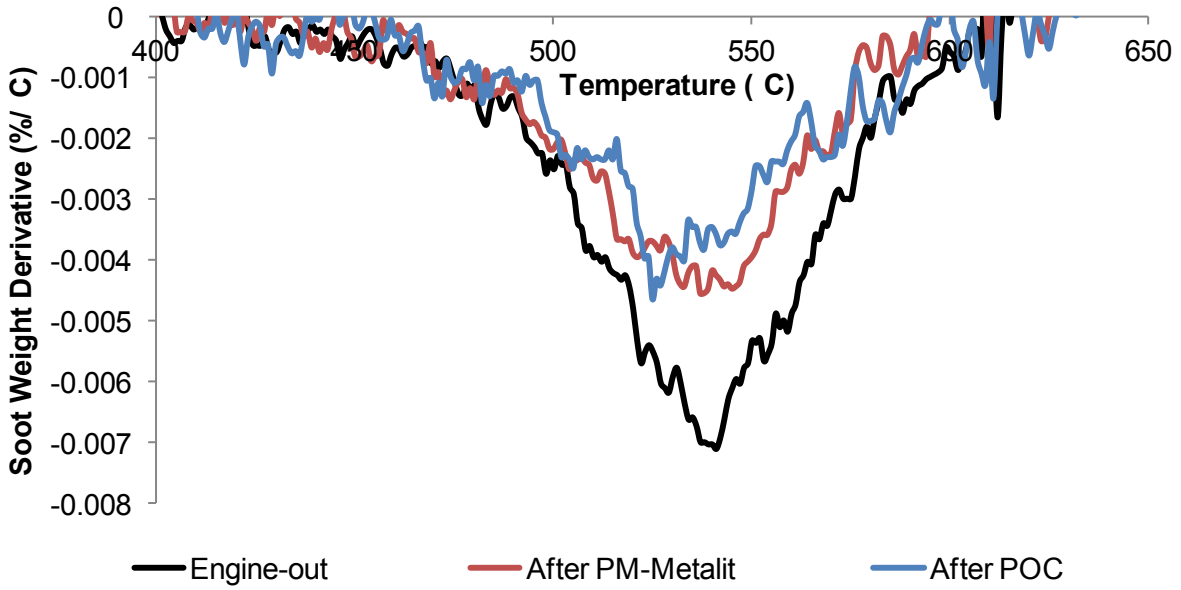


**Figure 6-46.** Weight derivative of the soot collected upstream and downstream of the PM-Metalit and the POC

### 6.4.2. Efficiency of a Combined PFF and DPF System

#### *6.4.2.1. Filtration Efficiency*

The filtration efficiency of the PM-Metalit+DPF and POC+DPF systems (Figure 6-47) was averaged over the 7 hour experiment. As expected for the DPF, the filtration efficiency remained over 99.5% over the duration of the experiment. The PM-Metalit showed a slight drop in filtration efficiency in terms of number, from 54% (beginning of the experiment) to 50% (end of experiment), while the efficiency remained the same in terms of mass. In contrast, the POC showed an increase in filtration efficiency from 34% at the beginning of the experiment to 55% in PM numbers and from 30% efficiency to 54% in PM mass. It was noticed previously that the POC required a certain period of use to reach its optimum filtration efficiency, as some particulate accumulation on the membrane could enhance the filtration, similarly to the mechanisms in wall-flow filters.

When comparing the filtration (Figure 6-47), the DPF in the POC+DPF system showed a slightly lower efficiency compared to the other DPFs. As proposed in section 6.3.1.1., the removal of a portion of particulates by the upstream PFF could reduce the soot cake formation within the DPF that further enhances the filtration efficiency. This could explain the slight reduction in filtration recorded for the DPFs fitted with an upstream PFF, although the DPF average filtration remained over 99% in each system. The overall filtration efficiencies of the PFF+DPF systems showed limited improvements compared to the standalone DPF, due to its high filtration efficiency that was difficult to further improve with the use of partial-flow filters with 40% to 60% filtration efficiency.

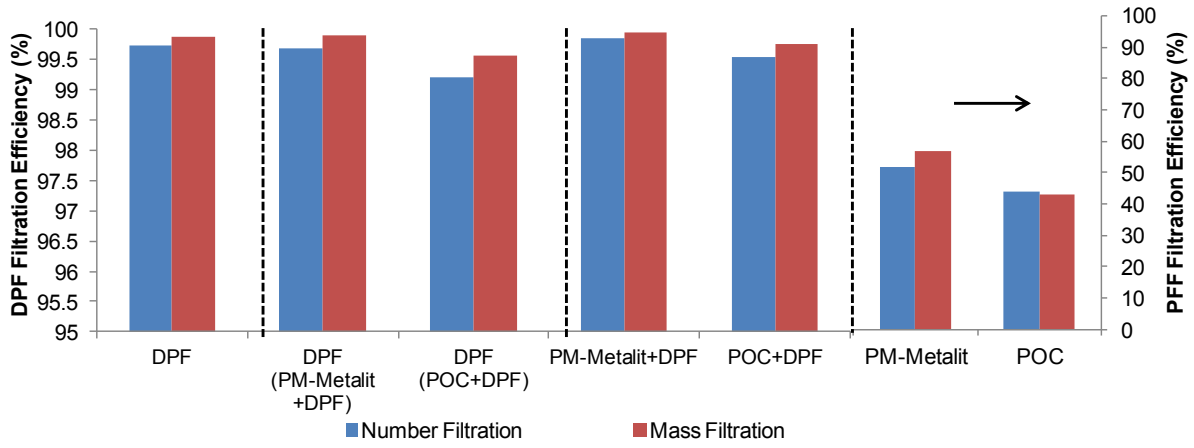


**Figure 6-47.** PM number and mass filtration for the DPF, PM-Metalit+DPF and POC+DPF configurations

In terms of removal efficiency for specific particulate sizes (Figure 6-48), the presence of the POC especially affected the DPF filtration efficiency of small particulates (below 20 nm). This confirms the hypothesis that the POC can reduce the soot cake accumulation in the DPF as this soot cake would reduce the wall porosity and enhance the removal of the small particulates (as recorded in the standalone DPF). At this condition, the POC appeared more efficient in trapping small particulates compared to the PM-Metalit, possibly due to the high exhaust gas temperature (340°C) favouring the oxidation of the volatile materials. However, the PM-Metalit showed greater filtration efficiency for the large PM, due to the high space velocity forcing a greater portion of exhaust gas towards the membrane but affecting its filtration for the small PM.

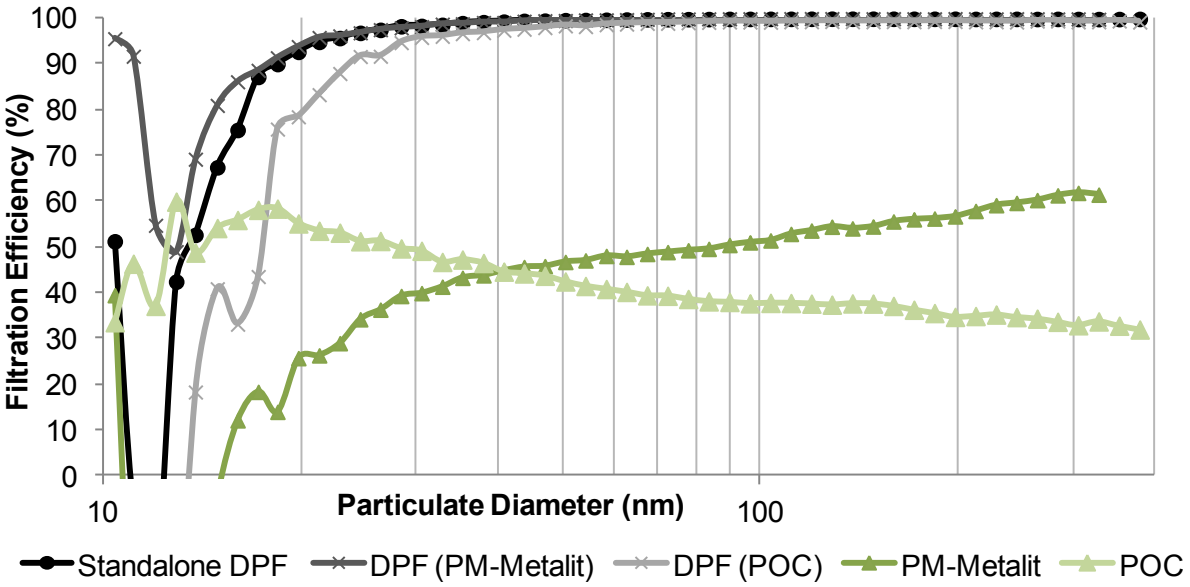


**Figure 6-48.** PM filtration efficiency based on the particulate diameter for the DPF, PM-Metalit and POC of the configurations studied

The combinations PFF+DPF showed similar filtration efficiencies over the studied particulate range compared to the standalone DPF (Figure 6-49), with a slight enhancement in the removal of the smallest PM (PM-Metalit+DPF). The engine condition used in this experiment did not favour the removal of the small particulates due to the high flow and high PM concentrations used to promote the DPF loading. At different operating conditions, the gain in small PM filtration could be enhanced as the PFFs previously showed greater sub-20 nm particulate removal.

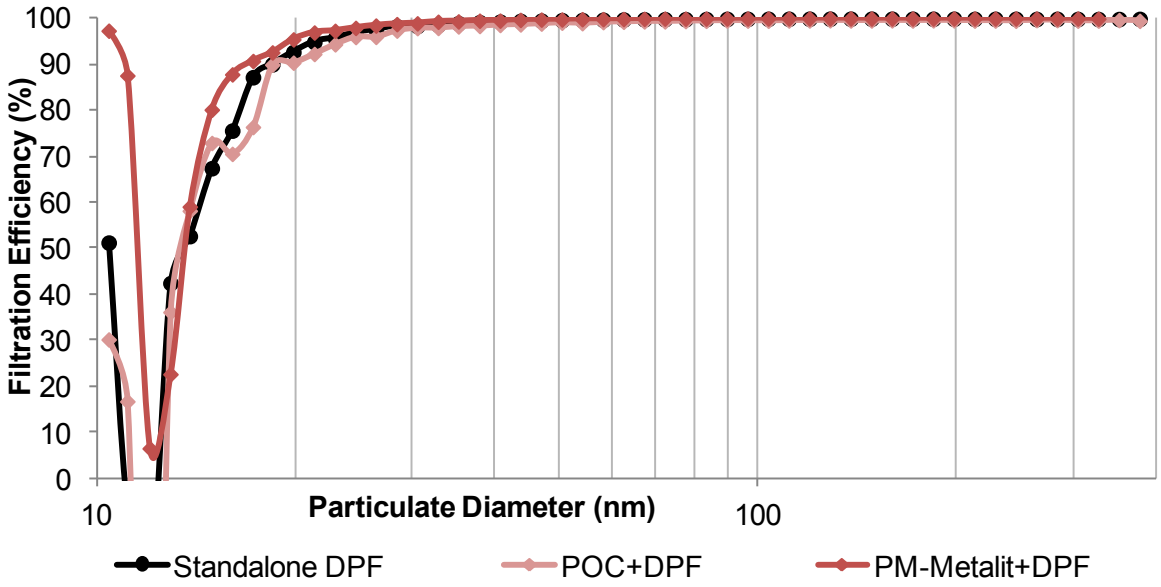


**Figure 6-49.** PM filtration efficiency based on the particulate diameter for the DPF, PM-Metalit+DPF and POC+DPF configurations

*6.4.2.2. Soot Accumulation and Pressure Increase in the DPF*

After the 7 hour test, the standalone DPF had accumulated 0.31 g of soot while the DPFs fitted with an upstream PFF (either PM-Metalit or POC) showed a soot mass accumulation of 0.22 g. This 30% soot mass reduction translated into a lower DPF pressure increase (Figure 6-50). Moreover, the DPF pressure increase profiles from the PFF+DPF configurations were steadier than in the case of the DPF alone. This would reduce the engine power loss created by a higher rate of backpressure increase. The critical point is to appropriately choose the PFF dimensions and the DPF regeneration strategy, to limit the creation of additional pressure in the partial-flow filter that would reduce the advantage of using a PFF+DPF system.

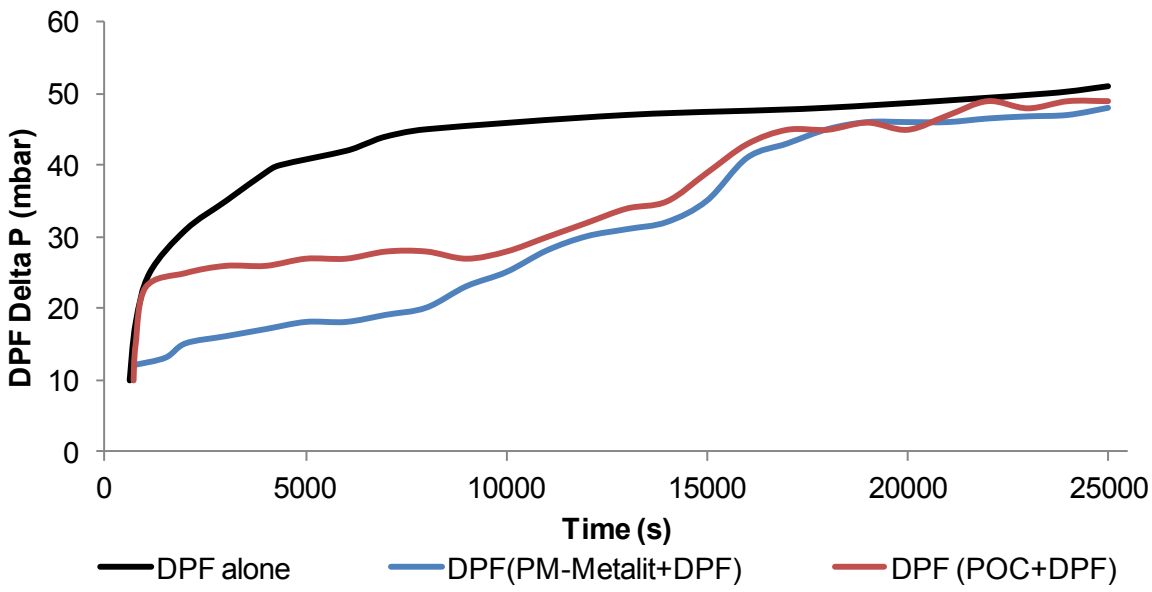


**Figure 6-50.** Pressure increase across the DPF during the loading period

## 6.5. SUMMARY AND CONCLUSIONS

The potential of using a partial-flow filter in replacement of the DOC was investigated in this chapter, from the perspective of filtration and oxidation efficiencies, long-term activity and effect on the downstream DPF when combined in a PFF+DPF system. The reduced soot mass loading in the DPF, associated with a lower pressure increase, showed the potential of the PFF+DPF combination to reduce the need for active regenerations, allowing either a longer DPF loading time (fewer active regenerations required) or a shorter regenerative event (reduced mass of soot to oxidise). This would translate into a reduction of the fuel penalty and hydrocarbon emissions caused by the use of active regenerations, combined with an increase in small particulate removal (from the PFF) over the aftertreatment system.

# 7. CONCLUSIONS AND FUTURE WORK

The aftertreatment strategies and design criteria developed in this research work were aimed at promoting the low-temperature removal of diesel pollutants (CO, HC and particulate matter) and provide solutions to the forthcoming reduction of exhaust gas temperature associated with modern engine development, to help achieving ever tightening emission legislation limits.

## 7.1. A THERMALLY EFFICIENT DOC CONFIGURATION TO IMPROVE LOW-TEMPERATURE ACTIVITY

This study demonstrates the possibility of improving the CO and HC conversion efficiency of an oxidation catalyst by enhancing its thermal behaviour through modification of the substrate cell density and wall thickness. This was achieved through a combination of two catalysts operating at complementary conditions (during warm up and cooling phases) to widen the catalyst activity temperature window. Improved oxidation efficiencies, especially for CO, were recorded at low temperatures with the proposed catalyst combinations compared to the baseline catalyst. This promotion of the catalyst low-temperature activity was not only due to the improved thermal behaviour of the component but also due to additional substrate physical properties (surface of contact and mass transfer) that enhanced the interactions between exhaust gas and catalytic material. The drawbacks related with these two-brick combinations are the potential backpressure increase, especially with the LS configurations, the additional cost from using two different coated substrates instead of one and the use of more costly metallic substrates (3 to 10 times more expensive than ceramic).

The choice of the substrate cell density and wall thickness in the two-catalyst configuration depends upon the engine exhaust characteristics (temperature and flow rate)

and operating conditions. The choice of the second substrate involves a compromise, as it can easily negatively influence hydrocarbon conversion efficiency.

This study could be extended towards the investigation of varying the distribution of the catalytic loading between the first and second brick to take advantage of the warmer, higher surface area of the first catalyst compared to the second one.

The design strategy developed in this chapter could also be applied to other types of flow-through catalysts, such as SCR or lean $NO_x$ trap, to enhance their efficiency over wider exhaust conditions. An additional relevant application of this two-brick configuration could be the coating of each component with a different catalyst that requires specific operating temperature window (e.g. copper and iron for $NO_x$ removal), to take advantage of the different temperature profiles reached in the catalysts. Finally, the two-brick configuration could also be optimised by using a coating with a different but complementary function in each brick, such as a lean $NO_x$ trap, followed by an SCR catalyst or two SCR catalysts using different reductants (i.e. HC or $NH_3$) to enhance the efficiency of the system.

## 7.2. EFFECT OF THE EXHAUST GAS COMPOSITION ON THE DOC ACTIVITY

### 7.2.1. Interactions Between Exhaust Gas Pollutants

The singularity of this investigation lies in the use of various “diesel” types of fuels and combustion modes to produce a variety of exhaust gases and highlight the interactions between exhaust gas pollutants in the DOC (adsorption competition onto the same catalytic sites). The outcomes of this study draw strategies to reduce the inhibitions (selective momentary control of some species) and enhance the promotion of the oxidation activity, especially at low temperature. By presenting these interactions as they take place in the catalyst, using genuine exhaust gases, the study also gives tools to qualitatively predict how

efficiently CO and different hydrocarbon species would be oxidised, based on the exhaust gas composition. This can help identifying synergies between engine calibrations (i.e. promotion of light alkenes during combustion instead of alkanes), fuel specifications and catalyst efficiency.

### 7.2.2. Oxygen Exhaust Gas Concentration

The addition of oxygen has the potential of enhancing the low-temperature catalytic oxidation of CO, especially under conditions where oxygen exhaust gas content is reduced (EGR strategy or lower air-fuel ratio operating conditions). The catalyst oxidation efficiency was particularly promoted at temperatures close to the light-off, but an increase in oxygen exhaust content could not trigger the reaction when the catalyst was still kinetically limited (low temperatures) or poisoned with carbonaceous species accumulated on the active sites.

An increase from limited conversion efficiency (few percentages) to 25-30% at 120°C from the addition of oxygen can significantly reduce CO tailpipe emissions, especially during cold start, when peaks of CO are produced and the engine could be running at lower air-fuel ratios. Moreover, timing oxygen injections with peaks of CO and alkenes emissions could take advantage and enhance the heat production from the exothermic oxidation reaction to efficiently increase the catalyst local temperature and promote greater conversion efficiency. This heating strategy would be more efficient than other heating techniques (catalyst or exhaust gas heating) as the heat would be directly produced where it is needed, i.e. on the active sites, limiting the heat losses. The gain in conversion efficiency even remained for some time after the oxygen addition had stopped due to the delay to cool down the active sites. The use of warmer oxygen could also further increase these beneficial effects, especially at cold start. The practical application of this experiment in an engine would be the addition of air rather than oxygen to the exhaust system, e.g. through optimisation of the

valve timing, by increasing the overlap phase, to allow some of the fresh air entering the combustion chamber to be sucked into the exhaust system by the exiting exhaust gas.

### 7.2.3. Effect of Soot Accumulation on the DOC Activity

The outcomes of the investigation on soot accumulation in high cell density flow-through oxidation catalyst showed limited effect on the activity, mainly affecting NO oxidation. Nevertheless, with further increase in cell density and subsequent reduction in the cell hydraulic diameter, the effect of soot accumulation in the channels could reach greater extent. The developments in engine injection and calibration strategies tend to decrease the diameter of the particulates exiting the combustion chamber, which would reduce the possibility of plugged channels. In addition, this study also provided an insight into the particulate removal efficiency in flow-through catalysts, highlighting a limited trapping performance and a "self-regenerating" or cleaning capacity through particulate blow-off. This limited filtration efficiency showed a potential for improvement.

## 7.3. COMBINATION OF FILTRATION AND OXIDATION FUNCTIONS TO IMPROVE THE DPF THERMAL MANAGEMENT

The investigation of the replacement of the DOC in the exhaust system by another aftertreatment component that would combine a filtration and oxidation function required the extensive study of specific parameters. First, the analysis of the filtration mechanisms of the selected components (partial-flow filters and flow-through catalysts) revealed great differences in their particulate removal efficiency at various engine operating conditions. Their oxidation capacity was also investigated and compared to the conventional DOC, as well as their long-term activity. Two components (PM-Metalit and POC) that showed

promising particulate filtration efficiency were selected, to be each fitted upstream of a DPF. The results of these PFF+DPF systems showed a 30% reduction in the total mass of soot accumulated in the DPF, which could be translated into a reduction in the need for active regenerations (frequency and/or duration). Additionally, the partial-flow filters improved the removal of small particulates (below 30 nm) that will become a greater concern in future legislation due to potential negative health effects. Further parameters still need to be investigated, such as the behaviour of the PFF during an active regeneration event, and the possibility of coating the PM-Metalit and its effect on the filtration efficiency.

The choice of components to be fitted upstream of the DPF is governed by specific parameters (requirement for minimum filtration efficiency, low-temperature oxidation capacity, limited pressure increase and cost) whose importance and rank will define the appropriate component for specific applications and requirements.

## 7.4. CLOSING REMARKS

A number of diverse strategies were investigated in this study, reaching towards different perspectives (exhaust gas and aftertreatment components) that could be combined together to widen the catalyst operating temperature window. The gains in conversion efficiency recorded for some of the proposed aftertreatment solutions (two-brick configurations, addition of oxygen, and control of the exhaust species interactions in the catalyst at low temperature) could also translate into a reduction of precious metal loading and therefore cost savings. While some of the approaches developed here could be considered costly, the ever tightening emission legislation will push forward the boundaries of what can and need to be achieved in terms of vehicle emission reductions. Aftertreatment research and development, with the help of multidisciplinary scientific collaborations, will have to look at new strategies and solutions that might not have been interesting in the past but that will become more

relevant in the future, due to the new requirements in terms of emissions and thermal management of the diesel exhaust aftertreatment system.

# AUTHOR PUBLICATIONS

- **Lefort, I**. and Tsolakis A. (2013) A Thermally Efficient DOC Configuration to Improve CO and THC Conversion Efficiency. **SAE Paper**, 2013-01-1582. *Presented by the author at SAE World Congress 2013 in Detroit, USA.*

- **Lefort, I.**, Herreros, J. M. and Tsolakis, A. (2014) Reduction of Low Temperature Engine Pollutants by Understanding the Exhaust Species Interactions in a Diesel Oxidation Catalyst. **Environmental Science & Technology**, 48: (4): 2361-2367**.**

- **Lefort, I.**, Herreros, J. M. and Tsolakis, A. (2015) The Use of a Partial-Flow Filter to Assist the Diesel Particulate Filter and Reduce Active Regeneration Events. **SAE Int. J. Engines***,* 7: (4): 1953-1960. *Presented by the author at the SAE Powertrain, Fuel and Lubricants 2014, Birmingham, UK.*

***Conference Paper***

- **Lefort, I.**, Herreros, J. M. and Tsolakis, A. (2014) Oxygen Exhaust Concentration Effect on Low Temperature CO Oxidation. *Presented by the author at the 1st International Conference on Engineering Science and Innovative Technology (ESIT) 2014 in Krabi, Thailand*.

***Collaboration Paper***

- Herreros, J.M., Gill, S.S., **Lefort, I.**, Tsolakis, A., Millington, P. and Moss, E. (2014) Enhancing the Low Temperature Oxidation Performance over a Pt and a Pt-Pd Diesel Oxidation Catalyst. **Appl. Catal. B: Environ.**, 147: (0): 835-841.

***Conference Posters***

- *Reduction of Low Temperature Pollutants by Understanding the Exhaust Species Interactions in a Diesel Oxidation Catalyst*, presented at the **Future Powertrain Conference** 2014, Solihull, UK.

- *Engaging Low Temperature Issues in Diesel Exhaust for Cleaner Vehicle Emissions*, presented at the **SAE Powertrain, Fuel and Lubricants** 2014, Birmingham, UK.

# AWARDS

**Engineering and Physical Sciences College Best Publication Award** for *Reduction of Low Temperature Engine Pollutants by Understanding the Exhaust Species Interactions in a Diesel Oxidation Catalyst*, University of Birmingham, January 2014.

**Outstanding Paper Award** in Automotive Engineering for *Oxygen Exhaust Concentration Effect on Low Temperature CO Oxidation*, at 1st International Conference on Engineering Science and Innovative Technology (ESIT) Conference, Krabi, Thailand, April 2014.

**Best Oral Presentation** at the 3rd Mechanical Engineering Symposium, University of Birmingham, May 2014.

**Austin Rover Prize (PG),** awarded annually to the most worthwhile thesis, project report or essay in the subject areas of the role, use and/or engineering aspects of the motor vehicle in modern society, University of Birmingham, December 2014.

# APPENDICES

## A.1. Legislation Driving Cycles

Driving cycles have been developed to reproduce a certain driving pattern and study the behaviour of a specific type of vehicle (from motorcycles to heavy goods vehicles (HGVs) and buses), in terms of performance and emissions. Some drive cycles are developed as part of a study or a project, while others are used to evaluate vehicle emissions and compare them to the limits imposed by the legislation.

Three main drive cycles are currently used worldwide to homologate a vehicle (here passenger cars) from the emissions point of view. These cycles were designed based on the local driving pattern (speed limit, driving conditions) and the typical vehicle power.

The New European Driving Cycle (NEDC) is composed of four repetitions of the ECE-15 urban driving cycle, first introduced in 1970 and one extra-urban driving cycle (EUDC), developed in 1990 (Figure A-1). A low-temperature test (-7°C) is also required for homologation. In addition to the usual emission limits on CO, THCs, $NO_x$ and particulate mass, the legislation imposes a limit on particulate numbers, to reduce the emissions of small particulates considered more dangerous for health (Figure 1-2) in the scope of Euro 6 legislation. Compared to the vehicles used at the time when the NEDC was designed, nowadays vehicles are more powerful and fitted with multiple features improving the driver comfort and entertainment but also increasing the engine load. Moreover, the development of more congested urban centres changed the driving pattern now encountered in Europe compared to the one in the 1970s. These changes make the European driving cycle, with its low acceleration and constant speed cruise phases, less representative of today's more transient and sharper driving habits. Therefore, from Euro 6.2 legislation onwards, the possibility of real-life driving emission assessment could be compulsory for homologation.

This new feature could impose the vehicle to either perform a random cycle on a bench or a real on-road drive, recording the emissions using portable emission measurement systems (PEMS).

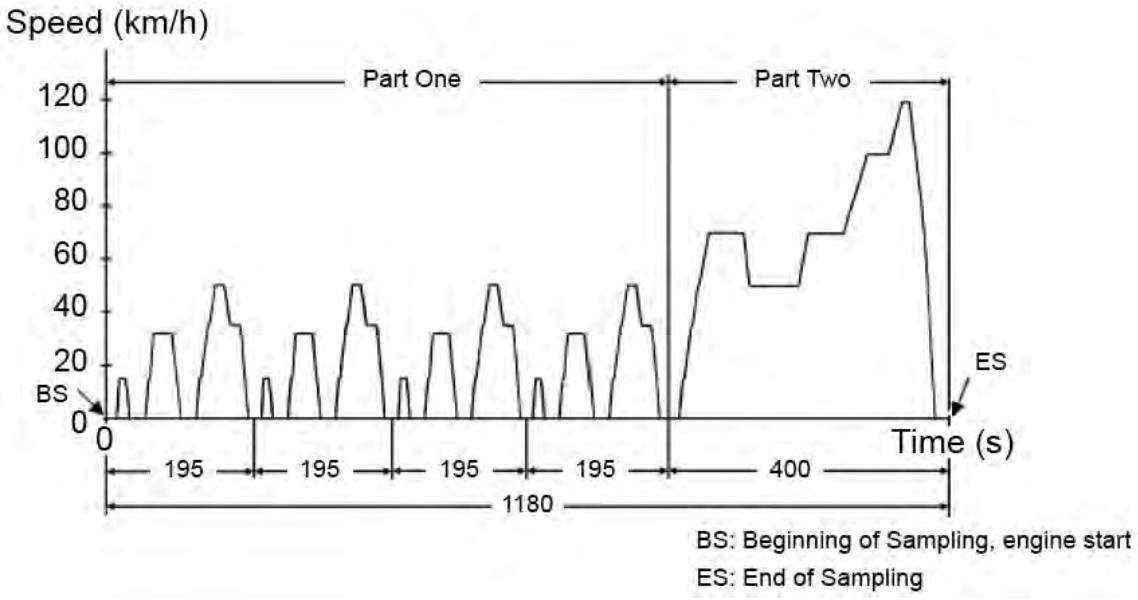


**Figure A-1.** Vehicle speed against time during an NEDC

In North America, the Environmental Protection Agency (EPA) developed its legislative driving cycle (FTP-75, Federal Test Procedure) in 1975 but it was updated in 2008 to include some additional specific driving phases to make it more representative of today's driving conditions (cold-start cycle test, highway fuel economy test (HWFET), aggressive driving (US06) and optional air conditioning driving) (Figure A-2).

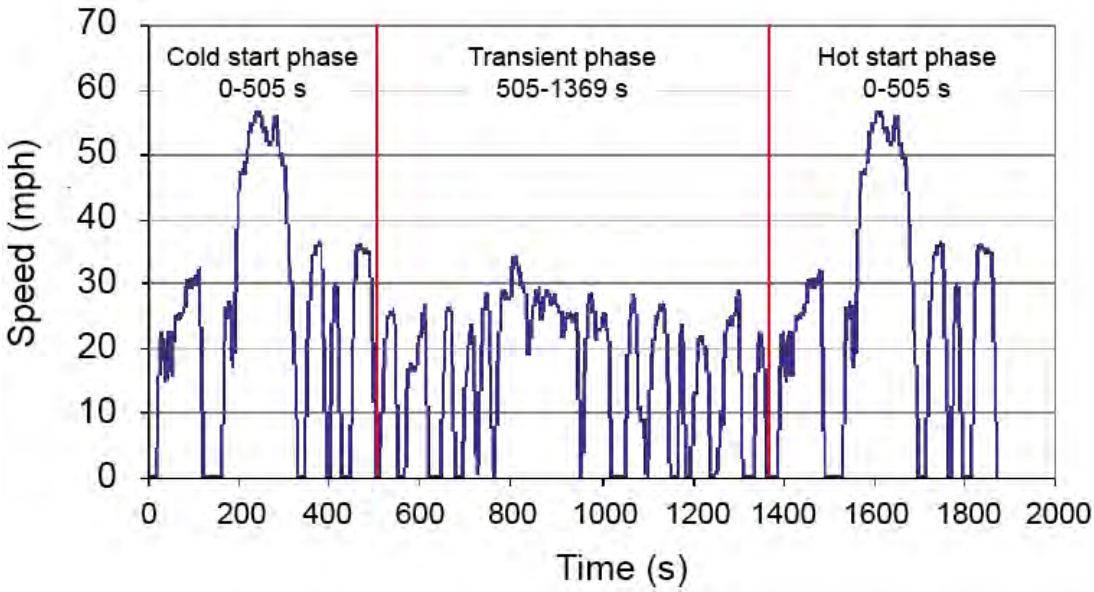


**Figure A-2.** Vehicle speed against time during the FTP-75

In Japan, the first cycle to be developed was the 10-15 mode cycle in 1983 which has now been replaced by the JC08, since 2008, which is a more representative version of urban driving conditions (Figure A-3), with more transient phases (acceleration/deceleration) and longer idle segments to simulate congestion traffic. A cold-start measurement was also added to the cycle.

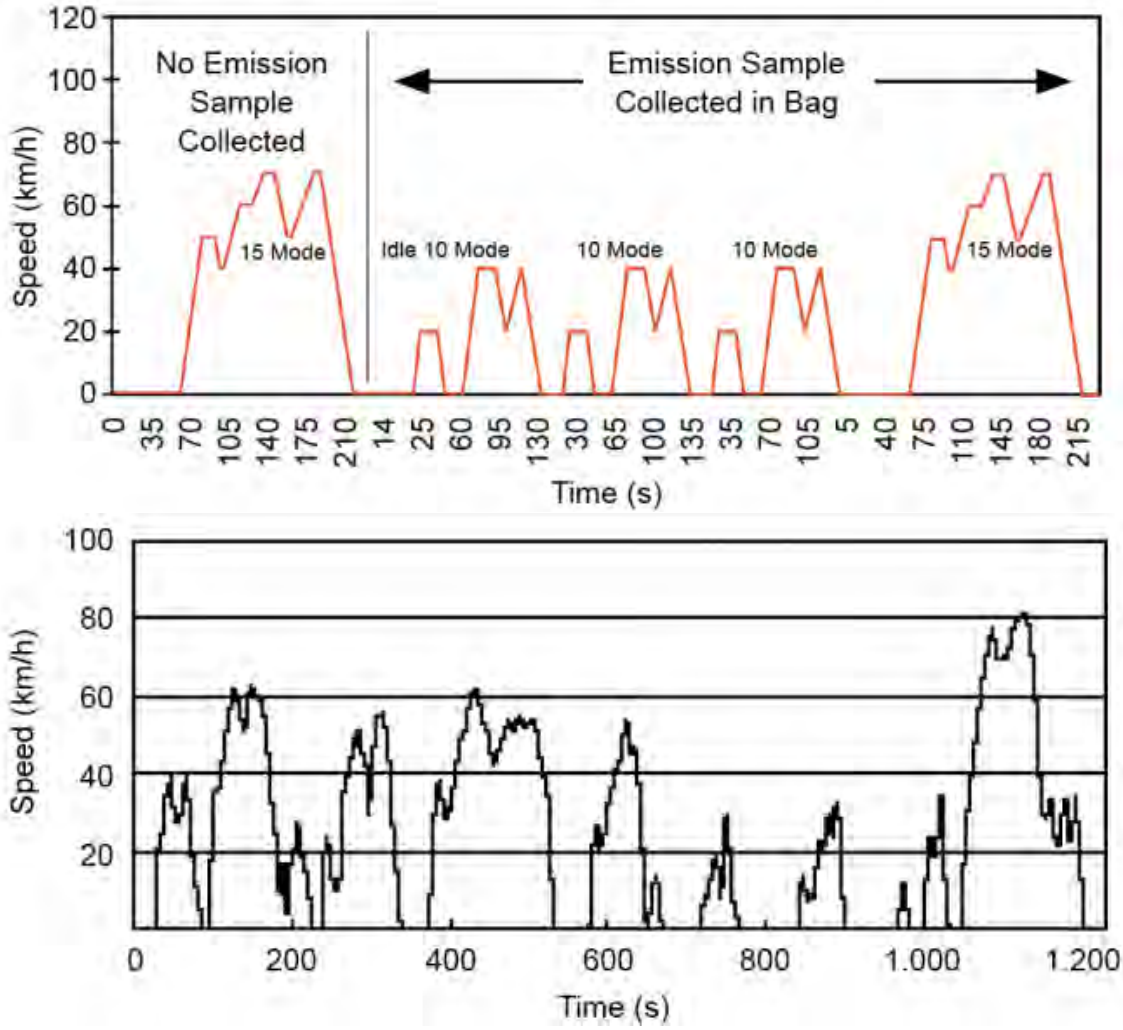


**Figure A-3.** Vehicle speed against time for the Japan 10-15 cycle (top) and more recent JC08 cycle (bottom)

These drive cycles need to be continuously updated with new features, as the driving pattern and vehicle specifications evolve, to maintain a similarity with real-life driving conditions. The main reproach usually made is that these cycles tend to reproduce smoother driving conditions than what can be met on-road, especially with acceleration and idle phases (Färnlund & Engström, 2001). Therefore, in order to remedy these limitations and allow a greater uniformity in world emission legislation, a worldwide harmonized light-duty vehicle test procedure (WLTP) is currently being developed under the guidelines of the United Nations World Forum for Harmonization of Vehicle Regulations (UNECE, 2012).

This cycle aims at reproducing conditions that are more representative of real-world driving situations and takes into account the additional use of lights, air conditioning and other equipments and options available on the vehicle. Three different cycles have been designed that will apply to vehicles depending on their ratio power/unloaded mass and the maximum vehicle speed. Special features will be added onto the cycle (e.g. extra high-speed part for Europe and the United States) depending on the region where the vehicle will be sold, in order to replicate local driving characteristics. This cycle will also feature more transient phases (abrupt accelerations) and lower speeds (10-20 km/h) compared to the driving conditions of the cycles currently used (Figure A-4).

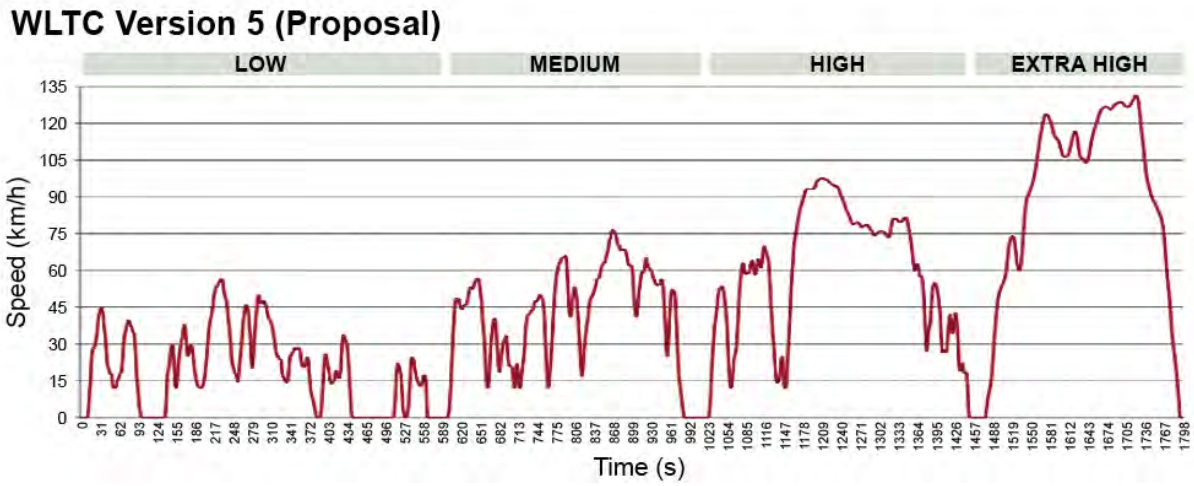


**Figure A-4.** Vehicle speed against time for the WLTP

Simultaneously to the evolution of these drive cycles, the emission limits for vehicle homologation are continuously reducing worldwide (Delphi, 2014). These limits impose the implementation of aftertreatment components in the exhaust system to promote the removal of pollutants before release to the atmosphere.

# REFERENCES


Adamczyk *et al.* (1999) Adamczyk, A.A., Hubbard, C.P., Ament, F., *et al.* (1999) Experimental and Modeling Evaluations of a Vacuum-Insulated Catalytic Converter. **SAE Paper**, 1999-01-3678.

Agarwal *et al.* (2011) Agarwal, D., Singh, S.K. and Agarwal, A.K. (2011) Effect of Exhaust Gas Recirculation (EGR) on Performance, Emissions, Deposits and Eurability of a Constant Speed Compression Ignition Engine. **Applied Energy**, 88: (8): 2900-2907.

Agarwal *et al.* (2004) Agarwal, A.K., Singh, S.K., Sinha, S.S., *et al.* (2004) Effect of EGR on the Exhaust Gas Temperature and Exhaust Opacity in Compression Ignition Engines. **Sadhana**, 29: (3): 275-284.

Al-Harbi *et al.* (2012) Al-Harbi, M., Hayes, R., Votsmeier, M., *et al.* (2012) Competitive NO, CO and Hydrocarbon Oxidation Reactions Over a Diesel Oxidation Catalyst. **The Canadian Journal of Chemical Engineering**, 90: (6): 1527-1538.

Alkidas *et al.* (2004) Alkidas, A.C., Battiston, P.A. and Kapparos, D.J. (2004) Thermal Studies in the Exhaust System of a Diesel-Powered Light-Duty Vehicle. **SAE Paper**, 2004-01-0050.

Andersson *et al.* (2007) Andersson, J., Antonsson, M., Eurenius, L., *et al.* (2007) Deactivation of Diesel Oxidation Catalysts: Vehicle - and Synthetic Aging Correlations. **Applied Catalysis B: Environmental**, 72: (1–2): 71-81.

Andreassi *et al.* (2002) Andreassi, L., Cordiner, S., Mulone, V., *et al.* (2002) Mixed Numerical-Experimental Analysis Procedure for Non-Blocking Metal Supported Soot Trap Design. **SAE Paper**, 2002-01-2782.

Babu *et al.* (2008) Babu, K.V.R., Dias, C., Waje, S., *et al.* (2008) PM Metalit® - A Continuously Regenerating Partial Flow Particulate Filter - Concept and Experience with Korean Retrofit Programme. **SAE Paper**, 2008-28-0008.

Bach & Eggenschwiler (2011) Bach, C. and Eggenschwiler, P. (2011) Ceramic Foam Catalyst Substrates for Diesel Oxidation Catalysts : Pollutant Conversion and Operational Issues. **SAE Paper**, 2011-24-0179.

Ballesteros *et al.* (2008) Ballesteros, R., Hernández, J.J., Lyons, L.L., *et al.* (2008) Speciation of the Semivolatile Hydrocarbon Engine Emissions from Sunflower Biodiesel. **Fuel**, 87: (10–11): 1835-1843.

Ballesteros *et al.* (2010) Ballesteros, R., Hernández, J.J. and Lyons, L.L. (2010) An Experimental Study of the Influence of Biofuel Origin on Particle-Associated PAH Emissions. **Atmospheric Environment**, 44: (7): 930-938.

Ballinger *et al.* (2009) Ballinger, T., Cox, J., Konduru, M., *et al.* (2009) Evaluation of SCR Catalyst Technology on Diesel Particulate Filters. **SAE Int. J. Fuels Lubr.**, 2: (1): 369-374.

Barnes & Klimisch (1973) Barnes, G.J. and Klimisch, R.L. (1973) Initial Oxidation Activity of Noble Metal Automotive Exhaust Catalysts. **SAE Paper**, 730570.

Berlowitz *et al.* (1988) Berlowitz, P.J., Peden, C.H.F. and Goodman, D.W. (1988) Kinetics of Carbon Monoxide Oxidation on Single-Crystal Palladium, Platinum, and Iridium. **The Journal of Physical Chemistry**, 92: (18): 5213-5221.

Bhatt *et al.* (2013) Bhatt, D., Waje, S., Babu, K.V.R., *et al.* (2013) Achieving BS-IV Emission Targets for Diesel Small Commercial Vehicle (SCV) with Close Coupled Advanced EnviCat ® DOC and Coated PM Metalit ® After - Treatment System. **SAE Paper**, 2013-26-0054.

Bollig *et al.* (2004) Bollig, M., Liebl, J., Zimmer, R., *et al.* (2004) Next Generation Catalysts are Turbulent:Development of Support and Coating. **SAE Paper**, 2004-01-1488.

Borland & Zhao (2002) Borland, M. and Zhao, F. (2002) Application of Secondary Air Injection for Simultaneously Reducing Converter-In Emissions and Improving Catalyst Light-Off Performance. **SAE Paper**, 2002-01-2803.

Bosch Mobility Solutions (2013) Bosch Mobility Solutions (2013) **Bosch Compact, Overview of diesel markets from China to the U.S.**, Press release [online]. Available from: http://www.bosch-presse.de/presseforum/details.htm?txtID=6355&tk_id=108 [Accessed 6 August 2013].

Brillant & Zikoridse (2005) Brillant, S. and Zikoridse, G. (2005) Metal Fibre Diesel Particulate Filter : Function and Technology. **SAE Paper**, 2005-01-0580.

Brück *et al.* (2001a) Brück, R., Kaiser, F.-W., Konieczny, R., *et al.* (2001a) Study of Modern Application Strategies for Catalytic Aftertreatment Demonstrated on a Production V6 Engine. **SAE Paper**, 2001-01-0925.

Brück *et al.* (2001b) Brück, R., Hirth, P., Reizig, M., *et al.* (2001b) Metal Supported Flow-Through Particulate Trap; a Non-Blocking Solution. **SAE Paper**, 2001-01-1950.

Brück *et al.* (2009) Brück, R., Müller-Haas, K., Holz, O., *et al.* (2009) "Application of PM-METALIT® and SCRi® Systems". **5th AVL International Commercial Powertrain Conference**. Graz, Austria.

Burch *et al.* (1998) Burch, R., Sullivan, J.A. and Watling, T.C. (1998) Mechanistic Considerations for the Reduction of $NO_x$ over $Pt/Al_2O_3$ and $Al_2O_3$ Catalysts Under Lean-Burn Conditions. **Catalysis Today**, 42: (1–2): 13-23.

Burch *et al.* (2002) Burch, R., Breen, J.P. and Meunier, F.C. (2002) A Review of The Selective Reduction of NOx with Hydrocarbons Under Lean-Burn Conditions with Non-Zeolitic Oxide and Platinum Group Metal Catalysts. **Applied Catalysis B: Environmental**, 39: (4): 283-303.

Burch & Biel (1999) Burch, S.D. and Biel, J.P. (1999) SULEV and "Off-Cycle" Emissions Benefits of a Vacuum-Insulated Catalytic Converter. **SAE Paper**, 1999-01-0461.

Burch & Millington (1995) Burch, R. and Millington, P.J. (1995) Selective Reduction of Nitrogen Oxides by Hydrocarbons Under Lean-Burn Conditions Using Supported Platinum Group Metal Catalysts. **Catalysis Today**, 26: (2): 185-206.

Campbell & Martin (1995) Campbell, M.G. and Martin, E.P. (1995) Substrate Selection for a Diesel Catalyst. **SAE Paper**, 950372.

Cant *et al.* (1978) Cant, N.W., Hicks, P.C. and Lennon, B.S. (1978) Steady-State Oxidation of Carbon Monoxide over Supported Noble Metals With Particular Reference to Platinum. **Journal of Catalysis**, 54: (3): 372-383.

Carberry *et al.* (2005) Carberry, B., Grasi, G., Guerin, S., *et al.* (2005) Pre-Turbocharger Catalyst - Fast Catalyst Light-Off Evaluation. **SAE Paper**, 2005-01-2142.

Carel (1998) Carel, R.S. (1998) "Chapter 3 - Health Aspects of Air Pollution". In Sher, E. (Ed.) **Handbook of Air Pollution From Internal Combustion Engines**. San Diego, Academic Press 42-64.

Carty & Lednor (1996) Carty, W.M. and Lednor, P.W. (1996) Monolithic Ceramics and Heterogeneous Catalysts: Honeycombs and Foams. **Current Opinion in Solid State and Materials Science**, 1: (1): 88-95.

Cavataio *et al.* (2009) Cavataio, G., Girard, J.W. and Lambert, C.K. (2009) Cu/Zeolite SCR on High Porosity Filters: Laboratory and Engine Performance Evaluations. **SAE Paper**, 2009-01-0897.

Chanda *et al.* (2000) Chanda, A.A., Richards, R.R. and J.T., V. (2000) "Method and System for Late Cycle Oxygen Injection in an Internal Combustion Engine". **United States Patent Office**. Patent NO. US006067973A.

Chen *et al.* (2003) Chen, Y., Bowman, J. and Harris, J. (2003) Catalyst Converter Canning Simulation Studies. **SAE Paper**, 2003-01-0666.

Cordiner *et al.* (2009) Cordiner, S., Mariani, A. and Mulone, V. (2009) Experimental-Numerical Analysis of Mass Transfer in Standard and Longitudinal Structured (LS) Substrates. **SAE Paper**, 2009-01-1270.

Dawson & Kramer (2006) Dawson, E.K. and Kramer, J. (2006) Faster is Better: The Effect of Internal Turbulence on DOC Efficiency. **SAE Paper**, 2006-01-1525.

Delphi (2014) Delphi (2014) Worldwide emissions standards, passenger cars and light duty vehicles 2014/2015 [online]. Available from: http://delphi.com/pdf/emissions/delphi-worldwide-emissions-standards-passenger-cars-lightduty-vehicles-2014-2015.pdf.

Diefke *et al.* (2003) Diefke, F., Nilsson, P., Brück, R. and Schaper, S. (2003) New Diesel Catalyst Systems to Achieve European 2005 Legislation – Tested on a Volvo S60 Passenger Car. May 2003. Communication published by Emitec.

Diehl *et al.* (2010) Diehl, F., Barbier Jr, J., Duprez, D., *et al.* (2010) Catalytic Oxidation of Heavy Hydrocarbons over $Pt/Al_2O_3$. Influence of the Structure of The Molecule on its Reactivity. **Applied Catalysis B: Environmental**, 95: (3–4): 217-227.

EAMA (2013) European Automobile Manufacturer's Association (2013) **Trends in New Car Registrations: Diesel Penetration** [online]. Available from: http://www.acea.be/statistics/tag/category/diesel-penetration.

Färnlund & Engström (2001) Färnlund, J. and Engström, C. (2001) The Representativeness of Driving Cycles in Real-World Traffic. Rototest A.B. Publication 2001:35/E, Document ID RP-010122. Rönninge, Sweden.

Gaiser & Mucha (2004) Gaiser, G. and Mucha, P. (2004) Prediction of Pressure Drop in Diesel Particulate Filters Considering Ash Deposit and Partial Regenerations. **SAE Paper**, 2004-01-0158.

Geiser & Kreyling (2010) Geiser, M. and Kreyling, W. (2010) Deposition and Biokinetics of Inhaled Nanoparticles. **Particle and Fibre Toxicology**, 7: (1): 1-17.

Gill *et al.* (2011) Gill, S.S., Turner, D., Tsolakis, A., *et al.* (2011) Understanding the Role of Filtered EGR on PM Emissions. **SAE Paper**, 2011-01-2080.

Glover *et al.* (2011) Glover, L., Douglas, R., McCullough, G., *et al.* (2011) Performance Characterisation of a Range of Diesel Oxidation Catalysts: Effect of Pt:Pd Ratio on Light Off Behaviour and Nitrogen Species Formation **SAE Paper**, 2011-24-0193.

Görsmann (2005) Görsmann, C. (2005) Catalytic Coatings for Active and Passive Diesel Particulate Filter Regeneration. **Monatshefte für Chemie / Chemical Monthly**, 136: (1): 91-105.

Grbic *et al.* (2004) Grbic, B., Radic, N. and Terlecki-Baricevic, A. (2004) Kinetics of Deep Oxidation of N-Hexane and Toluene over $Pt/Al_2O_3$ Catalysts: Oxidation of Mixture. **Applied Catalysis B: Environmental**, 50: (3): 161-166.

Gulati (2000) Gulati, S.T. (2000) Design Considerations for Advanced Ceramic Catalyst Supports. **SAE Paper**, 2000-01-0493.

Gulati (2001) Gulati, S.T. (2001) Design and Durability of Standard and Advanced Ceramic Substrates. **SAE Paper**, 2001-26-0011.

Gulati (2005) Gulati, S.T. (2005) "Ceramic Catalyst Supports for Gasoline Fuel". **Structured Catalysts and Reactors**. CRC Press 21-70.

Gulati *et al.* (2001) Gulati, S.T., Leonhard, T. and Roe, T.A. (2001) Shear Strength of Cordierite Ceramic Catalyst Supports. **SAE Paper**, 2001-01-0935.

Gulati *et al.* (2002) Gulati, S.T., Hampton, L.E. and Lambert, D.W. (2002) Thermal Shock Resistance of Advanced Ceramic Catalysts for Close-Coupled Application. **SAE Paper**, 2002-01-0738.

Hadavi *et al.* (2013) Hadavi, S.A., Li, H., Andrews, G., *et al.* (2013) Diesel Cold Start into Congested Real World Traffic: Comparison of Diesel, B50, B100 for Gaseous Emissions. **SAE Paper**, 2013-01-2528.

Happonen *et al.* (2013) Happonen, M., Matilainen, P., Kanniainen, K., *et al.* (2013) The Effect of a Particle Oxidation Catalyst (POC ® ) on Particle Emissions of a GDI Car during Transient Engine Operation. **SAE Paper**, 2013-01-0839.

Hauff *et al.* (2012) Hauff, K., Tuttlies, U., Eigenberger, G., *et al.* (2012) Platinum Oxide Formation and Reduction During NO Oxidation on a Diesel Oxidation Catalyst – Experimental Results. **Applied Catalysis B: Environmental**, 123–124: (0): 107-116.

Hawley *et al.* (1998) Hawley, J.G., Brace, C.J., Wallace, F.J., *et al.* (1998) "Chapter 10 - Combustion-Related Emissions in CI Engines". In Sher, E. (Ed.) **Handbook of Air Pollution From Internal Combustion Engines**. San Diego, Academic Press 280-357.

Heck *et al.* (2009) Heck, R.M., Farrauto, R.J. and Gulati, S.T. (2009) **Catalytic air pollution control: Commercial technology, 3rd Edition**. John Wiley & Sons.

Heikkilä *et al.* (2009) Heikkilä, J., Rönkkö, T., Lähde, T., *et al.* (2009) Effect of Open Channel Filter on Particle Emissions of Modern Diesel Engine. **Journal of the Air & Waste Management Association**, 59: (10): 1148-1154.

Hirose *et al.* (2012) Hirose, S., Miyairi, Y., Katsube, F., *et al.* (2012) Newly Developed Cordierite Honeycomb Substrate for SCR Coating Realizing System Compactness and Low Backpressure. **SAE Paper**, 2012-01-1079.

Holroyd (2006) Holroyd, J.A. (2006) "A Diesel Oxidation Catalyst with Low T50 Properties and a Wide Operating Temperature Range". **12th Annual MDEC Conference Mining Diesel Emissions Council**. Toronto North, Canada.

Honardar *et al.* (2011) Honardar, S., Busch, H., Schnorbus, T., *et al.* (2011) Exhaust Temperature Management for Diesel Engines Assessment of Engine Concepts and Calibration Strategies with Regard to Fuel Penalty. **SAE Paper**, 2011-24-0176.

Hori *et al.* (1992) Hori, M., Matsunaga, N., Malte, P.C., *et al.* (1992) The Effect of Low-Concentration Fuels on the Conversion of Nitric Oxide to Nitrogen Dioxide. **Symposium (International) on Combustion**, 24: (1): 909-916.

Hosogai *et al.* (2003) Hosogai, S., Komatsu, K. and Unno, Y. (2003) "The Hybrid Catalyst, a New Catalyst Concept to Improve Utilization of Exhaust Gas Energy and Increase the Efficiency of Diesel Catalyst Systems". **24th Vienna International Motor Symposium**. Vienna, Austria.

Houdry (1956) Houdry, E.J. (1956) "Catalytic Structure and Composition". **United States Patent Office**. Patent NO. US2742437A.

Hughes *et al.* (2006) Hughes, K.W., Gian, D. and Calleja, J. (2006) Relative Benefits of Various Cell Density Ceramic Substrates in Different Regions of the FTP Cycle. **SAE Paper**, 2006-01-1065.

Hughes & Flörchinger (2002) Hughes, K.W. and Flörchinger, P. (2002) Ultra Thinwall Light-off Performance - Varying Substrates, Catalysts, and Flow Rates; Models and Engine Testing. **SAE Paper**, 2002-01-0352.

IARC (2012) International Agency for Research on Cancer (2012) **Diesel Engine Exhaust Carcinogenic**, Press release n°213 [online]. Available from: http://www.iarc.fr/en/media-centre/pr/2012/pdfs/pr213_E.pdf.

Ichikawa *et al.* (1999) Ichikawa, Y., Umehara, K., Hijikata, T. (1999) Catalyst Layout Optimisation for Ultra Thin-Wall and High Cell-Density Ceramic Substrate. **SAE Paper**, 990019.

Imtenan *et al.* (2014) Imtenan, S., Varman, M., Masjuki, H.H., *et al.* (2014) Impact of Low Temperature Combustion Attaining Strategies on Diesel Engine Emissions for Diesel And Biodiesels: A Review. **Energy Conversion and Management**, 80: (0): 329-356.

Irani *et al.* (2009) Irani, K., Epling, W.S. and Blint, R. (2009) Effect of Hydrocarbon Species on NO Oxidation over Diesel Oxidation Catalysts. **Applied Catalysis B: Environmental**, 92: (3–4): 422-428.

Ishizaki *et al.* (2012) Ishizaki, K., Mitsuda, N., Ohya, N., *et al.* (2012) A Study of PGM-Free Oxidation Catalyst YMnO3 for Diesel Exhaust Aftertreatment. **SAE Paper**, 2012-01-0365.

Jacobs *et al.* (2006) Jacobs, T., Chatterjee, S., Conway, R., *et al.* (2006) Development of Partial Filter Technology for HDD Retrofit. **SAE Paper**, 2006-01-0213.

Jasper *et al.* (1991) Jasper, T.S., Robinson, K., Anderton, D., *et al.* (1991) "Monolith Substrate Effects on Catalyst Light-Off". In Crucq, A. (Ed.) **Studies in Surface Science and Catalysis**. Elsevier 523-535.

Jatkar (1997) Jatkar, A.D. (1997) A New Catalyst Support Structure for Automotive Catalytic Converters. **SAE Paper**, 971032.

Jayat *et al.* (2015) Jayat, F., Seifert, S., Babu, K.V.R., *et al.* (2015) Application of a LS Metal Catalyst Substrate for BS IV Two and Three Wheelers. **SAE Paper**, 2015-26-0098.

Jeong & Kim (2001) Jeong, S.-J. and Kim, W.-S. (2001) A New Strategy for Improving the Warm-Up Performance of a Light-Off Auto-Catalyst for Reducing Cold-Start Emissions. **Proceedings of the Institution of Mechanical Engineers, Part D: Journal of Automobile Engineering**, 215: (11): 1179-1196.

Johansen *et al.* (2007) Johansen, K., Dahl, S., Mogensen, G., *et al.* (2007) Novel Base Metal-Palladium Catalytic Diesel Filter Coating with $NO_2$ Reducing Properties. **SAE Paper**, 2007-01-1921.

Johnson & Kittelson (1994) Johnson, J.E. and Kittelson, D.B. (1994) Physical Factors Affecting Hydrocarbon Oxidation in a Diesel Oxidation Catalyst. **SAE Paper**, 941771.

Johnson & Kittelson (1996) Johnson, J.E. and Kittelson, D.B. (1996) Deposition, Diffusion and Adsorption in the Diesel Oxidation Catalyst. **Applied Catalysis B: Environmental**, 10: (1–3): 117-137.

Johnson Matthey (2014) Johnson Matthey (2014) **Metals Base Prices** [online]. Available from: http://www.platinum.matthey.com/.

Kalam *et al.* (2008) Kalam, M.A., Masjuki, H.H., Redzuan, M., *et al.* (2008) Development and Test of a New Catalytic Converter for Natural Gas Fueled Engine. **SAE Paper**, 2008-01-1550.

Kallinen *et al.* (2009) Kallinen, K., Moreno, A., Savimäki, A., *et al.* (2009) Pt/Pd Diesel Oxidation Catalyst : A Study on the Properties Enhanced by the Use of Pd. **SAE Paper**, 2009-26-0018.

Kandylas & Stamatelos (1999) Kandylas, I.P. and Stamatelos, A.M. (1999) Engine Exhaust System Design Based on Heat Transfer Computation. **Energy Conversion and Management**, 40: (10): 1057-1072.

Karjalainen *et al.* (2012) Karjalainen, P., Heikkilä, J., Rönkkö, T., *et al.* (2012) "Particle Emission Reduction in a SI-DI Vehicle by an Open Channel Filter". **16th ETH-Conference on Combustion Generated Nanoparticles**. Zurich, Switzerland.

Katare *et al.* (2007) Katare, S.R., Patterson, J.E. and Laing, P.M. (2007) Aged DOC is a Net Consumer of $NO_2$: Analyses of Vehicle, Engine-dynamometer and Reactor Data. **SAE Paper**, 2007-01-3984.

Kim *et al.* (2011) Kim, C.H., Schmid, M., Schmieg, S.J., *et al.* (2011) The Effect of Pt-Pd Ratio on Oxidation Catalysts Under Simulated Diesel Exhaust. **SAE Paper**, 2011-01-1134.

Kim *et al.* (2014) Kim, Y.-W., Van Nieuwstadt, M., Stewart, G., *et al.* (2014) Model Predictive Control of DOC Temperature during DPF Regeneration. **SAE Paper**, 2014-01-1165.

Kinnunen *et al.* (2012) Kinnunen, T., Matilainen, P., Scheder, D., *et al.* (2012) Particle Oxidation Catalyst (POC ® ) - From Diesel To GDI - Studies on Particulate Number and Mass Efficiency **SAE Paper**, 2012-01-0845.

Klingstedt *et al.* (2004) Klingstedt, F., Eränen, K., Lindfors, L.E., *et al.* (2004) A Highly Active Ag/Alumina Catalytic Converter for Continuous HC-SCR during Lean-Burn Conditions: From Laboratory to Full-Scale Vehicle Tests. **Topics in Catalysis**, 30-31: (1-4): 27-30.

Knafl *et al.* (2007) Knafl, A., Han, M., Bohac, S.V., *et al.* (2007) Comparison of Diesel Oxidation Catalyst Performance on an Engine and a Gas Flow Reactor. **SAE Paper**, 2007-01-0231.

Koebel *et al.* (2002) Koebel, M., Madia, G. and Elsener, M. (2002) Selective Catalytic Reduction of NO and $NO_2$ at Low Temperatures. **Catalysis Today**, 73: (3–4): 239-247.

Koltsakis *et al.* (2006) Koltsakis, G.C., Katsaounis, D.K., Samaras, Z.C., *et al.* (2006) Filtration and Regeneration Performance of a Catalyzed Metal Foam Particulate Filter. **SAE Paper**, 2006-01-1524.

Koltsakis *et al.* (2007) Koltsakis, G.C., Katsaounis, D.K., Markomanolakis, I.A., *et al.* (2007) Metal Foam Substrate for DOC and DPF Applications. **SAE Paper**, 2007-01-0659.

Koltsakis *et al.* (2008) Koltsakis, G.C., Katsaounis, D.K., Samaras, Z.C., *et al.* (2008) Development of Metal Foam Based Aftertreatment System on a Diesel Passenger Car. **SAE Paper**, 2008-01-0619.

Koltsakis *et al.* (2011) Koltsakis, G.C., Samaras, Z., Karvountzis-Kontakiotis, A., *et al.* (2011) Implications of Engine Start-Stop on After-Treatment Operation. **SAE Int. J. Engines**, 4: (1): 1571-1585.

Konieczny *et al.* (2008) Konieczny, R., Müller, W., Cherington, B., *et al.* (2008) Pre-Turbocharger-Catalyst - Catalytic Performances on an Euro V Type Diesel Engine and Robust Design Development. **SAE Paper**, 2008-01-0768.

Korin *et al.* (1999) Korin, E., Reshef, R., Tshernichovesky, D., *et al.* (1999) Reducing Cold-Start Emission from Internal Combustion Engines by Means of a Catalytic Converter Embedded in a Phase-Change Material. **Proceedings of the Institution of Mechanical Engineers, Part D: Journal of Automobile Engineering**, 213: (6): 575-583.

Kotrba *et al.* (2013) Kotrba, A., Gardner, T.P., Bai, L., *et al.* (2013) Passive Regeneration Response Characteristics of a DPF System. **SAE Paper**, 2013-01-0520.

Kramer *et al.* (2009) Kramer, J., Pfahl, U., Bruestle, C., *et al.* (2009) The PM-Metalit: A PM control technology for Tier 4 Off-Highway Applications. **SAE Paper**, 2009-01-2838.

Kyu-Hyun *et al.* (2000) Kyu -Hyun, L., Chang -Yeul, S. and Wan-Bum, K. (2000) Development of Dual Wall Air Gap Exhaust System **SAE Paper**, 2000-01-0205.

Ladommatos *et al.* (1996) Ladommatos, N., Abdelhalim, S.M., Zhao, H., *et al.* (1996) The Dilution, Chemical, and Thermal Effects of Exhaust Gas Recirculation on Diesel Engine Emissions - Part 1: Effect of Reducing Inlet Charge Oxygen. **SAE Paper**, 961165.

Ladommatos *et al.* (2000) Ladommatos, N., Abdelhalim, S. and Zhao, H. (2000) The Effects of Exhaust Gas Recirculation on Diesel Combustion and Emissions. **International Journal of Engine Research**, 1: (1): 107-126.

Lafossas *et al.* (2011) Lafossas, F., Matsuda, Y., Mohammadi, A., *et al.* (2011) Calibration and Validation of a Diesel Oxidation Catalyst Model: from Synthetic Gas Testing to Driving Cycle Applications. **SAE Int. J. Engines**, 4: (1): 1586-1606.

Lafyatis *et al.* (1998) Lafyatis, D.S., Ballinger, T.H., Lammey, G., *et al.* (1998) Ambient Temperature Light-off Aftertreatment System for Meeting ULEV Emission Standards. **SAE Paper**, 980421.

Lahiri *et al.* (1997) Lahiri, D., Mehta, P.S., Poola, R.B., *et al.* (1997) **Utilization of Oxygen-Enriched Air in Diesel Engines: Fundamental Considerations** [online]. http://www.osti.gov/scitech//servlets/purl/563183-i4sk1J/webviewable/ Madison, WI (United States) [Accessed 1 September 1997].

Lancefield *et al.* (2000) Lancefield, T., Methley, I., Räse, U., *et al.* (2000) The Application of Variable Event Valve Timing to a Modern Diesel Engine. **SAE Paper**, 2000-01-1229.

Lapuerta *et al.* (2003) Lapuerta, M., Armas, O. and Gómez, A. (2003) Diesel Particle Size Distribution Estimation from Digital Image Analysis. **Aerosol Science and Technology**, 37: (4): 369-381.

Lapuerta *et al.* (2006) Lapuerta M., Ballesteros, R., Martos F.J. (2006) A Method to Determine the Fractal Dimension of Diesel Soot Agglomerates. **Journal of Colloid and Interface Science**, 303: 149–158.

Lapuerta *et al.* (2010) Lapuerta M., Martos F.J., Martín–González G. (2010) Geometrical Determination of the Lacunarity of Agglomerates with Integer Fractal Dimension. **Journal of Colloid and Interface Science**, 346: 23–31.

Laurell *et al.* (2013) Laurell, M., Sjörs, J., Ovesson, S., *et al.* (2013) "The Innovative Exhaust Gas Aftertreatment System for the New Volvo 4 Cylinder Engines; A Unit Catalyst System for Gasoline and Diesel Cars". **22nd Aachen Colloquium Automobile and Engine Technology**. Aachen, Germany.

Lehtoranta *et al.* (2007) Lehtoranta, K., Matilainen, P., Åsenbrygg, J.-M., *et al.* (2007) Particle Oxidation Catalyst in Light Duty and Heavy Duty Diesel Applications. **SAE Paper**, 2007-24-0093.

Lehtoranta *et al.* (2009) Lehtoranta, K., Matilainen, P., Kinnunen, T.J.J., *et al.* (2009) Diesel Particle Emission Reduction by a Particle Oxidation Catalyst. **SAE Paper**, 2009-01-2705.

Li *et al.* (2012) Li, J., Szailer, T., Watts, A., *et al.* (2012) Investigation of the Impact of Real-World Aging on Diesel Oxidation Catalysts. **SAE Int. J. Engines**, 5: (3): 985-994.

Lindfors *et al.* (2004) Lindfors, L.E., Eränen, K., Klingstedt, F., *et al.* (2004) Silver/Alumina Catalyst for Selective Catalytic Reduction of $NO_x$ to $N_2$ by Hydrocarbons in Diesel Powered Vehicles. **Topics in Catalysis**, 28: (1-4): 185-189.

Liu *et al.* (2008) Liu, Y., Ba, G., Kim, W., *et al.* (2008) Continuously Regenerating Particulate Matter (PM Metalit®) in LDV & HDV Retrofit Application Experiences from the Korean Retrofit Programme. **SAE Paper**, 2008-01-1547.

Liu *et al.* (2013) Liu, Y., Zheng, Y., Harold, M.P., *et al.* (2013) Lean $NO_x$ Reduction on LNT-SCR Dual-Layer Catalysts by $H_2$ and CO. **Applied Catalysis B: Environmental**, 132–133: (0): 293-303.

Mabilon *et al.* (1995) Mabilon, G., Durand, D. and Courty, P. (1995) "Inhibition of Post-Combustion Catalysts by Alkynes: A Clue for Understanding their Behaviour under Real Exhaust Conditions". In Frennet, A. & Bastin, J.M. (Eds.) **Studies in Surface Science and Catalysis**. Elsevier 775-788.

Mallamo *et al.* (2013) Mallamo, F., Longhi, S., Millo, F., *et al.* (2013) Modeling of Diesel Oxidation Catalysts for Calibration and Control Purpose. **International Journal of Engine Research**.

Marsh *et al.* (2001) Marsh, P., Acke, F., Konieczny, R., *et al.* (2001) Application Guideline to Define Catalyst Layout for Maximum Catalytic Efficiency. **SAE Paper**, 2001-01-0929.

Mather *et al.* (2002) Mather, D.K., Foster, D.E., Poola, R.B., *et al.* (2002) Modeling the Effects of Late Cycle Oxygen Enrichment on Diesel Engine Combustion and Emissions. **SAE Paper**, 2002-01-1158.

Maus & Brück (2005) Maus, W. and Brück, R. (2005) "The Future of Heterogeneous Catalysis in Automotive Applications; “Turbulent“ Catalysts for Spark - and Compression Ignition Engines". **26th International Vienna Motor Symposium**. Vienna, Austria.

Maus & Brück (2007) Maus, W. and Brück, R. (2007) "Exhaust Gas Aftertreatment Systems for Commercial Vehicles - Technologies and Strategies for the Future". **4th AVL International Commercial Powertrain Conference**. Graz, Austria.

Mayer *et al.* (2009) Mayer, A., Czerwinski, J., Comte, P., *et al.* (2009) Properties of Partial-Flow and Coarse Pore Deep Bed Filters Proposed to Reduce Particle Emission of Vehicle Engines. **SAE Int. J. Fuels Lubr.**, 2: (1): 497-511.

McCullough & Douglas (1996) McCullough, G. and Douglas, R. (1996) Reaction Mapping During Light-Off in a Two-Stroke Oxidation Catalyst. **SAE Paper**, 961808.

McDonald *et al.* (1995) McDonald, J.F., Purcell, D.L., McClure, B.T., *et al.* (1995) Emissions Characteristics of Soy Methyl Ester Fuels in an IDI Compression Ignition Engine. **SAE Paper**, 950400.

Meng *et al.* (1997) Meng, M., Lin, P. and Fu, Y. (1997) The Catalytic Removal of CO and NO Over Co-Pt(Pd,Rh)/$\gamma$-$Al_2O_3$ Catalysts and Their Structural Characterizations. **Catalysis Letters**, 48: (3-4): 213-222.

Merlone Borla *et al.* (2011) Merlone Borla, E., Nicol, G., Brandstätter, W., *et al.* (2011) New Concepts and Technologies for Integrated Diesel Exhaust Gas Aftertreatment Systems. **SAE Paper**, 2011-24-0184.

Miller *et al.* (2002) Miller, R.K., Haberkamp, W.C., Badeau, K.M., *et al.* (2002) Design, Development and Performance of a Composite Diesel Particulate Filter. **SAE Paper**, 2002-01-0323.

Millet *et al.* (2009) Millet, C.-N., Chédotal, R. and Da Costa, P. (2009) Synthetic Gas Bench Study of a 4-Way Catalytic Converter: Catalytic Oxidation, $NO_x$ Storage/Reduction and Impact of Soot Loading and Regeneration. **Applied Catalysis B: Environmental**, 90: (3–4): 339-346.

Millo & Vezza (2012) Millo, F. and Vezza, D. (2012) Characterization of a New Advanced Diesel Oxidation Catalyst with Low Temperature $NO_x$ Storage Capability for LD Diesel **SAE Paper**, 2012-01-0373.

Mittendorfer *et al.* (2003) Mittendorfer, F., Thomazeau, C., Raybaud, P., *et al.* (2003) Adsorption of Unsaturated Hydrocarbons on Pd(111) and Pt(111): A DFT Study. **The Journal of Physical Chemistry B**, 107: (44): 12287-12295.

Morlang *et al.* (2005) Morlang, A., Neuhausen, U., Klementiev, K.V., *et al.* (2005) Bimetallic Pt/Pd Diesel Oxidation Catalysts: Structural Characterisation and Catalytic Behaviour. **Applied Catalysis B: Environmental**, 60: (3–4): 191-199.

Mueller-Haas *et al.* (2003) Mueller-Haas, K., Brueck, R., Rieck, J.S., *et al.* (2003) FTP and US06 Performance of Advanced High Cell Density Metallic Substrates as a Function of Varying Air/Fuel Modulation. **SAE Paper**, 2003-01-0819.

Mulla *et al.* (2005) Mulla, S.S., Chen, N., Delgass, W.N., *et al.* (2005) $NO_2$ Inhibits the Catalytic Reaction of NO and $O_2$ over Pt. **Catalysis Letters**, 100: (3-4): 267-270.

Mulla *et al.* (2006) Mulla, S.S., Chen, N., Cumaranatunge, L., *et al.* (2006) Reaction of NO and $O_2$ to $NO_2$ on Pt: Kinetics and Catalyst Deactivation. **Journal of Catalysis**, 241: (2): 389-399.

Nguyen *et al.* (2011) Nguyen, L.D.K., Sung, N.W., Lee, S.S., *et al.* (2011) Effects of Split Injection, Oxygen Enriched Air and Heavy EGR on Soot Emissions in a Diesel Engine. **International Journal of Automotive Technology**, 12: (3): 339-350.

Nohara & Komatsu (2014) Nohara, T. and Komatsu, K. (2014) Potential of PM Reduction with Diesel Particulate Filter-less System for Off-Road Engine Applications. **JSAE**, 45: (2).

Ntziachristos *et al.* (2004) Ntziachristos, L., Mamakos, A., Samaras, Z., *et al.* (2004) Overview of the European "Particulates" Project on the Characterization of Exhaust Particulate Emissions From Road Vehicles: Results for Light-Duty Vehicles. **SAE Paper**, 2004-01-1985.

Oh *et al.* (2011) Oh, H., Luo, J. and Epling, W. (2011) NO Oxidation Inhibition by Hydrocarbons over a Diesel Oxidation Catalyst: Reaction Between Surface Nitrates and Hydrocarbons. **Catalysis Letters**, 141: (12): 1746-1751.

Okawara *et al.* (2005) Okawara, S., Tsuji, S., Inoue, M., *et al.* (2005) Soot Trapping and Continuously Oxidizing Behavior by Flow-Through Metallic PM Filter. **SAE Paper**, 2005-09-28.

Onodera *et al.* (2008) Onodera, H., Nakamura, M., Takaya, M., *et al.* (2008) Development of a Diesel Emission Catalyst System for Meeting US SULEV Standards. **SAE Int. J. Fuels Lubr.**, 1: (1): 231-238.

Pace *et al.* (2005) Pace, L., Konieczny, R. and Presti, M. (2005) Metal Supported Particulate Matter-Cat, A Low Impact and Cost Effective Solution for a 1.3 Euro IV Diesel Engine. **SAE Paper**, 2005-01-0471.

Pace & Presti (2011) Pace, L. and Presti, M. (2011) An Alternative Way to Reduce Fuel Consumption During Cold Start: The Electrically Heated Catalyst. **SAE Paper**, 2011-24-0178.

Page *et al.* (1999) Page, D.L., MacDonald, R.J. and Edgar, B.L. (1999) The QuadCAT™ Four-Way Catalytic Converter: An Integrated Aftertreatment System for Diesel Engines. **SAE Paper**, 1999-01-2924.

Pannone & Mueller (2001) Pannone, G.M. and Mueller, J.D. (2001) A Comparison of Conversion Efficiency and Flow Restriction Performance of Ceramic and Metallic Catalyst Substrates. **SAE Paper**, 2001-01-0926.

Parker *et al.* (1989) Parker, D.H., Bartram, M.E. and Koel, B.E. (1989) Study of High Coverages of Atomic Oxygen on the Pt(111) Surface. **Surface Science**, 217: (3): 489-510.

Parks *et al.* (2007) Parks, J., Huff, S., Kass, M., *et al.* (2007) Characterization of In-Cylinder Techniques for Thermal Management of Diesel Aftertreatment **SAE Paper**, 2007-01-3997.

Pataky *et al.* (1994) Pataky, G.M., Baumgard, K.J., Gratz, L.D., *et al.* (1994) Effects of an Oxidation Catalytic Converter on Regulated and Unregulated Diesel Emissions. **SAE Paper**, 940243.

Patterson *et al.* (2000) Patterson, M.J., Angove, D.E. and Cant, N.W. (2000) The Effect of Carbon Monoxide on the Oxidation of Four C6 to C8 Hydrocarbons over Platinum, Palladium and Rhodium. **Applied Catalysis B: Environmental**, 26: (1): 47-57.

Pfeifer *et al.* (2007) Pfeifer, M., Kögel, M., Spurk, P.C., *et al.* (2007) New Platinum/Palladium Based Catalyzed Filter Technologies for Future Passenger Car Applications. **SAE Paper**, 2007-01-0234.

Phillips *et al.* (1999) Phillips, P.R., Chandler, G.R., Jollie, D.M., *et al.* (1999) Development of Advanced Diesel Oxidation Catalysts. **SAE Paper**, 1999-01-3075.

Pipho *et al.* (1991) Pipho, M.J., Kittelson, D.B. and Zarling, D.D. (1991) $NO_2$ Formation in a Diesel Engine. **SAE Paper**, 910231.

Poola *et al.* (2004) Poola, R.B., Lill, R.J., Gottemoller, P., *et al.* (2004) "Electronically-Controlled Late Cycle Air Injection to Achieve Simultaneous Reduction of $NO_x$ and Particulates Emissions from a Diesel Engine". **United States Patent Office**. Patent NO. US6752131B2.

Presti *et al.* (2006) Presti, M., Pace, L., Carelli, G., *et al.* (2006) Turbulent Flow Metal Substrates: A Way to Address Cold Start CO Emissions and to Optimize Catalyst Loading. **SAE Paper**, 2006-01-1523.

Rajkumar & Govindarajan (2011) Rajkumar, K. and Govindarajan, P. (2011) Impact of Oxygen Enriched Combustion on the Performance of a Single Cylinder Diesel Engine. **Frontiers in Energy**, 5: (4): 398-403.

Rakopoulos *et al.* (2004) Rakopoulos, C.D., Hountalas, D.T., Zannis, T.C., *et al.* (2004) Operational and Environmental Evaluation of Diesel Engines Burning Oxygen-Enriched Intake Air or Oxygen-Enriched Fuels: A Review. **SAE Paper**, 2004-01-2924.

Reizig *et al.* (2001) Reizig, M., Brück, R., Konieczny, R., *et al.* (2001) New Approaches to Catalyst Substrate Application for Diesel Engines. **SAE Paper**, 2001-01-0189.

Rice *et al.* (2008) Rice, M., Kramer, J., Mueller, R., *et al.* (2008) Development of an Integrated NOx and PM Reduction Aftertreatment System: SCRi™ for Advanced Diesel Engines. **SAE Paper**, 2008-01-1321.

Royer & Duprez (2011) Royer, S. and Duprez, D. (2011) Catalytic Oxidation of Carbon Monoxide over Transition Metal Oxides. **ChemCatChem**, 3: (1): 24-65.

Saichaitanya *et al.* (2013) Saichaitanya1, P., Simhadri, K., Vamsidurgamohan, G. (2013) Impact of Cold and Hot Exhaust Gas Recirculation on Diesel Engine. **Int. Journal of Engineering Research and Applications**, 3: (5): 430-434.

Salomons *et al.* (2007) Salomons, S., Hayes, R.E., Votsmeier, M., *et al.* (2007) On the Use of Mechanistic CO Oxidation Models with a Platinum Monolith Catalyst. **Applied Catalysis B: Environmental**, 70: (1–4): 305-313.

Saroglia *et al.* (2002) Saroglia, G., Basso, G., Presti, M., *et al.* (2002) Application of New Diesel Aftertreatment Strategies on a Production 1.9 L Common-Rail Turbocharged Engine. **SAE Paper**, 2002-01-1313.

Schejbal *et al.* (2010) Schejbal, M., Štěpánek, J., Marek, M., *et al.* (2010) Modelling of Soot Oxidation by $NO_2$ in Various Types of Diesel Particulate Filters. **Fuel**, 89: (9): 2365-2375.

Schmidt *et al.* (1999) Schmidt, J., Waltner, A., Loose, G., *et al.* (1999) The Impact of High Cell Density Ceramic Substrates and Washcoat Properties on the Catalytic Activity of Three Way Catalysts. **SAE Paper**, 1999-01-027.

Schreiber *et al.* (2007) Schreiber, D., Forss, A.M., Mohr, M., *et al.* (2007) Particle Characterisation of Modern CNG, Gasoline and Diesel Passenger Cars. **SAE Paper**, 2007-24-0123.

Seifert *et al.* (2011) Seifert, S., Jayat, F., Reck, A., *et al.* (2011) Benefits of LS-Design™, a Structured Metal Foil for Two and Three Wheelers Catalyst Substrates, to Minimize Catalyst Volumes, PGM Loads and the Route Towards Low NOx Emissions. **SAE Paper**, 2011-28-0042.

Sher (1998) Sher, E. (1998) "Chapter 2 - Environmental Aspects of Air Pollution". In Sher, E. (Ed.) **Handbook of Air Pollution From Internal Combustion Engines**. San Diego, Academic Press 27-41.

Shigapov *et al.* (2008) Shigapov, A., Dubkov, A., Ukropec, R., *et al.* (2008) Development of PGM-Free Catalysts for Automotive Applications. **Kinetics and Catalysis**, 49: (5): 756-764.

Shimizu & Ohtaka (2007) Shimizu, C. and Ohtaka, Y. (2007) Parametric Analysis of Catalytic Converter Plugging Caused by Manganese-Based Gasoline Additives. **SAE Paper**, 2007-01-1070.

Sim *et al.* (2001) Sim, H.S., Min, K. and Chung, S.H. (2001) Effect of Synchronized Secondary Air Injection on Exhaust Hydrocarbon Emission in a Spark Ignition Engine. **Proceedings of the Institution of Mechanical Engineers, Part D: Journal of Automobile Engineering**, 215: (4): 557-566.

Skoglundh *et al.* (1991) Skoglundh, M., Löwendahl, L.O. and Otterated, J.E. (1991) Combinations of Platinum and Palladium on Alumina Supports as Oxidation Catalysts. **Applied Catalysis**, 77: (1): 9-20.

Snyder *et al.* (1972) Snyder, P.W., Stover, W.A. and Lassen, H.G. (1972) Status Report on HC/CO Oxidation Catalysts for Exhaust Emission Control. **SAE Paper**, 720479.

Son *et al.* (1999) Son, G.S., Kim, D.J., Lee, K.Y., *et al.* (1999) A Study on the Practicability of a Secondary Air Injection for Emission Reduction. **SAE Paper**, 1999-01-1540.

Southward *et al.* (2010) Southward, B.W.L., Basso, S. and Pfeifer, M. (2010) On the Development of Low PGM Content Direct Soot Combustion Catalysts for Diesel Particulate Filters. **SAE Paper**, 2010-01-0558.

Sultana *et al.* (2009) Sultana, A., Haneda, M. and Hamada, H. (2009) A New Concept of Combined $NH_3$-CO-SCR System for Efficient NO Reduction in Excess Oxygen. **Applied Catalysis B: Environmental**, 88: (1–2): 180-184.

Sun *et al.* (2008) Sun, H., Zhang, Y., Quan, X., *et al.* (2008) Wire-Mesh Honeycomb Catalyst for Selective Catalytic Reduction of $NO_x$ Under Lean-Burn Conditions. **Catalysis Today**, 139: (1–2): 130-134.

Theis *et al.* (2011) Theis, J.R., Dearth, M. and McCabe, R. (2011) LNT+SCR Catalyst Systems Optimized for $NO_x$ Conversion on Diesel Applications. **SAE Paper**, 2011-01-0305.

Torbati *et al.* (2013) Torbati, R., Pidria, M.F., Cerciello, G., *et al.* (2013) A Fully Integrated Partial Flow Filter with a Specialized and Unique Engine Management System to Meet Tier 4 Emission Legislations. **SAE Paper**, 2013-01-2462.

Traa *et al.* (1999) Traa, Y., Burger, B. and Weitkamp, J. (1999) Zeolite-Based Materials for the Selective Catalytic Reduction of $NO_x$ with Hydrocarbons. **Microporous and Mesoporous Materials**, 30: (1): 3-41.

Umehara *et al.* (2000) Umehara, K., Makino, M., Brayer, M., *et al.* (2000) Prediction of Catalytic Performance for Ultra Thin Wall and High Cell Density Substrates. **SAE Paper**, 2000-01-0494.

UNECE (2012) UNECE (2012) **Worldwide harmonized Light vehicles Test Procedure (WLTP)** [online]. Available from: https://www2.unece.org/wiki/pages/viewpage.action?pageId=2523179.

Vaaraslahti *et al.* (2006) Vaaraslahti, K., Ristimäki, J., Virtanen, A., *et al.* (2006) Effect of Oxidation Catalysts on Diesel Soot Particles. **Environmental Science & Technology**, 40: (15): 4776-4781.

Vakkilainen & Lylykangas (2004) Vakkilainen, A. and Lylykangas, R. (2004) Particle Oxidation Catalyst (POC) for Diesel Vehicles. **SAE Paper**, 2004-28-0047.

Voltz *et al.* (1973) Voltz, S.E., Morgan, C.R., Liederman, D., *et al.* (1973) Kinetic Study of Carbon Monoxide and Propylene Oxidation on Platinum Catalysts. **Product R&D**, 12: (4): 294-301.

Watanabe *et al.* (2007) Watanabe, T., Kawashima, K., Tagawa, Y., *et al.* (2007) New DOC for Light Duty Diesel DPF System. **SAE Paper**, 2007-01-1920.

Watling *et al.* (2012) Watling, T.C., Ahmadinejad, M., Ţuţuianu, M., *et al.* (2012) Development and Validation of a Pt-Pd Diesel Oxidation Catalyst Model. **SAE Int. J. Engines**, 5: (3): 1420-1442.

Web of Science (2014) Web of Science (2014) **Catalytic Converters Citation Report** [online]. Available from: https://webofknowledge.com.

Wiebenga *et al.* (2012) Wiebenga, M.H., Kim, C.H., Schmieg, S.J., *et al.* (2012) Deactivation Mechanisms of Pt/Pd-Based Diesel Oxidation Catalysts. **Catalysis Today**, 184: (1): 197-204.

Windeatt *et al.* (2012) Windeatt, J., Brady, G., Usher, P., *et al.* (2012) Real World Cold Start Emissions from a Diesel Vehicle. **SAE Paper**, 2012-01-1075.

Winkler *et al.* (2009) Winkler, A., Ferri, D. and Aguirre, M. (2009) The Influence of Chemical and Thermal Aging on the Catalytic Activity of a Monolithic Diesel Oxidation Catalyst. **Applied Catalysis B: Environmental**, 93: (1–2): 177-184.

Yao (1980) Yao, Y.-F.Y. (1980) Oxidation of Alkanes over Noble Metal Catalysts. **Industrial & Engineering Chemistry Product Research and Development**, 19: (3): 293-298.

Yao (1984) Yao, Y.-F.Y. (1984) The Oxidation of CO and Hydrocarbons over Noble Metal Catalysts. **Journal of Catalysis**, 87: (1): 152-162.

Ye *et al.* (2011) Ye, S., Yap, Y.H., Kolaczkowski, S.T., *et al.* (2011) Catalyst 'Light-Off' Experiments on a Diesel Oxidation Catalyst Connected to a Diesel Engine-Methodology and Techniques. **Chemical Engineering Research and Design**, 90: (6): 834-845.

Zeldovich (1946) Zeldovich, Y.B. (1946) The Oxidation of Nitrogen in Combustion and Explosions. **Acta Physiochem**, URSS, 21: 577.

Zhang *et al.* (2010) Zhang, Z., Chen, M., Jiang, Z., *et al.* (2010) Performance and Mechanism Study for Low-Temperature SCR of NO with Propylene in Excess Oxygen over Pt/$TiO_2$ Catalyst. **Journal of Environmental Sciences**, 22: (9): 1441-1446.

Zheng & Altman (2000) Zheng, G. and Altman, E.I. (2000) The Oxidation of Pd(111). **Surface Science**, 462: (1–3): 151-168.